

# Driven-Dissipative Quantum Many-Body Systems

Thèse de doctorat de l'Université Paris-Saclay  
préparée à l'Université Paris-Sud  
à l'Institut de Physique Théorique - CEA/Saclay

Ecole doctorale n°564 École Doctorale Physique en Île-de-France (EDPIF)  
Spécialité de doctorat : Physique

Thèse présentée et soutenue à Gif-sur-Yvette, le 21/10/2019, par

**ORAZIO SCARLATELLA**

Composition du Jury :

Karyn Le Hur Directrice de Recherche CNRS, École Polytechnique	Président
Martin Eckstein Professor, FAU Erlangen-Nürnberg	Rapporteur
Jonathan Keeling Reader, University of St Andrews	Rapporteur
Cristiano Ciuti Professeur, Université de Paris (prev Univ. Paris Diderot)	Examinateur
Serge Florens Directeur de Recherche CNRS, Institut NEEL	Examinateur
Alessandro Silva Associate Professor, SISSA	Examinateur
Marco Schirò Chargé de recherche CNRS, IPhT - CEA/Saclay, Collège de France	Directeur de thèse

# Acknowledgements

This thesis contains results of original work I've carried out during my three years PhD. Many people contributed, in a direct or indirect way, to making those results possible. The first person I need to thank is my PhD advisor, Marco Schirò, who took me under his wing as his first PhD student. He supervised my work with great dedication and he was my main mentor, collaborator and source of knowledge. He was as well an invaluable source of motivation and encouragement, compensating for my natural propensity to be unsatisfied about my work. I really appreciated his effort in encouraging me to follow my research interests and to broaden my knowledge outside of my research subject.

I would like to thank Aashish Clerk, who was directly involved in my research and in particular in the work presented in Chapter 3 of this thesis, which he actively supervised and contributed to. I would like to thank Rosario Fazio, who was directly involved in supervising the work in Chapter 4, for his precious discussions and feedbacks.

I am very grateful to Jonathan Keeling and Martin Eckstein for reading meticolously my thesis and allowing me to defend my PhD and for their interesting feedback on my work. I would equally like to thank Karyn Le Hur, Cristiano Ciuti, Alessandro Silva and Serge Florens, for accepting to be part of my jury.

I also need to thank my tutors, Pierfrancesco Urbani and Grégoire Misguich, who followed my developments and achievements during those three years and gave me their feedback and advices. I would like to thank the postdocs of the group, Steven, Francesco and Huggai, for the discussions we've had, their advices and company.

My PhD was funded by École Doctorale Physique en Île-de-France (EDPIF) and was carried out at Institut de Physique Théorique (IPhT) - CEA/Saclay and Université Paris-Sud/Paris-Saclay. I am grateful to those institutions as my PhD wouldn't have been possible without their support. I would like to thank the staff of IPhT, in particular the secretaries Sylvie Zaffanella, who saw my name on too many Amazon packages and helped me with all sorts of bureaucracy, Laure Sauboy, Anne Angles, the great IT staff Patrick Berthelot and Laurent Sengmanivanh, Riccardo Guida, Sylvain Ribault and Marco Schirò for organizing the lab courses, my great french teacher Henriette Helleboid and François Gelis and Loïc Bervas.

I would like to thank the other PhD students and postdocs of the lab whose company I've enjoyed during those years: Lilian, who shared the office with me and ensured everything was covered enough with sheets of paper, Kemal, who was always very warm and joyful, Raphael, Benoît, Jonathan, Étienne, Romain, Thiago, Linnea, Laïs, Vardan,

Guillaume, Thibault, Valerio, Valentina, Riccardo, Juan Miguel, Alex, Long, Federico, Corentin, Debmalya, Sebastian, Soumya, Hannah, Riccardo, Luca, Niall, Santiago, Severin, Yifei, Sarah, Ben, Elba, Francesca, Benjamin, Felix, Christian, Federica, Marco, Ingrid, Maxence, Bruno.

I also need to thank College de France, in particular the group of Antoine Georges, where my supervisor obtained a position as young team leader and where I spent a considerable amount of time during the last year of my PhD. I would like to thank in particular Thomas, Giacomo, Alice, Fedor, Anna and Michel for their nice company and their support during this last year.

I was supposed to be done with writing my thesis before starting the 2019 Les Houches summer school on Dynamics and Disorder in Quantum Many Body Systems Far From Equilibrium, but this didn't happen and thesis writing filled my spare time at Les Houches. I want to thank the attendees, organizers and lecturers of the school for making this school so great, for the nice time spent together and for their encouragement to bring this thesis to its end.

The years of my PhD were also a very difficult period of my life as I was engaged in a daily fight with insomnia. This has been my naughtiest enemy so far, deeply affecting my professional and social life. I would like to thank Annabella Di Giorgio, Jean Maquet and my parents for helping me getting out of this (waking) nightmare.

Finally I need to thank my friends who shared with me fears and joys and supported me during those years. Thank you Ivan, Bartolo and Luca for putting up with me in our house in Parc de Sceaux. I really learned a lot from you and I found in you great friends. Thank you Rachele and Eleonora, for bringing owls and cakes in the house. Thank you the extended Parc de Sceaux house members Giulia and Stefano: at the same time it was painful and very pleasant to do sports with you. Thank you Tony and Marwa, always present to celebrate the important events. I also want to thank Filippo, sharing with me the challenge of understanding open quantum systems, for the interesting conversations and the nice time spent together. Thank you friends of the PCS master, because you're all so great and this allowed me to grow so much and to face this PhD.

Infine vorrei ringraziare la mia famiglia. Mamma, papà, mi sono allontanato da voi inseguendo le mie ambizioni, ma sappiate che vi sarò per sempre riconoscente per tutto quello che avete fatto e che fate per me e che vi stimo tanto. Sorella, auguro a tutti i fratelli del mondo di avere un rapporto così bello come lo abbiamo noi due. Nonna, vorrei tanto accontentarti e tornare a casa presto.

# Summary

My PhD was devoted to the study of driven-dissipative quantum many-body systems. These systems represent natural platforms to explore fundamental questions about matter under non-equilibrium conditions, having at the same time a potential impact on emerging quantum technologies. My goal was to investigate new physical phenomena determined by the interplay of interactions, dissipation and non-equilibrium conditions as well as to develop new techniques to study these systems.

The outline of the thesis is the following. In chapter 1 we will introduce the research field, at the boundaries of condensed matter physics, quantum optics and quantum information. We will discuss my motivations to do research in this field as well as the main ideas behind it, or at least my point of view, and go through some recent theoretical and experimental developments. In chapter 2 we will introduce some theoretical techniques and concepts that will be useful in the rest of the thesis. Rather than entering in technical details, for which we will refer to books and papers, we will try to make connections between different techniques that are not often discussed in literature. In chapter 3 we will discuss the spectral properties of Markovian open quantum systems, looking in particular at a quantum van der Pol oscillator, in presence of an additional non-linear term in its Hamiltonian. This chapter is mostly based on [1]. In chapter 4, we will study the phase transition between a normal and a superfluid phase in a prototype system of driven-dissipative bosons on a lattice, which is characterized by an instability of dynamical modes. This chapter is mostly based on [2]. In chapter 5 we will discuss the phase boundary of a Mott insulating phase stabilized by dissipation, which is potentially relevant for undergoing experiments. The results of this chapter are preliminary and unpublished. Finally, in chapter 6 we will discuss some developments towards using the technique of dynamical mean field theory (DMFT) for studying driven-dissipative lattice systems. We will revisit and extend some well known techniques for impurity systems in the context of Markovian open systems, which are potentially useful both in the context of DMFT and to go beyond Markovian master equations into more complicated scenarios of non-Markovian dissipation. This chapter is mostly based on [3].

# Contents

<b>1</b>	<b>Driven-Dissipative Quantum Many-Body Systems</b>	<b>7</b>
1.1	The basic ideas . . . . .	7
1.2	Experimental platforms . . . . .	9
1.3	Dissipation engineering . . . . .	13
1.4	Theoretical investigations . . . . .	15
<b>2</b>	<b>Theoretical Methods</b>	<b>19</b>
2.1	Non-equilibrium Green functions . . . . .	20
2.2	Non-Equilibrium contour and Keldysh field theory . . . . .	22
2.3	Markovian open quantum systems . . . . .	25
2.4	Markovian systems Green functions . . . . .	29
<b>3</b>	<b>Spectral Properties of a Quantum van der Pol Oscillator</b>	<b>34</b>
3.1	Introduction . . . . .	34
3.2	Spectral function . . . . .	36
3.3	Effective temperature . . . . .	38
3.4	The van der Pol oscillator . . . . .	39
3.5	Spectral properties of vdP oscillator . . . . .	42
3.6	Conclusions . . . . .	50
<b>4</b>	<b>Finite-Frequency Transition in Driven-Dissipative Bosons on a Lattice</b>	<b>52</b>
4.1	Introduction . . . . .	52
4.2	The model . . . . .	53
4.3	Finite-frequency instability of the normal phase . . . . .	57
4.4	Dissipative dynamics . . . . .	62
4.5	Conclusions . . . . .	67
<b>5</b>	<b>Dissipative Preparation of Photonic Mott Insulators</b>	<b>69</b>
5.1	The model . . . . .	70
5.2	Ground-state problem . . . . .	71
5.3	Driven-dissipative problem . . . . .	72
5.4	Changing the driving protocol . . . . .	77
5.5	Conclusions . . . . .	81

<b>6 Towards Dynamical Mean Field Theory for Driven-Dissipative Systems</b>	<b>82</b>
6.1 Driven-dissipative bosonic DMFT . . . . .	83
6.2 Auxiliary impurity problem . . . . .	85
6.3 Formulation of the impurity problem . . . . .	87
6.4 Hybridization expansion . . . . .	88
6.5 Diagrammatic rules and Dyson equation . . . . .	93
6.6 The Non-Crossing impurity solver . . . . .	96
6.7 Conclusions . . . . .	102
<b>7 General Conclusions</b>	<b>104</b>
<b>8 Résumé Substancial</b>	<b>106</b>
8.1 Introduction . . . . .	106
8.2 Spectral Properties of a Quantum van der Pol Oscillator . . . . .	109
8.3 Transition à fréquence finie dans des réseaux de bosons pilotés et dissipatifs	112
8.4 Préparation d'isolants de Mott à l'aide de la dissipation . . . . .	115
8.5 Vers une approche DMFT pour les réseaux de bosons dissipatifs pilotés . .	117
<b>A Energy-selective dissipator</b>	<b>120</b>
A.1 Derivation . . . . .	120
A.2 Cold and hot drives . . . . .	123
<b>B More on DMFT</b>	<b>125</b>
B.1 Delocalization transition in DMFT . . . . .	125
B.2 Hubbard-I impurity solver in the symmetric phase . . . . .	126
<b>C Details of the NCA solver</b>	<b>128</b>
C.1 Stationary state . . . . .	128
C.2 Derivation of NCA self-energy . . . . .	128
C.3 Trace preservation . . . . .	130
C.4 Hermiticity preservation . . . . .	131
C.5 Green Functions . . . . .	133

# Chapter 1

# Driven-Dissipative Quantum Many-Body Systems

Along this chapter we will motivate my interest in the theoretical investigation of driven-dissipative quantum many-body systems and make connections with the literature and with state-of-the-art experiments. In Sec. 1.1 we will introduce the main ideas behind this research field. In Sec. 1.2 we will describe experimental platforms that are emerging as quantum simulators, with a focus on circuit quantum electro-dynamics (circuit QED), while in Sec. 1.3 we will discuss the concept of dissipation engineering, turning dissipation from a decoherence machine into a resource to prepare quantum states. Finally, in Sec. 1.4 we will present some recent theoretical advances in this field, leaving a number of open questions for future investigations.

## 1.1 The basic ideas

The 10 years old field of **driven-dissipative quantum many-body systems** is a hybrid research field, intersecting ideas coming from traditionally different domains of physics, in particular atomic molecular and optical (AMO) physics, condensed matter physics and quantum information. Let's start by breaking down the parts composing the name of this research field. The **quantum many-body** problem could be traced back to Dirac's quote “*The general theory of quantum mechanics is now almost complete...the difficulty is only that the exact application of these laws leads to equations much too complicated to be soluble*” [4]. Quantum many-body physics has seen a series of breakthrough in its history, for example the BCS theory of superconductivity [5] or the understanding magnetic impurities in metals [6], leading to the development of renormalization group techniques. Collective phenomena arise when many particles interact with each other realizing spectacular macroscopic quantum states, such as for example Bose-Einstein condensates, superconductors or Mott insulators. The above Dirac quote continues with “*It therefore becomes desirable that approximate practical methods of applying quantum mechanics should be developed*” [4]. In fact, quantum many-body problems are very hard to solve, calling for a variety of approximated techniques, each of them tailored to address certain physical regimes.

While the computer era has significantly pushed the boundary of tractable problems, the exponential increase of the Hilbert space with the number of degrees of freedom limits the system sizes that can be treated numerically. The assumption, when verified, of thermodynamic equilibrium significantly simplifies the many-particles problem. A direct application of the thermodynamics ensembles of classical statistical mechanics to quantum particles, allows to obtain quantum statistics. These describe the equilibrium state obtained by putting a quantum system in contact with a reservoir with some well defined thermodynamic variables, such as temperature and chemical potential. The limit of this approach is that it does not allow to study the dynamics towards equilibration, that instead needs a more microscopic modeling of dissipation, nor more general non-equilibrium scenarios.

This microscopic modeling of **dissipation** in quantum mechanics was born in the 60's, stimulated by the invention of the laser. While in many cases one is interested in quantum systems which are as isolated as possible from their environment, as the coupling to the environment is detrimental for quantum features, this is not the case, for example, in the phenomenon of laser action, which needs a lossy cavity to take place [7]. While dissipative phenomena are easily described in classical Newtonian mechanics, for example drag forces in fluids or thermal losses in a circuit, the Hamiltonian formulation of quantum mechanics does not naturally allow for describing dissipative processes. The simplest idea of trying to quantize classical dissipative equations of motion unfortunately leads to the catastrophic consequence of breaking the quantum canonical commutation relations [7]. The effort to develop a dissipative quantum theory that would recover well known classical equations in the classical limit while preserving canonical commutation has led to the now commonly accepted "system plus reservoir" approach [8–10].

In order to compensate for losses of particles and energy, one can **drive** the system applying external forces on it, eventually establishing a dynamical balance between driving forces and losses. We will call such a system a **driven-dissipative** system. The dynamical balance between driving forces and losses is not expected, though, to lead to a thermodynamic state and rather it realizes a non-equilibrium stationary state. In fact, the drive plus dissipation mechanism explicitly breaks microscopic reversibility, or detailed balance, underlying thermodynamic equilibrium. In this dissertation we will focus on those non-equilibrium stationary states rather than on transient dynamics. We will mainly consider dissipative processes that can be described in terms of Lindblad master equations, that we will introduce in Ch. 2.

Combining the non-equilibrium conditions realized in driven-dissipative systems with the interest in collective phenomena arising when many particles interact with each other, gives rise to the new area of activity of driven-dissipative quantum many-body systems [11–26]. Relaxing the constraint of thermodynamic equilibrium opens the door to new, many-body phases, with no equilibrium counterpart. For example, there's no guarantee that a driven-dissipative system will ever reach a time-independent state and the onset of limit-cycles or chaos are valid alternatives [20, 27, 28]. Driven-dissipative stationary states can undergo phase-transitions when tuning some control knobs, called dissipative phase transitions, that are potentially different from ordinary quantum or thermal phase

transitions and therefore are attracting a lot of attention [29–55]. While driven-dissipative systems are very natural platforms to study out-of-equilibrium phenomena, dissipation is detrimental for quantum features and thus for observing interesting quantum mechanical behaviours. For example, most of the phase-transitions in those systems belong to thermal universality classes [18, 41, 45] even if this is not a general statement [41, 46, 53]. Nevertheless not all the quantum features get necessarily washed out by dissipation, to the point that dissipative processes can be engineered in such a way that they generate quantum states rather than suppressing them; this is the concept of dissipation engineering that we will discuss in section 1.3. In the next section, instead, we will discuss the experimental platforms that allow to realize and manipulate driven-dissipative quantum systems and that are pushing the technological boundaries towards the quantum simulation of many-body physics in these systems.

## 1.2 Experimental platforms

The last years have seen enormous advances in controlling and probing quantum systems, motivated by the wish to understand fundamental questions, but also with the goal of realizing technologies taking advantage of quantum mechanical effects. Those developments have been achieved in several branches of physics such as condensed matter physics, atomic physics, quantum optics and quantum information. They brought forth a number of highly controllable and measurable experimental platforms, which can simulate the behaviour of more complex, otherwise inaccessible many-body quantum systems: these platforms are called *quantum simulators*. The idea of quantum simulation was originally proposed by Feynman [56]. The necessity for a quantum platform to simulate quantum many-body systems comes from the observation that their Hilbert space grows exponentially with the number of degrees of freedom. An exponentially large amount of data would then be needed to encode a quantum many-body wavefunction in a classical computer, making the problem intractable for big systems. Rather than trying to solve a many-body Hamiltonian using a computer, one can take a physical system, that is ideally very easy to control and measure and that is modelled by that Hamiltonian, and study how that system behaves: this physical system realizes a quantum simulator. A series of quantum simulators nowadays allow to explore non-equilibrium many-body quantum physics, such as ultracold atomic gases [57, 58], quantum circuits [47, 59–63], optical cavities [35, 44], and trapped ions [64]. In the last 20 years, quantum simulators allowed to experimentally engineer many theoretically investigated Hamiltonians and to probe quantum phases of matter and phase transitions [65–69].

Platforms have emerged as well to simulate driven-dissipative many-body systems. Photonic systems are particularly suited to realize these systems as their particle number is hardly conserved in realistic situations. On the other hand photons are among the best examples of non-interacting particles in vacuum. If one is interested in studying many-body effects which arise thanks to the interactions amongst particles, interacting particles are needed. A first experimental challenge in those photonic platforms though,

was to make photons interact with each other [59, 70]. In order to do that, photons are coupled, through their electromagnetic field, to other interacting particles, which in turn mediate photon-photon interactions. Those mediated interactions need to be bigger than the photonic decay rate due to dissipation in order to play a major role [71]. Promising experimental platforms in which such strong interactions in driven-dissipative systems are achieved are: those involving photons with optical wavelengths [70, 72], and those based on superconducting circuits [59, 60, 63, 73] whose excitations are microwave photons. Photon-photon interactions are mediated by a non-linear component: the possibility of photons to excite electron-hole pairs in semiconductors for the first category, and the non-linear behaviour of Josephson junctions in the second. In the next section we will do a short overview of superconducting circuits, that are promising to realize scalable arrays of strongly-interacting photons [73–76].

### 1.2.1 Theory of superconducting circuits

Superconducting circuits [77] can be described by collective, mesoscopic variables, such as charge and flux, which show quantum mechanical behaviour if thermal fluctuations are smaller than the excitation energies of the circuit. The leads that are connected to the system in order to probe and control it, constitute an unavoidable electromagnetic environment responsible for losses of particles, energy and quantum coherence [63]. Those loss and decoherence processes can be usually modelled by a Lindblad master equation [63], that we will discuss in chapter 2. A natural way to probe such systems consists in driving them continuously with a microwave generator, thus realizing a balance of incoming and outgoing particles and energy. The simplest building blocks of superconducting circuit platforms are LC resonators, characterized by their inductance and capacitance with typical values around  $L = 1\text{ nH}$  and  $C = 10\text{ pF}$  leading to a resonant frequency of  $\omega_0/2\pi = 1/2\pi\sqrt{LC} \approx 1.6\text{ GHz}$ , in the microwave range [78]. An LC resonator can be quantized by writing down its classical Hamiltonian and promoting the conjugate classical variables,  $Q$  and  $\phi$ , that mimic respectively position and momentum, to quantum operators satisfying the canonical commutation rules  $[Q, \phi] = -i$ . The  $\hbar = 1$  units will be used throughout the thesis. The Hamiltonian of an LC resonator is simply the sum of the inductor and capacitance energies and it is formally equivalent to a mass connected to a spring, that is to an harmonic oscillator, thus it can be expressed in terms of annihilation and creation operators,  $a = \frac{1}{\sqrt{\omega_0}} \left( \frac{Q}{\sqrt{2C}} + i \frac{\phi}{\sqrt{2L}} \right)$ ,

$$H = \frac{\phi^2}{2L} + \frac{Q^2}{2C} = \omega_0 \left( a^\dagger a + \frac{1}{2} \right) \quad (1.1)$$

An LC resonator is a linear circuit element and its Hamiltonian is quadratic in  $a^\dagger$  and  $a$  operators. In order to make things more interesting, one needs to introduce non-linear elements in the circuit, such as Josephson junctions. These are made by sandwiching a thin insulating layer between two superconductors [79]. Josephson discovered that, without any voltage drop, such a junction sustains a current given by  $I = I_c \sin(\Delta\theta)$ , where  $\Delta\theta$  is the difference of the phase of the superconducting order parameter between the two sides of

the junction and  $I_c$  is the critical current above which dissipative conduction takes place: this is called the dc Josephson effect. The magnetic flux through a superconducting circuit is related to the gradient of the phase  $\Delta\theta$  of the superconducting order parameter by the local gauge invariance of the vector potential giving  $\phi/\phi_0 = \Delta\theta$ , where  $\phi_0 = 1/(2e)$  is the flux quantum [80]. A Josephson junction stores an energy of  $-E_J \cos(\phi/\phi_0)$ , with  $E_J = I_c \phi_0$ , consistently with the Josephson current just introduced ( $I = \dot{Q} = \partial H/\partial\phi$ ). The second order in  $\phi$  gives a linear inductance contribution to the Hamiltonian, with  $L_J = \phi_0^2/E_J$ , while higher orders introduce non-linearities in the model. The junction also has its own capacitance  $C_J$ , thus it is represented as a Josephson non-linear element (a cross in schematics) in parallel with  $C_J$ , with total Hamiltonian

$$H_J = \frac{Q^2}{2C_J} + \frac{\phi^2}{2L_J} + U_{NL}(\phi) \quad (1.2)$$

with non-linearities  $U_{NL}(\phi) = E_J \sum_{n>1} (-1)^{n+1} (\phi/\phi_0)^{2n} / (2n)!$ . Keeping the first non-linear contribution in the rotating-wave approximation, that is keeping only terms with equal number of annihilation and creation operators, we get the Hamiltonian

$$H = \omega_J a^\dagger a + \frac{U}{2} (a^\dagger a)^2 \quad (1.3)$$

If one puts two Josephson junctions in parallel to form a ring, realizing a superconducting quantum interference device (SQUID), they behave like a single effective junction for the rest of the circuit, but the Josephson energy  $E_J$  can be tuned by controlling a magnetic flux applied through the ring, which in turns allows to tune  $U$ . Devices featuring one or more Josephson junctions are called superconducting qubits [81]. Connecting two circuits elements,  $i$  and  $j$ , with a capacitive coupling gives rise to the hopping element (in the rotating wave approximation)

$$H_J = J \left( a_i^\dagger a_j + a_i a_j^\dagger \right) \quad (1.4)$$

Using those building blocks, or combining them in more sophisticated ways, allows to engineer a variety of many-body Hamiltonians describing bosonic particles on a lattice [60, 73, 82].

### 1.2.2 Many-body Hamiltonians with circuits

An array of coupled Josephson junctions is described by a Bose-Hubbard Hamiltonian [83].

$$H_{BH} = \sum_i \left( \omega_0 n_i + \frac{U}{2} n_i^2 \right) - J \sum_{\langle ij \rangle} \left( a_i^\dagger a_j + h.c. \right) \quad (1.5)$$

with  $n_i = a_i^\dagger a_i$ . When we will discuss, in Ch. 4.5 the Bose-Hubbard model with losses and driving terms, we will have this kind of experimental set-up in mind. Josephson junctions arrays were first realized in 1980's and Bose-Hubbard physics was investigated

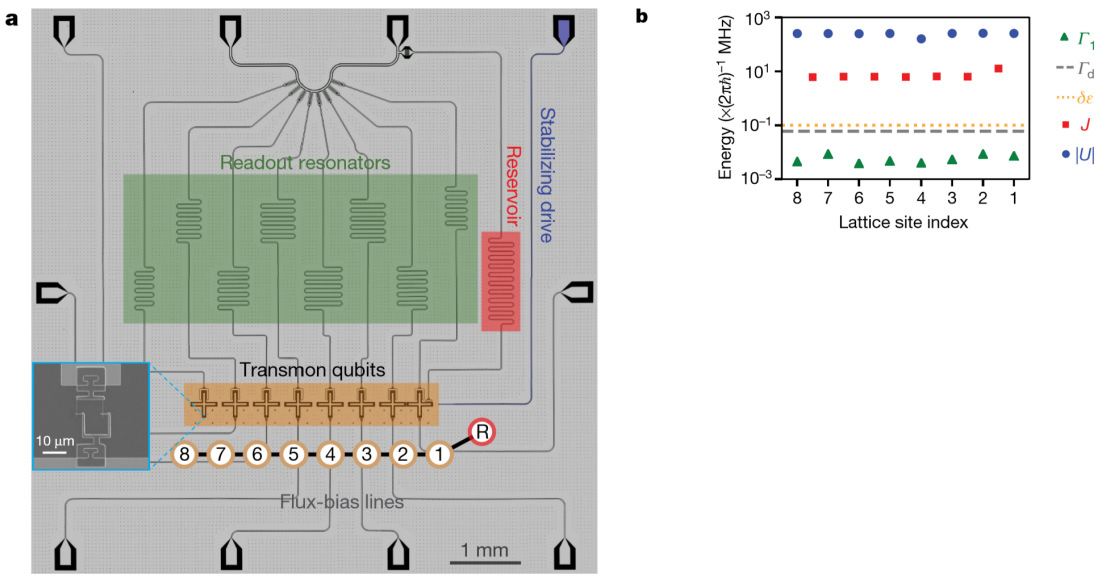


Figure 1.1: Picture from [62]. Bose–Hubbard lattice in a superconducting circuit. a) Optical image of the device. Superconducting transmon qubits (Q1–Q8; yellow) constitute lattice sites with energies tunable by individual fluxbias lines. Capacitive coupling between transmons leads to tunnelling  $J$ , and transmon anharmonicity gives the on-site interaction  $U$ . Readout resonators (green) enable site-resolved occupancy measurement via a common transmission line. A lossy resonator (red) acts as a cold reservoir for the stabilization process. A stabilization line (blue) drives only site Q1. Inset, close-up scanning electron microscope image of the transmon qubit, showing the bottom of the cross-shaped capacitor pad and the SQUID loop. b) Measured on-site interactions  $U$ , tunnelling rates  $J$ , single-photon losses  $\Gamma_1$ , dephasing rate  $\Gamma_d$  and on-site disorder  $\delta\epsilon$ , demonstrating a high-coherence, low-disorder Bose–Hubbard lattice in the strongly interacting regime.

already in the early 1990 [84]. One of the main advances of current architectures is that individual circuit elements are separated by larger distances on the chip and thus are individually accessible. Also there's much better control on disorder in the fabrication of chips, that was a significant limitation to experiments [73]. In [83, 85] the authors made a recent theoretical proposal using Josephson junctions embedded in LC resonators. A experimental platform on this line has recently been experimentally realized in [62], consisting in an array of 8 transmon qubits, that are SQUIDS in parallel with a large capacitance. Their circuit is shown in Fig. 1.1

Another Hamiltonian that received much attention in recent years, because it can be naturally realized in circuits [47, 61, 86, 87], is the Jaynes-Cummings Hubbard Hamiltonian [11, 13, 29, 33, 73, 88–90]. The on-site Jaynes-Cummings Hamiltonian is realized by coupling an LC resonator to a qubit [63]. This set-up features two bosonic modes per site, in contrast with the Bose-Hubbard, where there's only one mode per site: a linear mode inside the LC resonator and a non-linear mode in the qubit. If the Josephson non-linearity is bigger than all other energy scales, the qubit can be approximated with a 2-level system with raising and lowering operators  $\sigma^+$  and  $\sigma^-$ , thus realizing the Jaynes-Cummings lattice Hamiltonian

$$H_{JC} = \sum_i \left[ \omega_0 a_i^\dagger a_i + \varepsilon \sigma_i^+ \sigma_i^- + g (a_i \sigma_i^+ + a_i^\dagger \sigma_i^-) \right] - J \sum_{\langle ij \rangle} (a_i^\dagger a_j + h.c.) \quad (1.6)$$

The physics of the Jaynes-Cummings Hubbard and the Bose-Hubbard Hamiltonian is strictly related. Both of them feature a similar equilibrium phase diagram including a Mott and a superfluid phase with a transition between them belonging to the same universality classes [29, 90, 91].

### 1.3 Dissipation engineering

Quantum behaviour is very fragile and indeed our everyday world hardly shows any quantum feature. In fact, the interaction of a quantum system with its environment is responsible for destroying its quantum features and recovering the much more familiar to us classical behaviour. Despite the usual negative connotation associated with dissipation, dissipative processes can actually be turned into resources to prepare, rather than suppress, states with interesting quantum mechanical behaviour. This concept is known as *dissipation engineering* [92] and a major effort in this direction is currently being made in the quantum optics and quantum information communities. Dissipation engineering has been successfully employed to prepare quantum states in different contexts [62, 93–97] and it is promising for realizing autonomous quantum error correction [98–100]. In this section we will discuss two cases of experimental realizations of this concept. The first is the dissipative stabilization of a Mott insulating phase, realized experimentally in [62] and theoretically proposed in [93, 101, 102], which will be the subject of Ch. 5. In [62] the authors realized a 1D chain of 8 coupled transmons qubits, realizing a Bose-Hubbard Hamiltonian. Each site has intrinsic losses which would lead to an empty state. In order

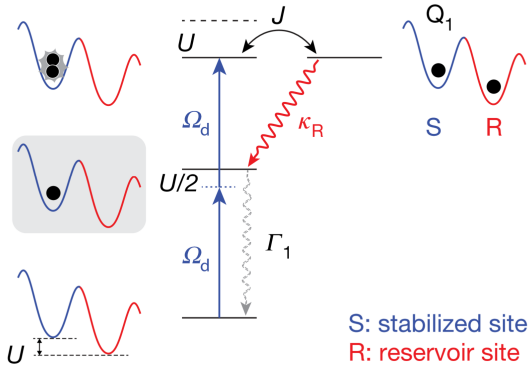


Figure 1.2: Picture from [62]. Scheme for the one-transmon dissipative stabilizer designed in [62]. An auxiliary transmon R acts as an environment for the  $n = 2$  state of the target site S, stabilizing the site in the  $n = 1$  state.

to stabilize a Mott insulating phase with exactly one photon on each site, the authors implemented two versions of a “dissipative stabilizer”, respectively involving one and two auxiliary transmons. We will describe the working principle of the stabilizer, in the scheme involving one auxiliary transmon for simplicity, first considering the case in which the system consists of a single site coupled to the auxiliary transmon as shown in Fig. 1.2. Say we want to put exactly one photon in the site. In order to populate the site, transitions are driven from the  $n = 0$  state to the  $n = 2$  state, with a classical field of frequency  $\omega_{02}/2$ . Due to the on-site Hubbard interaction  $U$ , the drive frequency is detuned from the transition from the  $n = 0$  to the  $n = 1$  state by  $U/2$ :  $\omega_{02}/2 \neq \omega_{01}$ . Once in the state with  $n = 2$ , the second photon with energy  $\omega_{12}$  rapidly tunnels to the auxiliary transmon, that is strongly lossy and eventually dissipates the photon in its environment. Eventually, the target site is left with exactly one photon. When considering the whole chain instead of a single site, the first site of the chain being the stabilized site, then the first site acts as a narrow-band photon source for the rest of the chain. Photons from this site tunnel into the others until filling them all. When all the sites are filled with one photon, then the stabilizer will be unable to inject additional photons, as this would require an energy higher than the source energy, because of the incompressibility of the Mott phase. A driving scheme in the same spirit of having an energy selective source of particles was proposed in [101] and will be discussed in Ch. 5, where we will study the phase diagram of such a dissipatively-stabilized Mott insulator. A second example of engineered dissipation is the experimental preparation [103, 104] of what are maybe the most paradigmatic example of non-classical states, Schrödinger cat states, through dissipation. In this experiment, the authors observe the two Schrödinger cat states obtained by the symmetric and antisymmetric superposition of two photonic coherent states with opposite phase squeeze out of vacuum in the dissipative dynamics. Their set-up consists of two superconducting resonators, named the *storage* and the *readout* cavity, coupled through a Josephson junction. The readout cavity is driven through a coherent tone and strongly coupled to a transmission line and it is meant to

evacuate entropy from the storage, as the auxiliary transmon of the experiment [62]. The coupling of the cavities through the Josephson junction and the pumping of the readout, stimulates the conversion of two storage photons into one readout photon, which is rapidly lost in the transmission line, and one pump photon. An effective description of the storage cavity involves terms in which a pair of photons are injected in the storage or dissipated from the storage. Additionally, dissipative processes involving only one storage photon at a time are also present. As a result of the processes involving photons pair creation and annihilation, the authors observe Schrödinger cats states squeezing out of the vacuum, before decaying into a classical state, because of the always present single-particle losses. This model has been investigated theoretically in [105], where an analytical solution for the steady state density matrix is found. Due to unavoidable single-particle losses, the authors show that the steady state density matrix is always a statistical mixture of the two cat states, but that the transient dynamics can pass through a metastable state lasting orders of magnitudes longer than the photon lifetime. With those two examples of engineered dissipation, that were chosen amongst others according to my personal taste, I hope I gave the reader the flavour of why dissipative quantum systems are more interesting than expected, in the sense that not only they are important to understand how a quantum system turns classical by the effect of the coupling to the environment, but that they can be equally used for engineering new out-of-equilibrium quantum phases of matter.

## 1.4 Theoretical investigations

In this last section we will discuss some recent theoretical investigations in the realm of driven-dissipative quantum many-body systems. This discussion is by no means exhaustive and the selection of topics is a personal choice. As a first example of a topic of current interest, optical bistability has recently been studied beyond its semi-classical solution, in the context of a single coherently driven non-linear resonator with one-particle Markovian losses [54, 106]. While in the semi-classical limit, in which the bosonic field is replaced by its expectation value, there is a region in the strength of the driving field with two dynamically stable solutions, in the same region the quantum solution obtained as the steady state of the corresponding Lindblad master equation has a single solution. These two pictures are reconciled by investigating the behaviour of the smallest eigenvalue of the Liouvillian super-operator, called the Liouvillian gap, in the same region. In the semi-classical limit of infinitely many-bosons this eigenvalue is vanishingly small and the master equation admits two stationary states, thus recovering the semi-classical bistability in this limit. The closing of the Liouvillian gap allows to interpret the phenomenon of optical bistability as a first order dissipative phase transition [37, 49]. This novel point of view attracted a new wave of interest on optical bistability and more generally on the possibility of having multiple steady-states of the Liouvillian in the thermodynamic limit. In [106] the authors claimed that a closing of the Liouvillian gap and thus a dissipative phase transition would also occur connecting many of those cavities in a lattice model. This time only a finite number of photons per site is needed, and a dissipative phase transition is supposed

to arise in the thermodynamic limit of infinitely many sites. Indeed, a following work [50] numerically showed that it is the case in 2D, where the Liouvillian gap closes point-wise for a critical drive strength, while in 1D the Liouvillian gap unexpectedly saturates to a finite value as the lattice size is increased. In a similar direction, a recent work [107] analysed a spin model for which the mean-field solution shows a bistable behaviour, with a method aimed at including quantum fluctuations beyond mean-field in a self-consistent way supported by MPO simulations. The numerical results of [107] show that bistability is completely washed away in 1D, while suggest the possibility of true bistability in the thermodynamic limit in 2D.

Another interesting front of current investigations is aimed at understanding universal phenomena in many-body driven-dissipative systems. Universal phenomena are intimately related to phase transitions and to fixed points of the renormalization group flows [108] and can characterize both non-equilibrium stationary states of driven-dissipative systems and their dynamics. The interest in critical phenomena in this novel class of systems is two-fold. The first reason of interest stems from the non-equilibrium nature of those systems. While equilibrium dynamical phase transitions have been classified by Hohenberg and Halperin [109], non-equilibrium conditions can lead to new universality classes which escape this classification. On the other hand, most of the phase transitions in driven-dissipative systems belong to thermal universality classes and are described by an emergent effective temperature, as quantum fluctuations are lost as a result of dissipation [18, 41, 45]. A current challenge is to understand to which extent quantum features can be present in the critical properties of those systems. Some progresses in both directions have been made. In [41], the authors study the Bose condensation transition in driven-dissipative systems using a functional renormalization group approach. They predict a new critical exponent, which describes how quantum coherent dynamics is washed away towards an effective thermal behaviour, which escapes the Hohenberg-Halperin classification of equilibrium critical dynamics and thus defines a new universality class. In this work, the renormalization group flow leads to a fixed point where all quantum coherence is lost and where only the dissipative couplings are non-zero and thus the phase-transition in the stationary state is then essentially classical. In [110], the authors discuss a novel universality class in one-dimensional driven open quantum system, which manifests in presence of strong diffusive noise on top of inevitable white noise. They predict a new non-equilibrium fixed point with mixed coherent and dissipative nature. In striking contrast with [41], quantum mechanical effects persist in the critical behaviour. This critical behaviour though, characterizes only intermediate length-scales, before the final onset of decoherence at the longest length-scales in the system. A relevant work in this context is the recent numerical study [53] of the critical behaviour of a model of a quadratically driven non-linear photonic lattice. Essentially, this is a lattice model obtained by coupling several cavities of the kind that were used to prepare cat states in [103]. Each site of the lattice features drive and dissipative processes involving two photons at a time as well as additional single-photon losses. The authors of [53] claim that, for small values of dissipation, the critical behaviour is determined by an underlying quantum critical point of

the quantum Ising universality class. For increasing photon loss rates, a departure from this quantum universal behaviour is interpreted as the onset of a quantum critical regime, akin of what one would expect by increasing temperature starting from a zero temperature quantum critical point [111, 112].

Finally, I would like to turn the attention to the possibility of breaking time-translational symmetry in many-body driven-dissipative systems. In the quantum world, the question of whether it is possible to break time-translational invariance, has recently attracted a lot of interest, starting the quest for time-crystals. Soon after the original proposal [113] of an oscillating ground-state of a quantum many-body system, no-go theorems showed that it is actually impossible to break continuous time-translational symmetry in ground-states [114–116]. Starting from this defeat, the focus has changed from looking for realizations of spontaneously broken continuous time-translational symmetry to investigating cases in which discrete time-translational symmetry is broken. The basic idea is looking at systems driven with a certain drive period, which show a dynamics with a period which is a multiple of the drive period: this is the class of Floquet time-crystals [117–121]. As the time-crystal behaviour is supposed to be an effect of many-body interactions, the spontaneous frequency of oscillations of the system should be robust to perturbations in the drive frequency. In driven-dissipative systems, nothing prevents from the possibility of breaking time-translational symmetry resulting in a non-equilibrium state which oscillates in time. A well known example is provided by exciton-polariton condensates where the superfluid order parameter oscillates at an effective chemical potential [30, 31, 70, 122]. The breaking of time-translational symmetry in those systems is associated with a dissipative phase transition, in which some eigenvalues of the Liouvillian become purely imaginary. An example of this time-crystal behaviour is given in the semi-classical spin model studied in the context of boundary time-crystals [28]. There, the possibility of time-crystal behaviour at the boundary of a closed many-body quantum systems is connected with a driven-dissipative problem showing time-crystal behaviour in its long time dynamics. In this semi-classical model, the authors show that indeed a large number of eigenvalues of the Liouvillian become purely imaginary in the thermodynamic limit, thus the limit cycle phase is characterized by several harmonics. Another interesting work in the context of spin models is [123], where the authors study an incoherent spin-model developing a time-crystal phase, relating it to models of synchronization of oscillators. Limit cycles are easily predicted at the mean-field level, but it is questionable whether they survive upon including fluctuations. In [20] for example, the authors investigate the robustness of limit cycles predicted in mean-field in a driven-dissipative Heisenberg lattice using beyond mean-field methods, and conclude that those oscillations are damped out in any physical dimension upon including beyond mean-field fluctuations. In [22], the authors show that dissipation can actually prevent systems, which would thermalize if they were isolated, from thermalizing. They show that a D-dimensional Hubbard model shows non-damped oscillations in presence of dissipation, which are damped out in absence the environment. This happens because the coherences that lead to dephasing in the isolated system get damped out by the dissipation. The authors formulate an algebraic condition for the

existence of purely imaginary eigenvalues of a Liouvillian which applies for special kinds of engineered dissipation. We will discuss breaking of time-translational symmetry in the context of strongly-interacting driven-dissipative bosons on a lattice in Ch. 4, resulting in a phase transition in which a finite frequency mode becomes unstable. In Ch. 5 we will discuss the phase diagram of dissipatively-stabilized Mott insulators, which is profoundly modified with respect to the ground state one due to the instability of dynamical modes.

The field of driven-dissipative quantum many-body systems is still young and rapidly growing. The topics covered in this chapter are not exhausting and are related to my personal point of view of the field. After this short, hopefully exciting introduction to the field, we are now ready to discuss some investigation I carried on during my PhD.

## Chapter 2

# Theoretical Methods

In this chapter we will introduce some theoretical tools we will make use of throughout the thesis. We are mainly interested in open quantum systems that can be described by Markovian master equations. Treating many-body systems using master equations though is a hard problem and we will resort to a field-theoretical approach based on Green functions, when this is advantageous. As we have discussed, driven-dissipative systems are naturally out-of-equilibrium, so we need to work in the non-equilibrium framework provided by Keldysh field theory. In order to make the discussion short and more interesting for the reader, well established topics will be introduced in a concise way, referring to textbooks and papers for technical details. We will rather concentrate on making connections amongst different techniques, as these connections are not so often discussed in the literature.

We will keep the discussion generic for bosonic and fermionic systems introducing the variable  $\xi$  such that

$$\begin{aligned}\xi &= 1 && \text{for bosons} \\ \xi &= -1 && \text{for fermions}\end{aligned}$$

We will give all definitions considering a single bosonic (fermionic) mode in second quantization, with creation and annihilation operators  $a$  and  $a^\dagger$  following the commutation (anti-commutation) relations

$$[a, a^\dagger]_\xi = 1$$

where  $[ , ]_\xi$  is the commutator (anti-commutator) for bosons (fermions).

The outline of the chapter is the following. In section 2.1 we will introduce non-equilibrium Green functions, which will be the main theoretical building block of our theoretical approach, giving a brief overview of why they are useful and which kind of information one can extract from them. In section 2.2 we will introduce the concept of the non-equilibrium contour and set the definitions of the main objects one has to deal with in Keldysh field theory. In section 2.3 we will discuss Markovian open quantum systems, we will introduce the Lindblad master equation, discuss super-operators and look at how

to make contact between master equations and Keldysh field theory. Finally, in Sec. 2.4 we will discuss Green functions of Markovian quantum systems, trying again to make contact with their definitions in Keldysh field theory, and we will discuss a useful spectral decomposition of such Green functions.

## 2.1 Non-equilibrium Green functions

When dealing with interacting many-body problems, diagonalizing the Hamiltonian is usually hard for big systems. Most of the methods of many-body theory are tailored at computing Green functions rather than at diagonalising the Hamiltonian. We generically call Green functions average values of strings of operators computed at different points in time or space. This definition can be made more precise and it doesn't justify the use of the name "Green functions". The content of this section with more details can be easily found in books [124, 125]. Green functions allow to extract physical information about the system, such as to describe the response to an applied perturbation or to describe correlations. For a generic interacting problem, they cannot be computed exactly, but many powerful approximations have been developed in the past years. One advantage of working with Green functions is that this allows for systematic perturbative expansions about the non-interacting limit, that can be evaluated by means of Wick's theorem.

Throughout this thesis we will mostly deal with one-particle Green functions, describing the creation and annihilation of one particle at different times. Let's consider a quantum system following the Hamiltonian dynamics described by von Neumann equation

$$\partial_t \rho(t) = -i [H, \rho(t)] \quad (2.1)$$

where  $H$  and  $\rho$  are the system Hamiltonian and density matrix. Out of equilibrium one can define two, independent, one-particle Green functions, the so-called greater and lesser. Those are given by

$$\begin{aligned} G^>(t, t') &= -i \langle a(t) a^\dagger(t') \rangle \\ G^<(t, t') &= -i \xi \langle a^\dagger(t') a(t) \rangle \end{aligned} \quad (2.2)$$

where  $\langle \dots \rangle = \text{tr}(\dots \rho(0))$ , where we assume the normalization  $\text{tr}\rho(0) = 1$ ,  $a(t)$  is the annihilation operator in the Heisenberg picture  $a(t) \equiv e^{iHt} a e^{-iHt}$  and  $a^\dagger(t)$  its conjugate. The  $>$  ( $<$ ) label indicates that the operator corresponding to the first time argument is applied after (before) the other one, i.e. the first time argument must be regarded as "greater (lesser)" than the other. An equivalent choice is to work with the symmetric and antisymmetric combinations of the greater and the lesser. It is actually useful to split the antisymmetric combination into its retarded and advanced components, as those are *response functions* describing the linear response of the system to an applied perturbation.

By doing so, one obtains the Keldysh and retarded one-particle Green functions

$$G^K(t, t') = G^>(t, t') + G^<(t, t') = -i\langle \{a(t), a^\dagger(t')\}_\xi \rangle \quad (2.3)$$

$$G^R(t, t') = \theta(t - t') (G^>(t, t') - G^<(t, t')) = -i\langle [a(t), a^\dagger(t')]_\xi \rangle \theta(t - t') \quad (2.4)$$

$$(2.5)$$

where  $\theta(t)$  is the step function,  $\theta(t) = 0$  for  $t \leq 0$ ,  $\theta(t) = 1$  for  $t > 0$ , and  $\{, \}_\xi$  is the anti-commutator (commutator) for bosons (fermions). The Keldysh Green function has the property  $G^K(t, t') = -[G^K(t', t)]^*$ . We left out the advanced Green function

$$G^A(t, t') = \theta(t' - t) (G^<(t, t') - G^>(t, t')) = i\langle [a(t), a^\dagger(t')]_\xi \rangle \theta(t' - t)$$

that depends on the retarded by the relation  $[G^A(t', t)]^* = G^R(t, t')$ . The lesser, greater, Keldysh, retarded and advanced Green functions naturally arise in the context of Keldysh field theory and are the most natural quantities one can aim at computing in such a framework.

Those quantities allow to extract a big amount of physical information. Coupling a classical, time-dependent field to the Hamiltonian,  $H_h = H + a^\dagger h(t) + a h^*(t)$ , the linear response is given by the retarded Green function through the Kubo formula

$$\langle a(t) \rangle_h = \langle a(t) \rangle_{h=0} + \int_{-\infty}^{\infty} G_{h=0}^R(t, t') h(t') \quad (2.6)$$

In a cavity set-up the intracavity fields are related to extracavity ones through input-output theory [126, 127] and the retarded Green function of intracavity fields can be measured directly through an homodyne detection measurement [128].

Green functions depend on two times for transient dynamics, but, if the system reaches a stationary state, i.e.  $\rho(t) = \rho_{ss}$ , for sufficiently long times, then in this stationary regime they depend only on time differences. Equivalently one says they become time-translational invariant. In this case it is usually advantageous to work in Fourier space, by introducing the Fourier transform of a function  $f(t)$  as  $f(\omega) = \int_{-\infty}^{\infty} dt f(t) e^{i\omega t}$ . As the retarded Green function is a causal function, i.e. it is zero for  $t < t'$ , the real and imaginary parts of its Fourier transform depend on each other through the Kramers-Krönig relations [129]:

$$\text{Re}G^R(\omega) = \mathcal{P} \int_{-\infty}^{\infty} \frac{d\omega'}{\pi} \frac{\text{Im}G^R(\omega')}{\omega' - \omega} \quad \text{Im}G^R(\omega) = -\mathcal{P} \int_{-\infty}^{\infty} \frac{d\omega'}{\pi} \frac{\text{Re}G^R(\omega')}{\omega' - \omega} \quad (2.7)$$

The Fourier transform of the retarded Green function is then completely determined by its imaginary part, called the spectral function

$$A(\omega) = -\frac{1}{\pi} \text{Im}G^R(\omega) = -\frac{1}{2\pi i} (G^R(\omega) - G^A(\omega)) = -\frac{1}{2\pi i} (G^>(\omega) - G^<(\omega)) \quad (2.8)$$

The second equality holds because in Fourier space  $[G^R(\omega)]^* = G^A(\omega)$ . One can show that  $\int_{-\infty}^{\infty} d\omega A(\omega) = 1$  due to commutation (anti-commutation) relations of annihilation

and creation operators, and the  $-1/\pi$  factor is a normalization constant. The spectral function measures how well adding one particle on top of a given state represents an excited state of the system. If adding one particle gives an exact excited state, then this state will never decay, as it is the case for free particles, and this gives a delta peak in  $A(\omega)$ . For an interacting system, instead, those delta peaks normally get renormalized by interactions getting a finite width.

In the case the system is in thermal equilibrium with inverse temperature  $\beta$ , then a very special relation holds, known as the *fluctuation-dissipation theorem* (FDT). This relates the Keldysh Green function to the spectral function

$$G^K(\omega) = -2\pi i(1 + 2\xi n_{\xi,\beta}(\omega))A(\omega) \quad (2.9)$$

where  $n_{\xi,\beta} = (\exp(\beta\omega) - \xi)^{-1}$  is the Bose(Fermi) distribution with inverse temperature  $\beta$  and zero chemical potential (in units of the Boltzmann constant, i.e.  $k_B = 1$ ). When FDT holds, i.e. in equilibrium, then the Keldysh Green function doesn't add any additional information with respect to the spectral function. Out of equilibrium, instead, the Keldysh Green function is an independent quantity that carries extra information. At equal times it gives the occupation of the mode at a given time

$$G^K(t, t) = -i \left( 1 + \xi 2\langle a^\dagger a \rangle(t) \right) \quad (2.10)$$

while the spectral function at equal-times information yields a constant, corresponding to its fixed area in Fourier space, thus it gives no information on the state.

Out of equilibrium one can parametrize the ratio between the Keldysh Green function and the spectral function, called the *distribution function*:

$$F(\omega) = \frac{G^K(\omega)}{-2\pi i A(\omega)} \quad (2.11)$$

This is a real function as  $A(\omega)$  is real by definition, while the  $G^K(\omega)$  is purely imaginary as it satisfies  $G^K(\omega) = -[G^K(\omega)]^*$ . In equilibrium this function would be fixed by FDT,  $F_{eq}(\omega) = (1 + 2\xi n_{\xi,\beta}(\omega))$ , while out of equilibrium it is completely arbitrary.  $F(\omega)$  allows to define effective thermodynamic quantities, in specific cases. For example, if for small frequencies the bosonic distribution function of a given system shows a  $1/\omega$  behaviour, one can define a low-energy effective temperature by analogy with the bosonic equilibrium distribution function by  $\beta_{\text{eff}} = 2/(\omega \lim_{\omega \rightarrow 0} F(\omega))$ . One must be careful, though, with effective thermodynamic quantities as there are several other ways to define them with different meanings. Also, those effective quantities describe observables, rather than the whole system, in the sense that different observables can yield different effective thermodynamic quantities [24, 130].

## 2.2 Non-Equilibrium contour and Keldysh field theory

We have already discussed the need for a non-equilibrium theoretical framework to deal with driven-dissipative systems. The formalism of the Schwinger/Keldysh *double-contour*[131,

[132] arises very naturally when considering the time-evolution of the density matrix of a quantum mechanical system. In this section we will introduce the double-contour and the formalism of Keldysh field theory.

To understand the idea behind the double-contour, consider the evolution of the density matrix according to the Von Neumann equation

$$\partial_t \rho(t) = -i [H, \rho(t)] \quad (2.12)$$

This equation is formally solved by introducing the evolution operator  $U(t, t') = e^{-iH(t-t')}$ . Considering an initial state  $\rho(t')$  then  $\rho(t) = U(t, t')\rho(t')U(t', t)$ . One is interested in computing average values. Let's consider an observable  $O$  at time  $t$ . Assuming the normalization  $\text{tr} \rho(t) = 1$ , its average value is given by

$$\langle O \rangle(t) = \text{tr} [O \rho(t)] = \text{tr} [U(t', t) O U(t, t') \rho(t')] \quad (2.13)$$

where we have used the cyclic property of the trace. This way of writing corresponds to applying a *forward* time evolution on  $\rho(t')$  up to time  $t$ , then picking up the operator  $O$  and applying a *backward* evolution from time  $t$  to  $t'$ . One can always extend the upper time  $t$  of forward and backwards evolutions up to  $\infty$  and we will assume this extension in the following. Also, we will consider systems that forget about their initial condition, thus we will take the limit  $t' \rightarrow -\infty$ . These forward and backwards time-evolutions from  $t' = -\infty$  to  $t = \infty$  define the two *branches* of the double-contour, that we will call  $C$ .

The Keldysh path integral can be derived by slicing time-evolutions in infinitesimal time-steps and introducing identities in terms of bosonic (fermionic) coherent states[133]<sup>1</sup>. If one is interested only in the ground state or in finite temperature equilibrium states, there are workarounds to avoid the double-contour evolution [133], leading to the zero temperature or finite temperature formulations path integrals.

In the following, we will give a pragmatic definition of the kind of objects one has to manipulate in Keldysh field theory, without entering in the details, for which we refer to textbooks [124, 133] and to the review [135] in the context of Markovian quantum systems.

In a coherent-states path integral formulation, a model is specified by its action rather than its Hamiltonian, which is a functional of time-dependent coherent fields. Given there are both a forward and backward evolution, there will be two kinds of fields, respectively belonging to the forward and backward *branches* of the double-contour. In order to distinguish between them, fields with time arguments belonging to the forward(backward) branch are assigned a  $+(-)$  label, so that the couple  $(t, \gamma)$ , with  $\gamma \in \{+, -\}$ , allows to locate one field on the double-contour. For a single-mode system, the Keldysh partition function is defined by

$$Z = \text{tr} \rho(\infty) = \int \mathcal{D} [a, \bar{a}] e^{iS[a, \bar{a}]} \quad (2.14)$$

---

<sup>1</sup>The coherent state path integral has been developed also for spin systems, see for example [134].

The action  $S[a, \bar{a}]$  is a functional of the time-dependent coherent fields  $a$  and  $\bar{a}$ , where the over-bar indicates complex conjugation. All the fields under the path integral sign are time-ordered by the contour time-ordering operator  $T_C$ . A time-ordering is defined on the double-contour, such that

$$\begin{aligned} (t, +) &> (t', +) && \text{if } t > t' \\ (t, -) &> (t', -) && \text{if } t' > t \\ (t, -) &> (t', +) && \forall t, t' \end{aligned}$$

In words, two fields belonging to the + branch follow standard time-ordering, those on the – branch are ordered in the opposite way and – fields come always after + ones. This time-ordering allows to define  $T_C$  by its action on two generic functions of coherent fields belonging to the plus or minus contour, that we call  $f$  and  $g$ , by

$$T_C f_\gamma(t) g_{\gamma'}(t') = f_\gamma(t) g_{\gamma'}(t') \quad \text{if } (t, \gamma) > (t', \gamma') \quad (2.15)$$

$$T_C f_\gamma(t) g_{\gamma'}(t') = \xi g_{\gamma'}(t') f_\gamma(t) \quad \text{if } (t, \gamma) < (t', \gamma') \quad (2.16)$$

According to this definition, bosonic fields commute in the path integral, while fermionic fields anti-commute, i.e. they are Grassman variables. We define contour integrals as  $\int_C dt f(t) \equiv \int_{-\infty}^{\infty} dt f_+(t) - \int_{-\infty}^{\infty} dt f_-(t)$ . This allows to write the action of a generic closed system in the compact continuous form

$$S[a, \bar{a}] = \int_C dt \bar{a}(t) i\partial_t a(t) - H(a(t), \bar{a}(t)) \quad (2.17)$$

where  $H(a(t), \bar{a}(t))$  is the Hamiltonian of the system, that is a function of coherent fields. Contour time-ordered averages can be also computed by the path integral, for example one-particle Green functions read

$$G^{\gamma, \gamma'}(t, t') = -i \langle a_\gamma(t) \bar{a}_{\gamma'}(t') \rangle = -i \int \mathcal{D}[a, \bar{a}] a_\gamma(t) \bar{a}_{\gamma'}(t') e^{iS[a, \bar{a}]} \quad (2.18)$$

where the average  $\langle \dots \rangle$  of Keldysh fields is a time-ordered average, i.e.  $\langle \dots \rangle \equiv \langle T_C \dots \rangle$ . We can defined a matrix  $G(t, t')$  of four Green functions in the contour indices  $\gamma, \gamma'$

$$G(t, t') = -i \begin{pmatrix} \langle a_+(t) \bar{a}_+(t') \rangle & \langle a_+(t) \bar{a}_-(t') \rangle \\ \langle a_-(t) \bar{a}_+(t') \rangle & \langle a_-(t) \bar{a}_-(t') \rangle \end{pmatrix} \quad (2.19)$$

The off-diagonal components correspond to the lesser and greater Green functions introduced in section 2.1:  $G^<(t, t') = G^{+-}(t, t')$  and  $G^>(t, t') = G^{-+}(t, t')$ . The diagonal components are combinations of  $G^<$  and  $G^>$ .

A change of basis in the contour indices, known as Keldysh rotation, is often convenient in calculations. This corresponds to introducing the classical and quantum fields

$$a_c(t) = \frac{a_+(t) + a_-(t)}{\sqrt{2}} \quad a_q(t) = \frac{a_+(t) - a_-(t)}{\sqrt{2}} \quad (2.20)$$

In this basis, the one-particle Green functions read

$$G(t, t') = -i \begin{pmatrix} \langle a_c(t) \bar{a}_c(t') \rangle & \langle a_c(t) \bar{a}_q(t') \rangle \\ \langle a_q(t) \bar{a}_c(t') \rangle & 0 \end{pmatrix} \quad (2.21)$$

where we called the matrix again  $G$  as (2.19), with an abuse of notation. Working in this basis is convenient because the  $G_{qq}$  component is identically zero. This corresponds to the relation  $G^{++}(t, t') + G^{--}(t, t') - G^{+-}(t, t') - G^{-+}(t, t') = 0$  between the Green functions in the other basis and can be proved by direct inspection. One can easily show [135] that the components of  $G(t, t')$  in this basis are the Keldysh, retarded and advanced Green functions introduced in section 2.1:  $G^{cc}(t, t') = G^K(t, t')$ ,  $G^{cq}(t, t') = G^R(t, t')$ , and  $G^{qc}(t, t') = G^A(t, t')$ .

## 2.3 Markovian open quantum systems

A quantum *system* that is decoupled from any *environment* – also called *bath* or *reservoir* – is said to be *closed*. Of course, no physical system is really closed, but in many cases this is a reasonable assumption to study quantum mechanical effects. In other situations, instead, one is interested in taking into account the environment, as this is crucial for describing the behaviour of the system. We will call *universe* the system plus reservoir ensemble. An environment is defined as an infinite set of degrees of freedom with a continuous spectrum. It is important that the spectrum is continuous to describe a true irreversible, dissipative dynamics; in this limit, the Poincaré recurrence theorem for quantum dynamics doesn't hold, the bath loses memory about its past and the dynamics becomes truly irreversible [136, 137]. The environment Hamiltonian can, in many cases, be modeled as an infinite set of free modes, known as the Caldeira-Leggett model [10]. If each mode is only weakly coupled to the system, this model is fairly general as the system is not expected to perturb sufficiently the environment modes to experience its non-linearities [10]. The Caldeira-Leggett model of the environment accounts for all memory-effects and it's very hard to treat if the system is interacting. We will develop a scheme to account for those memory effects in section 6, while in the rest of the thesis we will focus on Markovian open quantum systems, where memory of the environment is neglected.

This is a reasonable simplification in many physical scenarios, for example in typical quantum optics setups. A formal theory of Markovian open quantum systems have been developed [136, 138, 139], based on the semi-group property of Markovian time-evolution [136]. When dealing with open systems, one is interested in obtaining an effective dynamics for the reduced density matrix of the system, obtained by doing a partial trace  $\text{tr}_E$  on the environment degrees of freedom:

$$\rho = \text{tr}_E v$$

where  $v$  is the density matrix of the universe, i.e system plus environment. The physical assumption one needs to satisfy in order to neglect memory effects of the environment while doing such a trace is that

- the characteristic time of decay of bath correlations,  $\tau_B$ , is short compared to the relaxation time of the system  $\tau_R$  coupled to the bath

Under this assumption, the dynamics of the reduced density matrix takes the form of a quantum dynamical semigroup and it is described by a Lindblad master equation [136, 138, 139]<sup>2</sup>.

### 2.3.1 The Lindblad master equation

The Lindblad master equation, describing the evolution of the reduced density matrix under the above assumptions, reads

$$\begin{aligned}\partial_t \rho = \mathcal{L} \rho &= -i [H, \rho] + \mathcal{D} \rho \\ \mathcal{D} \rho &= \sum_{\alpha} \gamma_{\alpha} \left( L_{\alpha} \rho L_{\alpha}^{\dagger} - \frac{1}{2} \{ L_{\alpha}^{\dagger} L_{\alpha}, \rho \} \right)\end{aligned}\quad (2.22)$$

$\mathcal{L}$  will be referred to as the *Liouvillian/Lindblad* super-operator. The term  $\mathcal{D}$  is called Lindblad *dissipator* and it makes the effective dynamics substantially different from closed systems dynamics, in particular non-unitary. It is defined through the *jump operators*  $L_{\alpha}$ , that can be microscopically determined by specifying the coupling Hamiltonian between system and bath, and by the positive rates  $\gamma_{\alpha}$ . Assuming a time-independent  $\mathcal{L}$ , the Lindblad master equation is formally solved by the  $e^{\mathcal{L}t}$  propagator:

$$\rho(t) = e^{\mathcal{L}t} \rho(0)$$

It can be shown that the Lindblad master equation is a trace preserving and completely positive map [136], two fundamental properties for probabilities to be positive and conserved. In section 6 we will discuss those properties for a non-Markovian map, where it is highly non-trivial to develop approximated schemes that do not spoil those properties.

Throughout this thesis we will use weak-coupling master equations, which are derived assuming that the coupling with the reservoir is small. For those master equations, assumption 1 is not enough for those master equations to be of the Lindblad form (2.22), and thus to guarantee that probabilities are conserved and positive during the dynamics. One needs to make a second assumption in order to justify a secular approximation or rotating-wave approximation [136]:

- the typical time scale of the intrinsic evolution of the system,  $\tau_S$ , must be shorter than its relaxation time  $\tau_R$

We finally remark that coupling of the bath to the system not only gives rise to the dissipator, but it also gives an Hamiltonian contribution, known as the Lamb shift Hamiltonian. We will absorb this term in the definition of the original Hamiltonian, if not specified otherwise.

---

<sup>2</sup>Actually this was proven by Lindblad [139] only for a bounded generator  $\mathcal{L}$ . A discussion is reported in [136].

### 2.3.2 Super-operators

In the context of open systems we have to deal with operators acting on others operators, such as the Liouvillian on the density matrix: these will be called *super-operators*. In this section, we will first introduce the  $\pm$  notation for super-operators which makes formal contact with Keldysh field theory. Then we will introduce the Liouville space with the purpose of being able to represent super-operators, which are rank-4 tensors in the original Hilbert space, as matrices; this is advantageous for example to compute numerically the spectrum of the Liouvillian. The proper definition of a canonical algebra of annihilation and creation operators in the Liouville space leads to the so called third-quantization or super-fermionic representation [140–144], which is useful for an algebraic approach to many-body Markovian open systems, but it goes beyond the scope of this thesis and won't be addressed here.

Let's first introduce the  $\pm$  notation for super-operators. One can always promote operators to super-operators. Let's consider the two cases of an operator  $O$  applied to the right and left of another operator, that we will indicate with  $\bullet$ . We define the super-operators  $O_+$ ,  $O_-$ , as

$$\begin{aligned} O_+ &= O\bullet \\ O_- &= \bullet O \end{aligned}$$

The  $\bullet$  notation is useful to specify where the argument of a super-operator must be inserted, but becomes superfluous when using  $\pm$  indices. The following dagger rules are very useful

$$(O_+\bullet)^\dagger = O_-^\dagger \bullet^\dagger \quad (2.23)$$

$$(O_-\bullet)^\dagger = O_+^\dagger \bullet^\dagger \quad (2.24)$$

They follow from the definitions of  $O_\pm$ :  $(O_+\bullet)^\dagger = (O\bullet)^\dagger = \bullet^\dagger O^\dagger = O_-^\dagger \bullet^\dagger$  and  $(O_-\bullet)^\dagger = (\bullet O)^\dagger = O^\dagger \bullet^\dagger = O_+^\dagger \bullet^\dagger$ . The  $\pm$  notation, in which operators are promoted to super-operators, turns useful as one can write nested applications of super-operators without the need for parentheses specifying the argument of each super-operator, being understood that super-operators always apply on the whole string appearing to their right. To make an example, consider the nested expression  $\mathcal{S}(\mathcal{S}(\bullet)O)$ , where the parentheses are needed to specify the arguments of super-operators; in the  $\pm$  notation  $\mathcal{S}(\mathcal{S}(\bullet)O) = \mathcal{S}\mathcal{O}_-\mathcal{S}$  and no parentheses or bullets are needed. The most generic super-operator  $\mathcal{S}$  we will encounter can be written as  $\mathcal{S} = \sum_\alpha A_\alpha \bullet B_\alpha$ . As it is made up of operators acting from the right or left, it can be written analogously as  $\mathcal{S} = \sum_\alpha A_{\alpha,+}B_{\alpha,-} = \sum_\alpha B_{\alpha,-}A_{\alpha,+}$  in the  $\pm$  notation. In this notation the Lindblad super-operator takes the form

$$\mathcal{L} = -i(H_+ - H_-) + \sum_\alpha \gamma_\alpha \left( L_{\alpha,+} L_{\alpha,-}^\dagger - \frac{1}{2} \left( L_{\alpha,+}^\dagger L_{\alpha,+} + L_{\alpha,-} L_{\alpha,-}^\dagger \right) \right) \quad (2.25)$$

We remark the order of  $L_{\alpha,-}^\dagger$  and  $L_{\alpha,-}$  in the last term, as it could lead to mistakes:  $L_{\alpha,-} L_{\alpha,-}^\dagger = \bullet L_\alpha^\dagger L_\alpha$ .

We will now introduce the Liouville space. Super-operators are operators acting on others operators, such as the Liouvillian on the density matrix. It is natural to define a vector space  $H \otimes H$ , which is the tensor product of two copies of the original Hilbert space  $H$ , whose elements are the operators acting on  $H$ . Super-operators are then linear applications on this vector space of operators. This enlarged space is called Liouville space. Defining the inner product of two operators  $A, B$  as  $\langle A, B \rangle \equiv \text{tr}(A^\dagger B)$ , the Liouville space becomes a Hilbert space. Operators, for example the density operator  $\rho = \sum_{n,m} \rho_{nm} |n\rangle\langle m|$ , acting on the original space  $H$  and in the basis  $\{|n\rangle\}$ , become kets  $|\rho\rangle = \sum_{n,m} \rho_{nm} |n\rangle|m\rangle$  in the Liouville space. We will call this change of representation *vectorization*. We define bras as complex transpose of kets  $\langle \rho | = (\langle \rho |)^\dagger$ . We indicate super-operators in Liouville space with hats. The  $O_\pm$  super-operators defined above, in Liouville space become  $\hat{O}_+ = O \otimes \mathbb{1}$ ,  $\hat{O}_- = \mathbb{1} \otimes O^T$ . One can verify that this definition is the right one as applying  $\hat{O}_\pm$  on a ket, i.e.  $\hat{O}_\pm |\rho\rangle$ , yields the same result of vectorizing the operator  $O_\pm \rho \rightarrow |O_\pm \rho\rangle$ , using the vectorization rule given above. i.e.  $\hat{O}_\pm |\rho\rangle = |O_\pm \rho\rangle$ . Following from this last identity, the vectorized identity operator  $|\mathbb{1}\rangle$ , has the property  $\hat{O}_\pm |\mathbb{1}\rangle = |O\rangle$ . Also, the trace of an operator can be written using the identity ket or bra as  $\text{tr}O = \langle \mathbb{1}|O\rangle = \langle O^\dagger|\mathbb{1}\rangle$ , according to the definition of inner product. In Liouville space  $\mathcal{S} = \sum_\alpha A_{\alpha,+} B_{\alpha,-}$  becomes  $\hat{\mathcal{S}} = \sum_\alpha A_\alpha \otimes B_\alpha^T$ . The corresponding form of the Lindblad super-operator in Liouville space can be found with the rules just introduced and reads

$$\hat{\mathcal{L}} = -i(H \otimes \mathbb{1} - \mathbb{1} \otimes H^*) + \sum_\alpha \gamma_\alpha \left( L_\alpha \otimes L_\alpha^* - \frac{1}{2} (L_\alpha^\dagger L_\alpha \otimes \mathbb{1} + \mathbb{1} \otimes L_\alpha^T L_\alpha^*) \right) \quad (2.26)$$

This formula allows to simply represent  $\hat{\mathcal{L}}$  as a matrix in a code, using methods to perform the tensor (Kronecker) product of two matrices provided with standard libraries. Finally, we remark that in Liouville space the Lindblad master equation takes the form of a Schrödinger equation with non-Hermitian Hamiltonian  $\hat{\mathcal{L}}$ :  $\partial_t |\rho\rangle = \hat{\mathcal{L}} |\rho\rangle$ .

### 2.3.3 From Lindblad master equations to Keldysh action

The approaches of Keldysh field theory and master equations are closely related. The main formal difference is that while master equations are defined at the operator level, Keldysh field theory is a path integral approach. As it is described in detail in [135], writing the Keldysh action associated with a master equation is actually simple. Starting from a Lindblad master equation (2.22), the associated Keldysh action reads

$$S[a_+, \bar{a}_+, a_-, \bar{a}_-] = \int_{-\infty}^{\infty} dt ( \bar{a}_+ i \partial_t a_+ - \bar{a}_- i \partial_t a_- - i \mathcal{L}(a_+, \bar{a}_+, a_-, \bar{a}_-) ) \quad (2.27)$$

To obtain  $\mathcal{L}(a_+, \bar{a}_+, a_-, \bar{a}_-)$  entering the Keldysh action, one has to perform the following steps. First, the operators  $H$ ,  $L_\alpha$ ,  $L_\alpha^\dagger$  and  $L_\alpha^\dagger L_\alpha$ , defining the master equation (2.22) must be expressed in terms of  $a$  and  $a^\dagger$  operators and brought in normal ordered form, that is with all  $a^\dagger$  operators on the left of  $a$  operators. Then, the resulting “normal-ordered” Liouvillian must be written in the  $\pm$  notation for super-operators as in Eq. (2.25). Finally

$a_\pm^\dagger$  and  $a_\pm$  super-operators must be replaced with the corresponding coherent fields, giving  $\mathcal{L}(a_+, \bar{a}_+, a_-, \bar{a}_-)$  bit entering in the Keldysh action.

## 2.4 Markovian systems Green functions

For open systems, the Green functions of systems operators are naturally defined in the Hilbert space of the universe, which is a closed system as an ensemble; for example, being  $a, a^\dagger$  system operators, the greater and lesser one-particle Green functions are defined (as in (2.2)) by

$$\begin{aligned} G^>(t, t') &= -i\langle a(t)a^\dagger(t') \rangle_v \\ G^<(t, t') &= -i\xi\langle a^\dagger(t')a(t) \rangle_v \end{aligned} \quad (2.28)$$

where the average  $\langle \dots \rangle_v$  is performed on the universe density matrix  $\langle \dots \rangle_v = \text{tr}_v(\dots v(0))$  and  $a(t)$  is the annihilation operator in the Heisenberg picture  $a(t) \equiv e^{iH_v t}ae^{-iH_v t}$ , evolved with the universe Hamiltonian  $H_v$ . This definition is straightforward, but difficult to evaluate, and one is interested in deriving formulae to compute Green functions after removing the environmental degrees of freedom performing a partial trace. This is a non-trivial task as, even if  $a, a^\dagger$  are system operators, they are evolved with the universe Hamiltonian, which couples system and environment. For Markovian quantum systems, the partial trace on environment degrees of freedom can be performed and yields the quantum regression formulae that we will discuss in Sec. 2.4.1. In Ch. 6, we will derive analogous formulae for a non-Markovian propagator in a Non-Crossing approximation.

### 2.4.1 Lindblad Green functions: the quantum regression formulae

The Lindblad master equation (2.22) allows to compute the effective dynamics of the system density matrix, and thus of system observables, after removing the degrees of freedom of the environment with a partial trace. All the information needed to evolve the system reduced density matrix is contained in the Liouvillian super-operator. Green functions of system operators can be computed in the same spirit through the quantum regression formulae [145, 146] (also known as quantum regression theorem): one only needs to know the Liouvillian in order to compute them. We restrict to report the formulae for the lesser and greater one-particle Green functions we have introduced in section 2.1, but analogous formulae hold for n-particle Green functions, that we will use in section 6.4.2, where we will also give a proof for the n-particle case. We stress that the quantum regression formulae hold under the same assumptions one makes to derive the Lindblad master equation. A nice discussion and derivation of those formulae can be found in [7]. The quantum regression formulae for the greater and lesser, in the  $\pm$  notation introduced in 2.3.2 for super-operators, read:

$$G^>(t, t') = -i \text{tr} \left[ a_- e^{\mathcal{L}(t-t')} a_+^\dagger \rho(t') \right] \theta(t-t') - i \text{tr} \left[ a_+^\dagger e^{\mathcal{L}(t'-t)} a_- \rho(t) \right] \theta(t'-t) \quad (2.29)$$

$$G^<(t, t') = -i\xi \text{tr} \left[ a_+ e^{\mathcal{L}(t-t')} a_-^\dagger \rho(t') \right] \theta(t-t') - i\xi \text{tr} \left[ a_-^\dagger e^{\mathcal{L}(t'-t)} a_+ \rho(t) \right] \theta(t'-t) \quad (2.30)$$

where ‘‘tr’’ is the trace on system degrees of freedom only. The  $\theta$  step function appears as a result of the irreversibility of Lindblad dynamics [136]: as there’s no backward evolution propagator, one always has to reduce to forward in time propagations; this is achieved distinguishing the two cases in which  $t > t'$  and  $t < t'$ . Reporting those formulae, we used the  $\pm$  notation for super-operators introduced in section 2.3.2. Being familiar with the definition of non-equilibrium Green functions in Keldysh field theory in terms of  $+$  and  $-$  fields (2.19), its easy to remember the quantum regression formulae in this notation. For example, the lesser one-particle Green function in Keldysh field theory is given by

$$G^<(t, t') = G^{+-}(t, t') = -i\langle a_+(t)\bar{a}_-(t') \rangle$$

where  $a_+(t), \bar{a}_-(t')$  are fields on the double-contour. The  $<$  or  $+-$  label indicates that the field  $a$  ( $\bar{a}$ ) corresponding to the first (second) time argument must be placed on the  $+$  ( $-$ ) contour. To write the corresponding quantum regression formula, one needs to time-order the fields on Keldysh contour and distinguish the cases  $t > t'$  and  $t' > t$ :

$$G^<(t, t') = -i\langle a_+(t)\bar{a}_-(t') \rangle = -i\xi\langle \bar{a}_-(t')a_+(t) \rangle\theta(t-t') - i\xi\langle \bar{a}_-(t')a_+(t) \rangle\theta(t'-t)$$

Then one simply replaces the  $\bar{a}_-(t'), a_+(t)$  fields with  $a_-^\dagger, a_+$  super-operators. In this replacement, super-operators must be swapped to enforce their real-time ordering, rather than contour-time ordering, but this time without taking extra minus signs coming from fermionic anticommutation rules. For the lesser, this procedure gives Eq. (2.30):

$$G^<(t, t') = -i\xi \text{tr} \left[ a_+ e^{\mathcal{L}(t-t')} a_-^\dagger \rho(t') \right] \theta(t-t') - i\xi \text{tr} \left[ a_-^\dagger e^{\mathcal{L}(t'-t)} a_+ \rho(t) \right] \theta(t'-t)$$

To the best of my knowledge, this notation connecting quantum regression formulae and Green functions in Keldysh field theory has not been discussed elsewhere.

#### 2.4.2 Liouvillian spectrum

In this section we analyse the spectral properties of the Liouvillian super-operator. In particular we will need them to write a spectral representation of Green function in Sec. 2.4.3, but the spectral properties of the Liouvillian are interesting on their own, for example to study dissipative phase transitions[37, 49]. Let’s consider the Liouvillian super-operator in Liouville space  $\hat{\mathcal{L}}$ . It is a non-Hermitian matrix thus it has very different spectral properties from a Hermitian Hamiltonian. We consider the simplest case in which the Liouvillian can be diagonalized. The right-eigenvectors  $|r_\alpha\rangle$ , left-eigenvectors  $\langle l_\alpha|$ , and eigenvalues  $\lambda_\alpha$  of the Liouvillian are defined via

$$\hat{\mathcal{L}}|r_\alpha\rangle = \lambda_\alpha|r_\alpha\rangle \tag{2.31}$$

$$\langle l_\alpha|\hat{\mathcal{L}} = \langle l_\alpha|\lambda_\alpha \tag{2.32}$$

where  $\langle l_\beta|, |r_\alpha\rangle$  are biorthogonal (see e.g. [147]). We choose a normalization such that they are also biorthonormal:

$$\langle l_\beta|r_\alpha\rangle = \delta_{\beta\alpha} \tag{2.33}$$

Some properties of the eigenstates of the Liouvillian follow from its trace preservation property, that is  $0 = \partial_t \text{tr} \rho = \text{tr} \partial_t \rho = \text{tr} \hat{\mathcal{L}} \rho$ . In Liouville space this reads  $\langle \mathbb{1} | \hat{\mathcal{L}} | \rho \rangle = 0$ . As this is valid  $\forall \rho$ , it follows that  $\langle \mathbb{1} |$  is always a left-eigenvector of  $\hat{\mathcal{L}}$  with zero eigenvalue,  $\langle \mathbb{1} | \hat{\mathcal{L}} = 0$ , and we identify it with the  $\alpha = 0$  left-eigenvector:  $\langle \mathbb{1} | \equiv \langle l_0 |$  and  $\lambda_0 \equiv 0$ . As the eigenvalues  $\lambda_\alpha$  are unique for left and right-eigenvectors, there must be also at least one right-eigenvector with zero eigenvalue. We assume here that this right-eigenvector is unique and identify it with the steady state:  $|r_0\rangle \equiv |\rho_{ss}\rangle$ . It follows from the orthonormality condition (2.33) that, with the normalization fixed by the definition  $\langle \mathbb{1} | \equiv \langle l_0 |$ ,  $\rho_{ss}$  is normalized  $\text{tr} \rho_{ss} = \langle \mathbb{1} | \rho_{ss} \rangle = 1$ . There are interesting cases in which the Liouvillian has multiple steady states, but we won't discuss those cases [148]. Always from the orthonormality condition (2.33) and from the assumption of unique steady state, it follows that all the right eigenstates different from the steady state  $r_{\alpha \neq 0}$  are traceless:  $\langle \mathbb{1} | r_{\alpha \neq 0} \rangle = \delta_{0,\alpha \neq 0} = 0$ .

We can now interpret the eigenstates of the Liouvillian different from the steady state as decay modes of deviations from the stationary state. Suppose now that at  $t = 0$  the system starts in some state  $|\rho(0)\rangle$  that is not the stationary state. At later times, the system reduced density matrix will be given by

$$|\rho(t)\rangle = |\rho_{ss}\rangle + \sum_{\alpha \neq 0} c_\alpha e^{\lambda_\alpha t} |r_\alpha\rangle \quad (2.34)$$

with  $c_{\alpha \neq 0} = \langle l_\alpha | \rho(0) \rangle$  and  $c_0 = \langle \mathbb{1} | \rho_{ss} \rangle = 1$  by orthonormality (2.33). We can thus interpret each Liouvillian eigenmode  $\alpha \neq 0$  as a possible dynamical decay mode of some initial deviation from the steady state, with a decay rate given by  $-\text{Re} \lambda_\alpha$ . In general, a given decay mode will involve both diagonal elements of the density matrix in the energy-eigenstates basis (i.e. populations) as well as off-diagonal elements (i.e. coherences). However, in some cases the situation simplifies and one can cleanly separate the eigenmodes into processes only involving populations ( $T_1$  processes) or only involving coherences ( $T_2$  processes) as will be the case in Ch. 3.

#### 2.4.3 Spectral representation of Green functions

For closed systems in thermal equilibrium, it is extremely useful to relate Green functions directly to the energy eigenvalues and eigenstates of the system, obtaining their *Lehmann representation* [124, 125, 149, 150]. We introduce here a similar decomposition for Markovian open systems, which we will also call *Lehmann* or *spectral* representation. This section is mostly based on [1]. For those systems the relevant spectrum is not that of a system Hamiltonian, but rather of the system Liouvillian. Such spectral decompositions for open systems have been derived before, for example in the context of electron transport through correlated impurities [151, 152] or in the context of non-linear oscillators [153], where a “sum of partial spectra” was introduced. Nevertheless, the discussion of this decomposition in the literature was marginal, thus we reported a detailed discussion in [1], which is entirely contained in this section and in chapter 3.

To show how to derive a spectral representation let's consider the quantum regression formula for the lesser Green function in Eq. (2.30) and restrict to  $t > t' = 0$  for simplicity. We specialize to the case of a stationary density matrix  $\rho_{ss}$ , but the spectral representation can be equivalently derived for a time-dependent state. With these assumptions and in Liouville space, from the quantum regression formula (2.30) we get

$$i\xi G^<(t)\theta(t) = \langle a^\dagger(0)a(t)\rangle\theta(t) = \langle \mathbb{1}|a_+e^{\mathcal{L}t}a_-^\dagger\rho_{ss}\rangle\theta(t) \quad (2.35)$$

We note that the super-operator  $a_-^\dagger$  acting on steady state density matrix  $\rho_{ss}$  causes the system to deviate from the steady state. Just as in Eq. (2.34), this deviation can be expressed as a linear combination of right-eigenstates of the Liouvillian

$$|a_-^\dagger\rho_{ss}\rangle = \sum_\alpha |r_\alpha\rangle\langle l_\alpha|a_-^\dagger\rho_{ss}\rangle \quad (2.36)$$

eventually giving

$$i\xi G^<(t)\theta(t) = \sum_\alpha e^{\lambda_\alpha t} \langle \mathbb{1}|\hat{a}_+|r_\alpha\rangle\langle l_\alpha|\hat{a}_-^\dagger|\rho_{ss}\rangle \quad (2.37)$$

At an intuitive level,  $\hat{a}_-^\dagger$  “excites” the various dynamical eigenmodes of the Liouvillian; these modes then oscillate and decay as functions of time. The factor  $\langle \mathbb{1}|\hat{a}_+|r_\alpha\rangle = \text{tr}(ar_\alpha)$  corresponds to the change in  $\langle a \rangle$ , compared to the steady state value, associated with exciting a particular dynamical eigenmode  $\alpha$ , as we understand from Eq. (2.34). In many cases, one is interested in the connected average  $\langle a^\dagger(0)a(t)\rangle - \langle a^\dagger(0)\rangle\langle a(t)\rangle$ . In this case, the steady state mode with  $\alpha = 0$ , does not contribute to the sum in Eq. (2.37). The spectral decomposition of greater and lesser one-particle Green's function in Fourier space reads

$$G^>(\omega) = \sum_\alpha \left\{ \frac{1}{\omega - i\lambda_\alpha} \langle \mathbb{1}|\hat{a}_-|r_\alpha\rangle\langle l_\alpha|\hat{a}_+^\dagger|\rho_{ss}\rangle - \frac{1}{\omega + i\lambda_\alpha} \langle \mathbb{1}|\hat{a}_+^\dagger|r_\alpha\rangle\langle l_\alpha|\hat{a}_-|\rho_{ss}\rangle \right\} \quad (2.38)$$

$$G^<(\omega) = \xi \sum_\alpha \left\{ \frac{1}{\omega - i\lambda_\alpha} \langle \mathbb{1}|\hat{a}_+|r_\alpha\rangle\langle l_\alpha|\hat{a}_-^\dagger|\rho_{ss}\rangle - \frac{1}{\omega + i\lambda_\alpha} \langle \mathbb{1}|\hat{a}_-^\dagger|r_\alpha\rangle\langle l_\alpha|\hat{a}_+|\rho_{ss}\rangle \right\} \quad (2.39)$$

It is interesting to see how one recovers the standard closed-systems Lehmann representation by taking the zero-dissipation limit. This limit implies keeping only the Hamiltonian term in the Liouvillian, i.e. replacing  $\mathcal{L}$  with  $-i[H, \bullet]$ . Letting  $|\psi_i\rangle$  and  $E_i$  denote the eigenstates and eigenvalues of the Hamiltonian  $H$ , it is straightforward to find the dynamical eigenmodes of  $\mathcal{L}$ . Each dynamical eigenmode  $\alpha$  corresponds to a pair of energy eigenstates  $i, j$ :

$$r_{i,j}^{(0)} = l_{i,j}^{(0)} = |\psi_i\rangle\langle\psi_j| \quad (2.40)$$

$$\lambda_{i,j}^{(0)} = -i(E_i - E_j). \quad (2.41)$$

These modes have a simple interpretation. For a closed system, populations in the energy eigenstate basis are time-independent, corresponding to the zero-eigenvalue modes  $\lambda_{i,i}^{(0)}$ . Further, the coherences in the energy eigenstate basis have a simple undamped oscillatory

behaviour, corresponding to the  $i \neq j$  modes. We stress that in the purely closed system case, the dynamics no longer picks out a unique steady state, as any incoherent mixture of energy eigenstates is stationary. The only constraint from the dynamics to guarantee stationarity is that  $\rho_{ss}$  be diagonal in the energy eigenstate basis:  $\rho_{ss} = \sum_k p_k |\psi_k\rangle\langle\psi_k|$ . As usual, if the system is not coupled to an environment, one must then assume a distribution for the probabilities  $p_k$  when computing average values and correlation functions. For a system in thermal equilibrium, the  $p_k$  are Boltzmann weights. Plugging the closed systems eigenmodes (2.40) in Eq. (2.37) we obtain

$$\begin{aligned}\langle a^\dagger(0)a(t)\rangle\theta(t) &= \theta(t)\sum_{ij} e^{-i(E_i-E_j)t} \langle\psi_j|a|\psi_i\rangle\langle\psi_i|\rho_{ss}a^\dagger|\psi_j\rangle \\ &= \theta(t)\sum_{ij} e^{-i(E_i-E_j)t} \langle\psi_j|a|\psi_i\rangle\langle\psi_i|a^\dagger|\psi_j\rangle p_i\end{aligned}\quad (2.42)$$

The first line matches what one would obtain from a direct calculation using  $\langle a^\dagger(0)a(t)\rangle = \text{tr}(\rho_{ss}a^\dagger e^{iHt}ae^{-iHt})$ . In the second line, we have used the diagonal form of  $\rho_{ss}$ . This formula is actually valid both for  $t > 0$  and  $t < 0$  and it corresponds to the usual textbook thermal equilibrium Lehmann representation for the lesser one-particle Green function [112, 125].

The Lehmann representation is a powerful tool giving both physical insight on the meaning of Green functions and allowing to prove exact mathematical properties, such as sum rules, sign properties and the fluctuation dissipation theorem for equilibrium systems. In Ch. 3 we will discuss further the Lehmann representation for Markovian systems, focusing on the spectral function and in the context of a specific model of a quantum non-linear oscillator.

## Chapter 3

# Spectral Properties of a Quantum van der Pol Oscillator

In this chapter, we study the Green functions of Markovian driven-dissipative quantum systems, using the spectral representation of Green functions we discussed in section 2.4.3. Applying it to the prototype model of a quantum van der Pol oscillator with an additional non-linearity in its Hamiltonian, we predict phenomena that are not apparent in the steady-state density matrix. Unlike the steady state, the photonic spectral function of this model has a strong dependence on interaction strength. We point out that a sign property of spectral functions of equilibrium systems doesn't hold in the case of open systems. As a consequence of this, we find that the interplay of interaction and non-equilibrium effects can result in a surprising "negative density of states" with direct physical consequences as it can, for example, generate negative temperature states or produce finite-frequency instabilities in lattice models, as we will discuss in Ch. 4 and how it has been recently discussed in the context of quantum quenches [154]. In particular we find that the "negative density of states" can appear even in absence of steady state population inversion in the system density matrix. The results of this chapter have been published in [1].

### 3.1 Introduction

Driven-dissipative quantum systems typically have non-thermal steady states determined by the balancing of drive and dissipation. A vast amount of theoretical work has focused on finding (either exactly or approximately) the steady state of such systems, and the corresponding steady-state expectation values of observables [82, 155–158].

While describing steady states is clearly of interest, many experimental probes involve studying how a system responds to a weak applied perturbation. One is then naturally interested in understanding the Green functions that describe the linear response of the system to external perturbations, as we discussed in Sec. 2.1. For Markovian systems, these correlations functions can be readily computed using the quantum regression theorem, and have been studied in a variety of different contexts, from the standard example of resonance fluorescence of a driven two-level atom [159–161], recently discussed in the case

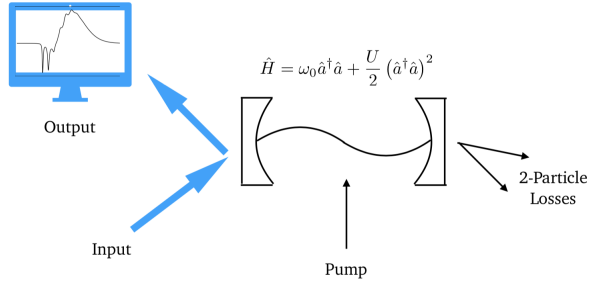


Figure 3.1: Schematic plot of the setup considered in this manuscript. A cavity mode with Kerr nonlinearity is driven by an incoherent pump and subject to two-photon losses. We investigate its spectral features, encoded in the cavity mode spectral function. This quantity could be directly measured by considering the reflection of a weak probe tone.

of arrays of coupled qubits [24], to the second-order correlations probing bunching/anti-bunching of time-delayed photons (see, e.g., [162]). The topic of correlation functions is also a standard topic in almost any quantum optics textbook (see, e.g., [7, 136]).

Despite this existing work, methods for obtaining physical intuition from the behaviour of Green functions remain of interest. For closed, equilibrium quantum many body systems, the Lehmann representation [125, 149, 150] is a powerful tool. It expresses a one-particle Green function in terms of the system energy eigenstates, and allows one to interpret the spectral function in terms of Fermi Golden rule rates for the addition (or removal) of a particle. This directly connects to experimental probes (e.g. angle-resolved photoemission spectroscopy (ARPES) or tunneling spectroscopy), and is invaluable in constructing intuitive pictures. Also, the Lehmann representation allows to prove exact mathematical properties, such as sum rules, sign properties and the fluctuation dissipation theorem for equilibrium systems.

In this chapter, we show that the Lehmann representation of Green functions of a driven dissipative system discussed in Sec. 2.4.3 also serves as a powerful interpretive tool. As a concrete example, we analyze a simple, but non-trivial model of a nonlinear quantum van der Pol oscillator, describing a single-mode bosonic cavity subject to incoherent driving and nonlinear loss (see Ref. [153] for a comprehensive review), with an additional Kerr interaction in its Hamiltonian. This model has recently received attention in the context of quantum synchronization with [163] and without [164, 165] Kerr interaction; it is also directly realizable in superconducting circuit architectures, where strong Kerr interactions and engineered two-photon losses have been experimentally achieved [103, 104]. Indeed, nonlinearities in those architectures are also of practical interest, inducing a photon blockade effect [166] which plays a crucial role to engineer states relevant for quantum computation [167–169]. While the model has a relatively simple steady state, its spectral features are instead remarkably rich [153, 170]. Unlike the steady state, the spectral function depends strongly on the size of the Kerr interaction, and reveals physics beyond that in the steady state density matrix. Specifically we show that the model features

both population inversion in the density matrix and a negative density of states (NDoS), two aspects which are tightly connected in equilibrium but whose interplay in the driven-dissipative case appears to be more complex. In particular we find a regime where NDoS emerges, even in absence of a population inversion in the stationary density matrix.

The chapter is organized as follows. In Sec. 3.2 we compare the Lehmann representation of the spectral function between the two cases of closed and open quantum systems, discussing a sign property of equilibrium spectral functions that doesn't hold instead for open systems. In Sec. 3.3 we discuss a notion of effective temperature with a direct operational meaning, directly probing the sign of the spectral function. In Sec. 3.4 we introduce the model of a van der Pol oscillator with Kerr nonlinearity and make some considerations on its symmetries, and in Sec. 3.5 we discuss its spectral properties and NDoS using the Lehmann representation and perturbation theory.

## 3.2 Spectral function

We will consider a bosonic system with a single mode, letting  $a$  denote its annihilation operator. We will study the retarded single-particle Green function,  $G^R(t)$ , introduced in Sec. 2.1, evaluated on a time-independent density matrix. As the state is assumed not to depend on time, Green functions depend only on time-differences. The definition of  $G^R(t)$  reads

$$G^R(t) = -i\theta(t)\langle [a(t), a^\dagger(0)] \rangle \quad (3.1)$$

This correlation function plays an important role in many different contexts. For example, via the Kubo formula, it describes the linear response of the system (see Sec. 2.1). In the case where  $a$  describes a photonic cavity mode,  $G^R(t)$  can be directly measured by weakly coupling the cavity to an input-output waveguide and measuring the reflection of a weak probe tone or by homodyne detection (see e.g. [128, 171, 172]).

### 3.2.1 Closed systems spectral representation

For a closed system in a time-independent statistical mixture, the Fourier transform of the Lehmann representation of the retarded Green function is [112]

$$G^R(\omega) = \sum_{i,j} \frac{|\langle \psi_j | a^\dagger | \psi_i \rangle|^2 (p_i - p_j)}{\omega - E_j + E_i + i\eta} \quad (3.2)$$

where  $\eta$  is a positive infinitesimal. Consistent with causality, this function is analytic in the upper half plane. It has simple poles with infinitesimal negative imaginary part, and with purely real weights. Of particular interest is the imaginary part of  $G^R(\omega)$ , which defines the one-particle spectral function or density of states  $A(\omega)$ :

$$A(\omega) = -\frac{1}{\pi} \text{Im} G^R(\omega). \quad (3.3)$$

For a closed system, the spectral function follows directly from Eq. (3.2):

$$\begin{aligned} A(\omega) &= \sum_{i,j} p_i \left( \left| \langle \psi_j | a^\dagger | \psi_i \rangle \right|^2 \delta(\omega - E_j + E_i) - \left| \langle \psi_j | a | \psi_i \rangle \right|^2 \delta(\omega - E_i + E_j) \right) = \\ &= \sum_{i,j} (p_i - p_j) \left| \langle \psi_j | a^\dagger | \psi_i \rangle \right|^2 \delta(\omega - E_j + E_i) \end{aligned} \quad (3.4)$$

The name one-particle spectral function or density of states comes from the fact that this function, for non-interacting systems, is a weighed sum of delta peaks located at the transition energies of the systems, thus it reveals the spectrum of the Hamiltonian. The first equality allows us to give a simple physical interpretation of  $A(\omega)$  in terms of Golden rule transition rates. The first term is naturally associated with adding a particle to the steady state and creating an excitation with energy  $\omega$ , whereas the second term is associated with removing a particle and creating an excitation with energy  $-\omega$ . For example the rate of going from state  $\psi_i$  to state  $\psi_j$  at long times as an effect of the perturbation  $a^\dagger e^{-i\omega t}$  is given by Fermi Golden rule by

$$\lim_{t \rightarrow \infty} P_{\psi_i \rightarrow \psi_j} = 2\pi \left| \langle \psi_j | a^\dagger | \psi_i \rangle \right|^2 \delta(\omega - E_j + E_i) \quad (3.5)$$

which, apart from a normalization, is the rate entering in  $A(\omega)$ .

The second equality in Eq. (3.4) also leads to an important result. If we assume that  $p_j \leq p_i$  whenever  $E_j \geq E_i$ , which is the case for an equilibrium Boltzmann distribution  $p_i = e^{-\beta E_i}$ , then we immediately can conclude:

$$A(\omega) \gtrless 0 \quad \text{for } \omega \gtrless 0, \quad (3.6)$$

i.e. the spectral function  $A(\omega)$  has the same sign as  $\omega$ . In particular this is valid for ground-states, for which  $p_0 = 1$  and  $p_{i \neq 0} = 0$ . A violation of this condition indicates the existence of *population inversion* in the steady state: a higher-energy eigenstate has a larger population in the steady state than a lower-energy eigenstate. While this is impossible in thermal equilibrium, it is indeed possible in a generic driven-dissipative non-thermal steady state.

### 3.2.2 Markovian open systems spectral representation

We can use the Lehmann representation for Green functions of Markovian open systems introduced in section 2.4.3, to obtain the corresponding formula to (3.2) for Markovian systems. Let's introduce the eigenvalues and right and left eigenstates of the Liouvillian  $\lambda_\alpha$ ,  $|r_\alpha\rangle$ ,  $\langle l_\alpha|$ , defined in Sec. 2.4.2. Then, the Lehmann representation for  $G^R(\omega)$  reads

$$G^R(\omega) = \sum_{\alpha} \frac{w_{\alpha}}{\omega + \text{Im}\lambda_{\alpha} - i\text{Re}\lambda_{\alpha}} \quad (3.7)$$

with

$$\begin{aligned} w_{\alpha} &= \langle \mathbb{1} | \hat{a}_- | r_{\alpha} \rangle \langle l_{\alpha} | \hat{a}_+^\dagger | \rho_{ss} \rangle - \langle \mathbb{1} | \hat{a}_+ | r_{\alpha} \rangle \langle l_{\alpha} | \hat{a}_-^\dagger | \rho_{ss} \rangle = \\ &= \text{tr}(ar_{\alpha}) \text{tr} \left( l_{\alpha}^\dagger [a^\dagger, \rho_{ss}] \right) \end{aligned} \quad (3.8)$$

There is clearly some similarity to the closed-system expression Eq.(3.2). Like the closed-system case, the Green function is decomposed into a sum of simple poles. However, whereas for the closed system poles occurred at energy differences that were infinitesimally shifted from the real axis, now the poles occur at eigenvalues of the Liouvillian, and will be shifted a finite distance below the real axis.

More intriguingly, the residues  $w_\alpha$  associated with the poles of  $G^R(\omega)$  are no longer necessarily real, as it must be for a closed system.

This has a direct consequence on the spectral function (c.f. Eq. (3.3)), which now takes the form

$$A(\omega) = -\frac{1}{\pi} \sum_{\alpha} z_{\alpha}(\omega) \frac{\text{Re}\lambda_{\alpha}}{(\omega + \text{Im}\lambda_{\alpha})^2 + (\text{Re}\lambda_{\alpha})^2} \quad (3.9)$$

where

$$z_{\alpha}(\omega) = \text{Re}w_{\alpha} + \text{Im}w_{\alpha} \frac{\omega + \text{Im}\lambda_{\alpha}}{\text{Re}\lambda_{\alpha}}. \quad (3.10)$$

It follows that the spectral function is no longer simply a sum of Lorentzians. An immediate corollary is that unlike the closed-system case (c.f. Eq.(3.6)), the sign of the spectral function is not controlled in a simple way by steady state probabilities. In other words, a driven-dissipative systems can have spectral functions which violate the sign property Eq. (3.6), without this necessarily coming from an inverted population of the stationary state, as it is the case for closed system.

We remark that the spectral function in Eq. (3.9) satisfies the sum rules originating from the commutation relations of operators at equal time:

$$\int_{-\infty}^{\infty} d\omega A(\omega) = \langle [a, a^\dagger] \rangle = 1, \quad (3.11)$$

as one can verify from Eq. (3.7). As a result, interactions, driving and dissipation can reshape  $A(\omega)$ , but they cannot change its area. Finally, this spectral decomposition of Markovian Green functions makes it clear that one can extract information on the eigenvalues of the Liouvillian from the poles of  $G^R(\omega)$ . In particular, it shows that the usual definition of second order phase transitions in terms of diverging susceptibilities coincides with the closure of the Liouvillian gap, namely the smallest non-zero eigenvalue of the Liouvillian vanishing, which is sometimes considered the hallmark of dissipative phase transitions [37, 49].

### 3.3 Effective temperature

As we have already discussed in Sec. 2.1 distribution function allows to define effective thermodynamic quantities out-of-equilibrium. In Sec. 2.1 we gave the example of the low energy effective temperature. We have also warned that there is no unique definition of those effective quantities and that different definitions bear different physical meanings. In this section it is significant to define the frequency dependent effective temperature  $T_{\text{eff}}(\omega)$  by

$$\frac{G^K(\omega)}{-2\pi i A(\omega)} \equiv \coth\left(\frac{\omega}{2T_{\text{eff}}(\omega)}\right) \quad (3.12)$$

by analogy with the FDT for bosons in equilibrium  $G^K(\omega)/(-2\pi i A(\omega)) = 1 + 2n_\beta(\omega) = \coth(\omega/(2T))$ , where  $T = 1/\beta$ . As discussed extensively in Ref. [130], this  $T_{\text{eff}}(\omega)$  has a direct operational meaning and is a useful quantity in many different physical contexts, e.g. the theory of optomechanical cavity cooling using driven resonators [173]. In general, if a second narrow-bandwidth auxiliary system interacts weakly with our main system via exchanging photons, it will equilibrate to a temperature  $T_{\text{eff}}(\omega_{\text{aux}})$ , where  $\omega_{\text{aux}}$  is the frequency of the auxiliary system. As example, the auxiliary system could be a qubit with splitting frequency  $\omega_{\text{aux}}$ , which interacts with the main system via  $H_{\text{int}} \propto (\sigma_+ a + \text{h.c.})$  [130, 172]. Note that for a general non-equilibrium system, there is no requirement that the effective temperature  $T_{\text{eff}}(\omega)$  be positive. Supposing  $iG^K(\omega) > 0$ , then the sign of  $A(\omega)$  dictates that of  $T_{\text{eff}}(\omega)$ . In particular, if the sign of  $A(\omega)$  obeys the equilibrium property Eq. (3.6), then  $T_{\text{eff}}(\omega) > 0 \forall \omega$ . If this is not true, then there will be frequency regions in which  $T_{\text{eff}}(\omega)$  is negative. We thus see that the anomalous sign of the spectral function discussed earlier is directly connected to the existence of negative effective temperatures. We stress that this negative temperature has physical consequences. Again, consider weakly coupling an auxiliary qubit to our system. If the qubit splitting frequency  $\omega_{\text{aux}}$  is such that  $T_{\text{eff}}(\omega_{\text{aux}}) < 0$ , the qubit would thermalize at negative temperature, implying an inversion of the qubit population, – namely a higher probability for the qubit to be in the excited state rather than its ground state.

### 3.4 The van der Pol oscillator

We now restrict to study a specific system. We consider the well-known quantum van der Pol (VdP) oscillator [153, 163] with an additional non-linear term in the Hamiltonian. The model thus describes a non-linear oscillator subject to incoherent single-particle driving and two particle losses. It is described by the master equation

$$\partial_t \rho = -i[H, \rho] + \gamma \left( r \mathcal{D}_p^{(1)} + \mathcal{D}_l^{(2)} \right) \rho \quad (3.13)$$

$$H = \omega_0 a^\dagger a + \frac{U}{2} (a^\dagger a)^2 \quad (3.14)$$

$$\mathcal{D}_p^{(1)} \rho = a^\dagger \rho \hat{a} - \frac{1}{2} \{ a a^\dagger, \rho \} \quad (3.15)$$

$$\mathcal{D}_l^{(2)} \rho = a a^\dagger \rho a^\dagger a - \frac{1}{2} \{ a^\dagger a^\dagger a a, \rho \} \quad (3.16)$$

Here  $\omega_0$  is the cavity frequency and  $U/2$  the strength of the Kerr (or Hubbard) interaction.  $\gamma$  is the two-photon loss rate, while  $\gamma r$  is the single photon pumping rate. We will set  $\omega_0 = 0$  in the following, as it can be eliminated by moving to a rotating frame.

Note first that the unique steady state density matrix of this model has been found analytically in Ref. [170, 174]. The steady state is an incoherent mixture of photon number Fock states; further, it is completely independent of the interaction strength  $U$ , and is only determined by the dimensionless parameter  $r$  (ratio of the driving to the nonlinear losses). The photon-number probabilities in the steady state are in fact determined by a classical

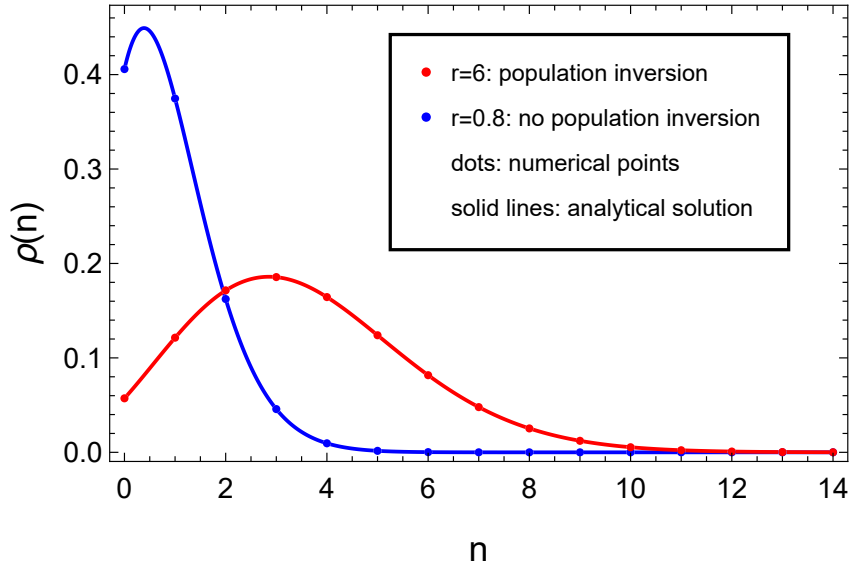


Figure 3.2: The stationary state density matrix is diagonal in the Fock basis. Its diagonal elements are plotted as a function of the number of bosons for two values of the pump-loss ratio  $r$ , showing a distribution with and without population inversion. The stationary state does not depend on the interaction  $U$ , resonator frequency  $\omega_0$  or dissipation scale  $\gamma$ . Numerical calculations use a Hilbert space cutoff  $N_{max} = 15$ . With this choice of cutoff the numerical solutions (dots) agree perfectly with the analytical predictions (solid lines).

master equation (i.e. coherences play no role) and they are given by

$$p_n = r^n \frac{\Gamma(r)\Phi(1+n, r+n, r)}{\Gamma(r+n)\Phi(1, r, 2r)} \quad (3.17)$$

where  $\Gamma(x)$  and  $\Phi(a, b, x)$  are the gamma function and the confluent hypergeometric function. In Fig. 3.2 we plot the probabilities  $p_n$  in the steady state for two different values of  $r$ . For the smaller value of  $r$ , those probabilities decay monotonically with  $n$ , whereas for large values, one obtains a peaked, non-monotonic distribution. As the Hamiltonian  $H$  dictates that energy increases with increasing photon number, this latter situation formally corresponds to a population inversion.

A natural question we now ask is whether this inversion effect (which is essentially classical) manifests itself in the cavity's spectral properties. We will answer this question in the rest of this chapter. We remark that the spectral properties of a related quantum van der Pol oscillator in different regimes were first discussed in a series of seminal works [153, 170] (see instead Ref. [175] for the undriven model). More recently, the power spectrum of a coherently driven quantum van der Pol oscillator was computed to investigate signatures of synchronization [165].

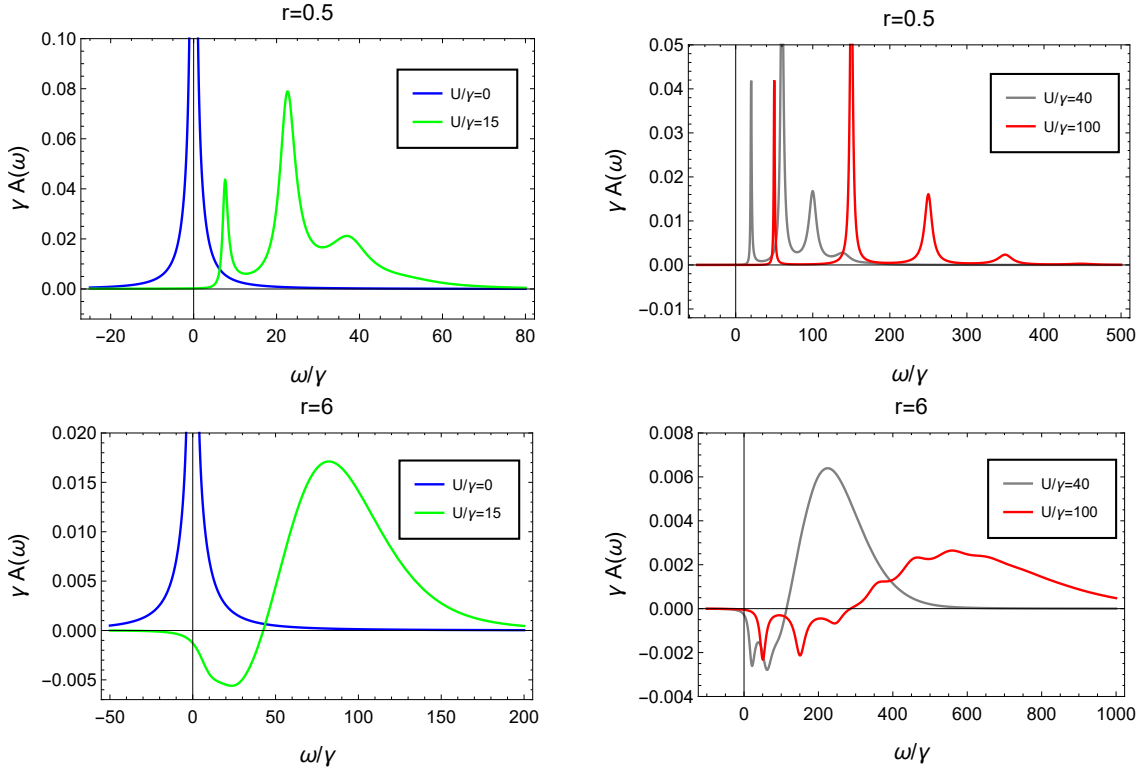


Figure 3.3: Evolution of the single-particle spectral function  $A(\omega)$  upon changing the interaction  $U$ , for two values of the parameter  $r$ , the ratio between drive and losses. For  $r = 0.5$  (top panel) we see that increasing the nonlinearity splits the single particle peak into a series of well separated resonances. For larger drive,  $r = 6$  (bottom panel), corresponding to an inverted steady state density matrix, a new feature appears for large enough interaction (bottom-right panel), namely the spectral function becomes negative over a range of frequencies. Parameters: resonator frequency  $\omega_0 = 0$ , Hilbert space cutoff  $N_{max} = 15$ .

### 3.4.1 Liouvillian eigenmodes and symmetry considerations

To understand the Green functions of our model, it will be useful to first discuss its symmetry properties. Due to driving and dissipation, the system does not conserve photon number. Nonetheless, the Liouvillian is invariant under the  $U(1)$  symmetry  $a \rightarrow ae^{i\theta}$ . This implies that the Liouvillian  $\mathcal{L}$  commutes with the superoperator  $\mathcal{K} = [a^\dagger a, \bullet]$  that generates the symmetry operation. As a result, the eigenvalues  $k$  of  $\mathcal{K}$  are quantum numbers which label the eigenstates of  $\mathcal{L}$ . We can use this to write the Liouvillian in the block-diagonal form  $\mathcal{L} = \bigoplus_k \mathcal{L}_k$ , where  $\mathcal{L}_k$  acts only within the eigensubspace of  $\mathcal{K}$  corresponding to the (integer) eigenvalue  $k$ . We denote the right eigenstates of a particular block  $\mathcal{L}_k$  by

$$r_{\alpha,k} = \sum_n r_{\alpha,k}^n |n+k\rangle \langle n| \quad (3.18)$$

In Fock space, we see that this is a matrix that only has non-zero elements along the  $k$ th off-diagonal.

The presence of this symmetry greatly reduces the numerical complexity of the problem, as we can diagonalize the different blocks separately. It also gives a simple physical way to label the different eigenmodes of  $\mathcal{L}$ . Eigenmodes corresponding to  $k = 0$  describe how diagonal elements of the density matrix (in the Fock basis) decay. Such decay modes conventionally referred to as  $T_1$  relaxation processes. In contrast, eigenmodes corresponding to  $k \neq 0$  describe how Fock-state coherences decay. These are generically referred to as  $T_2$  relaxation processes. In general, eigenmodes of the Liouvillian mix  $T_1$  and  $T_2$  processes; in this case, due to the presence of the  $U(1)$  symmetry,  $T_1$  and  $T_2$  processes correspond to different decay modes.

We make the crucial remark that different correlation functions will *only* be sensitive to a particular (small) subset of Liouvillian eigenmodes. For example, for the single particle Green function defined in Eq. (3.1), it is only the eigenmodes corresponding to  $k = 1$  that contribute. This follows immediately from the fact that the residues  $w_\alpha$  (3.8) of the poles of the retarded Green function Eq. (3.7) vanish for  $k \neq 1$  as

$$\text{tr}(ar_{\alpha,k}) = 0 \quad (k \neq 1) \quad (3.19)$$

Analogously, correlation functions like  $g^{(2)} = \langle a^\dagger(t)a^\dagger(t)a(0)a(0) \rangle$  would probe Liouvillian eigenmodes with  $k = 2$ , i.e.  $T_2$  processes involving coherences between states whose photon number differs by 2. Similarly, a correlation function destroying  $k$  bosons at  $t = 0$  and creating  $k$  bosons at time  $t$  would probe the decay of coherences between states whose photon numbers differ by  $k$ . It also follows that if one wishes to probe  $T_1$  processes (i.e.  $k = 0$ ), one needs to look at density-density correlation functions.

## 3.5 Spectral properties of vdP oscillator

We now turn to the spectral properties of the nonlinear van der Pol oscillator Eq. (3.13). We use the Lehmann representation given in Eq. (3.7) to compute the spectral functions numerically, by truncating the bosonic Hilbert space to a maximum number of states

$N_{\max} = 15$  and diagonalizing  $\mathcal{L}$ . The cutoff  $N_{\max} = 15$  is enough to obtain accurate results, as it is shown by the agreement of the steady state numerical solution with the analytical prediction in Fig. 3.2. We further checked that the results for the Green functions are stable by increasing  $N_{\max}$  and that they satisfy sum properties like Eq. (3.11).

### 3.5.1 Spectral function and the role of interactions

In Fig. 3.3 we plot the spectral function  $A(\omega)$  (c.f. Eq. (3.3)) of our system for several values of the dimensionless interaction strength  $U/\gamma$  and for two values of the drive/loss ratio  $r$ . An immediate result, visible in all four panels, is that the spectral functions strongly depend on the interaction strength. This is remarkably different from the steady state density matrix, which (as discussed in Sec. 3.4) is completely insensitive to  $U$ . Heuristically, while the steady state density matrix is completely independent of the system's coherent Hamiltonian dynamics, the system's response to perturbations retains a strong dependence on  $H$ .

For a more detailed analysis, consider first the regime of relatively weak driving where  $r = 0.5$  (top row of Fig. 3.3). To understand the lineshapes, recall from Sec. 3.4.1 that the spectral function is probing  $T_2$  decay modes which describe the decay of coherences between Fock states  $|n\rangle$  and  $|n+1\rangle$ . The oscillation frequency of these coherences is largely determined by the coherent Hamiltonian  $H$ . For  $U = 0$ , there is no Hamiltonian, and coherences do not oscillate; we thus obtain a single peak in the spectral function. As  $U/\gamma$  is increased, distinct peaks become visible in  $A(\omega)$  (each approximately Lorentzian), corresponding to different coherences and different decay modes; the peaks become more and more resolved with increasing  $U/\gamma$ .

For larger values of the driving parameter  $r$  (bottom row of Fig. 3.3,  $r = 6$ ), the situation is markedly different. For large driving and large enough interaction  $U$ , we find that the spectral function hits zero at a positive finite frequency, and for larger frequencies, becomes negative. We term this negativity of  $A(\omega)$  at  $\omega > 0$  “negative density of states” (NDoS). This is a clear indicator of non-equilibrium: as discussed in Sec. (3.2.1), this cannot happen in a closed system in thermal equilibrium. We also stress that (as discussed in Sec. 3.3 and in [172]), this NDoS corresponds to a negative effective temperature  $T_{\text{eff}}(\omega)$ ; this is shown in Fig. 3.4. We remark that this effective temperature, as defined by Eq. (3.12), is not a property of the stationary state and that it rather describes its excitations. As such, a population inversion of the stationary state is not sufficient for it to be negative and interactions are needed as well. As also discussed, this negative temperature effect could be directly probed by coupling the cavity weakly to an auxiliary probe qubit.

One might first think that the NDoS effect here is simply a reflection of the population inversion in the steady state photon number distribution, which occurs when  $r$  is sufficiently large. This is not the case: while the population inversion in the steady state is independent of  $U/\gamma$ ,  $A(\omega)$  only becomes negative at  $\omega > 0$  for sufficiently large  $U/\gamma$ . This is shown explicitly in Fig. 3.3. The relation between the NDoS effect in the spectral func-

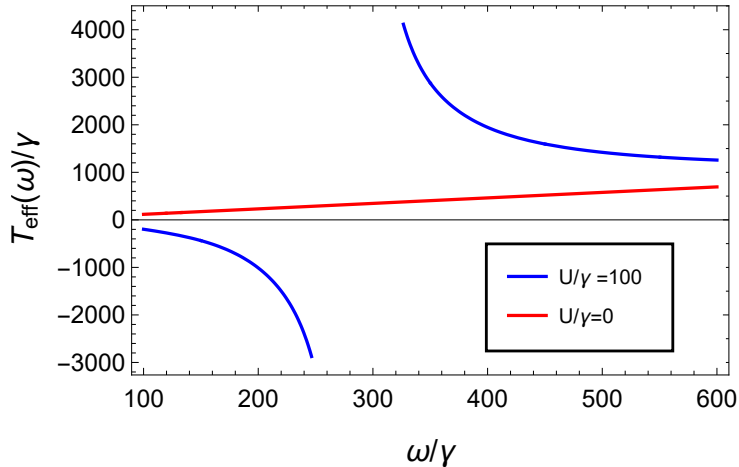


Figure 3.4: Frequency-dependent effective temperature  $T_{\text{eff}}(\omega)$  as defined in Eq. (3.12) in the regime of large pump-loss ratio ( $r = 6$ ). We notice that interaction  $U$  makes the effective temperature turn negative in some *positive* frequency region. For comparison we also plot the effective temperature of a  $U = 0$  cavity, which is always positive for  $\omega > 0$ . Parameters: resonator frequency  $\omega_0 = 0$ , Hilbert space cutoff  $N_{\max} = 15$ .

tion and population inversion in the steady state is thus not entirely trivial; we will explore this in more detail in the next sections. Note that similar spectral function negativity in presence of a population inversion has previously been identified in a related model of a quantum van der Pol oscillator in presence of negative damping and monochromatic drive [153, 170], as well as in parametrically driven bosonic systems [172].

### 3.5.2 Dissipation-induced lifetime

The results of the previous section show that the spectral properties of the nonlinear quantum VdP oscillator are richer than its steady state. In this section, we investigate the extent to which these can be understood using a perturbative approach where the only dynamical effect of dissipation and driving taken into account is to give a finite lifetime to the Fock-state eigenstates of the system Hamiltonian  $H$ .

Our starting point is the open-system Lehmann representation of Eq. (3.7). We will approximate the eigenstates of the Liouvillian to be the same as those of the closed system, e.g. simple outer products of Fock states (c.f. Eq. 2.40), ignoring their perturbative corrections due to dissipation for the time being. A special treatment will be reserved to the stationary state density matrix, whose populations  $p_n$  will be taken to follow Eq. (3.17), which is the exact distribution determined by dissipative processes. We will however take into account the modification of the Liouvillian's eigenvalues to leading order in the dissipation (i.e. in  $\gamma$ ). Formally, this procedure can be implemented using the Lindblad perturbation theory approach introduced in Ref. [176]. We write our full Liouvillian as  $\mathcal{L} = \mathcal{L}^{(0)} + \mathcal{D}$ , with the unperturbed Liouvillian  $\mathcal{L}^{(0)}\rho = -i[H, \rho]$  and the perturbation

$\mathcal{D} = \gamma \left( r\mathcal{D}_p^{(1)} + \mathcal{D}_l^{(2)} \right)$ . While  $\mathcal{L}^{(0)}$  is highly degenerate, we can still use the simple non-degenerate perturbation theory of [176] to compute the spectral function. In fact, due to the symmetry of  $\mathcal{L}$  discussed in Sec. 3.4.1, the eigenmodes determining the spectral function are only those with  $k = 1$ . We expand those eigenvalues and eigenvectors of the Liouvillian in powers of  $\gamma$ :

$$\begin{aligned}\lambda_\alpha &= \lambda_\alpha^{(0)} + \lambda_\alpha^{(1)} + O(\gamma^2) \\ r_\alpha &= r_\alpha^{(0)} + r_\alpha^{(1)} + O(\gamma^2) \\ l_\alpha &= l_\alpha^{(0)} + l_\alpha^{(1)} + O(\gamma^2)\end{aligned}$$

with the unperturbed quantities  $\lambda_\alpha^{(0)}, l_\alpha^{(0)}, r_\alpha^{(0)}$  defined by

$$r_{n+1,n}^{(0)} = l_{n+1,n}^{(0)} = |n+1\rangle\langle n| \quad (3.20)$$

$$\lambda_{n+1,n}^{(0)} = -i(E_{n+1} - E_n) = -i(\omega_0 + Un) \quad (3.21)$$

where  $E_n = \omega_0 n + U/2n^2$  are the eigenvalues of the Hamiltonian. As this set of zero-order eigenvalues  $\lambda_{n+1,n}^{(0)}$  are all distinct, we can apply non-degenerate perturbation theory. We retain the perturbative corrections to the eigenvalues, while ignoring for the time being any corrections to the eigenstates. The validity of such an approximation and the role of these corrections will be discussed later in the chapter. Perturbation theory tells us that the leading order correction to the Liouvillian eigenvalues  $\lambda_\alpha$  are given by  $\lambda_\alpha^{(1)} = \text{tr}[(l_\alpha^{(0)})^\dagger \mathcal{D} r_\alpha^{(0)}]$ . Accordingly, Eq. (3.7) yields the following approximate form for the spectral function:

$$A(\omega) = \frac{1}{\pi} \sum_{n=0}^{\infty} \frac{\Gamma_{n+1,n} |\langle n+1 | a^\dagger | n \rangle|^2 (p_n - p_{n+1})}{(\omega - E_{n+1,n})^2 + \Gamma_{n+1,n}^2} \quad (3.22)$$

where

$$\begin{aligned}E_{n+1,n} &= -\text{Im}(\lambda_{n+1,n}^{(0)} + \lambda_{n+1,n}^{(1)}) \\ &= E_{n+1} - E_n = \omega_0 + U/2 + Un\end{aligned} \quad (3.23)$$

$$\begin{aligned}\Gamma_{n+1,n} &= -\text{Re}(\lambda_{n+1,n}^{(0)} + \lambda_{n+1,n}^{(1)}) \\ &= 2\gamma n^2 + r\gamma(2n+3)\end{aligned} \quad (3.24)$$

Note that the first order correction to the  $\lambda_\alpha$  is purely real, implying there is no shift in the position of the spectral function resonances. The approximate spectral function in Eq. (3.22) is exactly the same as the equilibrium expression in Eq. (3.2), except that the populations  $p_n$  are non-thermal, and each resonance has a finite width  $\Gamma_{n+1,n}$ . While we have shown how this width can be calculated using formal perturbation theory, it also has a simple physical origin: it is the sum of the Fermi's Golden rule decay rates for the states  $|n\rangle$  and  $|n+1\rangle$ , forming the non-perturbed eigenstates (3.20) of the Liouvillian, i.e.

$$\begin{aligned}\Gamma_{n+1,n} &= \sum_m r\gamma \left( \left| \langle m | a^\dagger | n \rangle \right|^2 + \left| \langle m | a^\dagger | n+1 \rangle \right|^2 \right) + \\ &\quad + \sum_m \gamma \left( \left| \langle m | aa | n \rangle \right|^2 + \left| \langle m | aa | n+1 \rangle \right|^2 \right)\end{aligned} \quad (3.25)$$

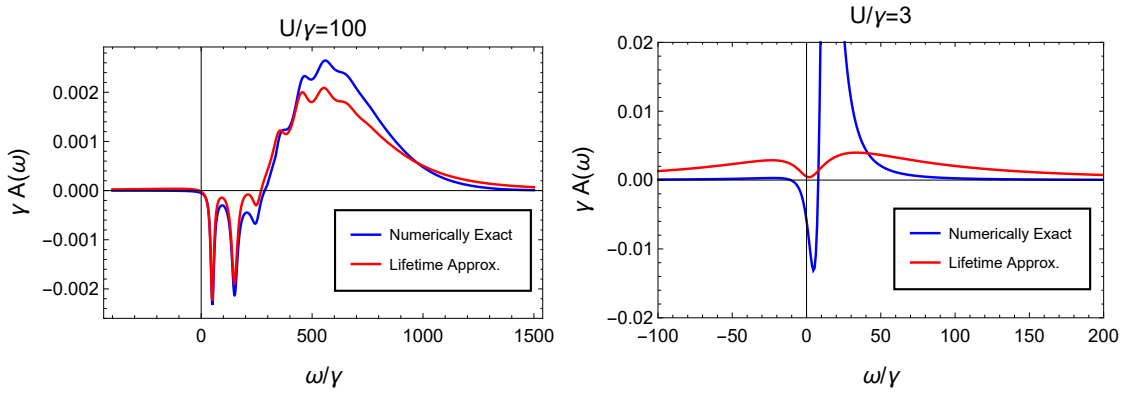


Figure 3.5: The spectral function  $A(\omega)$  obtained by numerical evaluation of the exact Lehmann representation, as well as that obtained using the lifetime approximation of Eq. (3.22). Top: The perturbative treatment of the lifetime is in good agreement with the exact result for a value of the interaction  $U/\gamma = 100$ . Bottom: Perturbation theory gets bad when the resonances are not well resolved. Here the interaction is  $U/\gamma = 3$ . Parameters: resonator frequency  $\omega_0 = 0$ , pump-loss ratio  $r = 6$ , Hilbert space cutoff  $N_{max} = 15$ .

The first line is the decay rate due to the incoherent driving, the second due to the two-photon loss. Basically, the first correction to the eigenvalues of the Liouvillian due to dissipation are the Fermi's Golden rule lifetimes of the non-perturbed eigenstates and they give the leading contribution to the width of the resonances of the spectral function. In Fig. 3.5 we compare the perturbative result with the full calculation obtained with the Lehmann representation for  $r = 6$  and two values of the Kerr interaction. We see that at large  $U/\gamma \simeq 100$  the perturbative approach captures rather well the main features of the spectrum, in particular the location of the peaks, their width and weight. However, upon decreasing the interaction, the agreement deteriorates, as we show for  $U/\gamma = 3$ . This behaviour is of course not surprising, as the perturbative approach is only valid in the small dissipation limit  $1 \ll U/\gamma, r \ll U/\gamma$ . As a rough rule of thumb, when resonances in Eq. (3.22) begin to overlap, perturbation theory starts getting bad, as the spacing between adjacent resonances is of order  $U$  and the width of the resonances of order  $\gamma$ .

Taking into account the dissipation-induced lifetime in Eq. (3.22) allows to uncover a mechanism by which dissipation can mask the effect of a population-inverted density matrix on the spectral function. Indeed, a population inversion in the stationary state, if there were no lifetime broadening, would certainly result in a violation of the Green functions sign property in Eq. (3.6), as one can see straight from Eq. (3.2). On the other hand, the lifetime broadens the resonances, making them overlap and possibly resulting in those with smaller weights to be completely masked by bigger ones. As a result, the spectral function in Eq. (3.22) does not obey anymore a precise sign rule which is dictated by the behaviour of populations of the density matrix, as in equilibrium (3.6). As a corollary, the presence of population inversion in the stationary state may not be revealed by a change of sign of the spectral function.

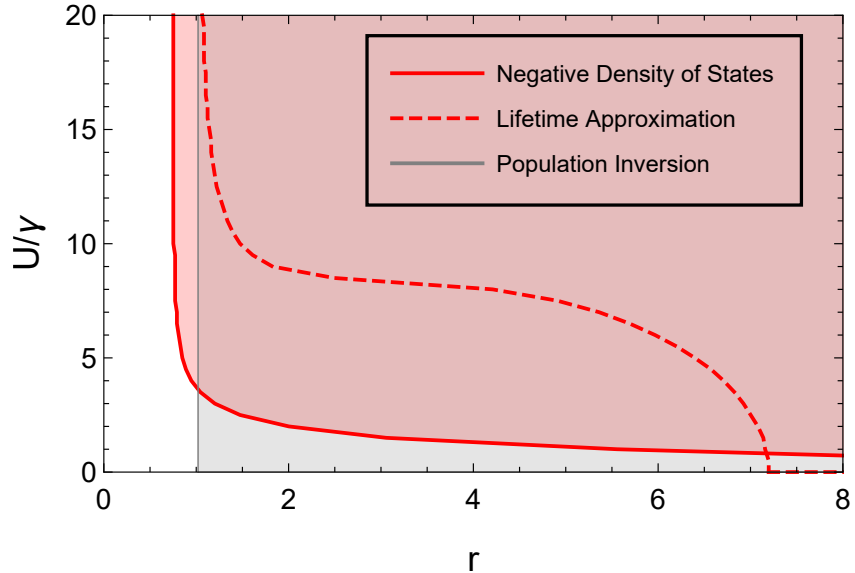


Figure 3.6: Region of parameters in the  $r$ - $U/\gamma$  plane where the spectral function  $A(\omega)$  is negative in some positive frequency range (NDoS), according to the exact result obtained by the Lehmann representation, Eq. (3.7), and to the lifetime approximation of Eq. (3.22). The vertical grey line shows the threshold value of  $r$  for which population inversion sets in the stationary state. According to the lifetime approximation, a NDoS is only possible with population inversion in the stationary state, while the exact result shows that this is not strictly necessary. Parameters: resonator frequency  $\omega_0 = 0$ , Hilbert space cutoff  $N_{max} = 15$ .

In Fig. 3.6, we summarize the above analysis by presenting a “phase” diagram, in the  $(r, U/\gamma)$  plane, of the regions of parameter space exhibiting the NDoS effect (i.e. the spectral function  $A(\omega)$  is negative at positive frequencies). The region  $r > 1$  (shaded grey) indicates where the steady-state exhibits a population inversion; this boundary can be determined analytically from the exact stationary state solution [174] and we remark that it is independent of  $U$ . In contrast, the spectral function is sensitive to both interaction and non equilibrium effects, resulting in a non-trivial value  $U_c(r)$  above which the negative density of state emerges. We plot this threshold interaction strength both for the numerically exact calculation of the spectral function (red-solid line), and for the approximate perturbative (lifetime broadening) calculation (red-dashed line). In general, the perturbative approach underestimates the NDoS effect; further, it fails to yield any population inversion in the region  $r < 1$ . In contrast, the numerically exact calculation reveals that NDoS can occur even for  $r < 1$ , i.e. in regions where the steady state photon number exhibits no population inversion. This is a remarkable result, which points toward yet another origin of NDoS, as we are going to further discuss below.

### 3.5.3 Dissipative effects beyond lifetime broadening

As demonstrated above, the simple perturbative lifetime broadening of eigenstates introduced in Eq. (3.22) was able to capture many aspects of the spectral function of our model. It however failed to describe the most interesting aspect of Fig. 3.6: there are parameter regions where the spectral function exhibits NDoS, even though the steady state density matrix does not exhibit population inversion. As we now show, this effect can also be captured in perturbation theory if we go beyond simply calculating a correction to the Liouvillian eigenvalues due to dissipation, but also calculate the change to the eigenmodes themselves. The leading eigenmode correction can cause the weight factors  $w_\alpha$  in Eqs. (3.7) and to acquire an imaginary part, implying that the spectral function is no longer a simple sum of Lorentzians. This provides a new route for NDoS.

Using the same perturbation theory used in Sec. 3.5.2, we can analytically compute the leading-order-in- $\gamma$  correction to the Liouvillian eigenmodes. Following [176] and assuming  $\mathcal{L}^{-1}$  exists, the first order corrections to the right and left eigenstates are given by:

$$r_\alpha^{(1)} = \sum_{\beta \neq \alpha} \frac{\text{tr} \left[ (r_\beta^{(0)})^\dagger \mathcal{D} r_\alpha^{(0)} \right]}{\lambda_\alpha^{(0)} - \lambda_\beta^{(0)}} r_\beta^{(0)} \quad (3.26)$$

$$l_\alpha^{(1)} = \sum_{\beta \neq \alpha} \frac{\text{tr} \left[ (l_\beta^{(0)})^\dagger \mathcal{D}^\dagger l_\alpha^{(0)} \right]}{\lambda_\alpha^{(0)*} - \lambda_\beta^{(0)*}} l_\beta^{(0)} \quad (3.27)$$

As expected, dissipation mixes the various eigenmodes together with a strength that is inversely proportional to the difference in eigenvalues. Here, the denominator is purely imaginary (as all unperturbed eigenvalues are imaginary).

As discussed, for the spectral function, the unperturbed modes of interest correspond to coherences between the  $|n\rangle$  and  $|n+1\rangle$  Fock states:

$$r_{n+1,n}^{(0)} = l_{n+1,n}^{(0)} = |n+1\rangle\langle n| \quad (3.28)$$

With dissipation, these modes acquire a real part to their eigenvalues, corresponding to dephasing. The first-order correction to the eigenstates takes the form:

$$\begin{aligned} r_{n+1,n}^{(1)} &= -i \frac{r\gamma}{U} 2\sqrt{(n+2)(n+1)} r_{n+2,n+1}^{(0)} + \\ &\quad + i \frac{\gamma}{U} n \sqrt{n^2 - 1} r_{n-1,n-2}^{(0)} \end{aligned} \quad (3.29)$$

$$\begin{aligned} l_{n+1,n}^{(1)} &= -i \frac{r\gamma}{U} 2\sqrt{(n+1)n} l_{n,n-1}^{(0)} + \\ &\quad + i \frac{\gamma}{U} (n+2) \sqrt{(n+1)(n+3)} l_{n+3,n+2}^{(0)} \end{aligned} \quad (3.30)$$

At a physical level, these corrections tell us that dephasing eigenmodes of the Liouvillian no longer correspond to a single Fock state coherence; rather, each mode involves three distinct coherences.

In Fig. 3.7 we show the effect of including these eigenmode corrections in the evaluation of the spectral function. We see that this modified approach is able to capture

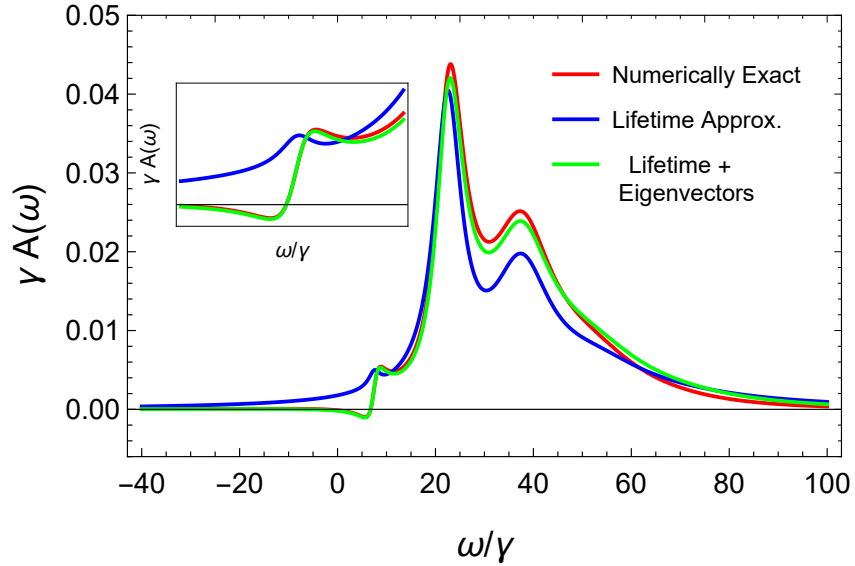


Figure 3.7: The spectral function  $A(\omega)$  for a value of  $r$  just below the threshold needed in order to have steady state population inversion. Strikingly, the spectral function  $A(\omega)$  (as computed numerically) still exhibits negativity at positive frequencies. This feature is missed if one calculates  $A(\omega)$  using the simple lifetime approximation of Eq. (3.22). Including the dissipative correction to the Liouvillian eigenstates (to leading order), one is then able to recover the negative part of  $A(\omega)$ . Parameters: resonator frequency  $\omega_0 = 0$ , interaction  $U/\gamma = 15$ , pump-loss rate  $r = 0.94$ , Hilbert space cutoff  $N_{max} = 15$ .

non-Lorentzian contributions to the spectral function, and to improve qualitatively and quantitatively the agreement with the exact numerical result. In particular, a region of negative density of states now appears at small frequency, an effect which is completely missed by the lifetime broadening approximation.

These eigenmode corrections can also be given a physical interpretation in terms of interference of different dephasing modes. Consider the contributions to the time-domain correlation function in Eq. (2.37) associated with a particular initial photon number  $m$ :

$$\sum_n e^{\lambda_{n+1,n} t} \left( \sum_l \langle l | a r_{n+1,n} | l \rangle \right) \langle m | l_{n+1,n}^\dagger a^\dagger | m \rangle \rho_{m,m} \quad (3.31)$$

Recall the interpretation: starting with  $m$  photons, we add a photon to the cavity, exciting a dephasing eigenmode  $\alpha = (n+1, n)$  of the Liouvillian. To 0-th order in dissipation, the time-independent weight factors are necessarily real. This follows from the fact that i)  $r_{n+1,n}^{(0)} = l_{n+1,n}^{(0)}$ , and ii) the only non-zero contribution is when  $l = n = m$ , i.e. adding a photon to  $|m\rangle$  excites a single, unique dephasing eigenmode.

Including dissipation to first order, both conditions (i) and (ii) no longer hold. In particular, as the dephasing eigenmodes no longer correspond to a single Fock coherence (c.f. Eq. (3.29)-(3.30)), adding a photon to  $|m\rangle$  can simultaneously excite several

distinct dephasing eigenmodes. It is the interference between these processes that give rise to complex weights and hence non-Lorentzian contributions to the spectral functions. The spectral function is thus sensitive to an interference in the dynamics, even though there is no coherence in the steady state density matrix. Stepping back, we thus see that even for weak dissipation, the spectral function is sensitive to more than just the lifetime-broadening effect of dissipation: the fact that dissipation can also create more complicated dephasing processes also directly impacts the form of  $A(\omega)$ . This gives rise to anti-Lorentzian contributions, and (in our model) negative density of states in regimes where the steady state exhibits no population inversion.

### 3.6 Conclusions

In this work we have studied the spectral properties of driven-dissipative quantum systems, taking the simple case of a quantum van der Pol oscillator with Kerr non-linearity as a working example. We have first derived some general results concerning the single particle Green function of systems described by a Lindblad master equation. Using a decomposition in terms of exact eigenstates of the Liouvillian we have compared the spectral representation for the Green function and compared it to the well known Lehmann representation for closed systems in thermal equilibrium. Such a spectral representation, in addition of being of practical relevance for numerical computations whenever the system is sufficiently small to be diagonalized exactly, has also a conceptual value. From one side it connects properties of the Liouville eigenvalues and eigenstates, which are of theoretical interest but often hard to access, to the behavior of the spectral functions, which are of direct experimental relevance. In addition it allows for a more transparent interpretation of spectral features in regimes far from equilibrium, for which a simple intuition is often lacking or misleading. As an example we have shown that the well known sign property of equilibrium Green functions, changing sign at zero frequency as a result of thermal occupation, can be violated in driven-dissipative systems and it is in general not directly constrained by the structure of the stationary state density matrix.

We have then applied our approach to the case of a quantum van der Pol oscillator with Kerr non-linearity. Such a model turns out to be a perfect case study, since the properties of its stationary density matrix are well known, while its spectral features reveal a number of surprises. In particular the resonator density of state shows a strong dependence from the strength of the Kerr nonlinearity, a feature completely absent in the steady state populations only set by pump/loss ratio. Even more interestingly, in the regime of large interaction and large non-equilibrium imbalance a NDoS emerges, an effect which would not be possible in thermal equilibrium.

We have summarized the behavior of the spectral function of this model in the phase diagram of figure (3.6) which shows that NDoS is not necessarily related to an inverted population in the steady state density matrix. In order to build physical intuition and to better understand the origin of this result we have developed a semi-analytical approach that starts from the spectral function of the isolated problem and adds a lifetime due to

dissipation in the spirit of a Fermi Golden Rule. This method, which turns out to be equivalent to a perturbation theory in the dissipation where only the eigenvalues of the Liouvillian are corrected, was able to partially capture the NDoS effect, at least for sufficiently large interaction and whenever the stationary density matrix shows population inversion. Finally we have shown that including the perturbative correction to the eigenstates of the Liouvillian results into a new mechanism for NDoS, due to the emergence of complex weights in the spectral function. This turns to be crucial to capture NDoS in the regime where the populations of the steady state are not yet inverted.

To conclude we mention that the approach outlined here is rather general and can be used to shed light on the spectral properties of other small driven-dissipative quantum models. Interesting future directions include for example the study of resonance fluorescence lineshapes beyond the two-level system limit [177, 178], the spectral features of a coherently driven cavity across a zero-dimensional dissipative phase transition [43, 47, 106] or applications related to quantum synchronization [164, 179, 180].

## Chapter 4

# Finite-Frequency Transition in Driven-Dissipative Bosons on a Lattice

Critical points and phase transitions are characterized by diverging susceptibilities, reflecting the tendency of the system toward spontaneous symmetry breaking. Equilibrium statistical mechanics bounds these instabilities to occur at zero frequency, giving rise to static order parameters. In this chapter we argue that a prototype model of correlated driven-dissipative lattice bosons, of direct relevance for upcoming generation of circuit QED arrays experiments, exhibits a susceptibility sharply diverging at a finite non-zero frequency, which is an emerging scale set by interactions and non-equilibrium effects. Our work, connecting breaking of time translational invariance to divergent finite-frequency susceptibilities, could potentially be extended to study other time-domain instabilities in non-equilibrium quantum systems, including Floquet time-crystals [118] and quantum synchronization [163, 164, 181, 182]. The results of this chapter have been published in [2].

### 4.1 Introduction

Second order phase transitions in systems at thermal equilibrium or in their ground state are characterized, according to the Landau paradigm, by the emergence of a static order parameter which spontaneously breaks a symmetry of the system, such as spin rotational invariance for magnetism or spatial translational invariance for crystals [111, 183]. The resulting criticality is described in terms of an instability of a symmetric phase, characterized by a singularity of a static susceptibility. For classical systems far away from thermal equilibrium, such as in presence of external forcing and dissipation, the variety of instabilities can be far richer, with both finite momentum and finite frequency modes going unstable and resulting in the formation of patterns, propagating fronts, spatio-temporal chaos, synchronization or other oscillatory behaviors [184–186]. Quantum many body sys-

tems in presence of both driving and dissipation mechanisms represent natural platforms to understand and explore such dynamical phases. A well known example is provided by exciton-polariton condensates where superfluidity has an order parameter oscillating in time [30, 31, 70, 122]. Yet the oscillating condensate is successfully described by semi-classical theories such as driven-dissipative Gross-Pitaevski equations that are valid in the regime of weak interactions. More recently the attention has shifted toward strongly correlated quantum lattice models with drive and dissipation, where several works have revealed the existence of limit cycles, i.e. non-stationary solutions of the quantum dynamics for a macroscopic order parameter, at least at the mean field level [16, 17, 20, 93, 187–189].

In this chapter we focus on a paradigmatic model of driven-dissipative interacting bosons on a lattice, which is directly relevant for the upcoming generation of circuit QED arrays experiments [61, 62, 86]. We argue that a dynamical susceptibility of such an open quantum many body system, which in thermal equilibrium is finite and small since non-zero frequency modes are typically damped by interactions, can display a genuine singularity at finite frequency, as a result of strong interactions and non-equilibrium effects. The critical frequency is non-trivial and set by a competition of interactions with drive and dissipation. Eventually, the system undergoes a dynamical phase transition where the order parameter emerges with a finite oscillation frequency and in the broken symmetry phase oscillates in time without damping, thus breaking the continuous time-translational symmetry. This stationary-state instability is controlled by both dissipative and coherent couplings, in particular by the ratio between hopping and local interaction, thus providing the strongly correlated analogue of weak coupling non-equilibrium bosons condensation.

The chapter is organized in the following way. In section 4.2 we introduce the many-body model in the framework of Keldysh field theory and we discuss our approach based on a strong-coupling effective action combined with the exact numerical solution of the single-site master equation. In section 4.3 we discuss the stationary-state instability of the normal phase characterized by a diverging finite-frequency susceptibility and we discuss how this is related to the physics of the single-site problem. In section 4.4 we present the consequences of this instability on the dynamics of the order parameter, first by a numerical mean-field calculation and then recovering this dynamics from the saddle point solution of our effective field theory.

## 4.2 The model

We consider the Bose-Hubbard (BH) Hamiltonian

$$H = -J \sum_{\langle ij \rangle} \left( a_i^\dagger a_j + \text{hc} \right) + \sum_i \left( \omega_0 n_i + \frac{U}{2} n_i^2 \right) \quad (4.1)$$

modelling a lattice of circuit QED resonators (see Sec. 1.2). Each lattice site hosts a single bosonic mode with annihilation and creation operators  $a_i, a_i^\dagger$ , with frequency  $\omega_0$  and local interaction  $U$ ;  $n_i = a_i^\dagger a_i$  is the occupation operator of site  $i$ .  $\sum_{\langle ij \rangle}$  is a sum on nearest-neighbours sites, which are coupled with hopping rate  $J$ . The Bose-Hubbard model is a

prototype model of interacting bosonic lattices and it has been intensively studied. We mainly refer to the important paper [91] and to the book [111]. We supplement the model with local pump and losses, necessary to drive the system into a non-equilibrium steady state. We anticipate that the results we are going to discuss do not depend on the specific model for drive and dissipation and we will highlight the key features a model needs to have for our results to apply. We formulate the many-body problem specifying its Keldysh action, which reads

$$S = \int_C dt \left( \sum_i \bar{a}_i i \partial_t a_i - H \right) + \sum_i (S_{l,i} + S_{\sigma,i}) \quad (4.2)$$

$$H = \sum_i \left( \omega_0 \bar{a}_i a_i + \frac{U}{2} \bar{a}_i \bar{a}_i a_i a_i \right) - \sum_{\langle ij \rangle} J (\bar{a}_i a_j + \text{hc}) \quad (4.3)$$

$S_{l,i}$  describes Markovian particle losses of each lattice site,

$$S_{l,i} = -i\kappa \int_{-\infty}^{\infty} dt \left( \bar{a}_{i-} a_{i+} - \frac{1}{2} \bar{a}_{i+} a_{i+} - \frac{1}{2} \bar{a}_{i-} a_{i-} \right) \quad (4.4)$$

and corresponds to a standard Lindblad term by the mapping introduced in Sec. 2.3.3.  $S_{\sigma,i}$  describes the coupling of each site to, for the time being generic and non-Markovian, reservoirs

$$S_{\sigma,i} = -i \int_C dt \int_C dt' \sum_i \bar{a}_i(t) C(t-t') a_i(t') \quad (4.5)$$

where  $C$  describes the bath correlations and it depends only on time-differences as we assume the reservoir to be in a stationary state. Both kinds of dissipations are local and homogeneous throughout the lattice. The reservoir (4.5) will describe the *drive*, that is the term injecting particles in the system. It is an incoherent drive, meaning that it exchanges, in particular injects, bosons without a well defined phase into the system. As a result, it preserves the  $U(1)$  symmetry, the invariance under  $a_i \rightarrow e^{i\phi} a_i$ , of the Hamiltonian in Eq. (4.1). This leaves open the possibility of a spontaneous breaking of this symmetry, that is what we are interested in studying. In other words, if we chose to drive the system with a coherent, classical field, i.e. with Hamiltonian  $H_d = a^\dagger F e^{-i\omega_d t} + a F^* e^{i\omega_d t}$  as in [15, 190, 191], this would explicitly spoil the  $U(1)$  symmetry, precluding the possibility of a spontaneous symmetry breaking.

#### 4.2.1 Strong-coupling approach

We now introduce a general strong-coupling approach to study driven-dissipative correlated lattice models, which generalizes the equilibrium approach of Ref [91] (see also [90, 111, 192]). We write down the Keldysh partition function

$$Z = \int \prod_i \mathbf{D}[\bar{a}_i, a_i] e^{iS[\{\bar{a}_i, a_i\}]} \quad (4.6)$$

where by  $\{\bar{a}_i, a_i\}$  we mean the set of bosonic coherent fields of all sites. We rewrite the effective action in the form

$$S = S_{loc} - \int_C dt \sum_{ij} \bar{a}_i J_{ij} a_j \quad (4.7)$$

$$S_{loc} = \sum_i (S_{u,i} + S_{l,i} + S_{\sigma,i}) \quad (4.8)$$

where  $S_{loc}$  describes decoupled sites, containing the term  $S_{u,i}$  describing unitary evolution and the dissipative contributions  $S_{l,i}, S_{\sigma,i}$ . The only term coupling different sites is the hopping term, where  $J_{ij}$  is the hopping matrix, being equal to  $-J$  for nearest neighbours sites and zero otherwise. We then decouple the hopping term through a Hubbard-Stratonovich transformation, by introducing an auxiliary bosonic field  $\psi_i$  for each site. This transformation corresponds formally to the Gaussian integral

$$\exp \left( -i \int_C dt \sum_{ij} \bar{a}_i J_{ij} a_j \right) = \frac{1}{\mathcal{N}} \int \prod_i \mathbf{D} [\bar{\psi}_i \psi_i] \exp \left\{ i \int_C dt \left[ \sum_{ij} \bar{\psi}_i J_{ij}^{-1} \psi_j + \sum_i (\bar{\psi}_i a_i + \psi_i \bar{a}_i) \right] \right\} \quad (4.9)$$

where  $J_{ij}^{-1}$  is the inverse hopping matrix and  $\mathcal{N}$  is a normalization constant coming from Gaussian integration that we don't need to compute. The field  $\psi_i$  plays the role of a local order parameter since, for small  $\langle a_i \rangle, \langle \psi_i \rangle$  is linearly related to  $\langle a_i \rangle$  [91]. By plugging this formula in the action (4.2), we are now left with a path integral on  $a_i, \bar{a}_i$  and  $\psi_i, \bar{\psi}_i$  fields. We can formally integrate on the  $a_i, \bar{a}_i$  fields

$$\begin{aligned} Z &= \int \prod_i \mathbf{D}[\bar{a}_i, a_i] e^{iS[\{\bar{a}_i, a_i\}]} = \\ &= \frac{1}{\mathcal{N}} \int \prod_i \mathbf{D}[\bar{\psi}_i, \psi_i] e^{i \int_C dt \sum_{ij} \bar{\psi}_i J_{ij}^{-1} \psi_j} \int \prod_i \mathbf{D}[\bar{a}_i, a_i] e^{iS_{loc}} e^{i \int_C \sum_i (\bar{\psi}_i a_i + \psi_i \bar{a}_i)} \end{aligned} \quad (4.10)$$

and define an effective action for the fields  $\psi_i, \bar{\psi}_i$  alone, of the form

$$\mathcal{S}_{\text{eff}} = \int_C dt \left( \sum_{ij} \bar{\psi}_i J_{ij}^{-1} \psi_j + \sum_i \Gamma[\bar{\psi}_i, \psi_i] \right) \quad (4.11)$$

where the second term represents the generating functional of the bosonic Green functions of isolated sites,  $\Gamma[\bar{\psi}_i, \psi_i] = -i \log \langle T_C e^{i \int_C dt (\bar{\psi}_i a_i + a_i^\dagger \psi_i)} \rangle_{loc}$ . We stress that the latter average is taken over the interacting driven-dissipative **decoupled** sites, which is much easier to compute than averages on the many-body problem. We will now describe the on-site dynamics by a Markovian master equation and we compute the Green function of isolated sites entering the effective action by exact diagonalization of the associated Liouvillian and using the spectral representation introduced in Sec. 2.4.3. Our approach therefore combines the strong coupling field theory (4.11) with the exact numerical solution of the single-site problem. As such, it could be applied to lattice models with any scheme of incoherent local drive and dissipation by just solving the appropriate local problem.

### 4.2.2 Single-site problem: driving protocol and master equation

In this chapter we consider the physical realization of the drive theoretically proposed in [101, 189, 193]. An ensemble of  $N_{at} \gg 1$  two-level emitters with randomly distributed frequencies is coupled to each resonator. The microscopic Hamiltonian for this driving scheme reads

$$H_d = \sum_i \sum_{n=1}^{N_{at}} \omega_{at}^{(n)} \sigma_i^{+(n)} \sigma_i^{-(n)} + g \sum_{i,n} \left( a_i^\dagger \sigma_i^{-(n)} + hc \right) \quad (4.12)$$

where  $\sigma_i^{-(n)}$ ,  $(\sigma_i^{+(n)})$  are the lowering (raising) operators for the two-level emitters and  $g$  is the single-emitter Rabi frequency. The transition frequencies  $\omega_{at}^{(n)}$  of the two-level systems are assumed to be uniformly distributed over a finite range. Each emitter is further incoherently pumped by an external pump in its excited state at a strong rate, such that the emitters are constantly maintained in their excited states, namely their population is kept perfectly inverted. As a consequence of this, the emitters cannot absorb particles from the system, but only inject particles into the system: as soon as one emitter relaxes to its ground state injecting a particle in the system, the pump will immediately bring it in its excited state again, before it can absorb any particle from the system. We refer to [101, 193] for more details about the physical realization of this scheme. In order to describe this driving scheme we have to specify the Keldysh components of its correlation function  $C$  entering the action (4.5). As the two-level emitters frequencies are uniformly distributed on a finite range, their spectrum of emission can be approximated by a box-shaped function. The absorption rate of the bath will be zero instead. In frequency domain, this corresponds to

$$C^{-+}(\omega) \equiv 0 \quad C^{+-}(\omega) \equiv f \Gamma^{+-}(\omega) \equiv f \theta(\sigma - |\omega|) \quad (4.13)$$

where  $\theta$  is the step function and  $\sigma$  is the bandwidth of the drive: the drive only exchanges, namely injects, particles with the system with energy lower than  $\sigma$ . Reservoirs selective in energy have been studied theoretically and experimentally in different works [93, 166, 193] and have been proposed to dissipatively stabilize gapped ground-states [101, 189], a challenge that has been experimentally achieved in [62]. We will discuss the phases ones can dissipatively stabilize using those kind of reservoirs in chapter 5.

The dynamics of an isolated site described by the action (4.8) can be described, in the Markovian approximation, by means of the master equation

$$\partial_t \rho = -i [H_{loc}, \rho] + \left( \kappa \mathcal{D}_l + f_g \tilde{\mathcal{D}}[a^\dagger, \tilde{a}_g^\dagger] + f_l \tilde{\mathcal{D}}[a, \tilde{a}_l] \right) \rho \quad (4.14)$$

with  $H_{loc} = \omega_0 n + \frac{U}{2} n^2$ .  $\mathcal{D}_l$  is a Lindblad dissipator describing single-particle losses with rate  $\kappa$

$$\mathcal{D}_l \rho = \left( a \rho a^\dagger - \frac{1}{2} \{ a^\dagger a, \rho \} \right) \quad (4.15)$$

The dissipator  $\tilde{\mathcal{D}}$  describes the reservoir (4.5) in a Markovian approximation. It is not of a Lindblad form, as no secular or rotating wave approximation is performed in order to

keep the frequency structure of the bath. This dissipator has been used in the literature in different contexts, for example in [101, 166, 193], and we report a derivation and other details about it in appendix A.1.  $\tilde{\mathcal{D}}$  is defined by

$$\tilde{\mathcal{D}}[X, Y] = X\rho Y^\dagger + Y\rho X^\dagger - X^\dagger Y\rho - \rho Y^\dagger X \quad (4.16)$$

and it is evaluated in the modified bosonic operators  $\tilde{a}_g, \tilde{a}_l$ , which are dressed by the drive correlation functions. Our model of the drive (4.13) corresponds to  $f_l = 0, f \equiv f_g$ . The modified annihilation operator  $\tilde{a}_g$  is given by

$$\tilde{a}_g = \sum_n \Gamma_{+-}^R(\varepsilon(n+1) - \varepsilon(n)) \langle n|a|n+1\rangle |n\rangle \langle n+1| \quad (4.17)$$

while we don't need  $\tilde{a}_l$  as  $f_l = 0$  (its definition is reported in appendix A.1). The function  $\Gamma_{+-}^R(\omega)$  is evaluated in  $\varepsilon(n+1) - \varepsilon(n) = Un + (\omega_0 + U/2)$ , the level spacing of the isolated single-site Hamiltonian, and it is the retarded part of the box-shaped lesser defined in (4.13), namely  $\Gamma_{+-}^R(t) \equiv \Gamma_{+-}(t)\theta(t)$  and reads

$$\Gamma_{+-}^R(\omega) = \frac{1}{2}\theta(\sigma - |\omega|) - \frac{i}{2\pi} \log \left| \frac{\sigma - \omega}{\sigma + \omega} \right| \quad (4.18)$$

Some more details about those functions are reported in appendix A.1. The imaginary part of  $\Gamma_{+-}^R(\omega)$  is a Lamb-shift term. This terms becomes important when  $\sigma \simeq |\varepsilon(n+1) - \varepsilon(n)|$  because it diverges logarithmically. Staying away from those points and for small dissipation, the Lamb-shift does not affect the results of this chapter, thus we will neglect it.

### 4.3 Finite-frequency instability of the normal phase

The effective action (4.11) is exact, but we need to approximate the generating functional  $\Gamma[\bar{\psi}_i, \psi_i]$  to actually compute some observables. We expand Eq. (4.11) in the fields  $\psi, \bar{\psi}$  and truncate at second order in those fields, performing a gaussian approximation. A gaussian approximation of the effective action is well suited within the normal phase, where the order parameter fluctuates around zero. It is equivalent to a strong-coupling resummation of the perturbation theory in the hopping  $J$  often referred to as random phase approximation (RPA) around the atomic limit [89, 194] and it is well known to capture qualitatively the instability of the Mott phase, as for example discussed in Refs. [91, 111]. We explicit the gaussian action in the Keldysh basis, introducing the classical and quantum components of the fields and grouping them in the vector  $\Psi_i^\dagger = (\psi_{i,c}^*, \psi_{i,q}^*)$ . In this notation, we obtain the effective action

$$\mathcal{S}_{\text{eff}} = \int_{-\infty}^{\infty} \int_{-\infty}^{\infty} dt dt' \sum_{ij} \Psi_i^\dagger(t) \chi_{ij}^{-1}(t - t') \Psi_j(t') \quad (4.19)$$

As we are interested in computing Green functions in the stationary state of the dissipative dynamics, assuming such a stationary state exists, the order parameter inverse Green

function  $\chi_{ij}^{-1}$  will depend only on time differences. In terms of its Keldysh components it reads

$$\chi_{ij}^{-1}(t - t') = \begin{pmatrix} 0 & J_{ij}^{-1} - G_{loc}^A(t - t') \\ J_{ij}^{-1} - G_{loc}^R(t - t') & -G_{loc}^K(t - t') \end{pmatrix} \quad (4.20)$$

where  $G_{loc}^{R/A/K}(t - t')$  are the single-site retarded, advanced and Keldysh Green functions, defined in section 2.2, evaluated in the stationary state of the single-site problem, i.e. at  $J = 0$ . The susceptibility of the order parameter, which corresponds to the retarded component of  $\chi$ , is finally given by

$$\chi^R(q, \omega) = \frac{1}{J_q^{-1} - G_{loc}^R(\omega)} \quad (4.21)$$

$J_q = -2J \sum_{\alpha=1}^d \cos q_\alpha$  is the dispersion of a hypercubic lattice, where the sum is on spatial dimensions, and  $J_q^{-1} = 1/J_q$ . In thermal equilibrium, the  $U(1)$  susceptibility Eq. (4.21) is well known to show a zero-frequency singularity at a critical value of the hopping, at which the Mott insulating phase becomes unstable towards superfluidity [91, 111]. As we are going to show, the behavior of the same quantity in our non-equilibrium state is remarkably different. As it happens for example in [30], out of equilibrium both the unstable mode and the critical hopping have to be determined by setting to zero the denominator of the susceptibility (4.21). It's easy to check that increasing  $J$  the first unstable mode occurs for  $q = 0$ , as long as  $\text{Re}G_{loc}^R(\Omega_*) < 0$ , which is the case here. This leads to the two conditions for the critical point

$$\begin{aligned} 0 &= \text{Im}G_{loc}^R(\Omega_*) \\ 1/(zJ_c) &= -\text{Re}G_{loc}^R(\Omega_*) \end{aligned} \quad (4.22)$$

involving the retarded Green function of the single-site problem.  $z = 2d$  is the coordination number, i.e. the number of neighbours of one site, of the hypercubic lattice; we will absorb it in the hopping parameter redefining it through  $zJ \rightarrow J$  in the rest of the chapter. The first condition determines the frequency of the unstable mode,  $\Omega_*$ , while the second determines the critical hopping  $J_c$ . In figure 4.1 we plot the  $q = 0$  susceptibility, probing the instability of the homogeneous normal phase, for different values of the hopping strength  $J$ , showing a pole at  $\omega = \Omega_*$  when the critical hopping  $J_c$  is reached. Right at  $J_c$  the susceptibility diverges as a power law around  $\Omega_*$ ,  $\chi^R(q = 0, \omega) = \chi_0 / (\omega - \Omega_*)^\alpha$ , with mean-field exponent  $\alpha = 1$ . The appearance of a singularity at finite frequency is a remarkable result with no counterpart in systems in thermal equilibrium, where one expects finite frequency modes to be damped by interactions thus acquiring a finite lifetime, ultimately cutting off the singularity of any dynamical susceptibility. In section 4.3.1, we will interpret  $\Omega_*$  as an effective chemical potential for bosons.

### 4.3.1 Results on the single-site problem

In this section we analyse the one-particle Green functions of the single-site problem, which enter in the effective action (4.19). While consisting only of a single site, this problem

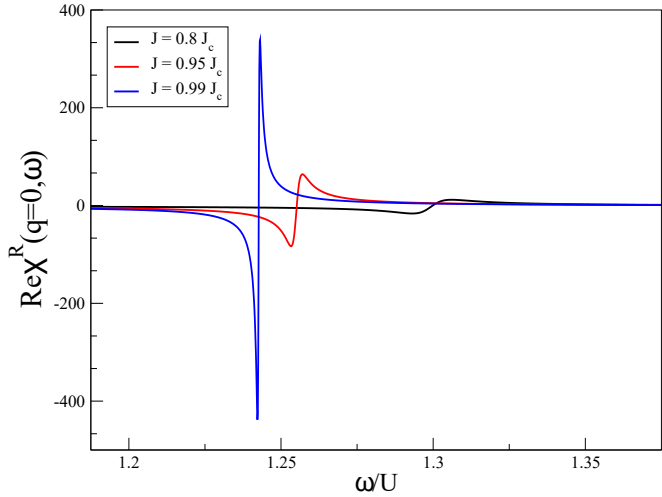


Figure 4.1: Normal phase susceptibility in the gaussian approximation, Eq. (4.21), as a function of frequency and for different values of the hopping  $J$ . The real part of the susceptibility goes through a zero with a characteristic two-peaks structure which gets sharper as the critical value  $J_c$  is approached, turning into a genuine singularity at  $\Omega_*$ . Parameters: Drive amplitude  $f = 0.125U$ , bandwidth  $\sigma = U$ , loss rate  $\kappa = 0.0064U$ , resonator frequency  $\omega_0 = 0.0$ , interaction  $U = 8$ .

remains quite non-trivial due to non-linearity and dissipation and cannot be solved exactly, as in the equilibrium analog [111]. The analysis of this section is based on the drive scheme introduced in section 4.2.2, but the results can be extended to other driving schemes as we will discuss in section 4.3.2. We compute the single-site retarded and Keldysh Green functions – defined in Sec. 2.1 – in the stationary state of the single-site problem. In order to do that we use their Lehmann representation (see Sec. 2.4.3) and a numerical diagonalization of the Liouvillian, truncating the bosonic Fock space to  $N_H = 11$  states. We are interested in the strong-drive  $f \gg \kappa$  and strongly-interacting  $U \gg f, \kappa$  regime for which the finite-frequency transition occurs and we will briefly discuss the opposite regimes in Sec. 4.3.2. In this regime, as we see in the main panel of figure 4.2, the spectral function of single-particle excitations,  $\text{Im}G_{loc}^R$ , features two atomic-like excitations separated by  $U$ . As it has been extensively discussed in Ch. 3, the spectral function of bosonic systems in thermal equilibrium or in their ground state, is constrained to change sign at zero frequency. In the non-equilibrium conditions we consider, the spectral function in 4.2 changes sign at a non-zero frequency which depends on interactions, drive and dissipation. This is precisely  $\Omega_*$ , the unstable mode of the many-body problem at the critical hopping, for which the susceptibility 4.21 diverges. In the inset of figure 4.2 we show that  $\Omega_*$  increases with the drive amplitude  $f$ . This frequency can be interpreted as an emergent chemical potential for bosons, as we can deduce from the bosonic distribution function,

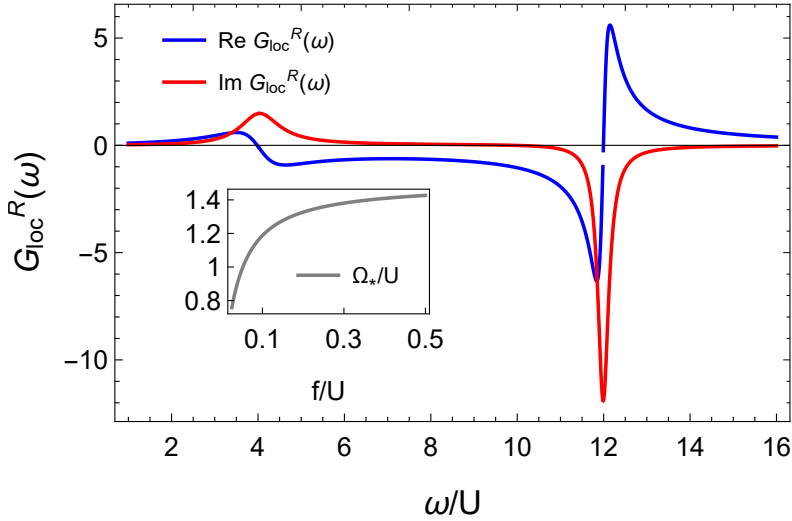


Figure 4.2: Retarded Green function of the interacting single-site problem in Eq. (4.1) with drive and dissipation in the strong-drive regime  $f \gg \kappa$ . The imaginary part, describing the spectral function, shows two peaks separated by a gap of order  $U$ . Crucially, the two peaks are not placed around zero frequency, i.e. the imaginary part changes its sign at a finite frequency  $\Omega_*$ . This emergent frequency is not fixed a priori but rather fully tunable and depending from the amplitude and bandwidth of the drive. The inset shows how it changes with the drive amplitude. Parameters: drive amplitude  $f = 0.125U$ , bandwidth  $\sigma = U$ , loss rate  $\kappa = 0.0128U$ , resonator frequency  $\omega_0 = 0.0$ , interaction  $U = 8$ .

which contains information on the occupation of bosonic modes. We recall that the bosonic distribution function (Sec. 2.1) is defined by

$$F_{loc}(\omega) = \frac{G_{loc}^K(\omega)}{2i\text{Im}G_{loc}^R(\omega)} \quad (4.23)$$

In thermal equilibrium the fluctuation-dissipation theorem (FDT) constraints the distribution function of bosons to  $F_{eq}(\omega) = \coth((\omega - \mu) / (2T))$ . In the non-equilibrium conditions determined by drive and dissipation, FDT does not hold and the distribution function is arbitrary and determined by the dynamics. We plot in figure 4.3 the distribution function for a given value of interaction, drive and dissipation. While its overall shape shows departures from the thermal equilibrium case, we find that around the critical frequency  $\Omega_*$  the system develops a singularity of the form  $F(\omega) \simeq 2T_{\text{eff}} / (\omega - \Omega_*)$ , arising from the fact that  $\text{Im}G_{loc}^R(\omega)$  has a zero at  $\Omega_*$  while the Keldysh component is finite around the same frequency range. By analogy with the low frequency behaviour of the equilibrium distribution function, and discussed in Sec. (2.1), this suggests an asymptotic thermalization around the frequency  $\Omega_*$ . The frequency  $\Omega_*$  thus plays the role of an effective chemical potential for single particle excitations.

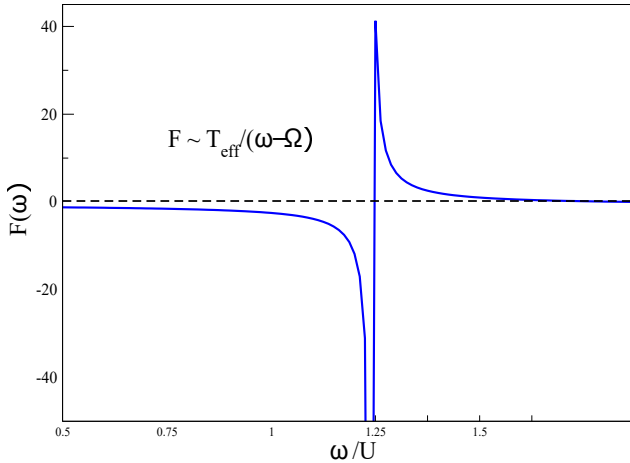


Figure 4.3: Effective Distribution Function as a function of frequency around  $\Omega_*$  for fixed value of interaction, drive and dissipation. Around the frequency  $\Omega_*$  the system develops a singularity which allows to define an effective temperature  $T_{\text{eff}}$ , whose dependence from the drive bandwidth is plotted in the inset. Parameters: loss rate  $\kappa = 0.0128U$ , resonator frequency  $\omega_0 = 0.0$ , drive bandwidth (left panel)  $\sigma = U$ , drive amplitude (right panel)  $f = 0.125U$ , interaction  $U = 8$ .

#### 4.3.2 Discussion on the finite-frequency transition

A zero of the single site spectral function  $\text{Im}G_{loc}^R(\omega)$  at a finite frequency  $\Omega_*$  is the essential feature to get the finite-frequency transition. We discussed in Ch. 3 that a change of sign of the spectral function at finite frequency can be related to a population inversion in the density matrix. Provided drive and dissipation can make the spectral function change sign at a non-zero frequency, then the details about the driving scheme don't matter; our results then apply to a large class of driven-dissipative bosonic lattices. We will discuss an alternative driving scheme, which equally realizes a finite-frequency transition, at the end of Ch. 5. Our finite-frequency phase transition can equally be connected with phenomena of quantum synchronization [163, 164, 181, 182]. The relation of negative spectral functions with dynamical phase transition in the context of quantum quenches has been recently discussed in [154].

For our choice of the drive, such a non-trivial zero is essentially related to the existence of the two-peakes of the spectral function in Fig. 4.2. This structure is there in the strong-drive regime  $f \gg \kappa$ , for which the drive prompts an inversion of populations. In this regime, one also needs that the interaction  $U$  is sufficiently strong with respect to dissipation such that the width of the peaks is smaller compared to  $U$ : by decreasing  $U$  the two peaks merge in a single one, recovering a single-peaked spectrum akin to that of a driven-dissipative linear oscillator, as we discussed in Sec. 3.5.1. Consequently,

there's no zero in the spectral function for small  $U$  and no phase transition in the lattice problem is predicted. As driven-dissipative condensates have been predicted in the weak coupling regime [41], this is a clear artifact of our strong-coupling approach. Namely the field-theoretical approach we use and the weak coupling master equation describing the single-site problem, are both valid for  $U \gg f, \kappa$ . Till now, we considered the strong-drive condition  $f \gg \kappa$ . In the opposite regime  $f \lesssim \kappa$  the zero of the spectral function is also washed away and no phase transition is predicted. This agrees with the existence of a critical drive-to-loss ratio for getting non-equilibrium condensates as in [41].

The evidence of a finite-frequency mode of correlated driven-dissipative bosonic lattices becoming unstable at the critical hopping  $J_c$  is one of the main results of this work. Also, our strong coupling approach shows the existence of a normal phase for  $J < J_c$  in the strong drive regime  $f > \kappa$ , where weak coupling approaches to non-equilibrium condensation in extended systems predict a superfluid phase [41]. In fact, in [41], the condensation transition happens in the drive to loss ratio, regardless of the hopping. In [41] the driven-dissipative condensate oscillates at an effective chemical potential arising at the condensation transition, which is determined semiclassically and it is proportional to the condensation order parameter [41]. Right at the condensation transition, though, where the superfluid order parameter vanishes, a vanishing effective chemical potential is predicted. By contrast, our effective chemical potential,  $\Omega_*$ , is finite at the condensation transition. In fact  $\Omega_*$  equally affects the transient dynamics of the incoherent normal phase where the superfluid order parameter is exactly zero, as we will show in 4.4. This difference comes from our strong-coupling approach around the atomic limit. As such, an accurate quantum-mechanical treatment of interactions, resulting in atomic-like excitations of the single-site problem, is needed to determine  $\Omega_*$ . In section 4.4.1, we derive a field theory describing the transition by expanding the effective action around the unstable mode. The scale  $\Omega_*$ , generated by local interactions and dissipation, is then a parameter entering the effective field theory, that is microscopically determined by (4.22).

## 4.4 Dissipative dynamics

We now discuss the consequences of the finite-frequency instability of the normal phase we have presented so far and investigate the dissipative dynamics of the lattice problem for different values of the hopping  $J$  close to the critical value. To this extent, we use a time-dependent Gutzwiller (tdG) decoupling of the density matrix, i.e.  $\rho(t) = \prod_i \rho_i(t)$  that we further assume homogeneous in space,  $\rho_i(t) \equiv \rho_{loc}(t)$ . This approximation results in an effective single-site problem  $\partial_t \rho_{loc}(t) = -i[H_{\text{eff}}(t), \rho_{loc}(t)] + \mathcal{D}_{loc}[\rho_{loc}]$  where  $H_{\text{eff}}(t) = \omega_0 n + Un^2/2 + zJ(a^\dagger \psi(t) + hc)$  with  $z$  the coordination number of the lattice,  $\mathcal{D}_{loc}$  is the local dissipator including incoherent drive and losses, while  $\psi(t) = \text{tr}(\rho_{loc}(t)a)$  is a self-consistent time-dependent field. We expect this approximation to capture some qualitative features of the dynamics across the phase transition, at least in high enough dimensions, where its mean field description is supposed to be accurate. In figure 4.4 we plot the dynamics of the bosonic order parameter  $\psi(t) = \langle a(t) \rangle$  as a function of time for different

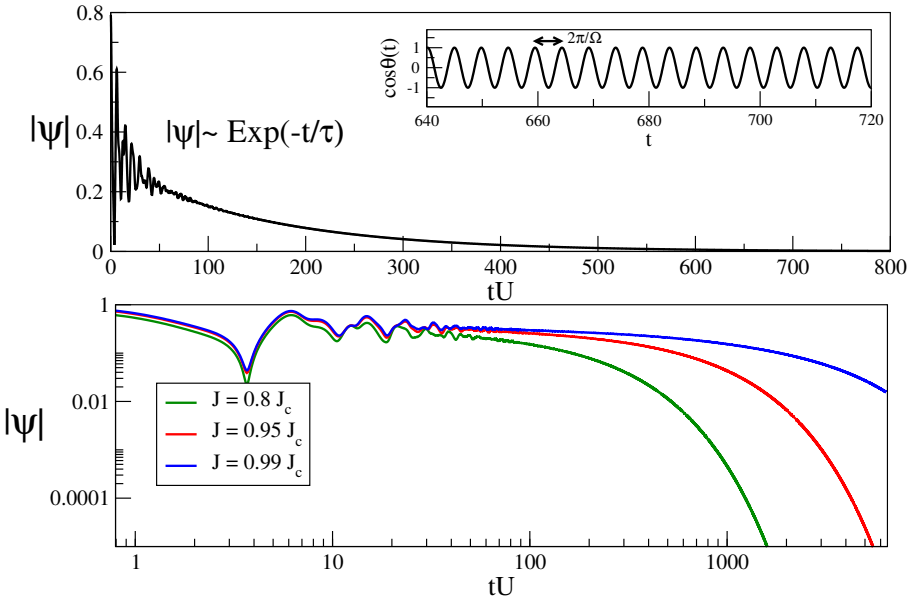


Figure 4.4: Dynamics of the order parameter  $\psi(t) = |\psi(t)|e^{i\theta(t)}$  obtained from the tdG method, for different values of the hopping strength  $J$ . The initial condition is unimportant at long times. (Top Panel) Normal phase,  $J = 0.8J_c$ , exponential decay of the order parameter toward an incoherent stationary state  $|\psi(t \rightarrow \infty)| \sim e^{-t/\tau(J)}$ , with oscillations at frequency  $\Omega(J)$  (see inset) due to the phase linearly growing in time. (Bottom Panel, log scale) Approaching the critical point  $J_c$ , the dynamics slows down suggesting a power-law decay right at the transition, as we show analytically. Parameters: drive amplitude  $f = 0.125U$ , bandwidth  $\sigma = U$ , loss rate  $\kappa = 0.0064U$ , resonator frequency  $\omega_0 = 0.0$ , interaction  $U = 8$ .

values of the hopping  $J \lesssim J_c$ . Introducing a polar representation,  $\psi(t) = |\psi(t)|e^{i\theta(t)}$ , we see that the absolute value of the order parameter shows an exponential relaxation toward zero,  $|\psi(t)| \sim e^{-t/\tau(J)}$ , indicating an incoherent stationary state, while the phase grows linearly in time with finite angular velocity  $\Omega$ ,  $\theta(t) = \Omega(J)t + \theta_0$ . A closer inspection reveals that the characteristic frequency  $\Omega(J)$  differs from the value  $\Omega_*$  previously identified by an amount  $\delta\Omega(J) = |\Omega(J) - \Omega_*|$  which depends on the hopping rate  $J$  and vanishes at the critical point  $J = J_c$  with a characteristic power law,  $\delta\Omega \sim (J_c - J)$ , as shown in the top panel of figure 4.5. Similarly the relaxation time diverges upon approaching the critical hopping  $J_c$ ,  $\tau \sim 1/(J_c - J)$  (see figure 4.5) and the order parameter shows a characteristic critical slowing down, as shown in the bottom panel of figure 4.4.

#### 4.4.1 Nonequilibrium field theory of finite frequency criticality

We now proceed to set up a Keldysh non-equilibrium field theory for the finite-frequency transition, which allows us to obtain a complete analytical picture of the mean field dynamics and sets the stage to discuss the role of quantum fluctuations beyond mean field. The starting point is to expand the effective action (4.11) for  $q \rightarrow 0$  and  $\omega \rightarrow \Omega_*$  and then

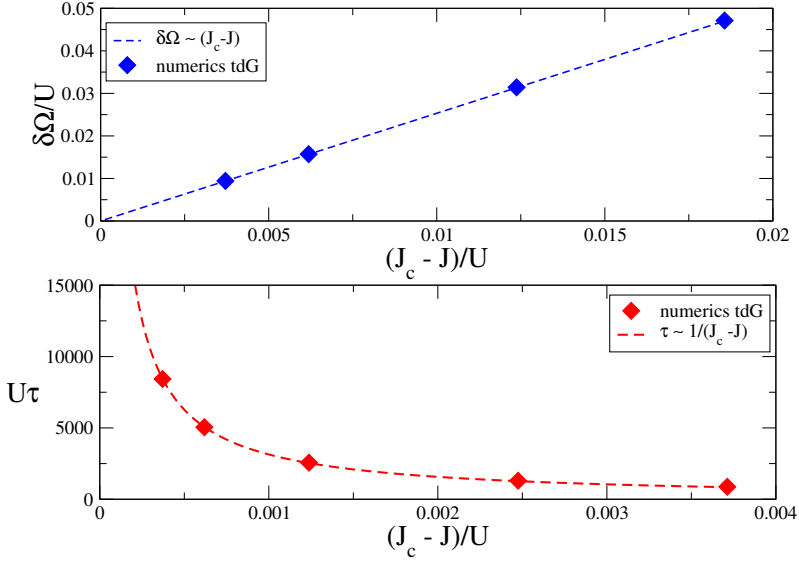


Figure 4.5: Comparison of the results obtained from the tdG method and from Eq. (4.25) for the two scales  $\delta\Omega$  (slow frequency oscillation mode, top panel) and  $\tau$  (relaxation time to reach a steady state, bottom) as a function of the distance from the critical point,  $J_c - J$ . The dissipative dynamical transition is characterized by both energy scales becoming critical. Parameters: drive amplitude  $f = 0.125U$ , bandwidth  $\sigma = U$ , loss rate  $\kappa = 0.00648U$ , resonator frequency  $\omega_0 = 0.0$ , interaction  $U = 8$ .

move to a rotating frame where the field is oscillating at frequency  $\Omega_*$ . Introducing the fields  $\tilde{\psi}_{c,q}(x, t) = e^{-i\Omega_* t} \psi_{c,q}(x, t)$ , we obtain

$$\begin{aligned} \mathcal{S}_{\text{eff}} = & \int dt dx \tilde{\psi}_c^* \left( -r + K_1 i \partial_t + \frac{K_2}{2} \partial_t^2 - K_3 \nabla^2 \right) \tilde{\psi}_q + hc \\ & + \mathcal{S}_{\text{noise}} + \mathcal{S}_{\text{int}} \end{aligned} \quad (4.24)$$

where  $r = 1/zJ + \text{Re}G_{\text{loc}}^R(\Omega_*) = (J_c - J)/J_c^2$  is the distance from the dissipative phase transition while  $K_3 = 1/zJ^2$ . Differently from the weak-coupling action [135] yielding a Gross-Pitaevski equation for the condensate dynamics, the effective action (4.24) features both first and second time-derivative terms, with complex coefficients  $K_{1,2} = \partial_\omega^{1,2} G_{\text{loc}}^R(\Omega_*)$ , a feature of the strong-coupling limit around which we expand. In equilibrium  $K_1, K_2$  play a crucial role for the critical behavior of the transition, which changes universality class at the tip of the Mott lobes, where  $K_1 = 0$ . In the present case we always find numerically  $K_1 \neq 0$  for finite dissipation, suggesting a single universality class for our driving scheme, but this point need to be investigated further. Assuming  $K_1 \neq 0$ ,  $K_2$  is irrelevant under renormalization, as one can tell by scaling arguments and it can be neglected to study the critical dynamics. In Eq. (4.24),  $\mathcal{S}_{\text{noise}} = \int dx dt dt' \tilde{\psi}_q^*(x, t) G_{\text{loc}}^K(t - t') \tilde{\psi}_q(x, t')$  represents the noise contribution, which depends on the Keldysh Green function of the single site. Around  $\Omega_*$  this gives a finite time-local contribution, and thus we can disregard retardation and obtain a purely time local quadratic action with noise term  $\mathcal{S}_{\text{noise}} = D \int dx dt \tilde{\psi}_q^*(x, t) \tilde{\psi}_q(x, t)$ . Here  $D$  plays the role of effective diffusion coefficient in

the equivalent stochastic (Langevin) dynamics and it is indeed given by  $D \simeq G_{loc}^K(\Omega_*) \sim T_{\text{eff}}$ . Finally  $\mathcal{S}_{int}$  accounts for the non-linearities and it is completely determined by the multi-particle Green functions of the driven-dissipative single site problem. If we restrict to interaction terms with one quantum and three classical fields, which is valid in high enough dimensions according to canonical power counting [135], we can write this term as  $\mathcal{S}_{int} = u \int dx dt \tilde{\psi}_q^*(x, t) \tilde{\psi}_c^*(x, t) \tilde{\psi}_c^2(x, t) + hc$ . We can now take the saddle point equation  $\delta S / \delta \tilde{\psi}_q^*(x, t) = 0$  and obtain the equation of motion

$$(iK_1 \partial_t - K_3 \nabla^2 - r) \tilde{\psi}_c + u |\tilde{\psi}_c|^2 \tilde{\psi}_c = 0 \quad (4.25)$$

which takes the form of a complex Ginzburg-Landau equation, well known as a phenomenological description of pattern formation in classical non-equilibrium systems [184–186]. The spatially homogeneous solution of equation (4.25) can be obtained in closed form, as we discuss in the next section, and it describes a transition between a phase where  $\tilde{\psi}_c \rightarrow 0$  for  $t \rightarrow \infty$  and a phase where the modulus of the order parameter saturates to a finite value. We remark that this semi-classical dynamics only describes the evolution in a frame rotating at frequency  $\Omega_*$ . The origin of this energy scale, which is not contained in Eq. (4.25), is instead genuinely quantum mechanical and rooted in the solution of the quantum single site problem, as previously discussed.

#### 4.4.2 Analytical solution of saddle point dynamics

We discuss here more in detail the solution of equation (4.25). Assuming an homogeneous solution and introducing polar coordinates for absolute value and phase of the order parameters  $\tilde{\psi}_c(t) \equiv |\tilde{\psi}_c(t)| e^{i\tilde{\theta}(t)}$  one obtains two separate equations for  $|\tilde{\psi}_c(t)|$  and  $\tilde{\theta}(t)$ , whose solution reads

$$|\tilde{\psi}_c(t)| = |\tilde{\psi}_c(0)| \frac{e^{-\tilde{r}_I t}}{\sqrt{1 + \alpha (1 - e^{-2\tilde{r}_I t})}} \quad (4.26)$$

$$\tilde{\theta}(t) = -\tilde{r}_R t + \tilde{u}_R \int_0^t dt' |\tilde{\psi}_c(t')|^2 \quad (4.27)$$

where  $\tilde{r}, \tilde{u}$  are complex coefficients given by

$$\tilde{r} \equiv \tilde{r}_R + i\tilde{r}_I = r/K_1 \quad (4.28)$$

$$\tilde{u} \equiv \tilde{u}_R + i\tilde{u}_I = u/K_1 \quad (4.29)$$

while  $\alpha = |\tilde{\psi}_c(0)| |\tilde{u}_I| / \tilde{r}_I$ . This solution describes a dynamical transition close to the critical point  $J_c$ . Specifically for  $J < J_c$  the order parameter shows damped oscillations toward zero

$$\tilde{\psi}_c(t) \sim e^{-t/\tau} e^{-i\delta\Omega t} \quad (4.30)$$

with a divergent relaxation time and an oscillation frequency going to zero approaching the transition

$$\tau = 1/\tilde{r}_I \sim 1/(J_c - J) \quad (4.31)$$

$$\delta\Omega = \tilde{r}_R \sim (J_c - J) \quad (4.32)$$

Upon crossing the critical point, for  $J > J_c$ , the dynamics shows instead an amplification of the order parameter which saturates at long times into a train of finite amplitude oscillations

$$\tilde{\psi}_c(t) \sim |\tilde{\psi}_c(\infty)| e^{-i\delta\Omega_{sf}t} \quad (4.33)$$

with  $|\tilde{\psi}_c(\infty)| = \sqrt{|\tilde{r}_I|/|\tilde{u}_I|} \sim \sqrt{J - J_c}$  and  $\delta\Omega_{sf} \sim (\tilde{r}_R + \tilde{r}_I\tilde{u}_R/\tilde{u}_I) \sim (J - J_c)$ . In the normal phase, where the non-linearity  $u$  disappears from the solution (4.27) at long times because  $\tilde{\psi}_c(t) = 0$ , the transient dynamics shows harmonic oscillations while in the broken symmetry phase multiple frequencies are present, at least on intermediate time scales, as encoded in the phase dynamics (4.27). Right at the transition, for  $J = J_c$  when  $\tilde{r}_{R,I} = 0$ , the amplitude of the order parameter decays towards zero as a power-law [34, 36] while the angular velocity vanishes and the phase grows in time only logarithmically,

$$|\tilde{\psi}_c(t)| \sim 1/\sqrt{t} \quad (4.34)$$

$$\tilde{\theta}(t) \sim \log(1 + 2\tilde{u}_I|\tilde{\psi}_c(0)|t) \quad (4.35)$$

By this field-theoretical treatment we found microscopic expressions for the critical scales  $\delta\Omega$  and  $\tau$  (4.31), which determine the mean-field dynamics of the order parameter close to criticality. In Fig. 4.5 we compare those expressions with the numerical values found fitting the Gutzwiller dynamics, finding perfect agreement, which confirms the validity of our analysis.

#### 4.4.3 Discussion

In the previous section we have shown that disregarding (i) retardation effects in the effective action, i.e. expanding all local correlators around the critical frequency  $\Omega_*$ , as well as (ii) disregarding terms higher than quadratic in the quantum fields allow to fully reproduce the results obtained by time-dependent Gutzwiller decoupling, describing the finite-frequency dynamical transition at the mean field level. Still the full effective action in Eq. (4.24) includes the effect of non linearities, noise and quantum fluctuations beyond this semiclassical mean field dynamics that could renormalize the oscillation frequency. These can be captured with a renormalization group treatment of the finite-frequency criticality, along the lines discussed for the equilibrium Bose Hubbard model [195] as well as for weakly interacting non-equilibrium superfluids [41, 46]. Particularly interesting in this respect is the role under renormalization of higher order expansion coefficients in the effective action, such as  $K_1, K_2$  and the next order noise term controlled by  $\partial_\omega G_{loc}^K(\Omega_*)$ . The former are related to emergent symmetries, such as particle-hole in the equilibrium Bose-Hubbard model [111] or the asymptotic equilibrium symmetry in the driven-dissipative condensation, whose deviation results in a KPZ like critical phase dynamics [135]. A term analogous to the latter was shown instead to give rise to non-trivial critical behavior in diffusively driven one dimensional bosons [110]. An interesting question is whether the inclusion of fluctuations beyond the gaussian level could completely wash away the finite-frequency transition or renormalize the critical frequency  $\Omega_*$  down to zero, resulting

in a static transition. While answering this question certainly deserves further investigation, our results suggest that, provided the effective action (4.24) in the rotating frame admits a non-vanishing  $U(1)$  order parameter  $\tilde{\psi}_c \neq 0$ , then the broken symmetry phase in the original frame will display undamped oscillations and breaking of time-translational invariance.

## 4.5 Conclusions

In this chapter we have shown that a prototype model of correlated driven-dissipative lattice bosons develops, for a critical value of the hopping rate, a diverging susceptibility at a non-zero frequency  $\Omega_*$ . The resulting finite-frequency criticality corresponds to the dissipative dynamics lacking of a stationary state and rather oscillating in time without damping. Writing down the effective Keldysh field theory for this finite frequency transition we have obtained its semiclassical limit which we show to reproduce the results of a time-dependent Gutzwiller decoupling of the density matrix. We emphasize that capturing the critical frequency  $\Omega_*$  requires the quantum solution of the single-site dissipative interacting problem and it is therefore not contained in the semi-classical equation of motion we derived, which only describes the dynamics in the frame rotating at  $\Omega_*$ . Our results differ from other studies of limit cycles instabilities in driven-dissipative systems, such as exciton-polariton condensates described by Gross-Pitaevski (GP) types of equation and it could be seen as the strongly correlated version of them. Indeed our transition shares genuine features of a dissipative Mott-superfluid quantum phase transitions being tuned both by coherent couplings and pump/loss rates. In particular our incoherent phase exists at small hopping even beyond the standard threshold of pump greater than losses, an effect which is genuinely quantum mechanical due to the Hubbard repulsion favouring Fock-like states rather than coherent states. Furthermore the frequency of the limit cycle is finite at the transition point, where the superfluid order parameter vanishes, and influences also the normal phase dynamics, while in GP theories it vanishes at that point, being proportional to the superfluid order parameter. Our work suggests several interesting future directions. From one side it would be interesting to include dynamical and spatial fluctuations to study the fate of this dissipative dynamical transition in finite dimensions, following similar investigations done for dynamical transitions in isolated quantum systems [196–198]. Another intriguing open question is whether a similar finite-frequency criticality exists in models of driven-dissipative systems with discrete broken symmetry phases [16] or even in presence of a purely coherent drive, as for example in the context of optomechanical platforms [172, 199] or coherently driven quantum spin chains [188]. Finally, while our work focuses on a paradigmatic model of driven-dissipative bosons which is relevant for the upcoming generation of circuit QED arrays experiments [61, 62, 93], it also outlines a generic framework to study dynamical instabilities in non-equilibrium quantum systems, by focusing on frequency dependent response functions and their divergences. Such a framework has the potential to be applied in a wide range of contexts, including for example driven and isolated Floquet systems, where breaking of discrete time-translational

symmetry has been predicted [118, 119, 200] and observed [121, 201], quantum systems undergoing various forms of synchronization [163, 164, 179, 181, 182, 199, 202] as well as electronic systems under pump-probe optical-irradiation [203]

## Chapter 5

# Dissipative Preparation of Photonic Mott Insulators

The recent experimental advances in controlling dissipation has brought forth the possibility to engineer dissipative processes in order to obtain entangled quantum phases of matter as stationary states of the dissipative dynamics. This follows the concept of dissipative engineering introduced in Sec. 1.3. In Ch. 4 we studied a model of driven-dissipative bosonic lattices and we concentrated on the finite-frequency phase transition driven by the hopping term, that is not related to the specific choice of the drive. In this chapter, instead, we will study the properties of the normal phase stabilized by the driving scheme introduced in 4.2.2, which depend crucially on the choice of the drive. This driving scheme was proposed in [101] to stabilize a Mott insulating phase as the stationary state of the dissipative dynamics. An interesting question to ask is how different this Mott insulating phase is from the equilibrium one. In [101], the authors showed that the stationary state of such a driven-dissipative Bose-Hubbard chain in 1D is very close to the ground state of a 1D Bose-Hubbard model with a proper chemical potential. This similarity extends across both the Mott phase and the superfluid phase and suggests that, out of drive and dissipation, one can get as close as wanted to the ground state. Remarkably though, in [101], the non-equilibrium nature of the problem plays no major role. Their phase diagram for the driven-dissipative stationary state matches pretty well the ground state one in 1D, showing the well known Mott lobes structure [88, 204]. There's no hint in [101] of the finite-frequency transition we discussed in Ch. 4 and even the superfluid phase is stationary. The numerical methods used in [101] are, in fact, tailored to compute the time-independent stationary state of the model, but give no access to dynamical features. On the other hand, driven-dissipative superfluids are well known oscillate in time [30, 41] at an effective chemical potential. Also, in [189], where a similar problem in the hard-core bosons limit is analysed, limit cycles are predicted. It is indeed puzzling to reconcile the completely static, ground-state-like picture of [101], with the dynamical non-equilibrium features predicted for example in [1, 30, 41, 189] for driven-dissipative systems. In this chapter we provide a comprehensive picture allowing to reconcile these results. The dissipative preparation of Mott insulators is relevant for current experiments. In [62], that

we have already briefly discussed in Sec. 1, the authors use energy selective reservoirs to dissipatively stabilize a Mott insulating phase. Their experiment features a 1D chain of 8 non-linear superconducting resonators in a circuit. The chain realizes a lossy Bose-Hubbard model, where the last site is coupled to an energy-selective reservoir that injects photons with energy lower than the many-body gap. In contrast with the model of [101] and with our model (4.2), where each site is driven, in [62] only one site is connected to the reservoir.

In this chapter we study the stability of dissipatively stabilized Mott insulators, obtaining a mean-field phase diagram and making contact with the ground-state problem. The chapter is organized as follows. In 5.1 we introduce the driven-dissipative lattice model. In section 5.2 we discuss the ground-state properties of the single-site problem and the ground-state phase diagram. In section 5.3 we study the driven-dissipative single-site problem, drawing analogies with the ground-state case, and discuss the non-equilibrium phase diagram. Finally, in section 5.4 we discuss a different driving protocol, stabilizing a mixed phase rather than a Mott insulator, and discuss the role of effective thermal fluctuations.

## 5.1 The model

We consider the Bose-Hubbard model already defined in Sec. 4.2, reporting its action (4.2)

$$S = \int_C dt \left( \sum_i \bar{a}_i i \partial_t a_i - H \right) + \sum_i (S_{l,i} + S_{\sigma,i}) \quad (5.1)$$

$$H = \sum_i \left( \omega_0 \bar{a}_i a_i + \frac{U}{2} \bar{a}_i \bar{a}_i a_i a_i \right) - \sum_{\langle ij \rangle} J (\bar{a}_i a_j + \text{hc}) \quad (5.2)$$

where  $H$  is the Bose-Hubbard Hamiltonian and  $S_{l,i}$ ,  $S_{\sigma,i}$  describe the dissipative terms (4.4), (4.5). In Sec. 4.2.1 we discussed how to use a Hubbard-Stratonovich transformation to decouple the hopping term, reducing the lattice problem to computing momenta of its single-site problem. We then truncated the effective action at Gaussian level in Sec. 4.3, which is a well suited approximation to describe the normal phase where the order parameter fluctuates around zero, obtaining the mean-field critical point equation

$$1/(zJ_c) + G_0^R(\Omega_*) = 0 \quad (5.3)$$

This equation determines both  $J_c$  and  $\Omega_*$ , the critical hopping and the mode becoming critical and  $G_0^R$  is the retarded Green function of the single-site problem, which in the following will be either the ground-state one or that of the driven-dissipative stationary-state. We absorb the coordination number  $z$  in the hopping parameter redefining it through  $zJ \rightarrow J$ . We consider the driving scheme already introduced in sections 4.2.2, 4.2.2, which we will refer to as the *cold drive* because, as we will show in section 5.3.1 that it allows to prepare almost pure states with low temperature excitations 5.4.

## 5.2 Ground-state problem

It is interesting, in order to understand the driven-dissipative case, to summarize the ground-state properties of the Bose-Hubbard single-site problem and to discuss how those are related to the ground-state phase diagram in mean-field. As we will see, the cold drive leads to a stationary state of the single-site problem which is very similar to its ground-state, in agreement with the discussions of [101].

### 5.2.1 Single-site ground state

The Bose-Hubbard site Hamiltonian reads

$$H_g = -\mu_g n + \frac{U}{2} n^2 \quad (5.4)$$

where  $\mu_g > 0$  is the chemical potential. It is diagonal in Fock states and the energy of a state with  $n$  bosons is  $\varepsilon(n) = \frac{U}{2} (n - \frac{\mu_g}{U})^2 - \frac{\mu_g^2}{2U}$ , which is a parabola centered at  $-\mu_g/U$ . The ground-state occupation  $n_g > 0$  minimizing the energy therefore is

$$n_g - \frac{1}{2} < \frac{\mu_g}{U} < n_g + \frac{1}{2} \quad (5.5)$$

The ground-state occupation  $n_g$  stays constant for a finite range of chemical potential values given by (5.5). Equivalently  $n_g = \text{ceiling}(\frac{\mu_g}{U} - \frac{1}{2})$ , where  $\text{ceiling}(x)$  is the smallest integer bigger than  $x$ . The one-particle retarded Green function can be easily computed through a spectral decomposition and in the ground-state, given by (5.5), it takes the form

$$G_g^R(\omega) = \frac{n_g + 1}{\omega - \omega_{g+} + i0} - \frac{n_g}{\omega - \omega_{g-} + i0} \quad (5.6)$$

It probes the processes of adding or removing a particle from the ground state, with excitation energies  $\omega_{g+}$  and  $\omega_{g-}$ , which are given by

$$\omega_{g+} = \varepsilon(n_g + 1) - \varepsilon(n_g) = -\mu_g + U \left( n_g + \frac{1}{2} \right) \quad (5.7)$$

$$\omega_{g-} = \varepsilon(n_g) - \varepsilon(n_g - 1) = -\mu_g + U \left( n_g - \frac{1}{2} \right) \quad (5.8)$$

They are respectively positive and negative, as  $\varepsilon(n_g)$  is the ground-state energy, such that  $\varepsilon(n_g) > \varepsilon(n_g + 1), \varepsilon(n_g - 1)$ . The imaginary part  $i0$  is a vanishingly small regularization term. The imaginary part of (5.6) is the sum of two delta functions centered at  $\omega_{g+}, \omega_{g-}$ , while its real part has simple poles at those frequencies. Increasing the chemical potential at fixed  $n_g$ , the excitations  $\omega_{g+}, \omega_{g-}$  shift towards lower energies. The ground state condition (5.5) directly translates into the following bounds for  $\omega_{g+}$  and  $\omega_{g-}$ :

$$-U < \omega_{g-} < 0 \quad 0 < \omega_{g+} < U \quad (5.9)$$

### 5.2.2 Mean-field phase diagram

The ground-state mean-field phase diagram is given by the critical point equation (5.3) for the  $\Omega_* = 0$  mode. The condition  $\text{Im}G_g^R(0) = 0$  is always satisfied in equilibrium, in particular for ground-states, as we discussed in Sec. 3.2.1. The critical hopping is given by

$$1/J_{g,c} = -\text{Re}G_g^R(0) \quad (5.10)$$

Injecting  $G_g^R$  from (5.6), one obtains

$$J_{g,c} = \frac{(U/2)^2 - (Un_g - \mu_g)^2}{\mu_g + U/2} \quad (5.11)$$

yielding the well known Mott lobes in the  $\mu_g/U, J_{g,c}/U$  plane.

## 5.3 Driven-dissipative problem

We now move to analysing the driven-dissipative Bose-Hubbard model (5.1), starting from its single-site problem.

### 5.3.1 Driven-dissipative single-site problem

The master equation of the driven-dissipative Bose-Hubbard site, which we already introduced in Sec. 4.2.2, reads

$$\partial_t \rho = -i [H_s, \rho] + \kappa \left( a \rho a^\dagger - \frac{1}{2} \{ a^\dagger a, \rho \} \right) + r \kappa \left( a^\dagger \rho \tilde{a}_g + \tilde{a}_g^\dagger \rho a - a \tilde{a}_g^\dagger \rho - \rho \tilde{a}_g a^\dagger \right) \quad (5.12)$$

The Hamiltonian  $H_s = \omega_0 n + \frac{U}{2} n^2$  is the same considered for the ground state, with the substitution  $-\mu_g \rightarrow \omega_0 > 0$ . The last term in the master equation describes the cold drive 4.2.2 and we already discussed it in Sec. 4.2.2. We define the drive-to-loss ratio  $r$  and the overall dissipative scale  $\kappa$  and we report the expression of the modified creation operator  $\tilde{a}_g^\dagger$ , which is the hermitian conjugate of (4.17).

$$\tilde{a}_g^\dagger = \sum_n \Gamma_{+-}^A (\varepsilon(n) - \varepsilon(n-1)) \langle n | a^\dagger | n-1 \rangle | n \rangle \langle n-1 | \quad (5.13)$$

$\Gamma_{+-}^A(\omega)$  is evaluated in  $\varepsilon(n) - \varepsilon(n-1) = \omega_0 + U(n - \frac{1}{2})$ , the level spacing of the site Hamiltonian. For the box-shaped lesser  $\Gamma_{+-}(\omega) = \theta(\sigma - |\omega|)$ , we have

$$\Gamma_{+-}^A(\omega) = \frac{1}{2} \theta(\sigma - |\omega|) + \frac{i}{2\pi} \log \left| \frac{\sigma - \omega}{\sigma + \omega} \right| \quad (5.14)$$

that is the conjugate of (4.18). This model is essentially the same as proposed in [101], with a simplification that needs a comment. We considered the box-function  $\Gamma_{+-}(\omega) = \theta(\sigma - |\omega|)$ , while in [101] the authors consider a more physical smoothly-decaying function. Strictly speaking, the markovian approximation leading to the master equation (5.12) is violated by our choice, but, in the small dissipation limit  $\kappa \rightarrow 0$  we will consider, our

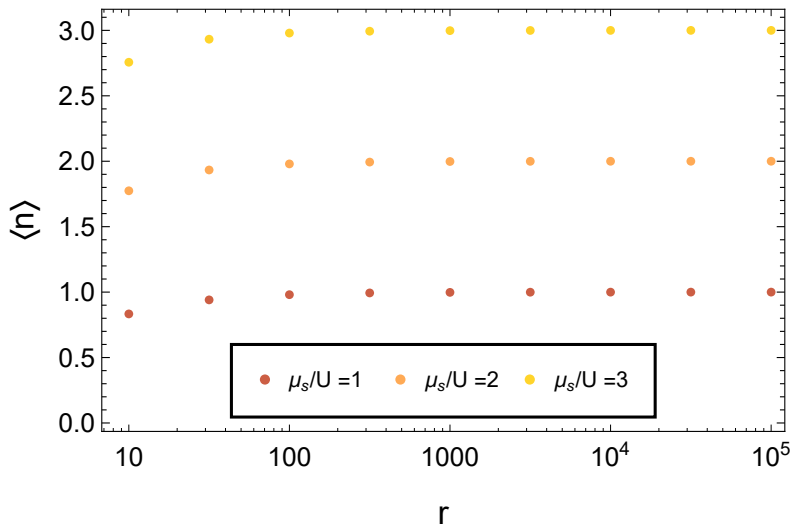


Figure 5.1: Driven-dissipative single-site steady-state average population  $\langle n \rangle$  as a function of the drive-to-loss ratio  $r$ , for different values of  $\mu_s/U$ . For  $r$  sufficiently big, say  $r \gg 1$ , the average population takes almost integer values; the corresponding density matrix is almost pure and only the Fock state with  $n = \langle n \rangle$  is populated. The population changes stepwise with  $\mu_s/U$ , in a photon blockade fashion. Parameters:  $\mu_s/U = 1/2 + 10^{-2}$ ,  $k/U = 10^{-6}$ ,  $\sigma/U = 3.5$ .

choice is consistent and equivalent to their model. A more detailed discussion can be found in appendix A.1. Let's describe the steady state populations of this model, that can be computed analytically. One can easily show that stationary state populations depend only on the drive-to-loss ratio  $r$  and not on the overall dissipative rate  $\kappa$  and that they are determined only by the real part of  $\Gamma_{+-}^A$  which is the theta function  $\frac{1}{2}\theta(\sigma - |\varepsilon(n) - \varepsilon(n-1)|)$ . Consequently only Fock states with up to  $n$  bosons can be populated, with the energy of the  $n$ -th boson such that  $\varepsilon(n) - \varepsilon(n-1) = \omega_0 + U(n - \frac{1}{2}) < \sigma$ , where  $\sigma$  is the bandwidth of the drive. In Fig. 5.1 we show the numerical calculations of the average population as a function of the drive-to-loss ratio  $r$ . For  $r$  sufficiently big, say  $r \gg 1$ , the average population takes almost integer values; the corresponding density matrix is almost pure and only the Fock state with the highest possible occupation, that we call  $n_s$ , is populated. This second condition can be written as  $\omega_0 + U(n_s + \frac{1}{2}) \gtrsim \sigma$ . Defining  $\mu_s = \sigma - \omega_0$ , those two conditions are summarized by

$$n_s - \frac{1}{2} < \frac{\mu_s}{U} \lesssim n_s + \frac{1}{2} \quad (5.15)$$

which is analogous to the ground state condition (5.5) with  $\mu_s$  in place of  $\mu_g$ . Equivalently, the steady state population is  $n_s \approx \text{ceiling}(\frac{\mu_s}{U} - \frac{1}{2})$  as we also show in figure 5.1. Let's now consider the one-particle retarded Green function of the driven-dissipative single-site problem. In the spirit of adding the effect of dissipation on Green functions in perturbation theory, as we have done in Ch. 3, the residues and the poles of the Green function get corrected by dissipative contributions. The retarded one-particle Green function, for  $r \gg 1$

will have main contributions

$$G_s^R(\omega) \approx \frac{n_s + 1 + O(\kappa)}{\omega - \omega_{s+} + i\Gamma(\kappa) + \delta(\kappa)} - \frac{n_s + O(\kappa)}{\omega - \omega_{s-} + i\Gamma(\kappa) + \delta(\kappa)} \quad (5.16)$$

where the lifetime  $\Gamma(\kappa)$  and energy-shift  $\delta(\kappa)$  vanish for  $\kappa \rightarrow 0$ . For small dissipation, the real part of the poles is essentially the same as for the closed system, replacing  $-\mu_g$  with  $\omega_0$ . Recalling that  $\omega_0 = \sigma - \mu_s$ , we get

$$\omega_{s+} \simeq \varepsilon(n_s + 1) - \varepsilon(n_s) = \sigma - \mu_s + U \left( n_s + \frac{1}{2} \right) \quad (5.17)$$

$$\omega_{s-} \simeq \varepsilon(n_s) - \varepsilon(n_s - 1) = \sigma - \mu_s + U \left( n_s - \frac{1}{2} \right) \quad (5.18)$$

Those excitation energies are very similar the ground-state ones (5.7), with  $\mu_s$  in place of  $\mu_g$ , but that they are globally shifted by  $\sigma$ . The stationary state condition (5.15) translates in the bound for  $\omega_{s+}$ ,  $\omega_{s-}$

$$\sigma - U < \omega_{s-} < \sigma \quad \sigma < \omega_{s+} < \sigma + U \quad (5.19)$$

which is analogous to the ground state one (5.9). We remark that even if the stationary state (5.15) of (5.12) is very close to the ground state of a Bose-Hubbard site (5.4) with chemical potential  $\mu_s$ , the excitation energies of the driven-dissipative stationary state are shifted by  $\sigma$  with respect to the ground-state ones, telling that this is a high-energy state rather than the ground-state. The ground-state and stationary-state Green functions coincide in the limit of small dissipation

$$\lim_{\kappa \rightarrow 0} G_s^R(\omega + \sigma) \rightarrow G_g^R(\omega)|_{\mu_s} \quad (5.20)$$

### 5.3.2 Non-equilibrium versus ground-state phase diagram

We now focus on the mean-field phase diagram and take the limit of small dissipation  $\kappa \rightarrow 0$ , while keeping the drive-to-loss ratio large  $r \gg 1$ . In this limit we have shown in 5.3.1 that the properties of the driven-dissipative single site, its occupation and spectrum, resemble those of the ground state of a Bose-Hubbard isolated site, therefore one could expect a ground-state-like phase diagram. We will show that instead the phase diagram of the driven-dissipative model is remarkably different. The equation for the critical point (5.3) is the same as for the ground-state case. Nevertheless, as we already discussed in Ch. 4, under the non-equilibrium conditions determined by drive and dissipation, the mode becoming unstable at the phase transition is not necessarily the  $\omega = 0$  mode, as for ground states, but it must be determined from the critical point equation itself, giving the two conditions for  $\Omega_*$  and  $J_c$

$$0 = \text{Im}G_s^R(\Omega_*) \quad (5.21)$$

$$1/J_c = -\text{Re}G_s^R(\Omega_*) \quad (5.22)$$

The phase-diagram obtained by solving this equations is shown in Fig. 5.2. Some com-

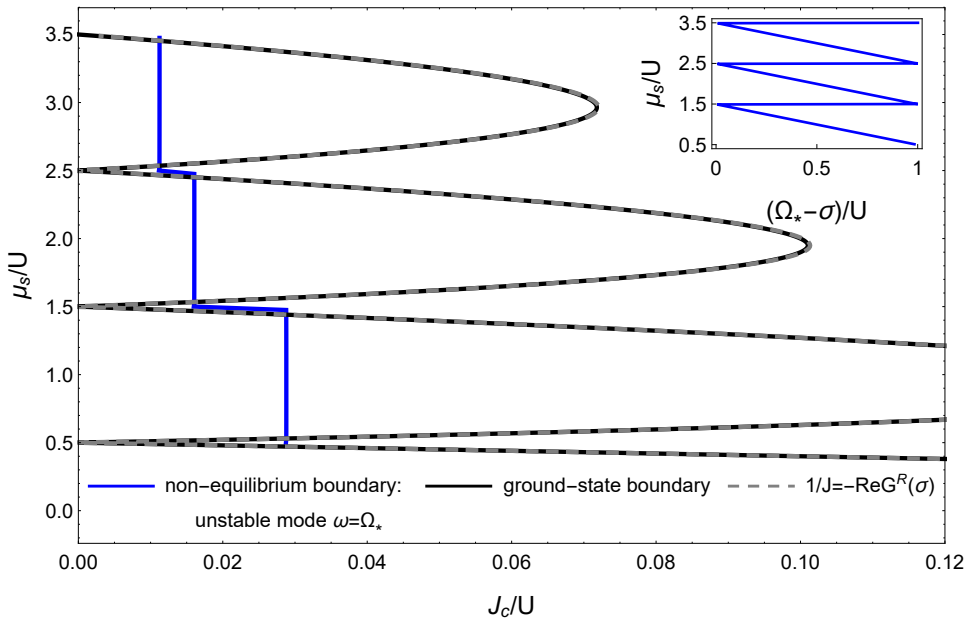


Figure 5.2: Mean-field phase diagram in the  $\mu_s/U$  versus  $J_c/U$  plane featuring a Mott insulating phase on the left and a superfluid phase on the right. Black line: ground state phase diagram of a Bose-Hubbard Hamiltonian with chemical potential  $\mu_s$ . Blue line: non-equilibrium phase diagram of the driven-dissipative Bose-Hubbard model. The dissipatively stabilized Mott insulator becomes unstable at lower hopping than in the ground-state case due to finite-frequency modes instabilities. Dashed-gray line: ground-state-like boundary computed from the driven-dissipative problem solving  $1/J = -\text{Re}G^R(\sigma)$ , which coincides with the ground-state boundary; this is not the phase diagram of the driven-dissipative model. Inset: the critical mode  $\Omega_*$  changes linearly with  $\mu_s/U$  jumping when going from one Mott lobe to the other. Parameters:  $\kappa/U = 10^{-5}$ ,  $\sigma/U = 3.5$ ,  $r = 10^2$ .

ments are due to explain Fig. 5.2, which is one of the most important results of this chapter. The solid black line shows the ground-state phase diagram of a Bose-Hubbard Hamiltonian with chemical potential  $\mu_s$ ; it is obtained from Eq. 5.11, with the replacement  $\mu_g \rightarrow \mu_s$ , and it will serve as a reference for comparison with our non-equilibrium results. Solving (5.22) for both  $J_c$  and the unstable mode  $\Omega_*$ , the non-equilibrium phase-diagram of system is given by the blue line in Fig. 5.2. The critical hopping  $J_c$  is much smaller than the corresponding ground-state value. As a result, the Mott phase is remarkably shrunk with respect to the ground state case and the Mott lobes get “cut off” by finite-frequency modes becoming unstable. The inset of Fig. 5.2 shows the dependence of the unstable mode  $\Omega_*$  on  $\mu_s/U$ . We see that  $\Omega_*$  is linear in  $\mu_s/U$  and it jumps when going from one lobe to the other. This inset is important as it shows that the unstable mode  $\Omega_*$  changes with  $\mu_s/U$ . This is in remarkable contrast with the ground-state critical point equation (5.10), in which the critical mode  $\omega = 0$  doesn’t change with  $\mu_g/U$  and it is the reason why the non-equilibrium phase diagram is remarkably different from the ground-state one. For different values of  $\mu_s/U$  different dynamical modes become unstable determining the “flattening” of the Mott lobes. A priori, due to the analogies between the single-site stationary-state and ground-state, one could have expected that, in the limit of vanishing dissipation  $\kappa \rightarrow 0$ , one would have had  $\Omega_* \rightarrow \sigma$ . In this case, the phase diagram would have been given by the dashed-gray line which coincides with the ground-state phase diagram. The dashed-gray line has been obtained by solving  $1/J = -\text{Re}G_0^R(\sigma)$  at fixed frequency  $\omega = \sigma$  and it coincides with the ground state boundary because the stationary state Green function coincides with the ground state one in this limit (5.20). This coincidence probably justifies the ground-state-like phase diagram found in [193], where the authors study the time-independent stationary state of the many-body master equation, but have no access to dynamical modes. We checked that the limit  $\kappa \rightarrow 0$  is numerically achieved, by showing that the critical hopping  $J_c$  attains a constant value for small enough  $\kappa$ , while keeping the drive-to-loss ratio  $r \gg 1$  fixed. This is shown in Fig. 5.3. We conclude this section by remarking that the small dissipation limit  $\kappa \rightarrow 0$  makes a huge difference in determining the critical point with respect to the ground-state, as it selects the unstable mode driving the transition. For  $\kappa = 0$  strictly, in fact, the equation  $\text{Im}G_g^R(\omega) = 0$  is satisfied for all  $\omega \neq \omega_{g,\pm}$ , while for any finite  $\kappa$  this degeneracy is lifted and there are isolated points at which  $\text{Im}G_s^R(\omega) = 0$ . The limit  $\kappa \rightarrow 0$  is thus non-trivial as it leads to a finite frequency criticality and thus to the spontaneous break of time-translational symmetry.

### 5.3.3 Mott phase stability to drive protocol

In the previous section we have identified a non-trivial non-equilibrium phase-diagram in the limit of small dissipation  $\kappa \rightarrow 0$ , while keeping fixed the drive-to-loss ratio  $r \gg 1$ ; the Mott phase stabilized by drive and dissipation is considerably shrunk in Fig. 5.2 with respect to the ground-state phase diagram as a result of dynamical modes becoming unstable. In this section we will explore the effect of changing  $r$  on the phase diagram. Let’s first recall the effect of  $r$  on populations, which is shown in Fig. 5.1. By decreasing  $r$ , the steady state becomes less pure, departing from the ground-state of a Bose-Hubbard

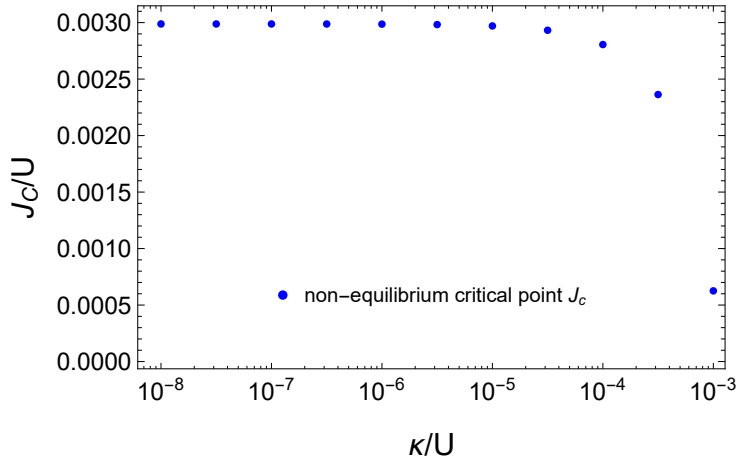


Figure 5.3: Critical hopping  $J_c$  as a function of  $\kappa/U$  at fixed  $r$ . For small enough  $\kappa$ ,  $J_c$  reaches a constant value. Parameters:  $\mu_s/U = 1$ ,  $k/U = 10^{-6}$ ,  $\sigma/U = 3.5$ ,  $r = 10^3$ .

site. In Fig. 5.1 we see that already for  $r = 10$  there's an important departure of population from integer values,  $\langle n \rangle \simeq 0.83$ , while for  $r = 100$  the average population is very close to integer,  $\langle n \rangle \simeq 0.98$ . In Fig. 5.4 we show how the non-equilibrium phase diagram changes by changing  $r$ . We observe the remarkable result that, for increasing values of  $r$  the Mott phase shrinks, until disappearing. This is also shown in the inset of Fig. 5.4 at fixed  $\mu_s/U$ . The other way around, decreasing  $r$  the “Mott” phase expands to higher values of  $J$ ; nevertheless, at the same time it gets less “Mott”, as on-site populations depart from the integer values characterizing a Mott insulator. Our results suggest that there is a trade off between the fidelity of the dissipatively stabilized phase to the Mott ground-state and the robustness of such a phase at finite hopping. A very interesting quantity to look at is the on-site occupation at finite  $J$  as a function of  $r$ . This quantity can be computed in our strong-coupling approach and its calculation will be addressed in the future. For the moment, we can't tell much about the Mott nature of this phase for  $r \gg 1$ , for example about its compressibility, but the numerical results of [101] show that the stationary state of their 7-sites 1D chain reproduces a Mott insulator with very high fidelity. The analysis of this section eventually suggests that the more mixed the “Mott” phase becomes, which at some point will call normal phase rather than Mott, the more this normal phase survives at finite hopping. In the next section we will consider a different driving scheme, that allows to stabilize a much more mixed steady-state, and show that the corresponding phase diagram agrees with this observation.

## 5.4 Changing the driving protocol

In this section we discuss a second driving protocol, that was experimentally realized in [166]. A random classical stochastic field  $\eta$  is modulated with a coherent tone  $\omega_L$  described

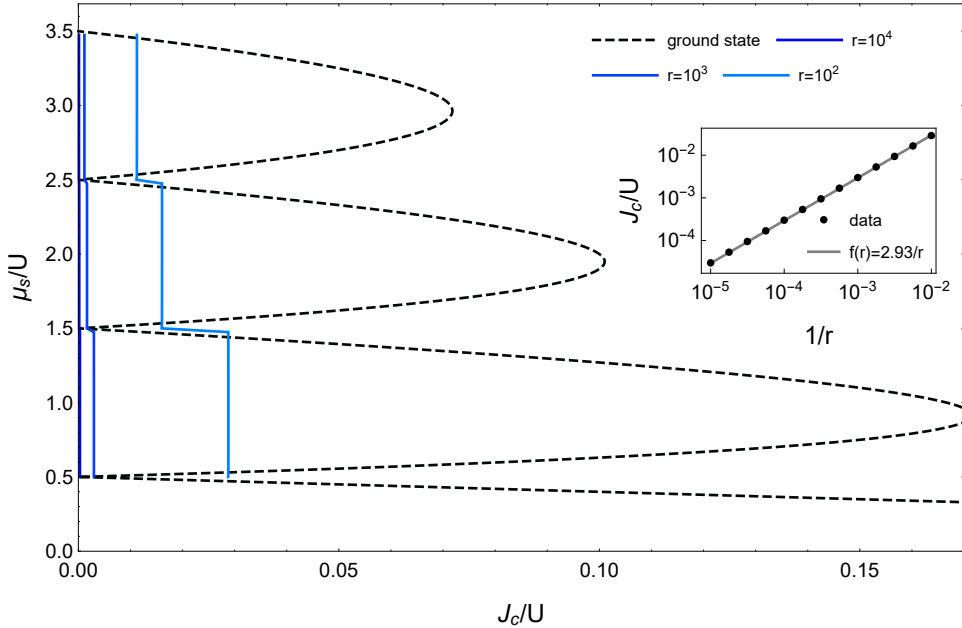


Figure 5.4: Mean-field phase diagram in the  $\mu_s/U$  versus  $J_c/U$  plane featuring a Mott insulating phase on the left and a superfluid phase on the right. Black like: ground state phase diagram of a Bose-Hubbard Hamiltonian with chemical potential  $\mu_s$ . Blue lines: non-equilibrium phase diagram of the driven-dissipative Bose-Hubbard model changing the drive-to-loss ratio  $r$ . Inset:  $J_c/U$  versus  $1/r$  at fixed  $\mu_s/U = 1$ . The region of Mott insulator stability shrinks increasing  $r$ . Parameters:  $kr/U = 10^{-3}$ ,  $\sigma/U = 3.5$ .

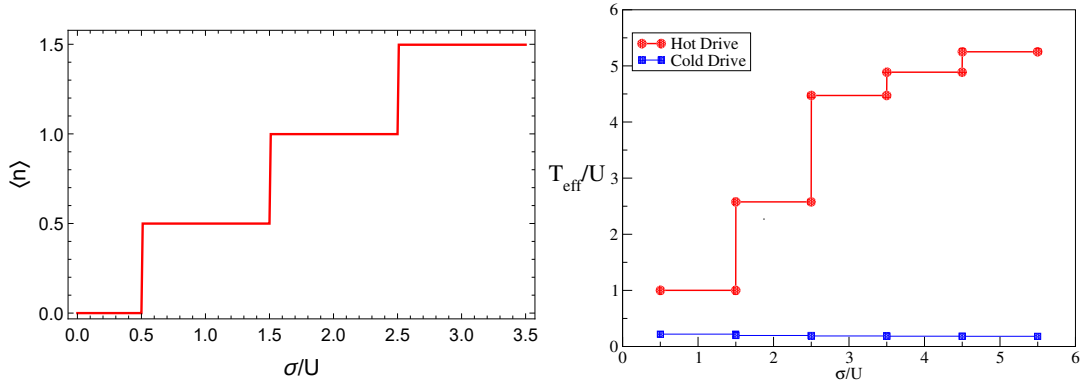


Figure 5.5: Left panel: average stationary state population  $\langle n \rangle$  obtained with the hot drive versus the drive bandwidth  $\sigma/U$ . The occupation increases stepwise showing photon blockade. The hot drive stabilizes half-integer values of the average population for  $r \gg 1$ . Parameters:  $\omega_0 = 0$ ,  $k/U = 10^{-6}$ ,  $\sigma/U = 3.5$ ,  $r = 10^3$ . Right panel: Effective temperature  $T_{\text{eff}}$  as a function of the drive bandwidth  $\sigma$  for the two driving protocols considered. We notice that while in the cold drive case  $T_{\text{eff}}$  depends only weakly on  $\sigma$  and stay small, for the hot drive case it substantially increases as  $\sigma$  (and therefore the number of photons) increases. Parameters:  $\kappa/U = 0.0128$ ,  $\omega_0 = 0$ ,  $\sigma/U = 0.625$ ,  $r = 9.77$ .

by the time-dependent Hamiltonian

$$H_{\text{hot}}(t) = \left( e^{i\omega_L t} a^\dagger \eta(t) + h.c. \right) \quad (5.23)$$

$\eta(t)$  is assumed to have Gaussian statistics with zero average,  $\langle \eta(t) \rangle = 0$ , and two-point correlations with Fourier transform  $\langle \eta(\omega) \eta(\omega') \rangle = f \delta(\omega - \omega') \theta(\sigma - |\omega|)$ . We will refer to this implementation as to the *hot drive* in the following, as opposed to the cold drive considered before. This drive can be described by the already introduced master equation (4.14) involving the modified dissipator (4.16), with  $f_g = f_l = f$  and  $\tilde{a}_g = \tilde{a}_l$  and with equal absorption and emission spectra

$$\Gamma_{+-}^R(\omega) = \Gamma_{-+}^R(\omega) = \frac{f}{2} \theta(\sigma - |\omega|) - i \frac{f}{2\pi} \log \left| \frac{\sigma - \omega}{\sigma + \omega} \right| \quad (5.24)$$

This drive acts both as a source and as a sink of particles with equal rates, much like a high-temperature bath, justifying the name *hot drive*. The corresponding density matrix is diagonal in Fock space and all the Fock states with  $n < \mu_s/U + \frac{1}{2}$  are populated. For  $r \gg 1$  those states get evenly populated, mocking an infinite temperature density matrix with a cut-off, which results in quasi-half-integer populations as we show in Fig. 5.5.

This opposes to the cold drive we previously considered, that stabilizes an almost pure Fock state in the same regime. This discussion about the “temperature” of steady-state populations is corroborated with the calculation of the effective temperature of one-particle excitations. As discussed in 4.3.1, for  $r \gg 1$  one-particle excitations are thermally distributed around  $\Omega_*$ , and thus  $\Omega_*$  can be interpreted as a chemical potential for those

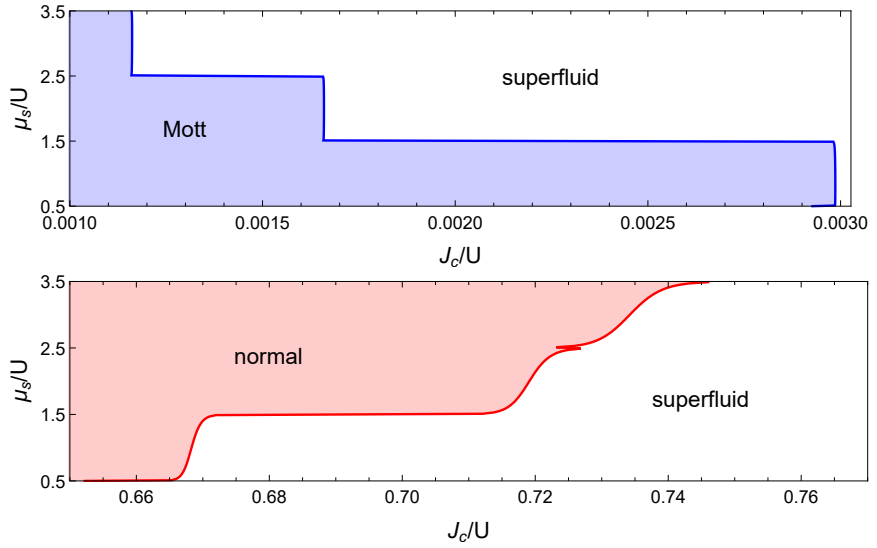


Figure 5.6: Stationary state phase diagram in the  $\mu_s/U$  versus  $J_c/U$  plane, for the two driving protocols considered, namely the cold drive (top panel) and hot drive (bottom panel). For increasing values of  $\mu_s/U$  the critical hopping decreases with the cold drive, as in the ground-state case, and increases with the hot drive, as an effect of effective thermal fluctuations. Parameters:  $k/U = 10^{-6}$ ,  $\sigma/U = 3.5$ ,  $r = 10^3$ .

excitations. The corresponding effective temperatures  $T_{\text{eff}}$  as a function of the drive bandwidth  $\sigma$ , for the two cases of the cold and hot drive, are shown in Fig. 5.5. The dependence of  $T_{\text{eff}}$  is remarkably different between the two cases. Indeed, upon increasing  $\sigma$ , the effective temperature increases for the hot drive while slightly decreases for the cold drive.

#### 5.4.1 Phase diagram

We compare the phase diagram of the cold drive, dissipatively stabilizing a Mott-like phase, with that of the hot drive, creating an incoherent mixed phase, in Fig. 5.6. Some interesting observations follow from this plot. First, we note that the values of critical hopping  $J_c$  for the hot drive are much bigger than for the cold case (the same parameters are used for both drives). Secondly, we notice that, for the cold drive (top panel), by increasing  $\mu_s$  and thus the local occupation, the region in which the normal phase is stable shrinks and the critical hopping  $J_c$  decreases, analogously to the ground-state phase diagram. Vice-versa, with the hot drive (bottom panel) we find the opposite behaviour, namely the critical hopping increases with  $\mu_s$  and the region of normal phase stability expands. We can understand this behaviour from the discussion about the effective temperature of one-particle excitations. Increasing  $\mu_s$ , the effective temperature of excitations increases for the hot drive, with the result of shrinking the broken symmetry region due to the increased thermal fluctuations. This also agrees with the observation that, for the cold drive, the critical hopping increases the more the density matrix is mixed, that is by decreasing  $r$ .

## 5.5 Conclusions

In this chapter we discussed the phase diagram of photonic Mott insulators, dissipatively stabilized using the scheme proposed in [101]. We discussed the similarity between the driven-dissipative stationary state of the single-site problem with the ground-state of a Bose-Hubbard site. This similarity at the single-site level extends to the 7-sites 1D chain studied in [101], where the authors find that this driven-dissipative model has a stationary state reproducing a Mott insulator with very high fidelity. We studied the mean-field phase-diagram of such a dissipatively stabilized Mott insulator in the limit of vanishing dissipation, for which the physics of one isolated site is very close to its ground state. We predicted that, surprisingly, the region of stability of such a phase is remarkably shrunk with respect to the ground-state phase diagram of the corresponding Bose-Hubbard Hamiltonian, due to the onset of dynamical modes instabilities. We found that the bigger the drive-to-loss ratio, the smaller the critical hopping for which the Mott phase becomes unstable. For bigger drive-to-loss ratio, the stationary state is also expected to be closer to the Mott ground state. Accordingly, our results suggest that there is a trade off between the fidelity of the stationary phase to a Mott insulator and robustness of such a phase at finite hopping. The validity of our results beyond mean-field needs to be asserted with more powerful methods. Indeed mean-field theory tends to favour the broken symmetry phase, thus one could expect that fluctuations beyond mean-field would push the Mott-superfluid phase boundary to larger values of the hopping. We expect though that the qualitative trend of the critical hopping decreasing with the drive strength, that arises from the local physics, would remain valid beyond mean-field. We finally studied the phase diagram of a different driving scheme, stabilizing a mixed incoherent normal phase rather than a Mott insulator, showing that effective thermal fluctuations increase the stability region of the normal phase, as expected. The results of this chapter are preliminary and mostly unpublished. The very interesting limit of vanishing dissipation can be solved analytically, computing the Green functions in perturbation theory as we did in Ch. 3. The occupation of the many-body stationary state can be equally computed using our strong-coupling approach. This driven-dissipative model thus turns out to be a very nice toy model to discuss dissipatively stabilized Mott insulators, being at the same time relevant for current experiments [62].

## Chapter 6

# Towards Dynamical Mean Field Theory for Driven-Dissipative Systems

Dynamical mean field theory (DMFT) has emerged in the last two decades as a very powerful approach to study strongly-interacting quantum many-body systems [205]. As for any quantum many-body problem, the exponential scaling of the size of the Hilbert space with the number of degrees of freedom makes it difficult to address big systems numerically. Markovian open systems suffer even more of this limitation, as the natural space to numerically treat those problems is the Liouville space (Sec. 2.3), whose size is the square of that of the original Hilbert space. Several methods have recently been proposed, which are mostly limited to 1D or to small system sizes. Tensor network schemes [206–208] are very efficient for 1D systems, but are still limited in higher dimensionalities despite the ongoing efforts [209]. A promising method for 2D is the corner space renormalization method [53, 156]. Recently a Monte Carlo method has been proposed [210], but its applicability it's limited by its sign problem. Beyond mean field methods such as cluster methods [157, 211] and the self-consistent projection operator [20, 212] are also promising techniques. Finally, four groups have independently proposed a neural-network ansatz for the density matrix of many-body open systems [213–216], following the proposal for closed system [217]. This approach looks promising, but its strengths and limitations still need to be assessed. Developing a DMFT approach to driven-dissipative quantum many-body systems would fill a gap in this scenario. DMFT is a non-perturbative strong-coupling technique that maps a lattice many-body problem in the thermodynamic limit onto an auxiliary problem describing a single-site coupled to a self-consistent bath, that we will call *impurity problem*. This is in the spirit of standard mean field theory, where a lattice problem is mapped onto a single-site problem in a self-consistent field. The qualitative difference is that the effective problem in mean-field is described by an Hamiltonian, while in DMFT retardation effects that one site experiences as an effect of the rest of the lattice are taken into account and the effective theory must be described in terms of an action,

which is non-local in time, hence the name dynamical mean field theory. Being formulated directly in the thermodynamic limit, DMFT is not limited to small system sizes as most of the already existing methods. The bottleneck of DMFT is that solving the auxiliary impurity problem is not an easy task, but it is still by far easier than solving the original lattice problem. As a result, one needs appropriate methods, which we will call *impurity solvers*, to solve the auxiliary problem.

The work presented in this chapter is the first attempt towards solving DMFT for driven-dissipative lattice problems. In section 6.1 we will introduce DMFT for driven-dissipative bosonic particles on a lattice, compare it with mean field theory and in 6.2 we will discuss the need for developing a tailored impurity solver for driven-dissipative systems. The development of the impurity solver will occupy the core of the chapter from section 6.3 on and a more detailed outline of the chapter will be given at the end of Sec. 6.2.

## 6.1 Driven-dissipative bosonic DMFT

DMFT was developed [218, 219] to give new insights on strongly-correlated fermionic systems in equilibrium, for example to shed light on the Hubbard model conundrum [205, 220]. Following its success for fermionic systems in equilibrium, it has been extended to bosons [221, 222] and to out-of-equilibrium conditions [223–225]. We will discuss DMFT in the context of bosonic systems, as we have in mind the experimental realizations discussed in Ch. 1 which involve bosonic particles. As we are interested in driven-dissipative systems, we must use the real-time, non-equilibrium formulation of DMFT, which for bosons was derived in [226] and that we will briefly discuss in this section. For bosons, the standard mean-field theory, that consists in decoupling the hopping introducing a self-consistent external field, becomes exact in the  $z \rightarrow \infty$  limit, where  $z$  is the coordination number of the lattice, i.e. the number of neighbours of each site. Bosonic DMFT improves on mean-field theory by adding first-order corrections in  $1/z$  or, equivalently, by adding second-order corrections in the fluctuations of the bosonic field [221, 226]. This is very different for fermions, for which DMFT is the theory recovered in the limit  $z \rightarrow \infty$  [205, 219].

We consider a generic problem of bosonic particles on a lattice with on-site drive and dissipation described by a Markovian master equation with jump operators  $L_{i\alpha}$ ; each site has Hamiltonian  $H_{0,i}$ , possibly strongly-interacting, and nearest-neighbours sites are coupled with a hopping term with strength  $J$ . The Keldysh action describing the problem, following the mapping of section 2.3, reads

$$S = \sum_i S_{0,i} + \sum_{\langle ij \rangle} \frac{J}{z} \int_C dt (\bar{a}_i a_j + \text{hc}) \quad (6.1)$$

$$S_{0,i} = \int_C dt (\bar{a} i \partial_t a - H_{0,i}) - i \int_{-\infty}^{\infty} dt \sum_{\alpha} \gamma_{\alpha} \left( L_{i\alpha+} \bar{L}_{i\alpha-} - \frac{1}{2} (\bar{L}_{i\alpha+} L_{i\alpha+} + L_{i\alpha-} \bar{L}_{i\alpha-}) \right) \quad (6.2)$$

The rescaling of the hopping strength  $J$  with the lattice coordination number  $z$  is necessary

to yield the correct  $z \rightarrow \infty$  limit [221]; the scaling for fermions would be instead  $J/\sqrt{z}$  [205]. We make the further assumption that all lattice sites are equivalent. DMFT maps the action (6.1) onto an effective action  $S_{\text{eff}}$  describing a single-site, that we will call the impurity, coupled to a field  $\Phi_{\text{eff}}$  and to a bath  $\Delta$ <sup>1</sup>:

$$S_{\text{eff}} = S_0 + \int_C dt \Phi_{\text{eff}}^\dagger(t) \mathbf{a}(t) - \frac{1}{2} \int_C dt dt' \mathbf{a}^\dagger(t) \Delta(t, t') \mathbf{a}(t') \quad (6.3)$$

$$\Phi_{\text{eff}}^\dagger = J \Phi^\dagger(t) + \int_C dt' \Phi^\dagger(t') \Delta(t', t) \quad (6.4)$$

We have dropped the site indices as all the terms in (6.3) refer to the same site. We refer to [226] for the derivation of this action and we remark that their derivation naturally applies also to our case of driven-dissipative lattices as long as drive and dissipation do not couple different lattice sites. The boldened fields  $\mathbf{a}, \Phi_{\text{eff}}, \Phi$  represent Nambu vectors, for example  $\mathbf{a}^\dagger = (\bar{a}, a)$ , which one needs to introduce in order to describe bosonic condensates, while  $\Delta$  is a matrix in this space. The action  $S_0$  describes the local, interacting driven-dissipative single-site problem, that we can solve numerically formulating it in terms of a Markovian master-equation, as we have done in Ch. 4 and 5.

The field  $\Phi$  and the bath  $\Delta$  need to be determined self-consistently from the effective action  $S_{\text{eff}}$  itself. The self-consistent condition for the first is simply given by  $\Phi = \langle \mathbf{a} \rangle$ . The key approximation of DMFT allows to determine a self-consistent condition for  $\Delta$ . This approximation consists in taking the lattice self-energy to be local in space

$$\Sigma_{ij}(t, t') \simeq \Sigma(t, t') \delta_{ij} \quad (6.5)$$

The Green function of the original lattice model is then given by the Dyson equation

$$\mathbf{G}_{ij}(t, t')^{-1} = \delta_{ij} [\mathbf{G}_{ni}(t, t')^{-1} - \Sigma(t, t')] - J_{ij} \mathbf{I} \quad (6.6)$$

where  $\mathbf{G}_{ij}(t, t') = -i \langle T_C \mathbf{a}_i(t) \mathbf{a}_j^\dagger(t') \rangle + i \Phi_i(t) \Phi_j^\dagger(t')$  is the connected part of the Green function,  $\mathbf{G}_{ni}^{-1}$  is the inverse, non-interacting Green function of the single-site problem and  $\mathbf{I}$  is the identity in Nambu space. The inverse Green function of the impurity computed by the effective action (6.3) is given by

$$\mathbf{G}(t, t')^{-1} = \mathbf{G}_{ni}(t, t')^{-1} - \Delta(t, t') - \Sigma(t, t') \quad (6.7)$$

In order for the effective impurity (6.3) to represent the original lattice problem, the Green function of the impurity must be the same as the local Green function of the lattice, that is  $\mathbf{G}(t, t') = \mathbf{G}_{ii}(t, t')$ , where to obtain  $\mathbf{G}_{ii}(t, t')$  one needs to invert  $\mathbf{G}_{ij}(t, t')^{-1}$ . Equations (6.6) and (6.7) provide the implicit relation between  $\mathbf{G}(t, t')$  and  $\Delta(t, t')$ . This relation can be made more formal in terms of Hilbert transforms, as in [205, 221] and involves the non-interacting density of states of the lattice. Taking the  $z \rightarrow \infty$  limit,  $\Delta \propto 1/z$  vanishes and (6.3) reduces to describing an isolated site in an external field, recovering standard mean-field theory.

---

<sup>1</sup>Note that here we use the convention  $Z = \int e^{iS}$  rather than  $Z = \int e^{-iS}$  that is used in [226].

## 6.2 Auxiliary impurity problem

In order to solve DMFT, one needs to solve the auxiliary impurity problem, where by “solving” we mean computing  $\langle \mathbf{a} \rangle$  and  $\mathbf{G}$  from the effective action (6.3). If one is able to compute those quantities, then the  $\Phi$  and  $\Delta$  can be updated using the self-consistent conditions described above, determining a new effective action; one then iterates this procedure until a fixed-point is reached, corresponding to the solution of the impurity problem. Unfortunately, solving the auxiliary impurity problem is not an easy task. In appendix B.2, we discuss a simple approximation which allows to solve the impurity problem analytically in the symmetric phase, which is known as the Hubbard-I approximation. This approximation allows for example to compute the local occupation and the one-particle spectral function at finite hopping. This already goes beyond simple mean-field theory, which describes the symmetric phase as a bunch of decoupled sites, giving no information on the hopping dependence of any quantity. The Hubbard-I approximation can be shown to coincide [227] with the strong-coupling Gaussian approximation 4.2.1 we used in Ch. 4.5. In particular, when applied to the Bose-Hubbard model we discussed in Ch. 4, it yields the same phase boundary for the normal to superfluid transition as mean-field. This is discussed more in details in appendix B, where we actually derive a non-trivial equation for the critical point in DMFT which goes beyond the mean-field equation (4.22) and we show that it reduces to mean-field in the Hubbard-I approximation. As a result, we need a more powerful impurity solver to go beyond the strong-coupling Gaussian description of Ch. 4.5 with DMFT and to obtain a beyond mean-field phase diagram. This motivates the rest of the chapter, in which we will derive a solver for the DMFT auxiliary impurity problem, tailored to address driven-dissipative lattice models.

Methods to solve the dynamics of quantum impurity models have flourished in recent years. The motivation comes from studying models of quantum dissipation and macroscopic quantum tunneling in the early days of Caldeira-Leggett and spin-boson models [228, 229] which keep attracting a lot of interest [230–232] or from diluted magnetic impurities in metals [233] and transport through quantum dots and single molecules attached to leads [234–236] leading to fermionic realizations of so called quantum impurity models. These consist of a small quantum systems with few interacting degrees of freedom, the impurity, coupled via hybridization to a gapless reservoir of fermionic or bosonic excitations. The dynamical correlations of such reservoirs, which decay in time as power laws at zero temperature and feature strong memory effects [237], together with local interactions, make quantum impurity physics highly non-trivial. The non-equilibrium impurity solvers may be classified into two classes: diagrammatic approaches and methods based on Hamiltonian diagonalization [225]. The most powerful techniques are based on diagrammatic Monte Carlo [238–246], giving numerically exact results in some cases, but in many cases these are affected by a nasty sign problem, limiting their application. We will develop an approximate technique, based on a self-consistent diagrammatic resummation known as the Non-Crossing Approximation [226, 247–251].

In the context of driven-dissipative lattice systems, the auxiliary impurity problem

(6.3) describes a driven-dissipative site, where losses and pump are described in terms on a Markovian master equation, which is further coupled to the self-consistent bath  $\Delta$  (and field  $\Phi$ ). An ideal impurity solver would allow to describe the physical, Markovian dissipation using the efficient formalism of Markovian master equations, while resorting to more involved methods to take into account the effect of the self-consistent, non-Markovian bath  $\Delta$  introduced by DMFT.

Apart from using it for DMFT, such a solver would allow to study models of quantum impurities in presence of both Markovian and non-Markovian losses. The two paradigms of Markovian and non-Markovian dissipation represent two well studied, yet substantially separated, paradigms of open quantum systems. The former has mostly been investigated in the context of quantum optics, quantum electronics and quantum information science where major efforts are devoted to design non-linear dissipative processes which act as a resource for quantum state preparation (see Sec. 1.3). The latter has been studied in the context of impurity in metals and transport through quantum dots, as we have already mentioned. The interest around quantum impurity problems featuring both Markovian and non-Markovian dissipation has recently grown [252–254]. Mesoscopic quantum devices have been successfully coupled to electromagnetic resonators hosting dissipative photon fields [255–258] offering the possibility to investigate the fate exotic many body phases such as the Kondo effect in presence of Markovian dissipation.

Taking inspiration from recent developments in quantum impurity physics [238–241] we develop an hybridization expansion for the real-time evolution operator of the impurity, in presence of both Markovian and non-Markovian dissipation. The final result naturally generalizes the well known real-time hybridization expansion [225, 240, 259] to impurities with an intrinsic quantum Markovian, rather than unitary, dynamics. In addition to its own interest and potential for the development of diagrammatic Monte Carlo sampling, this expansion allows us to formulate a Non-Crossing Approximation. We derive and discuss in details this approach and test it on a simple fermionic model coupled to a zero temperature bath and in presence of Markovian dissipation. Those results have been published in [3].

The rest of the chapter is organized as follows. In section 6.3 we give a general formulation of the impurity model and we introduce its reduced dynamics. Section 6.4 is devoted to derive the hybridzation expansion for the real-time impurity propagator, after tracing out the non-Markovian bath (section 6.4.1) and the Markovian environment (section 6.4.2). In section 6.5 we define diagrammatic rules and obtain a Dyson equation for the impurity propagator. In section 6.6 we develop a self-consistent resummation based on the Non-Crossing Approximation, while in section 6.6.3 we apply this method to a simple model of a fermionic impurity, showing interesting effects due to the simultaneous presence of Markovian and non-Markovian dissipative processes.

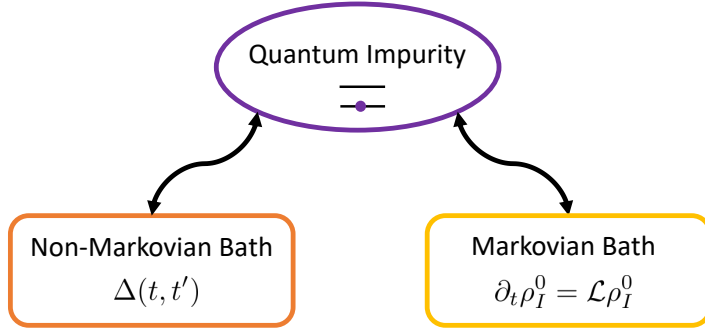


Figure 6.1: Schematic plot of the setup considered in this manuscript. A small quantum system (impurity) is (i) bilinearly coupled to a quantum bath whose non-trivial correlations, encoded in the hybridization function  $\Delta(t, t')$ , lead to non-Markovian behavior and (ii) coupled non-linearly to a Markovian bath whose effect on the impurity is described by a Lindblad master equation. The resulting quantum impurity model with mixed Markovian and non-Markovian dissipation is studied using hybridization expansion techniques.

### 6.3 Formulation of the impurity problem

We consider a model of a quantum impurity, a small quantum system with a finite number of bosonic (fermionic) degrees of freedom  $[d_a, d_b^\dagger]_\pm = \delta_{ab}$  and with Hamiltonian  $H_I[d_a, d_a^\dagger]$ , coupled to two different quantum baths (see figure 6.1). We will denote the Hamiltonian of the baths with  $H_M$  and  $H_{\bar{M}}$ , where the subscripts refer to the fact that  $\bar{M}$  is a non-Markovian bath and  $M$  is a Markovian one. We describe the two environments as a collection of non-interacting bosonic (fermionic) modes, respectively for a bosonic (fermionic) impurity:

$$H_M = \sum_p \omega_p b_p^\dagger b_p \quad H_{\bar{M}} = \sum_k \varepsilon_k c_k^\dagger c_k \quad (6.8)$$

The total Hamiltonian therefore reads

$$H = H_I + H_M + H_{IM} + H_{\bar{M}} + H_{I\bar{M}}$$

where we have introduced the two coupling terms between the impurity and the  $M$  and  $\bar{M}$  baths. We will consider the impurity to be bilinearly coupled to the  $\bar{M}$  bath, i.e. through a coupling Hamiltonian of the form

$$H_{I\bar{M}} = \sum_{ka} V_{ka} (d_a^\dagger c_k + h.c.) \quad (6.9)$$

while the coupling between the impurity and the  $M$  bath is taken of the most general form for which one can derive a Lindblad master-equation [136]:

$$H_{IM} = \sum_\alpha X_\alpha B_\alpha \quad (6.10)$$

with  $X_\alpha = X_\alpha^\dagger$ ,  $B_\alpha = B_\alpha^\dagger$  generic operators respectively of the impurity and of the Markovian bath.

Defining the time evolution operator of the entire system as  $U(t, 0) = e^{-iHt}$  and given an initial condition for the system density matrix  $\rho(0)$  we can formally write down the reduced density matrix of the impurity at time  $t$ , tracing out the degrees of freedom of the two environments

$$\rho_I(t) = \text{tr}_{M\bar{M}} [U(t, 0)\rho(0)U^\dagger(t, 0)] \quad (6.11)$$

from which the dynamics of simple impurity observables can be readily obtained as  $O_I(t) = \text{tr}[\rho_I(t)O_I]$ . With the assumption that the initial density operator of the environment and the impurity factorizes [136], we can define the evolution operator of the reduced dynamics

$$\rho_I(t) = \mathcal{V}(t, 0)\rho_I(0) \quad (6.12)$$

This reduced density operator and its evolution operator are the key quantities over which we will focus our attention throughout the chapter. Performing the trace over the environment degrees of freedom is a highly non-trivial problem. In the following we will obtain two main results. The first one is a formal series from  $\mathcal{V}$  to all orders in the coupling with the non-Markovian bath, called hybridization expansion, and the second one is a closed equation for  $\mathcal{V}$ , based on a self-consistent resummation of the series. We stress that the order in which the trace over the two environments is taken in Eq. (6.11) is not crucial. While in this work we will proceed by first taking the trace over the non-Markovian environment, resulting in an hybridization expansion, and then over the Markovian one, we could have equally reversed this choice and still obtain the same final result.

## 6.4 Hybridization expansion

In this section we derive a formal hybridization expansion (6.26) for the reduced density matrix of the impurity. Such an expansion is usually derived in the context of quantum impurity models coupled to a single bath, as a starting point to develop exact Monte-Carlo sampling [239, 240] or approximated resummation techniques [225, 250] to solve the problem. There the formulation is typically done at the level of the partition function, i.e. tracing out also the impurity degrees of freedom, while we are interested in the reduced density matrix and the evolution operator, see Eq. (6.12), therefore we will not perform such a trace, a fact that will result in some formal difference in the approach. More importantly, here the quantum impurity is also coupled to a second Markovian environment that we will need to trace out as well and this can be done exactly under the assumption that the  $IM$  subsystem obeys a Markovian Lindblad master equation [7, 136].

### 6.4.1 Tracing over the non-Markovian bath

We begin by performing the trace over the non-Markovian environment which is quadratic in terms of bath operators and bilinearly coupled to the impurity. Such a trace could be performed exactly within a path integral formulation leading to an effective Keldysh action

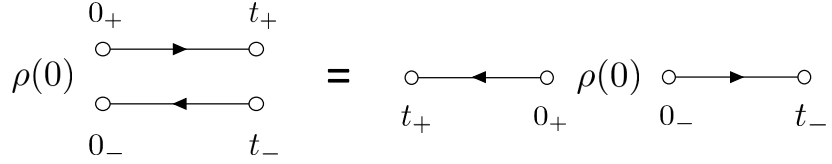


Figure 6.2: Two equivalent pictorial representations of the Schwinger/Keldysh contour  $C(t, 0)$ , describing the non-equilibrium evolution of an initial density operator  $\rho(0)$  from time 0 to time  $t$ . The two branches of the contour are usually called + and - and they correspond to the two time evolution operators applied to the left and to the right of the initial density operator, as in Eq. (6.13).

which is non-local in time. Here we proceed instead at the operator level by noticing that the trace could be taken exactly order by order in an expansion in the the coupling between the non-Markovian environment and the impurity.

In order to derive this expansion, we write down the full Hamiltonian of the system as  $H = H_0 + H_{\bar{M}} + H_{I\bar{M}}$ , describing respectively the impurity embedded in the Markovian bath ( $H_0 = H_I + H_M + H_{IM}$ ), the non-Markovian environment and its coupling to the impurity. We then move to the interaction picture with respect to the Hamiltonian  $H_0 + H_{\bar{M}}$ . Introducing the standard time-ordering and anti-time-ordering operators  $T_t$  and  $\check{T}_t$ , the density operator becomes

$$\begin{aligned} \rho(t) = & e^{-i(H_0+H_{\bar{M}})t} T_t e^{-i \int_0^t dt' H_{I\bar{M}}(t')} \rho(0) \times \\ & \times \check{T}_t e^{i \int_0^t dt' H_{I\bar{M}}(t')} e^{i(H_0+H_{\bar{M}})t} \end{aligned} \quad (6.13)$$

We will perform a simultaneous expansion in powers of  $H_{I\bar{M}}(t')$  both on the left and on the right of the initial density operator  $\rho(0)$ . A formal way to manage a single series expansion and to write all the operators on the left side of the density operator, is to use the formalism of the Schwinger/Keldysh double contour [131, 132] (see Sec. 2.2). Actually, the contour we consider does not extend up to infinite times, thus we call it  $C(t, 0)$ , and it is an “open” version of the Keldysh contour (Fig. 6.2); the reason for this difference is that we are not performing the trace on the impurity degrees of freedom, as it is done in the Keldysh path integral. Operators on the left (right) side of  $\rho(0)$  are assigned a + or - label, so that the couple  $(t, \gamma)$  with  $\gamma \in \{+, -\}$ , allows to locate one operator on the double contour. For convenience, we will attach the  $\pm$  indices to times, rather than to operators, as it is usually done in Keldysh field theory (the reader can compare the notation with Sec. 2.2). We will use the short notation  $t_\gamma \equiv (t, \gamma)$ . The fact that the contour is “open” means the maximum times on the different branches do not coincide:  $t_+ \neq t_-$ . The time-ordering on the contour is defined as usual, as well as the contour-time-ordering operator  $T_C$ , with the understanding that once time ordered, the operators belonging to the - branch of the contour have to be brought on the right side of the density matrix, as if we were exploiting the cyclic property of a trace.

Finally we define contour integrals as  $\int_{C(0,t)} dt \equiv \int_0^{t+} dt_+ - \int_0^{t-} dt_-$ . One can show

that the density operator evolution (6.13) can be written in the compact form

$$\rho(t) = T_C e^{-i(H_0 + H_{\bar{M}})(t_+ - t_-)} e^{-i \int_{C(0,t)} dt' H_{I\bar{M}}(t')} \rho(0)$$

and, accordingly, the evolution operator defined in (6.12) can be written as

$$\mathcal{V}(t, 0)\rho_I(0) = \text{tr}_{M\bar{M}} \left[ T_C e^{-iH_0(t_+ - t_-)} e^{-i \int_{C(0,t)} dt' H_{I\bar{M}}(t')} \rho(0) \right] \quad (6.14)$$

where we dropped  $H_{\bar{M}}$  using the cyclic property of  $\text{tr}_{\bar{M}}$ . In order to perform the partial trace on the non-Markovian environment, we assume that at time  $t = 0$  there's no entanglement between the non-Markovian bath and the rest of the system, such that the density operator factorizes  $\rho(0) = \rho_{IM}(0) \otimes \rho_{\bar{M}}(0)$ , with  $\rho_{\bar{M}}(0)$  quadratic in bosonic (fermionic) operators. Initial thermal states could be taken into account considering a third, imaginary time branch of the non-equilibrium contour [260–262], but this is beyond the interest of this work.

We then Taylor-expand the time-ordered exponential in powers of the impurity-bath hybridization  $H_{I\bar{M}}$  and perform the trace over the bath degrees of freedom, which immediately reduces the expansion to only even order terms. Then using Wick's theorem and performing the sums over  $\{b_i, b_i^\dagger\}$ , we can write the final result in terms of the bath hybridization function

$$\Delta_{a'a}^{\gamma'\gamma}(t', t) \equiv \sum_{b'} V_{a'b'} V_{ab'}^* G_{b'}^{\gamma', \gamma}(t', t) \quad (6.15)$$

where  $G_{b'}^{\gamma', \gamma}(t', t) = -i \langle T_C c_{b'}(t'_{\gamma'}) c_{b'}^\dagger(t_\gamma) \rangle$  is the contour ordered bath Green function. Finally, we obtain the hybridization expansion [225, 240, 259]:

$$\begin{aligned} \mathcal{V}(t, 0)\rho_I(0) &= \sum_{k=0}^{\infty} \frac{(-i)^k}{k!^2} \sum_{\gamma_1 \dots \gamma'_k} \prod_i \gamma_i \gamma'_i \sum_{a_1 \dots a'_k} \\ &\quad \int_0^t dt_1 \dots \int_0^t dt'_k \text{tr}_M \left[ T_C e^{-iH_0(t_+ - t_-)} d_{a'_k}^\dagger(t'_k, \gamma'_k) d_{a_k}(t_k, \gamma_k) \dots d_{a_1}(t_1, \gamma_1) \rho_{IM}(0) \right] \\ &\quad \sum_{\sigma \in P} \xi^{\text{sign}(\sigma)} \Delta_{a'_1 a_{\sigma(1)}}^{\gamma'_1 \gamma_{\sigma(1)}}(t'_1, t_{\sigma(1)}) \dots \Delta_{a'_k a_{\sigma(k)}}^{\gamma'_k \gamma_{\sigma(k)}}(t'_k, t_{\sigma(k)}) \end{aligned} \quad (6.16)$$

$\gamma_i, \gamma'_i$  are contour indices  $\gamma \in \{+, -\}$ . We notice that the hybridization function  $\Delta_{a'_i a_j}^{\gamma'_i, \gamma_j}(t'_i, t_j)$  connects the  $d_{a_j}(t_j, \gamma_j)$  operator with the  $d_{a'_i}^\dagger(t'_i, \gamma'_i)$  one. We can interpret this construction as follows. The  $d$  operator creates a "hole" in the impurity, which is propagated through the system and then annihilated by a  $d^\dagger$  operator. To this hole it corresponds (from the definition of  $\Delta$ ) a particle of the environment which is created, propagated and annihilated. Thus, the series eventually describes processes in which particles hop from the impurity to the environment and back to the impurity.

### 6.4.2 Tracing over the Markovian bath

#### Super-operators formalism

It is useful to describe time-evolution using super-operators (see Sec. 2.3.2), as these are natural objects to describe the dynamics of open systems and since they provide a useful framework to work out the trace on the Markovian environment in Eq. (6.16). We recall that a super-operator is operator acting on another operator. The focus is shifted from the standard evolution operator  $U(t, 0) = e^{-iHt}$ , which evolves a pure state (a ket) in time, to the super-operator  $\mathcal{U}(t, 0)$  which time-evolves a density operator and is defined by

$$\rho(t) = U(t, 0)\rho(0)U(0, t) \equiv \mathcal{U}(t, 0)\rho(0) \quad (6.17)$$

We can write a generic time-ordered string of operators, like it appears in Eq. (6.16), in the Schrödinger's picture and in a compact form, using the super-operators notation introduced in Sec. 2.3.2. We promote  $d, d^\dagger$  operators in the Schrödinger's picture to super-operators

$$d_\gamma^\dagger \bullet = \begin{cases} d^\dagger \bullet & \text{if } \gamma = + \\ \bullet d^\dagger & \text{if } \gamma = - \end{cases} \quad (6.18)$$

We trivially generalize the contour time-ordering operator  $T_C$  to the super-operators notation

$$\begin{aligned} T_C X_{1(t, \gamma)} \mathcal{U}_0(t, t') X_{2(t', \gamma')} &= \\ &= \begin{cases} X_{1(t, \gamma)} \mathcal{U}_0(t, t') X_{2(t', \gamma')} & \text{for } (t, \gamma) > (t', \gamma') \\ \xi X_{2(t', \gamma')} \mathcal{U}_0(t', t) X_{1(t, \gamma)} & \text{for } (t, \gamma) < (t', \gamma') \end{cases} \end{aligned} \quad (6.19)$$

The  $X_{t, \gamma}$  super-operators are objects in Schrödinger's picture and their time label  $t$  is just meant to know how to order them.

We also need to introduce a further “forward” time-ordering operator  $T_F$ , that orders two super-operators according to their time labels  $t, t'$ , regardless of their contour index:

$$\begin{aligned} T_F X_{1(t, \gamma)} \mathcal{U}_0(t, t') X_{2(t', \gamma')} &= \\ &= \begin{cases} X_{1(t, \gamma)} \mathcal{U}_0(t, t') X_{2(t', \gamma')} & \text{for } t > t' \\ X_{2(t', \gamma')} \mathcal{U}_0(t', t) X_{1(t, \gamma)} & \text{for } t < t' \end{cases} \end{aligned} \quad (6.20)$$

This definition is the same for both fermions and bosons, with no extra minus signs for fermions.

Using these definitions, we can write the following identity

$$\begin{aligned} T_C e^{-iH_0(t_+ - t_-)} d^\dagger(t'_k) \dots d(t_1) \rho_{IM}(0) &= \\ &= T_F T_C \mathcal{U}_0(t, t'_k) d_{t'_k \gamma'_k}^\dagger \mathcal{U}_0(t'_k, t_{k-1}) \dots d_{t_1 \gamma_1} \mathcal{U}_0(t_1, 0) \rho_{IM}(0) \end{aligned} \quad (6.21)$$

The second line is a chain of subsequent time-evolutions operated by  $\mathcal{U}_0$ , going overall from time 0 to time  $t$ , alternated with the application of  $d_\gamma, d_\gamma^\dagger$  super-operators. We remark

that the two time-order operators  $T_C$  and  $T_F$  do not commute. In order to evaluate the second line of Eq. (6.21), one has first to order the super-operators according to  $T_C$ ; this first ordering is necessary in order to compute the non-trivial sign factor obtained by swapping fermionic operators. Then the super-operators must be re-ordered according to the “forward” time-ordering operator  $T_F$ . This ensures that, in order to evaluate Eq. (6.21), one has to apply only forward in time evolutions; this is necessary as in the next section  $\mathcal{U}_0$  will become a Markovian evolution, which cannot be performed backwards in time.

### Performing the partial trace

We now aim at performing the partial trace on the Markovian environment which is left in Eq. (6.16). This trace is taken on a contour time-ordered string of impurity operators. The latter are nevertheless evolved by the joint dynamics of the impurity plus the remaining bath, making the partial trace non-trivial to evaluate. Assuming that the impurity-bath dynamics is governed by a Lindblad master equation, then the partial trace becomes trivial, as shown in [126] and also explained in [7]. We report a proof here as this is a crucial step to obtain the hybridization expansion (6.26). We recall the Lindblad master equation [7, 136]:

$$\partial_t \rho_I^0 = -i [H_I, \rho_I^0] + \sum_{\alpha} \gamma_{\alpha} \left( L_{\alpha} \rho_I^0 L_{\alpha}^{\dagger} - \frac{1}{2} \{ L_{\alpha}^{\dagger} L_{\alpha}, \rho_I^0 \} \right) \quad (6.22)$$

where  $L_{\alpha}$  are the jump operators, microscopically determined by the environment-impurity coupling (6.10).  $\rho_I^0(t)$  must not be confused with  $\rho_I(t) = \text{tr}_M \rho_{IM}(t)$ , as the former is the density operator obtained by evolving  $\rho(0)$  in presence of the Markovian environment alone.  $\rho_I(t)$  instead is obtained by evolving  $\rho(0)$  with a dynamics that includes both the Markovian and non-Markovian environments. Defining the Markovian evolution super-operator,  $\mathcal{V}_0(t-t') = e^{\mathcal{L}(t-t')}$ , with  $t > t'$ , then

$$\rho_I^0(t) = \mathcal{V}_0(t-t') \rho_I(0) \quad (6.23)$$

We remark that  $\mathcal{V}_0$  depends only on time differences as it formally solves (6.22). This is equivalent to

$$\rho_I^0(t) = \text{tr}_M \rho_{IM}^0(t) = \text{tr}_M [\mathcal{U}_0(t, t') \rho_{IM}^0(t')] = \mathcal{V}_0(t-t') \text{tr}_M \rho_{IM}^0(t') = \mathcal{V}_0(t-t') \rho_I(0) \quad (6.24)$$

In order to show how to perform the trace of the string of super-operators in (6.21), let's assume time ordering is already enforced so that we don't have to care about it. Defining  $r_1(t) = \mathcal{U}_0(t, t'_k) r_1(t'_k)$  and  $r_1(t'_k) = d_{t'_k \gamma'_k}^{\dagger} \mathcal{U}_0(t'_k, t_{k-1}) \dots d_{t_1 \gamma_1} \mathcal{U}_0(t_1, 0) \rho_{IM}(0)$ , we can break down the trace operation as follows:

$$\begin{aligned} \text{tr}_M [\mathcal{U}_0(t, t'_k) d_{t'_k \gamma'_k}^{\dagger} \dots d_{t_1 \gamma_1} \mathcal{U}_0(t_1, 0) \rho_{IM}(0)] &= \\ \text{tr}_M r_1(t) &= \text{tr}_M [\mathcal{U}_0(t, t'_k) r_1(t'_k)] = \mathcal{V}_0(t-t') \text{tr}_M r_1(t'_k) \end{aligned} \quad (6.25)$$

The last equality is analogous to Eq. (6.24) and holds under the same assumptions leading to Lindblad master equation. One can iterate this procedure, as now  $\text{tr}_M r_1(t'_k) = d_{t'_k \gamma'_k}^{\dagger} \text{tr}_M [\mathcal{U}_0(t'_k, t_{k-1}) r_2(t_{k-1})]$ , to turn all the  $\mathcal{U}_0$  super-operators in Eq. (6.16) in  $\mathcal{V}_0$  ones.

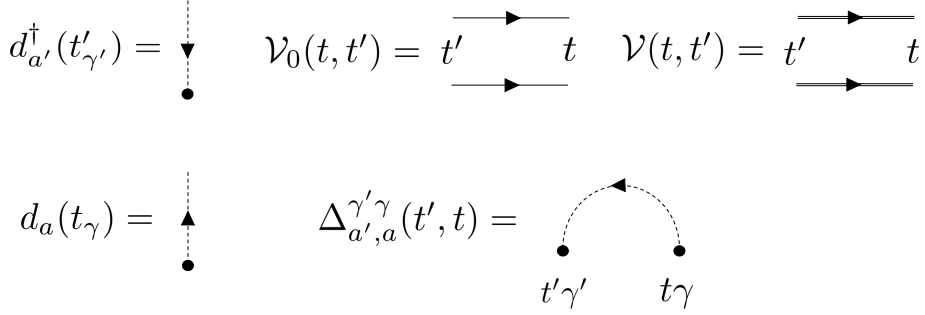


Figure 6.3: The Feynman rules to represent the hybridization expansion (6.26). The arrow of the hybridization line  $\Delta$  goes from a  $d$  super-operator to a  $d^\dagger$  one.

### Generalized hybridization expansion

We then get to the final form of the hybridization expansion in presence of both a non-Markovian and Markovian environment, that is one of the main results of this work:

$$\begin{aligned} \mathcal{V}(t, 0) = & \sum_{k=0} \frac{(-i)^k}{k!^2} \sum_{\gamma_1 \dots \gamma'_k} \prod_i \gamma_i \gamma'_i \sum_{a_1 \dots a'_k} \\ & \int_0^t dt_1 \dots \int_0^t dt'_k T_F T_C \mathcal{V}_0(t, t'_k) d_{a'_k(t'_k \gamma'_k)}^\dagger \mathcal{V}_0(t'_k, t_{k-1}) \dots d_{a_1(t_1 \gamma_1)} \mathcal{V}_0(t_1, 0) \times \quad (6.26) \\ & \times \sum_{\sigma \in P} \xi^{\text{sign}(\sigma)} \Delta_{a'_1 a_{\sigma(1)}}^{\gamma'_1 \gamma_{\sigma(1)}}(t'_1, t_{\sigma(1)}) \dots \Delta_{a'_k a_{\sigma(k)}}^{\gamma'_k \gamma_{\sigma(k)}}(t'_k, t_{\sigma(k)}) \end{aligned}$$

This series can be sampled using stochastic sampling techniques [239, 240, 263] or approximately resummed [225, 250]. For both purposes, it is useful to define the Feynman rules for the series (6.26). Each term of the hybridization expansion (6.26) must be understood as a composition of applications of super-operators, from the right-most to the left-most one, on the initial density operator. This becomes a simple matrix product in Liouville space, where super-operators are represented by matrices (see Sec. 2.3.2). Using “hats” to indicate super-operators in Liouville space, we have

$$\begin{aligned} & \mathcal{V}_0(t, t'_k) d_{a'_k(t'_k \gamma'_k)}^\dagger \dots d_{a_1(t_1 \gamma_1)} \mathcal{V}_0(t_1, 0) \rho_I(0) \\ \rightarrow & \hat{\mathcal{V}}_0(t, t'_k) \hat{d}_{a'_k(t'_k \gamma'_k)}^\dagger \dots \hat{d}_{a_1(t_1 \gamma_1)} \hat{\mathcal{V}}_0(t_1, 0) |\rho_I(0)\rangle \end{aligned} \quad (6.27)$$

## 6.5 Diagrammatic rules and Dyson equation

### 6.5.1 Feynman rules

The Feynman rules to draw the hybridization expansion (6.26) are represented in figure 6.3. We will use these rules to draw a term with  $2k$  annihilation plus creation super-operators, with a particular ordering for the times  $\{t_i, t'_i \dots t_1, t'_1\}$  and a choice of a permutation

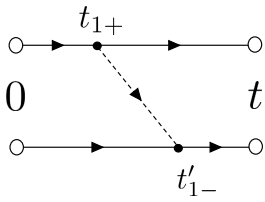


Figure 6.4: The Feynman diagram representing Eq. (6.28)

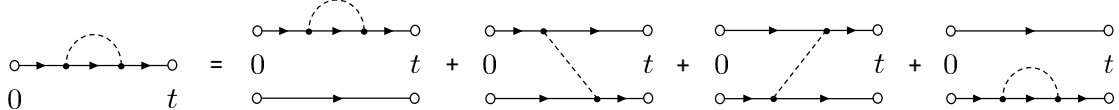


Figure 6.5: Compact diagrams represent an ensemble of diagrams hiding the double contour structure. By omitting the arrows on hybridization (dashed) lines, we mean the sum of all the possible arrows choices.

$\{\sigma(1), \sigma(2) \dots \sigma(k)\}$ . To do that, we draw a couple of parallel axes representing the double contour from time  $t = 0$  to time  $t$ .  $d_\gamma$  ( $d_\gamma^\dagger$ ) super-operators are represented as dashed half-lines with outwards (inwards) arrows, stemming from the contour branch  $\gamma$ . The dashed half-lines corresponding to the super-operators  $d_{a'_i(t'_i\gamma'_i)}^\dagger$  and  $d_{a_j(t_j\gamma_j)}$  are joined together to form a hybridization line, representing the hybridization function  $\Delta_{a'_i a_j}^{\gamma'_i \gamma_j}(t'_i, t_j)$ , which has an arrow going from  $d$  to  $d^\dagger$ . Then, each part of the double contour between two integration times, drawn as two parallel solid segments, represents a time-propagation super-operator  $\mathcal{V}_0$ . The dressed evolution operator  $\mathcal{V}$  is drawn by replacing the contour solid lines by double lines. As an example, the diagram corresponding to

$$i \int_0^t dt_1 \int_0^{t_1} dt'_1 \mathcal{V}_0(t, t'_1) d_{a'_1-}^\dagger \mathcal{V}_0(t'_1, t_1) d_{a_1+} \mathcal{V}_0(t_1, 0) \Delta_{a'_1 a_1}^{-+}(t'_1, t_1) \quad (6.28)$$

is shown in figure 6.4. All the diagrams with  $2k$  annihilation and creation super-operators are generated by connecting  $d^\dagger$  super-operators to  $d$  ones in all possible choices of permutations  $\sigma$  and considering all possible time orderings of integration times.

### 6.5.2 Compact diagrams

In this section we start from the hybridization expansion derived in section III, which involves bare diagrams to all orders, and use the Feynman rules to introduce diagrammatic resummation techniques.

To proceed further it is useful to draw more compact diagrams where the double contour is collapsed on a single time-axis and thus a time propagation  $\mathcal{V}_0$  is represented by a single line, as we show in figure 6.5. These compact diagrams represent an ensemble of diagrams drawn with the rules we introduced in 6.3. The advantage of this notation is that all the diagrams represented by a single compact diagram have the same topology in

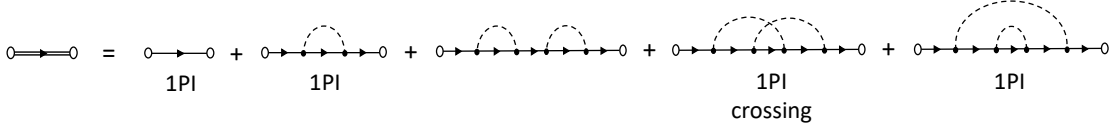


Figure 6.6: 1PI diagrams of the hybridization expansion in Eq. (6.26)

terms of being 1-particle irreducible or non-crossing. Figure 6.6 shows the hybridization expansion drawn using these compact diagrams.

### 6.5.3 Dyson equation

As a first step it is useful to distinguish diagrams which are one-particle irreducibles, i.e. compact diagrams which cannot be separated, by cutting a solid line, in two parts that are not connected by any hybridization line, as indicated in figure 6.6. Then, we introduce the self-energy  $\Sigma$  as the sum of one particle irreducible (1PI) diagrams. All the non-1PI diagrams can be obtained by joining some 1PI diagrams with solid lines, thus the whole series can be written as

$$\mathcal{V} = \mathcal{V}_0 + \mathcal{V}_0 \circ \Sigma \circ \mathcal{V}_0 + \mathcal{V}_0 \circ \Sigma \circ \mathcal{V}_0 \circ \Sigma \circ \mathcal{V}_0 + \dots$$

We remark that the objects composing this series,  $\mathcal{V}_0$  and  $\Sigma$ , are super-operators and the series must be understood as a composition of applications of super-operators, from the right-most to the left-most one, on a target operator. Self-energies and propagators are joined by the circle operation,  $\circ$ , standing for a super-operator application and a partial time convolution. Using brackets to stress that we refer to a super-operator application and the symbol  $\bullet$  to indicate a target operator, we have

$$\Sigma(t, t_1) \circ \mathcal{V}_0(t_1, t') \equiv \int_{t'}^t dt_1 \Sigma(t, t_1) [\mathcal{V}_0(t_1, t') [\bullet]]$$

The series above sums up to the Dyson equation  $\mathcal{V} = \mathcal{V}_0 + \mathcal{V}_0 \circ \Sigma \circ \mathcal{V} = \mathcal{V}_0 + \mathcal{V} \circ \Sigma \circ \mathcal{V}_0$ , or equivalently, in integro-differential form

$$\partial_t \mathcal{V}(t, t') = \mathcal{L} \mathcal{V}(t, t') + \int_{t'}^t dt_1 \Sigma(t, t_1) \mathcal{V}(t_1, t') \quad (6.29)$$

When the self-energy of the non-Markovian environment  $\Sigma$  is set to zero, this equation yields  $\mathcal{V}(t) = e^{\mathcal{L}t}$ , which is the Lindblad, Markovian evolution.

One of the main effects of dissipative dynamics is that the system may forget about initial conditions and reach the same stationary state for any initial condition. Assuming a stationary state exists for a non-Markovian map  $\mathcal{V}$  defined by the Dyson equation (6.29), then it satisfies

$$\left( \mathcal{L} + \int_0^\infty dt_1 \Sigma(\infty, t_1) \right) \rho_{ss} = 0 \quad (6.30)$$

Setting the non-Markovian self-energy to zero, this equation reduces to the Lindblad condition for the stationary state. The derivation of this equation invokes the finite memory of  $\Sigma$  and the stationarity of  $\mathcal{V}$  and is reported in appendix C.1.

$$\sum = \text{Diagram 1} + \text{Diagram 2} + \text{Diagram 3} + \text{Diagram 4} + \text{Diagram 5} = \text{Diagram 6}$$

Figure 6.7: The NCA series of the self-energy  $\Sigma$ . The resummed series for  $\Sigma$  corresponds to its  $k = 1$  diagrams, where the bare propagator  $\mathcal{V}_0$  is replaced with the dressed one  $\mathcal{V}$ .

## 6.6 The Non-Crossing impurity solver

The non-crossing approximation (NCA) corresponds to approximating the series for  $\mathcal{V}$ , and thus also for  $\Sigma$ , by considering only the compact diagrams 6.5.2 in which the hybridization lines do not cross [247–250]. The NCA diagrams composing the self-energy are shown in figure 6.7. In order to prove the second equality in figure 6.7, we remark that the first and last times of a self-energy diagram must be connected together by an hybridization line. If it's not the case, in fact, the resulting diagram is either non-1PI or it's crossed. Then all the diagrams of  $\Sigma$  (in NCA) are obtained connecting the intermediate times to form all the possible non-crossing diagrams (not only the 1PI ones this time). But the latter all non-crossing diagrams in turn define the NCA series for  $\mathcal{V}$ . This proves the second equality in figure 6.7. We remark that then, the NCA self-energy coincides with its contributions (with  $k = 1$ ), where the bare propagator  $\mathcal{V}_0$  is replaced with the dressed one  $\mathcal{V}$ .

To obtain an analytic expression of the self-energy, we have to cast the  $k = 1$  term of the hybridization expansion (6.26) in a form in which the innermost integration time is lower than the outermost, that is of the form  $\int_{t'}^t dt_1 \int_{t'}^{t_1} dt_2$ . In doing so, one must deal with the signs coming out of the time ordering. We report the calculation in appendix C.2. The expression for the self-energy eventually reads

$$\Sigma(t_1, t_2) = \sum_{\substack{\alpha\beta \\ ab}} -\alpha^{(1+\xi)/2} \beta i \left[ \Delta_{ba}^{\beta\alpha}(t_1, t_2) d_{\beta b}^\dagger \mathcal{V}(t_1, t_2) d_{\alpha a} + \xi \Delta_{ab}^{\alpha\beta}(t_2, t_1) d_{\beta b} \mathcal{V}(t_1, t_2) d_{\alpha a}^\dagger \right] \quad (6.31)$$

where  $\alpha, \beta \in \{+, -\}$  are contour indices,  $a, b$  are the fermionic generic indices. We can interpret the two terms in Eq. (6.31) as follows. The first term propagates a hole in the impurity (applies  $d^\dagger$  first and then  $d$ ) and a particle in the bath, the latter being described by a hybridization function with the same time arguments of  $\mathcal{V}$ ; The second term propagates a particle in the impurity and a hole in the bath with a hybridization function with opposite time arguments than  $\mathcal{V}$ .

Few comments are in order here, concerning the above result. First, in absence of the Markovian environment, that is by replacing  $\mathcal{V}(t, t')$  and  $\mathcal{V}_0(t, t')$  with  $\mathcal{U}(t, t')$  and  $\mathcal{U}_0(t, t')$ , our results are equivalent to non-equilibrium NCA schemes for unitary dynamics [226, 249, 251]. There is a formal difference consisting in our super-operators formulation of the hybridization expansion and of the Dyson equation, that is necessary to consider the additional Markovian environment without further approximations, but this difference is only formal and does not affect the results. In fact, if  $N$  is the dimensionality of the impurity Hilbert space, the usual non-equilibrium NCA propagator [226, 251] has different

Keldysh components, each of them being an  $N \times N$  matrix, while our  $\mathcal{V}$  propagator is a  $N^2 \times N^2$  matrix with no Keldysh components.

Furthermore, the result obtained for the NCA self-energy in Eq. (6.31) makes it clear that for a bath hybridization which is delta-correlated in time, the resulting self-energy contribution to the Dyson equation takes the form of a Lindblad dissipator. Indeed, one can recover the Lindblad master equation from our diagrammatic NCA approach doing the usual approximations one makes to derive master equations [136], and possibly discuss corrections to the master equation from higher order terms, as recently done [264].

### 6.6.1 Properties of the NCA propagator

The propagator  $\mathcal{V}(t, t')$  obtained in NCA is the time-evolution super-operator of the reduced density operator of the impurity. Assuming to switch on the interaction with the baths at time  $t = 0$ , then the density operator of the impurity at time  $t$  is given by  $\rho_I(t) = \mathcal{V}(t, 0)\rho_I(0)$ . A time evolution super-operator must be a convex-linear, completely positive and trace-preserving map [136]. It is natural to ask which of these properties are preserved by the NCA approximation.  $\mathcal{V}$  is obviously a linear map, implying it is also convex linear. We proved that it is trace-preserving and that it preserves hermiticity (see appendix C), while proving or disproving whether the map is completely positive is a tough task [265] that will be addressed in the future. We stress that  $\mathcal{V}(t, t')$  describes a non-Markovian evolution, so it does not form a semi-group, that is  $\mathcal{V}(t, t') \neq \mathcal{V}(t, t_1)\mathcal{V}(t_1, t')$  with  $t' < t_1 < t$ . Time-evolution super-operators have also interesting spectral properties following from trace preservation, akin to Lindblad master equations 2.4.2. We refer to appendix C for the proof. We call  $\lambda_i(t, t')$ ,  $v_i^R(t, t')$  the eigenvalues and right-eigenvectors of  $\mathcal{V}(t, t')$ , both depending on time. As it preserves the trace,  $\mathcal{V}(t, t')$  must have at least one eigenvalue equal to one, say  $\lambda_0 \equiv 1$ . If we assume this eigenvalue is non-degenerate, then all the others eigenvectors with  $i \neq 0$ , are traceless. As a consequence of these properties, if one evolves an initial state  $\rho(0)$  and expands  $\rho(t)$  on the instantaneous eigenvectors  $v_i^R(t, 0)$ , then those eigenvectors with  $i \neq 0$  will represent decay modes of the dynamics as they will be suppressed by their corresponding vanishing eigenvalues for long times, while  $v_{i=0}^R(t, 0)$  will evolve in time undamped until reaching a stationary value, representing the stationary state of the non-Markovian evolution. This discussion is analogous to the one in 2.4.2 about eigenmodes of the Liouvillian, with the formal difference that here we are looking at the evolution operator, rather than at its generator. We will numerically check these properties in figure 6.8 of the next section, where we will apply our NCA algorithm to a specific example.

### 6.6.2 Impurity Green functions

For using this NCA impurity solver in DMFT, one needs to compute one-particle Green functions, given the propagator  $\mathcal{V}$ . The expression for those Green functions generalizes the quantum regression formulae for Markovian master equations discussed in section 2.4.1

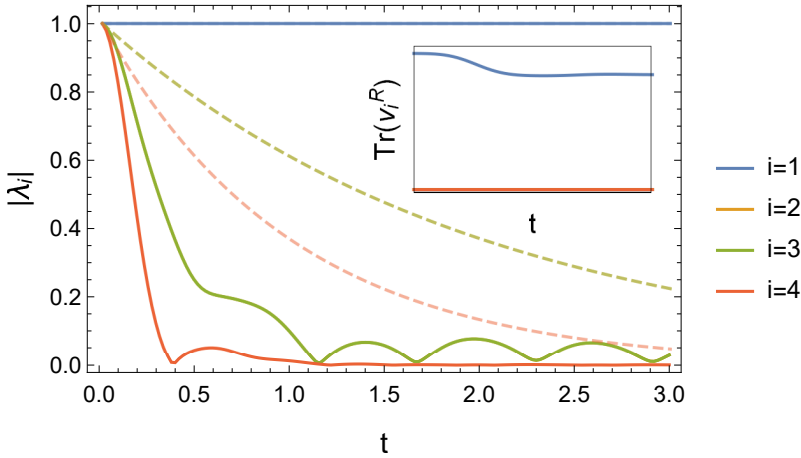


Figure 6.8: Real-time evolution of the absolute value of the eigenvalues of the impurity propagator. While an eigenvector with eigenvalue one is present at all times, all the other eigenvalues decay to zero at long times. The  $i = 2$  and  $i = 3$  curves coincide because the corresponding eigenvalues are complex conjugates. The decay is purely exponential for a purely Markovian system, which corresponds to the dashed lines, while strong deviations appear in the non-Markovian case. The inset shows that the right eigenstates of  $\mathcal{V}(t)$  with different-from-one eigenvalues are traceless, while the right eigenstate with eigenvalue one has a finite (unnormalized) trace. Parameters:  $\epsilon_0 = 5$ ,  $\gamma = \gamma_l = \gamma_p = \gamma_d = 0.5$ ,  $w = 10$ ,  $\eta = 1$ ,  $\Delta t = 0.02$ ,  $\rho_0 = |0\rangle\langle 0|$ .

and takes the form

$$G_{ab}^{\alpha\beta}(t, t') = -i \left\{ \beta^{(1-\xi)/2} \text{tr} \left[ d_{\alpha a} \mathcal{V}(t, t') d_{\beta b}^\dagger \mathcal{V}(t', 0) \rho_0 \right] \theta(t - t') + \xi \alpha^{(1-\xi)/2} \text{tr} \left[ d_{\beta b}^\dagger \mathcal{V}(t', t) d_{\alpha a} \mathcal{V}(t, 0) \rho_0 \right] \theta(t' - t) \right\} \quad (6.32)$$

We report a derivation of this formula in appendix C.5.

### 6.6.3 Case study: spin-less fermionic impurity

As a non-trivial application of the NCA approach for open system described so far, we consider here a model of a single-mode, spin-less fermionic impurity with Markovian losses, pump and dephasing and further coupled to a non-Markovian fermionic environment, with coupling Hamiltonian (6.8). We notice that the model in absence of dephasing, also known as Resonant Level Model, is quadratic in all the fermionic degrees of freedom and therefore easily solvable, with analytical expressions known for the wide-band limit. At finite dephasing this is no longer the case and the model cannot, to the best of our knowledge, be solved by simple means. This could be understood naturally in the Keldysh approach, where the dephasing would result in density-density type of coupling between different Keldysh branches.

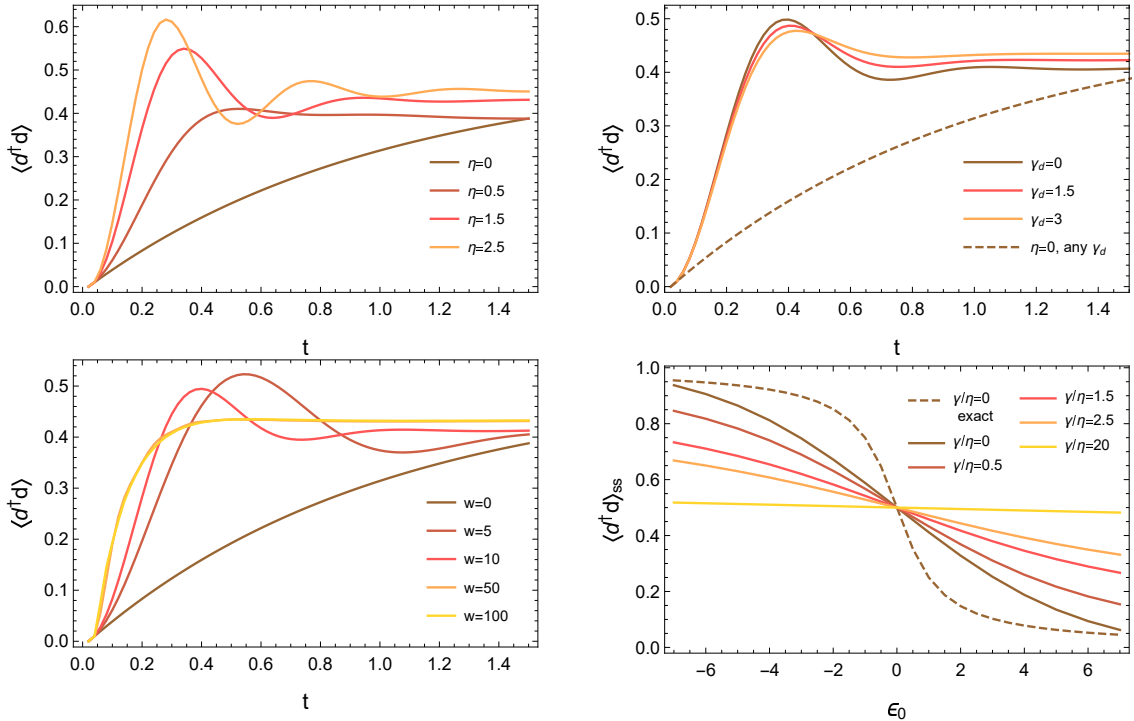


Figure 6.9: Dynamics of the number of fermions for different sets of parameters, namely changing the hybridization strength (Top left) the bandwidth (bottom left) and the dephasing rate (top right). Average population of the stationary state as a function of the energy level (bottom right). Parameters:  $\epsilon_0 = 1$ ,  $\gamma = \gamma_l = \gamma_p = \gamma_d = 0.5$ ,  $w = 10$ ,  $\eta = 1$ ,  $\Delta t = 0.02$ ,  $\rho_0 = |0\rangle\langle 0|$ .

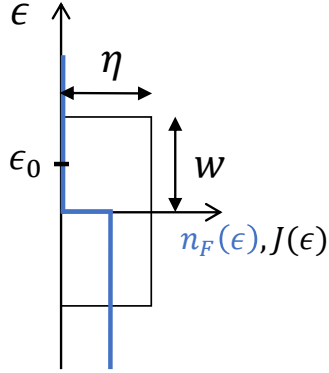


Figure 6.10: The density of states  $J(\epsilon)$  of the bath with bandwidth  $2w$  and particle-hole symmetric. In blue, the Fermi function  $n_F(\epsilon)$  at zero temperature and zero chemical potential.  $\epsilon_0$  is the energy of the impurity level.

The Markovian dynamics is described by a Lindblad master equation

$$\begin{aligned}\partial_t \rho_I^0 &= \mathcal{L} \rho_I^0 = -i [H_I, \rho_I^0] + (\gamma_l \mathcal{D}_l + \gamma_p \mathcal{D}_p + \gamma_d \mathcal{D}_d) \rho_I^0 \\ H_I &= \epsilon_0 d^\dagger d \\ \mathcal{D}_l \rho_I^0 &= d \rho_I^0 d^\dagger - \frac{1}{2} \{d^\dagger d, \rho_I^0\} \\ \mathcal{D}_p \rho_I^0 &= d^\dagger \rho_I^0 d - \frac{1}{2} \{d d^\dagger, \rho_I^0\} \\ \mathcal{D}_d \rho_I^0 &= d^\dagger d \rho_I^0 d^\dagger d - \frac{1}{2} \{d^\dagger d, \rho_I^0\}\end{aligned}$$

where  $\epsilon_0$  is the energy of the fermionic level.

The effect of the non-Markovian environment on the impurity is completely determined by its hybridization function (6.15). Here we choose a zero temperature, particle-hole symmetric, fermionic bath with constant density of states,  $J(\epsilon)$ , of bandwidth  $2w$  and with coupling strength to the impurity  $\eta$  as sketched in Fig 6.10. In this case the hybridization function depends only on time-differences. As a consequence, one can show that also  $\mathcal{V}$  and  $\Sigma$  depend only on time differences and we will set  $t' = 0$ . With these definitions we get for the hybridization functions

$$\begin{aligned}\Delta^{+-}(t) &= i \int_{-\infty}^{\infty} J(\epsilon) n_F(\epsilon) e^{-i\epsilon t} = 2i\eta e^{iwt/2} \sin(wt/2) / t \\ \Delta^{-+}(t) &= -i \int_{-\infty}^{\infty} J(\epsilon) (1 - n_F(\epsilon)) e^{-i\epsilon t} = -2i\eta e^{-iwt/2} \sin(wt/2) / t\end{aligned}$$

To solve the Dyson equation (6.29) numerically we use the simple forward discretization scheme  $\partial f(t) = [f(t + \Delta t) - f(t)] / \Delta t$ ,  $\int_0^t dt_1 f(t_1) = \Delta t / 2 \sum_{l=0}^{t/\Delta t - 1} [f((l + 1)\Delta t) + f(l\Delta t)]$ , with time-step  $\Delta t$ . More refined integration methods are explained in detail in [225]. The Hilbert space of the impurity has size  $N = 2$ , so that the super-operator  $\mathcal{V}$  has size  $N^2 \times N^2 = 4 \times 4$ .

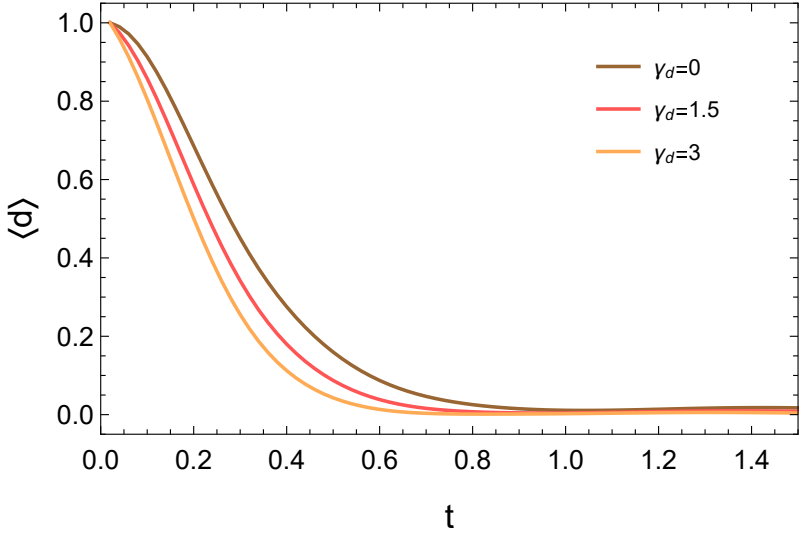


Figure 6.11: Dynamics of the density matrix coherence for different values of the dephasing. Parameters:  $\epsilon_0 = 1$ ,  $\gamma = \gamma_l = \gamma_p = \gamma_d = 0.5$ ,  $w = 10$ ,  $\eta = 1$ ,  $\Delta t = 0.02$ ,  $\rho_0 = |0\rangle\langle 0| + |0\rangle\langle 1| + |1\rangle\langle 0|$ .

## Results

We start analyzing the spectral properties of the propagator  $\mathcal{V}(t)$ , which have been discussed generically in section 6.6.1, and are reported in figure 6.8. In the main panel we plot the time dependence of the absolute value of the eigenvalues of  $\mathcal{V}(t)$ , both in the purely Markovian case (dashed lines) as well in presence of both Markovian and non-Markovian dissipations. In both cases there is an eigenvalue which remains equal to one, while the others decay to zero at long times, as pointed out in section 6.6.1. However the nature of this decay is rather different in the two cases, showing a faster dynamics and long time oscillations in the non-Markovian case as opposed to a pure exponential decay in the Markovian one. The inset of figure 6.8 shows instead that all the right-eigenstates of  $\mathcal{V}(t)$  with different-from-one eigenvalues are traceless, while the right eigenstate with eigenvalue one has a finite trace (that we could normalize to one at every time).

We then consider the dynamics of a simple observable, such as the density of fermions in the impurity level, as a function of time and for different parameters (see the different panels of figure 6.9). In the left figures we plot the dynamics for different values of the coupling  $\eta$  (top) and bandwidth  $w$  (bottom) of the non-Markovian environment, in presence of fixed Markovian losses, pump and dephasing. We see that with respect to the purely Markovian dynamics, characterized by a simple exponential relaxation, the NCA approach captures aspects related to the non-Markovian nature of the environment. In particular the dynamics becomes characterized by oscillations whose amplitude and frequency increase with the coupling  $\eta$ . Similarly, increasing the bandwidth of the non-Markovian environment reduces the oscillations characterizing the short-time population dynamics  $t \lesssim 1/w$ , which disappear in the large bandwidth limit, as it is the case for the

unitary dynamics of the Resonant Level Model.

Overall the non-Markovian environment makes the dynamics substantially faster. In the top-right plot we discuss the role of dephasing, that is actually very interesting as it shows an effect of the combined Markovian and non-Markovian environments. The dashed line shows that, for Markovian dissipation only, the dephasing does not affect the population dynamics; this is well understood as the dephasing dissipator commutes with the number operator. It's interesting to see that, instead, combined with a non-Markovian environment the dephasing has an impact on the dynamics of populations; this is a smaller effect as it involves both the Markovian and the non-Markovian environments. This effect can be understood as follows: let's consider a process in the time-evolution in which the non-Markovian environment applies a  $d_+^\dagger$  super-operator on the density matrix and then, after some time, a  $d_+$  super-operator. The application of the creation super-operator converts populations of the density matrix into coherences. Then the Markovian dephasing damps those coherences, which are then converted back to populations when the non-Markovian environment applies the annihilation operator. As a net effect, the dephasing has produced a change into populations, as it is shown in the top-right plot. We also note that not only the dynamics, but also the stationary values of the occupation change with the dephasing. A more direct effect of the dephasing appears in the coherences, i.e. in the off-diagonal elements of the density matrix, which decay to zero faster as  $\gamma_d$  is increased, as we show in figure 6.11. For what concerns the stationary state, we notice from the bottom-right plot that the average density would be independent of the energy of the fermionic level in the purely Markovian case, which leads to a infinite-temperature fully-mixed stationary state for the chosen dissipation rates. This makes sense as a Markovian bath has no energy structure, thus the level effectively sees always the same bath even if it's shifted in energy. On the other hand the coupling to the non-Markovian bath makes populations depend strongly on the position of the energy level and gives a result which is in good agreement with exact analytical calculations (dashed line); to justify the quantitative discrepancy with this analytical result, we stress that for the non-interacting limit we consider here, the NCA approximation, which is based on a strong coupling expansion, is not expected to be exact.

## 6.7 Conclusions

In this chapter we reported our developments towards a Dynamical Mean Field Theory (DMFT) approach to driven-dissipative lattice systems. Those efforts are justified by the current lack of established methods to study those systems. We introduced DMFT in the context of driven-dissipative models, we discussed how it compares to standard mean field theory and we derived a beyond mean field critical point equation for the delocalization transition on the Bethe lattice.

In order to solve DMFT, we developed a method to solve the auxiliary problem of a single impurity, which in our context is coupled simultaneously to a Markovian and a non-Markovian environment. We derived a formal hybridization expansion for the evo-

lution super-operator of the impurity, obtained after tracing out all the bath degrees of freedom. This result generalizes to non-unitary, Markovian case the hybridization expansion obtained for unitary quantum impurity models. As such it provides the natural starting point for the development of stochastic sampling techniques of the dissipative real-time dynamics of the impurity based on Diagrammatic Monte Carlo, that we leave for future studies. Starting from this expansion we define real-time diagrammatic rules and write down a Dyson Equation for the impurity propagator that we evaluate retaining only non-crossing diagrams, an approximation which is known to capture some aspects of the impurity physics at strong coupling. The resulting approach leads to a trace and hermiticity preserving non-Markovian dynamical map, with consequences on the spectral properties of the evolution super-operator, while proving its complete positivity in full generality remains an open question.

It is interesting to comment on the relation between our approach and related methods to deal with impurity models coupled to multiple baths. While in principle both the hybridization expansion [266] as well as the strong-coupling diagrammatic resummation [267] can be generalized in presence of multiple environments, taking the Markovian limit from the start has some practical and conceptual advantage. In particular, we can take direct advantage of the local nature of the Markovian evolution and perform an expansion around an *atomic-limit* which now contains not only local interactions, but also drive and dissipation. This limit can be easily solved by direct diagonalization of a Lindbladian, as opposed to treating the Markovian environment as an additional NCA self-energy. The key idea is therefore to treat on equal footing all the energy scales related to fast processes, while resorting to perturbation theory when dealing with processes leading to slowing decay correlations such as the coupling to gapless reservoirs.

As an application, we solved numerically the Dyson equation for the simple model of a fermionic, single-mode impurity, with Markovian losses, pump and dephasing and coupled to a non-Markovian, zero temperature environment. This model is non-trivial for the presence of dephasing, which is a quartic term in fermionic operators. This simple implementation allowed to check the spectral properties of the evolution super-operator and to study how Markovian dynamics gets modified by coupling to a non-Markovian environment. In particular our method allowed to show a physical consequence of coupling simultaneously to Markovian and non-Markovian environments: Markovian dephasing combined with non-Markovian processes leads to a change in impurity occupations. Future directions include the exploration of more complex impurity models involving internal degrees of freedom such as the Anderson Impurity model as well as bosonic extensions and to use of this NCA solver to solve DMFT for driven-dissipative lattices.

## Chapter 7

# General Conclusions

In this thesis we discussed the investigations I have been carrying on during my PhD in the realm of driven-dissipative quantum many-body systems. Chapter 1 was an introduction to this research field, highlighting my motivations and my point of view. Chapter 2 was devoted to introduce well known theoretical techniques, with an effort to make contact between Lindblad master equation and Keldysh field theory. In chapter 3 we discussed a spectral or Lehmann decomposition of single-particle Green functions of Markovian open systems. We applied such a spectral representation to a model of a quantum van der Pol oscillator with an additional non-linear term in its Hamiltonian. We pointed out that a sign property of spectral functions of equilibrium systems doesn't hold in the case of open systems. As a consequence of this, we found that the interplay of interaction and non-equilibrium effects can result in a surprising "negative density of states" with direct physical consequences as it can, for example, generate negative temperature states or produce finite-frequency instabilities in lattice models, as we discussed in Ch. 4. In particular we found that the "negative density of states" can appear even in absence of steady state population inversion in the system density matrix. In chapter 4, we studied the phase transition between a normal and a superfluid phase in a prototype system of driven-dissipative bosons on a lattice, which is expected to occur in a wide class of driven-dissipative models. This transition is characterized by a dynamical mode becoming unstable, determined by interactions and non-equilibrium conditions. We emphasize that capturing the critical mode requires the quantum solution of the single-site dissipative interacting problem and thus it is not a semiclassical result. The resulting finite-frequency criticality corresponds to the spontaneous break of time-translational invariance and to the lack of a time-independent stationary state. Writing down the effective Keldysh field theory for this finite frequency transition we have obtained its semiclassical limit which we show to reproduce the results of a time-dependent Gutzwiller decoupling of the density matrix. The theoretical strong-coupling framework we used has the potential to be applied in a wide range of contexts, including for example driven and isolated Floquet systems and problems of quantum synchronization. In chapter 5 we discussed the mean-field phase diagram a Mott insulating phase stabilized by dissipation, which is potentially relevant for ongoing experiments. We predicted that the region of stability of such a phase is remarkably shrunk with respect

to the ground-state phase diagram of a Bose-Hubbard Hamiltonian, due to the onset of dynamical modes instabilities. Our results suggest that there is a trade off between the fidelity of the stationary phase to a Mott insulator and robustness of such a phase at finite hopping. These results are preliminary and mostly unpublished. Finally we discussed the effects of effective thermal fluctuations on the phase diagram. Future developments include going further with analytical calculations, computing properties of the dissipative stabilized Mott at finite hopping and compute the non-equilibrium phase diagram beyond mean-field. Finally, in chapter 6 we discussed some developments towards using dynamical mean field theory (DMFT) for studying driven-dissipative lattice systems. We introduced DMFT in the context of driven-dissipative models and we discussed how it compares to standard mean field theory. In order to solve DMFT, we developed a method to solve the auxiliary problem of a single impurity, which is coupled simultaneously to a Markovian and a non-Markovian environment. We derived an hybridization expansion for the evolution super-operator of the impurity, generalizing to additional Markovian dissipation the well known hybridization expansion for quantum impurity models and providing the natural starting point for the development of stochastic sampling of the dissipative real-time dynamics of the impurity based on Diagrammatic Monte Carlo, that we leave for future studies. We developed an Non-Crossing Approximation (NCA) of the expansion, leading to a trace and hermiticity preserving non-Markovian dynamical map, while proving its complete positivity in full generality remains an open question. As a test, we applied this novel method to a simple model of a fermionic, single-mode impurity, with Markovian losses, pump and dephasing and coupled to a non-Markovian, zero temperature environment. In particular our method allowed to show effects of the interplay of Markovian and non-Markovian environments. Future directions include the exploration of more complex impurity models involving internal degrees of freedom such as the Anderson impurity model as well as bosonic extensions and to use of this method to solve DMFT for driven-dissipative lattices.

# Chapter 8

## Résumé Substancial

### 8.1 Introduction

Le jeune domaine des **systèmes quantiques à plusieurs corps dissipatifs pilotés** est un champ de recherche hybride, qui croise des idées issues de domaines de la physique traditionnellement différents, en particulier la physique atomique moléculaire et optique (AMO), la physique de la matière condensée et l'information quantique. Commençons par décomposer les éléments composant le nom de ce domaine de recherche. Le problème de **systèmes quantiques à plusieurs corps** pourrait être remonté à la citation de Dirac “*The general theory of quantum mechanics is now almost complete...the difficulty is only that the exact application of these laws leads to equations much too complicated to be soluble*” [4]. La physique quantique à plusieurs corps a connu une série de percées dans son histoire, par exemple la théorie BCS de la supraconductivité [5] ou la compréhension des impuretés magnétiques dans les métaux [6], conduisant au développement de techniques de groupe de renormalisation. Des phénomènes collectifs se produisent lorsque de nombreuses particules interagissent les unes avec les autres, réalisant des états quantiques macroscopiques spectaculaires, tels que par exemple des condensats de Bose-Einstein, des supraconducteurs ou des isolants de Mott. La citation de Dirac ci-dessus continue avec “*It there fore becomes desirable that approximate practical methods of applying quantum mechanics should be developed*” [4]. En fait, les problèmes quantiques à plusieurs corps sont très difficiles à résoudre, nécessitant une variété de techniques approchées, chacune d'entre elles étant adaptées à certains régimes physiques. Alors que l'ère de l'informatique a considérablement repoussé les limites des problèmes traitables, l'augmentation exponentielle de l'espace de Hilbert avec le nombre de degrés de liberté limite les tailles de système pouvant être traitées numériquement. L'hypothèse, une fois vérifiée, de l'équilibre thermodynamique simplifie considérablement le problème des particules multiples. Une application directe des ensembles thermodynamiques de la mécanique statistique classique aux particules quantiques permet d'obtenir les statistiques quantiques. Celles-ci décrivent l'état d'équilibre obtenu en mettant un système quantique en contact avec un réservoir avec des variables thermodynamiques bien définies, telles que la température et le potentiel chimique. La limite de cette approche est qu'elle ne permet pas d'étudier la dynamique vers

l'équilibrage, qui nécessite plutôt une modélisation plus microscopique de la dissipation, ainsi que des scénarios plus généraux de non-équilibre.

Cette modélisation microscopique de **dissipation** en mécanique quantique est née dans les années 60, stimulée par l'invention du laser. Bien que dans de nombreux cas on s'intéresse aux systèmes quantiques aussi isolés que possible de leur environnement, le couplage à l'environnement étant préjudiciable aux caractéristiques quantiques, il n'en va pas ainsi, par exemple, du phénomène d'action laser, qui nécessite une cavité avec pertes pour avoir lieu [7]. Bien que les phénomènes dissipatifs soient facilement décrits dans la mécanique newtonienne classique, par exemple les forces de trainée dans les fluides ou les pertes thermiques dans un circuit, la formulation hamiltonienne de la mécanique quantique ne permet pas naturellement de décrire les processus dissipatifs. L'idée la plus simple d'essayer de quantifier les équations dissipatives classiques du mouvement conduit malheureusement à la conséquence catastrophique de rompre les relations de commutation quantiques canoniques [7]. L'effort de développer une théorie quantique dissipative qui permettrait de récupérer les équations classiques bien connues dans la limite classique tout en préservant la commutation canonique a conduit à l'approche "système plus réservoir" [8–10].

Pour compenser les pertes de particules et d'énergie, on peut **piloter** le système en lui appliquant des forces externes, et établissant un équilibre dynamique entre les forces motrices et les pertes. Nous appellerons un tel système un système **dissipatif piloté**. L'équilibre dynamique entre les forces motrices et les pertes ne devrait toutefois pas conduire à un état thermodynamique, mais plutôt à un état stationnaire hors d'équilibre. En fait, le mécanisme pilotage plus dissipation rompt explicitement la réversibilité microscopique, ou équilibre détaillé, sous-jacent l'équilibre thermodynamique. Dans cette thèse, nous allons nous concentrer sur ces états stationnaires hors d'équilibre plutôt que sur une dynamique transitoire. Nous considérerons principalement les processus dissipatifs qui peuvent être décrits en termes d'équations-maîtresses de Lindblad.

La combinaison des conditions de non-équilibre réalisées dans les systèmes dissipatifs pilotés avec l'intérêt pour les phénomènes collectifs apparaissant lorsque de nombreuses particules interagissent entre elles donne naissance au nouveau domaine d'activité des systèmes quantiques à plusieurs corps dissipatifs pilotés[11–26]. Le relâchement de la contrainte de l'équilibre thermodynamique ouvre la porte à de nouvelles phases à plusieurs corps, sans contrepartie à l'équilibre. Par exemple, rien ne garantit qu'un système dissipatif déterminé atteindra jamais un état indépendant du temps et des cycles limites ou du chaos sont des alternatives valables [20, 27, 28]. Les états stationnaires dissipatifs-pilotés peuvent subir des transitions de phase lors du réglage de paramètres de contrôle, appelées transitions de phase dissipatives, qui sont potentiellement différentes des transitions de phase quantiques ou thermiques ordinaires et attirent donc beaucoup d'attention [29–55]. Bien que les systèmes dissipatifs pilotés soient des plates-formes très naturelles pour étudier les phénomènes hors d'équilibre, la dissipation est préjudiciable pour les caractéristiques quantiques et donc pour l'observation des comportements particuliers de la mécanique quantique. Par exemple, la plupart des transitions de phase dans ces systèmes

appartiennent aux classes d'universalité thermique [18, 41, 45]. Néanmoins, toutes les caractéristiques quantiques ne sont pas nécessairement effacées par la dissipation, au point que les processus dissipatifs peuvent être conçus de manière à générer des états quantiques plutôt qu'à les supprimer; C'est le concept de l'ingénierie de la dissipation.

## 8.2 Spectral Properties of a Quantum van der Pol Oscillator

Dans ce chapitre, nous étudions les fonctions de Green des systèmes quantiques markoviens dissipatifs pilotés, en utilisant une représentation spectrale de ces fonctions. En l'appliquant au modèle prototype d'un oscillateur quantique van der Pol avec une non-linéarité supplémentaire dans son hamiltonien, nous prédisons des phénomènes qui n'apparaissent pas dans la matrice de densité stationnaire. Contrairement à l'état stationnaire, la fonction spectrale photonique de ce modèle dépend fortement de la force de l'interaction. Nous soulignons qu'une propriété de signe des fonctions spectrales des systèmes d'équilibre ne tient pas dans le cas des systèmes ouverts. En conséquence, nous constatons que la coopération d'interactions et d'effets hors équilibre peut donner lieu à une surprenante "densité d'états négative" avec des conséquences physiques directes, dans la mesure où elle peut générer des états de température négatifs ou des transitions de phase à fréquences finies dans des modèles de réseau, comme nous le verrons dans le chapitre 8.3 et comment cela a été discuté récemment dans le contexte des quenches quantiques [154]. Nous trouvons en particulier que la "densité d'états négative" peut apparaître même en l'absence d'inversion de population dans l'état stationnaire. Les résultats de ce chapitre ont été publiés dans [1].

### 8.2.1 Introduction

Les systèmes quantiques dissipatifs-pilotés ont généralement des états stationnaires non thermiques déterminés par l'équilibrage de le pilotage et de la dissipation. Un grand nombre de travaux théoriques ont été consacrés à la recherche (exacte ou approximative) de l'état stationnaire de tels systèmes et des valeurs correspondantes attentes des observables. [82, 155–158].

Bien que la description des états stationnaires présente clairement un intérêt, de nombreuses sondes expérimentales impliquent d'étudier comment un système répond à une perturbation appliquée faible. On cherche alors naturellement à comprendre les fonctions de Green qui décrivent la réponse linéaire du système aux perturbations externes. Pour les systèmes markoviens, ces fonctions de corrélation peuvent être facilement calculées à l'aide du théorème de régression quantique et ont été étudiées dans divers contextes différents, à partir de l'exemple standard de la fluorescence d'un atome à deux niveaux piloté [159–161] au cas récemment discuté des reseaux de qubits couplés [24]. Le sujet des fonctions de corrélation est également un sujet standard dans presque tous les manuels d'optique quantique (voir, par exemple, [7, 136]).

Malgré ces travaux, les méthodes permettant d'obtenir une intuition physique à partir du comportement des fonctions de Green restent intéressantes. Pour les systèmes de nombreux corps quantiques fermés et à l'équilibre, la représentation de Lehmann est un outil puissant [125, 149, 150]. Il exprime une fonction de Green à une particule en termes d'états propres de l'hamiltonien du système et permet d'interpréter la fonction spectrale en termes de taux de règle d'or de Fermi pour l'ajout (ou le retrait) d'une particule. Ceci se connecte directement aux sondes expérimentales (par exemple, ARPES ou spec-

troscopie à effet tunnel) et est inestimable pour la construction d'images intuitives. En outre, la représentation de Lehmann permet de prouver des propriétés mathématiques exactes, telles que les règles de somme, les propriétés de signe et le théorème de dissipation de fluctuation pour les systèmes à l'équilibre. Dans ce chapitre, nous montrons que la représentation de Lehmann des fonctions de Green d'un système dissipatif piloté constitue également un puissant outil d'interprétation. Comme exemple concret, nous analysons un modèle simple, mais non trivial, d'un oscillateur de van der Pol quantique non linéaire, décrivant une cavité bosonique monomode sujette à un pilotage incohérente motrice et à une dissipation non linéaire (voir Réf. [153] pour plus de détails.), avec une interaction de Kerr supplémentaire dans son hamiltonien. Ce modèle a récemment retenu l'attention dans le contexte de la synchronisation quantique avec l'interaction de Kerr [163] et sans [164, 165]; il est également directement réalisable dans les architectures de circuits supraconducteurs, où de fortes interactions de Kerr et des pertes artificielles à deux photons ont été obtenues expérimentalement [103, 104]. En effet, les non-linéarités dans ces architectures présentent également un intérêt pratique, induisant un effet de blocage de photons [166] qui joue un rôle crucial dans l'ingénierie d'états pertinents pour le calcul quantique [167–169]. Bien que le modèle ait un état stationnaire relativement simple, ses caractéristiques spectrales sont remarquablement riches [153, 170]. Contrairement à l'état d'équilibre, la fonction spectrale dépend fortement de la taille de l'interaction de Kerr et révèle la physique au-delà de celle de la matrice de densité en état d'équilibre. Nous montrons en particulier que le modèle présente à la fois une inversion de population dans la matrice de densité et une densité d'états négative (NDoS), deux aspects étroitement liés à l'équilibre mais dont l'interaction dans le cas piloté-dissipatif apparaît plus complexe. Nous trouvons en particulier un régime dans lequel la NDoS émerge, même en l'absence d'inversion de population dans la matrice de densité stationnaire.

### 8.2.2 Résultats

Dans ce travail, nous avons étudié les propriétés spectrales des systèmes quantiques dissipatifs pilotés. Prenons le cas simple d'un oscillateur quantum van der Pol avec la non-linéarité de Kerr. Nous avons d'abord tiré quelques résultats généraux concernant la fonction de Green à une particule de systèmes décrite par une équation de Lindblad. En utilisant une décomposition en termes d'états propres exacts du Liouvillien, nous avons comparé la représentation spectrale de la fonction de Green à la bien connue représentation de Lehmann pour les systèmes fermés en équilibre thermique. Une telle représentation spectrale, en plus de présenter un intérêt pratique pour les calculs numériques lorsque le système est suffisamment petit pour être diagonalisé exactement, a également une valeur conceptuelle. D'un côté, il relie les propriétés des valeurs propres et des états propres de Liouville, qui présentent un intérêt théorique mais qui sont souvent difficiles d'accès, au comportement des fonctions spectrales, qui présentent une pertinence expérimentale directe. De plus, cela permet une interprétation plus transparente des caractéristiques spectrales dans des régimes éloignés de l'équilibre, pour lesquels une simple intuition est souvent absente ou trompeuse. A titre d'exemple, nous avons montré que la propriété

bien connue des fonctions de Green à l'équilibre, qui changent de signe à une fréquence nulle comme conséquence de l'occupation thermique, peut être violée dans les systèmes dissipatifs pilotés et qu'elle n'est en général pas directement contrainte par la structure de la matrice de densité stationnaire du système.

Nous avons ensuite appliqué notre approche au cas d'un oscillateur quantique de van der Pol avec une non-linéarité de Kerr. Un tel modèle s'avère être une étude de cas parfaite, car les propriétés de sa matrice de densité stationnaire sont bien connues, tandis que ses caractéristiques spectrales révèlent un certain nombre de surprises. En particulier, la densité d'état du résonateur montre une forte dépendance vis-à-vis de la force de la non-linéarité de Kerr, une caractéristique totalement absente des populations à l'état d'équilibre, définie uniquement par le rapport pompe/perte. Encore plus intéressant, sous le régime de fortes interactions et d'un important déséquilibre, une NDoS apparaît, effet qui ne serait pas possible en équilibre thermique.

Nous avons résumé le comportement de la fonction spectrale de ce modèle dans un diagramme de phase qui montre que la NDoS n'est pas nécessairement lié à une population inversée dans la matrice de densité stationnaire. Afin de construire une intuition physique et de mieux comprendre l'origine de ce résultat, nous avons développé une approche semi-analytique qui part de la fonction spectrale du problème isolé et ajoute une durée de vie due à la dissipation dans l'esprit de la règle d'or de Fermi. Cette méthode, qui s'avère équivalente à une théorie de perturbation dans la dissipation où seules les valeurs propres du liouvillien sont corrigées, a pu capturer partiellement l'effet de la NDoS, au moins pour une interaction suffisamment grande et chaque fois que la matrice de densité stationnaire montre une inversion de population. Enfin, nous avons montré que l'inclusion de la correction perturbative des états propres du Liouvillian détermine un nouveau mécanisme pour avoir une NDoS, du fait de l'émergence de poids complexes dans la fonction spectrale. Cela s'avère crucial pour capturer les NDoS dans le régime où les populations de l'état stationnaire ne sont pas encore inversées.

Pour conclure, nous mentionnons que l'approche décrite ici est plutôt générale et peut être utilisée pour faire la lumière sur les propriétés spectrales d'autres modèles quantiques dissipatifs pilotés. Parmi les orientations futures intéressantes, citons par exemple l'étude des formes de lignes de fluorescence au-delà de la limite du système à deux niveaux [177, 178], les caractéristiques spectrales d'une cavité pilotée de manière cohérente à travers une transition de phase dissipative de dimension zéro [43, 47, 106] ou des applications liées à la synchronisation quantique [164, 179, 180].

## 8.3 Transition à fréquence finie dans des réseaux de bosons pilotés et dissipatifs

Les points critiques et les transitions de phase sont caractérisés par des susceptibilités divergentes, reflétant la tendance du système à la rupture spontanée de symétrie. La mécanique statistique d'équilibre oblige ces instabilités à se produire à une fréquence nulle, donnant lieu à des paramètres d'ordre statiques. Dans ce chapitre, nous expliquons qu'un modèle de prototype de bosons sur réseau dissipatifs piloté et corrélés, qui présente un intérêt direct pour la prochaine génération d'expériences avec les circuits quantiques, présente une susceptibilité divergeant à une fréquence finie non nulle, une échelle émergente définie par des interactions et par les effets de non équilibre. Nos travaux, établissant un lien entre l'invariance par translation dans le temps et les susceptibilités divergentes en fréquence finie, pourraient éventuellement être étendus à l'étude d'autres instabilités dans le domaine temporel dans des systèmes quantiques hors équilibre, notamment les cristaux de temps de Floquet [118] et la synchronisation quantique [163, 164, 181, 182]. Les résultats de ce chapitre ont été publiés dans [2].

### 8.3.1 Introduction

Les transitions de phase de second ordre dans les systèmes à l'équilibre thermique ou dans leur état fondamental sont caractérisées, selon le paradigme de Landau, par l'émergence d'un paramètre d'ordre statique qui rompt spontanément une symétrie du système, telle que l'invariance de rotation du spin pour le magnétisme ou la translation spatiale pour les cristaux [111, 183]. La criticité qui en résulte est décrite en termes d'instabilité d'une phase symétrique, caractérisée par la singularité d'une susceptibilité statique. Pour les systèmes classiques éloignés de l'équilibre thermique, comme en présence de forçage et de dissipation externes, la variété des instabilités peut être beaucoup plus riche, les modes à la fois l'impulsion finie et la fréquence finie devenant instables et conduisant à la formation de chaos temporel, synchronisation ou autres comportements oscillatoires [184–186]. Les systèmes quantiques à plusieurs corps dissipatifs et pilotés, représentent des plateformes naturelles pour comprendre et explorer de telles phases dynamiques. Un exemple bien connu est fourni par les condensats d'excitons et polaritons où la superfluidité apparaît avec un paramètre d'ordre oscillant dans le temps [30, 31, 70, 122]. Pourtant, le condensat oscillant est décrit avec succès par des théories semi-classiques telles que les équations de Gross-Pitaevski qui sont valables dans le régime des interactions faibles. Plus récemment, l'attention s'est tournée vers les modèles de réseau fortement corrélés avec pilotage et dissipation, plusieurs travaux ayant révélé l'existence de cycles limites, à savoir des solutions non stationnaires de la dynamique quantique pour un paramètre d'ordre macroscopique, au moins au niveau du champ moyen [16, 17, 20, 93, 187–189].

Dans ce chapitre, nous nous intéressons à un modèle paradigmique de bosons en interaction dissipative-forcés sur un réseau, qui est directement pertinent pour les expériences de la prochaine génération de matrices de circuits QED [61, 62, 86]. Nous soutenons qu'une susceptibilité dynamique d'un tel système quantique ouvert aux nombreux corps,

qui en équilibre thermique est fini et petit car les modes de fréquence non nuls sont généralement amortis par des interactions, peut afficher une véritable singularité à fréquence finie, à la suite d'interactions fortes et des effets de non équilibre. La fréquence critique est non triviale et définie par une compétition d'interactions entre dynamisme et dissipation. Finalement, le système subit une transition de phase dynamique où le paramètre d'ordre émerge avec une fréquence d'oscillation finie et dans la phase de symétrie brisée oscille dans le temps sans amortissement, rompant ainsi la symétrie de translation dans le temps continu. Cette instabilité à l'état stationnaire est contrôlée à la fois par des couplages dissipatifs et cohérents, en particulier par le rapport entre le paramètre de saut et l'interaction locale, fournissant ainsi l'analogie fortement corrélée de la condensation de bosons hors équilibre à couplage faible.

### 8.3.2 Résultats

Dans ce chapitre, nous avons montré qu'un modèle prototype de bosons sur réseau dissipatifs et pilotés, développe pour une valeur critique du taux de sauts une susceptibilité divergente à une fréquence non nulle  $\Omega_{\text{crit}}$ . La criticité à fréquence finie obtenue correspond à une dynamique dissipative dépourvue d'état stationnaire et oscillant plutôt dans le temps sans amortissement. En notant la théorie du champ de Keldysh effectif pour cette transition de fréquence finie, nous en avons obtenu la limite semi-classique, que nous montrons reproduire les résultats d'un découplage de Gutzwiller dépendant du temps et de la matrice de densité. Nous soulignons que la capture de la fréquence critique  $\Omega_{\text{crit}}$  nécessite la solution quantique du problème d'un site isolé avec interaction et dissipation et qu'elle ne figure donc pas dans l'équation semi-classique du mouvement que nous avons dérivée, qui ne décrit que la dynamique du cadre en rotation à la fréquence  $\Omega_{\text{crit}}$ . Nos résultats diffèrent des autres études sur les instabilités en cycles limites dans les systèmes dissipatifs pilotés, tels que les condensats de excitons et polaritons décrits par les équations de type Gross-Pitaevski (GP), et pourraient en être considérées comme la version fortement corrélée. En effet, notre transition partage les caractéristiques authentiques d'une transition de phase quantique dissipative de Mott-superfluide, étant contrôlée à la fois par des couplages cohérents et par les taux de pompage/pertes. En particulier, notre phase incohérente existe par petits taux de saut, même au-delà du seuil standard de la pompe supérieur aux pertes, un effet véritablement quantique dû à la répulsion de Hubbard favorisant les états de type Fock plutôt que les états cohérents. De plus, la fréquence du cycle limite est finie au point de transition, où le paramètre d'ordre superfluide disparaît et influence également la dynamique de phase normale, tandis que dans les théories GP, elle s'annule à ce point, étant proportionnelle au paramètre d'ordre superfluide.

Nos travaux suggèrent plusieurs directions futures intéressantes. D'un côté, il serait intéressant d'inclure des fluctuations dynamiques et spatiales pour étudier le sort de cette transition dynamique dissipative en dimensions finies, à la suite d'enquêtes similaires effectuées pour les transitions dynamiques dans les systèmes quantiques isolés [196–198]. Une autre question ouverte intrigante consiste à savoir s'il existe une criticité similaire à fréquence finie dans les modèles de systèmes dissipatifs et pilotés avec phases de symétrie

discrètes brisées [16] ou même en présence d'un pilotage purement cohérent, comme par exemple dans le contexte de plates-formes optomécaniques [172, 199] ou des chaînes de spin quantiques pilotés de manière cohérente [188].

Enfin, alors que nos travaux portent sur un modèle paradigmique de bosons dissipatifs entraînés, pertinents pour la prochaine génération d'expériences sur les matrices de circuits QED, [61, 62, 93], il décrit également un cadre générique pour l'étude des instabilités dynamiques dans systèmes quantiques hors d'équilibre, en se concentrant sur les fonctions de réponse dépendant de la fréquence et leurs divergences. Un tel cadre pourrait être appliqué dans un large éventail de contextes, y compris par exemple les systèmes de Floquet pilotés et isolés, dans lesquels une rupture de la symétrie temps-translation discrète a été prédite [118, 119, 200] et observée [121, 201], systèmes quantiques soumis à diverses formes de synchronisation [163, 164, 179, 181, 182, 199, 202] ainsi que des systèmes électroniques sous irradiation optique pompe-sonde [203].

## 8.4 Préparation d'isolants de Mott à l'aide de la dissipation

Les progrès expérimentaux récents en matière de contrôle de la dissipation ont donné la possibilité de mettre au point des processus dissipatifs afin d'obtenir des phases quantiques enchevêtrées de la matière en tant qu'états stationnaires de la dynamique dissipative. Cela fait suite au concept d'ingénierie dissipative. Dans le chapitre 8.3, nous avons étudié un modèle de réseaux bosoniques dissipatif et piloté et nous nous sommes concentrés sur la transition de phase aux fréquences finies entraînée par le paramétrage de saut, qui n'est pas liée au choix spécifique du mécanisme de pilotage. Dans ce chapitre, nous étudierons plutôt les propriétés de la phase normale stabilisée par le schéma de pilotage proposé par [101]. Ce schéma de pilotage a été proposé dans [101] pour stabiliser une phase isolante de Mott en tant qu'état stationnaire de la dynamique dissipative. Une question intéressante à poser est la différence entre cette phase isolante de Mott et la phase d'équilibre. Dans [101], les auteurs ont montré que l'état stationnaire d'une telle chaîne de Bose-Hubbard pilotée et dissipative en 1D est très proche de l'état fondamental d'un modèle de Bose-Hubbard 1D avec un potentiel chimique approprié. Cette similitude s'étend à la fois à la phase de Mott et à la phase superfluide et suggère que, en contrôlant le pilotage et de la dissipation, on peut s'approcher autant que souhaité de l'état fondamental. De manière remarquable, cependant, dans [101], le caractère de non équilibre du problème ne joue aucun rôle majeur. Leur diagramme de phase pour l'état stationnaire piloté et dissipatif correspond assez bien à l'état fondamental un en 1D, montrant la structure bien connue des lobes de Mott [88, 204]. Il n'y a aucune indication dans [101] de la transition en fréquence finie dont nous avons parlé dans le chapitre 8.3 et même la phase superfluide est stationnaire. Les méthodes numériques utilisées dans [101] sont en fait adaptées pour calculer l'état stationnaire indépendant du temps du modèle, mais ne donnent pas accès aux caractéristiques dynamiques. D'autre part, on sait bien que les superfluides pilotés et dissipatifs oscillent dans le temps [30, 41] à un potentiel chimique efficace. De même, dans [189], où un problème similaire de la limite des bosons à noyau dur est analysé, des cycles limites sont prédits. Il est en effet déroutant de réconcilier l'image complètement statique de l'état fondamental de [101] avec les caractéristiques de non-équilibre dynamiques prédites par exemple dans [1, 30, 41, 189]. Dans ce chapitre, nous fournissons une image complète permettant de réconcilier ces résultats. La préparation dissipative des isolantes de Mott est pertinente pour les expériences en cours. Dans [62] les auteurs utilisent des réservoirs sélectifs en énergie pour stabiliser de manière dissipative une phase isolante de Mott. Leur expérience comprend une chaîne 1D de 8 résonateurs supraconducteurs non linéaires dans un circuit. La chaîne réalise un modèle de Bose-Hubbard avec pertes, dans lequel le dernier site est couplé à un réservoir sélectif en énergie qui injecte des photons avec une énergie inférieure à celle du gap de la phase de Mott. Contrairement au modèle de [101] et à notre modèle, où chaque site est piloté, à [62], un seul site est connecté au réservoir.

### 8.4.1 Résultats

Dans ce chapitre, nous avons abordé le diagramme de phase des isolants photoniques de Mott, stabilisés de manière dissipative, selon le schéma proposé dans [101]. Nous avons discuté de la similarité entre l'état stationnaire dissipatif du problème de site unique et l'état fondamental d'un site de Bose-Hubbard. Cette similitude au niveau des sites uniques s'étend à la chaîne 1D de 7 sites étudiée dans [101], où les auteurs ont constaté que ce modèle dissipatif et piloté présente un état stationnaire reproduisant avec une très haute fidélité un isolant de Mott. Nous avons étudié le diagramme de phase en champ moyen d'un tel isolant de Mott stabilisé par voie dissipative dans la limite de la dissipation nulle, pour laquelle la physique d'un site isolé est très proche de son état fondamental. Nous avions prédit que, de manière surprenante, la région de stabilité d'une telle phase est remarquablement réduite par rapport au diagramme de phase de l'état fondamental de l'hamiltonien de Bose-Hubbard correspondant, en raison de l'apparition d'instabilités de modes dynamiques. Nous avons constaté que plus le ratio pilotage/perte est important, plus le taux de saut critique pour lequel la phase de Mott devient instable est petit. Pour un rapport pilotage/perte supérieur, l'état stationnaire devrait également être plus proche de l'état fondamental de Mott. En conséquence, nos résultats suggèrent qu'il existe un compromis entre la fidélité de la phase stationnaire à un isolant de Mott et la robustesse d'une telle phase à taux de saut finis. La validité de nos résultats au-delà du champ moyen doit être affirmée avec des méthodes plus puissantes. En effet, la théorie du champ moyen tend à favoriser la phase de symétrie interrompue. On peut donc s'attendre à ce que des fluctuations au-delà du champ moyen poussent la limite de phase de Mott-superfluide à des valeurs plus grandes du saut. Nous nous attendons cependant que la tendance qualitative du taux de saut critique qui décroisse avec la force du pilotage, résultant de la physique locale, reste valable au-delà du champ moyen. Nous avons finalement étudié le diagramme de phase d'un schéma de pilotage différent, en stabilisant une phase normale mixte incohérente plutôt qu'un isolant de Mott, montrant que les fluctuations thermiques effectives augmentent la région de stabilité de la phase normale, comme prévu. Les résultats de ce chapitre sont préliminaires et pour la plupart non publiés. La limite très intéressante de dissipation évanescante peut être résolue analytiquement, en calculant les fonctions de Green dans la théorie des perturbations. L'occupation de l'état stationnaire à plusieurs corps peut également être calculée en utilisant notre approche de couplage fort. Ce modèle à dissipation pilotée s'avère donc être un très simple modèle pour discuter des isolants Mott stabilisés par dissipation, tout en étant pertinent pour les expériences en cours [62].

## 8.5 Vers une approche DMFT pour les réseaux de bosons dissipatifs pilotés

La théorie du champ moyen dynamique (DMFT) est apparue au cours des deux dernières décennies comme une approche très puissante pour étudier les systèmes quantiques à plusieurs corps fortement en interaction [205]. Comme pour tout problème quantique à plusieurs corps, la mise à l'échelle exponentielle de la taille de l'espace de Hilbert avec le nombre de degrés de liberté rend difficile la résolution numérique de gros systèmes. Les systèmes ouverts markoviens souffrent encore plus de cette limitation, car l'espace naturel pour traiter numériquement ces problèmes est l'espace de Liouville, dont la taille est le carré de celui de l'espace de Hilbert original. Plusieurs méthodes ont récemment été proposées, qui sont généralement limitées à 1D ou à des systèmes de petite taille. Les schémas de réseau de tenseurs [206–208] sont très efficaces pour les systèmes 1D, mais sont encore limités dans les dimensions supérieures malgré les efforts en cours [209]. Une méthode prometteuse en 2D est la méthode “corner space renormalization group” [53, 156]. Récemment, une méthode de Monte Carlo a été proposée [210], mais son applicabilité est limitée par son problème de signe. Au-delà des méthodes de champ moyen telles que les méthodes de cluster [157, 211] et l'opérateur de projection auto-cohérent [20, 212] sont également des techniques prometteuses. Enfin, quatre groupes ont indépendamment proposé un réseau de neurones pour la matrice de densité des systèmes ouverts à plusieurs corps [213–216], à la suite de la proposition pour les systèmes quantiques fermé [217]. Cette approche semble prometteuse, mais ses forces et ses limites doivent encore être évaluées. Développer une approche DMFT pour les systèmes quantiques à plusieurs corps quantiques dissipatifs et pilotés comblerait une lacune dans ce scénario. DMFT est une technique de couplage fort non perturbative qui mappe un problème de réseau dans la limite thermodynamique sur un problème auxiliaire décrivant un site unique couplé à un bain autocohérent, que nous appellerons *problème d'impureté*. C'est dans l'esprit de la théorie du champ moyen standard, où un problème de réseau est mappé sur un problème à site unique dans un champ autocohérent. La différence qualitative est que le problème effectif en champ moyen est décrit par un hamiltonien, tandis que les effets de retardement de DMFT qu'un site expérimente en tant qu'effet du reste du réseau sont pris en compte et que la théorie effective doit être décrite en termes de une action, qui n'est pas locale dans le temps, d'où le nom de théorie des champs moyens dynamiques. Formulé directement dans les limites thermodynamiques, DMFT ne se limite pas aux systèmes de petite taille, comme la plupart des méthodes existantes. Le goulot d'étranglement de DMFT réside dans le fait que la résolution du problème des impuretés auxiliaires n'est pas une tâche facile, mais elle reste de loin plus facile que de résoudre le problème du réseau initial. En conséquence, nous avons besoin de méthodes appropriées, que nous appellerons *résolveurs d'impuretés*, pour résoudre le problème auxiliaire. Le travail présenté dans ce chapitre constitue la première tentative vers la résolution de la DMFT pour des problèmes de réseau dissipatifs pilotés. Ces résultats ont été publiés dans [3].

### 8.5.1 Résultats

Dans ce chapitre, nous présentons nos développements vers une approche DMFT (Dynamical Mean Field Field) à pour étudier de systèmes à réseaux dissipatifs pilotés. Ces efforts sont justifiés par l'absence actuelle de méthodes bien établies pour étudier ces systèmes.

Afin de résoudre DMFT, nous avons développé une méthode pour résoudre le problème auxiliaire d'une seule impureté, qui dans notre contexte est couplé simultanément à un environnement markovien et à un environnement non-markovien. Nous avons dérivé une expansion formelle d'hybridation pour le super-opérateur d'évolution de l'impureté, obtenue après avoir tracé tous les degrés de liberté du bain. Ce résultat généralise au cas d'une dynamique markovienne non unitaire l'expansion d'hybridation obtenu pour les modèles unitaires d'impuretés quantiques. En tant que tel, il constitue le point de départ naturel pour le développement de techniques d'échantillonnage stochastique de la dynamique dissipative en temps réel de l'impureté basées sur Diagrammatic Monte Carlo, que nous laisserons pour des études ultérieures. À partir de cette expansion, nous définissons des règles de diagramme en temps réel et écrivons une équation de Dyson pour le propagateur d'impuretés que nous évaluons en ne retenant que les diagrammes non croisés, une approximation connue pour capturer certains aspects de la physique des impuretés à couplage fort.

Il est intéressant de commenter la relation entre notre approche et les méthodes associées pour traiter les modèles d'impuretés couplés à plusieurs bains. Alors qu'en principe l'expansion d'hybridation [266] ainsi que la résumation schématique à couplage fort [267] peuvent être généralisées en présence de plusieurs environnements, prendre la limite markovienne dès le début présente un avantage pratique et conceptuel. En particulier, nous pouvons tirer directement parti de la nature locale de l'évolution markovienne et effectuer un développement autour d'une limite atomique qui contient maintenant non seulement des interactions locales, mais également le pilotage et la dissipation. Cette limite peut être facilement résolue par la diagonalisation directe d'un Lindbladien, par opposition au traitement de l'environnement markovien comme une self-énergie dans l'approximation NCA. L'idée clé est donc de traiter sur un pied d'égalité toutes les échelles d'énergie liées aux processus rapides, tout en recourant à la théorie des perturbations pour traiter les processus conduisant à des corrélations lentes telles que le couplage à des réservoirs sans gap.

En tant qu'application, nous avons résolu numériquement l'équation de Dyson pour le modèle simple d'une impureté fermionique, avec pertes markoviennes, pompage et déphasage et couplé à un environnement à température nulle non markovien. Ce modèle n'est pas trivial pour la présence de déphasage, qui est un terme quartique dans les opérateurs fermioniques. Cette implémentation simple a permis de vérifier les propriétés spectrales du super-opérateur d'évolution et d'étudier comment la dynamique markovienne est modifiée par couplage à un environnement non-markovien. En particulier, notre méthode a permis de mettre en évidence une conséquence physique du couplage simultané à des environnements markoviens et non-markoviens: le déphasage markovien associé à des processus non-markoviens entraîne une modification des occupations des impuretés.

Les orientations futures comprennent l'exploration de modèles d'impuretés plus complexes faisant intervenir des degrés de liberté internes, tels que le modèle d'Anderson, ainsi que des extensions bosoniques, ainsi que l'utilisation de ce solveur NCA pour résoudre DMFT en réseaux dissipatifs pilotés.

# Appendix A

## Energy-selective dissipator

### A.1 Derivation

In this appendix we derive the dissipator defined in section 4.2 for the coupling to an energy selective reservoir. The derivation follows that of a Lindblad master equation, but we won't do the rotating-wave or secular approximation. We mainly follow [136] for the derivation of master equations.

Let's consider a Bose-Hubbard site with Hamiltonian  $H_S = \omega_0 a^\dagger a + U/2 (a^\dagger a)^2$ , with eigenvalues  $\varepsilon(n) = \omega_0 n + U/2n^2$  in terms of the eigenvalues of  $a^\dagger a$ , namely the Fock states. We consider this site to be coupled to a two-level system environment with coupling Hamiltonian

$$H_{SR} = \sum_k V_k (a^\dagger \sigma_k^- + \text{hc}) \quad (\text{A.1})$$

where  $\sigma_k^-$ ,  $\sigma_k^+$  are spin-flip operators. We consider a spin environment having in mind the physical implementation proposed in [101], but this choice is not crucial for the derivation. We leave the environment hamiltonian  $H_R$  unspecified. The total Hamiltonian of the system+reservoir is  $H = H_0 + H_{SR}$ , where we defined  $H_0 = H_S + H_R$ . We denote by  $v$  the total density matrix of system+reservoir, obeying the Von-Neumann equation.

$$\partial_t v = -i [H, v] \quad (\text{A.2})$$

We move to the interaction picture; the density matrix and operators in the interaction picture are defined as

$$v^{\text{ip}}(t) = e^{iH_0 t} v(t) e^{-iH_0 t} \quad H_{SR}^{\text{ip}}(t) = e^{iH_0 t} H_{SR} e^{-iH_0 t} \quad (\text{A.3})$$

In the interaction picture time evolution is in terms on  $H_{SR}^{\text{ip}}(t)$  and the Von-Neumann equation reads

$$\partial_t v^{\text{ip}}(t) = -i [H_{SR}^{\text{ip}}(t), v^{\text{ip}}(t)] \quad (\text{A.4})$$

Integrating this equation one gets  $v^{\text{ip}}(t) = v^{\text{ip}}(0) - i \int_0^t dt' [H_{SR}^{\text{ip}}(t'), v^{\text{ip}}(t')]$ , and plugging it back in (A.4), we get

$$\partial_t v^{\text{ip}}(t) = -i [H_{SR}^{\text{ip}}(t), v^{\text{ip}}(0)] - \int_0^t dt' [H_{SR}^{\text{ip}}(t), [H_{SR}^{\text{ip}}(t'), v^{\text{ip}}(t')]] \quad (\text{A.5})$$

The reduced density matrix of the system is defined by  $\rho = \text{tr}_R v$ . Performing a partial trace on the environment, and assuming

$$\text{tr}_R \left[ H_{SR}^{\text{ip}}(t), v^{\text{ip}}(0) \right] = 0 \quad (\text{A.6})$$

which is an easy condition to verify [7], we get

$$\partial_t \rho^{\text{ip}}(t) = - \int_0^t dt' \text{tr}_R \left[ H_{SR}^{\text{ip}}(t), \left[ H_{SR}^{\text{ip}}(t'), v^{\text{ip}}(t') \right] \right] \quad (\text{A.7})$$

We perform the Born approximation, which is a weak coupling approximation. It assumes that the bath density matrix is not changed by the coupling with the system:  $v^{\text{ip}}(t) \simeq \rho^{\text{ip}}(t)\rho_R$ . The Born approximation, and a change in integration variables, leads to

$$\partial_t \rho^{\text{ip}}(t) = - \int_0^t d\tau \text{tr}_R \left[ H_{SR}^{\text{ip}}(t), \left[ H_{SR}^{\text{ip}}(t-\tau), \rho^{\text{ip}}(t-\tau)\rho_R \right] \right] \quad (\text{A.8})$$

We now perform the Markov approximation. It consists in assuming that the integrand vanishes for  $\tau > \tau_B$ , where  $\tau_B$  is the relaxation time for bath correlations, so that we can let the upper limit of integration go to infinity. Also, one assumes that for  $\tau < \tau_B$  the system density matrix  $\rho^{\text{ip}}(t-\tau)$  doesn't change much, thus  $\rho^{\text{ip}}(t-\tau) \simeq \rho^{\text{ip}}(t)$ . Under these assumptions we get a time local equation

$$\partial_t \rho^{\text{ip}}(t) = - \int_0^\infty d\tau \text{tr}_R \left[ H_{SR}^{\text{ip}}(t), \left[ H_{SR}^{\text{ip}}(t-\tau), \rho^{\text{ip}}(t)\rho_R \right] \right] \quad (\text{A.9})$$

Performing an additional secular or rotating-wave approximation we would get a Lindblad master equation. We won't do it, thus we will get a dissipator that cannot be written Lindblad form, thus it is not guaranteed to yield a positive-definite density matrix [136, 193] and positivity must be checked a posteriori. By expanding the commutators we get

$$\partial_t \rho^{\text{ip}}(t) = \int_0^\infty d\tau \text{tr}_R \left( H_{SR}^{\text{ip}}(t-\tau)\rho^{\text{ip}}(t)\rho_R H_{SR}^{\text{ip}}(t) - H_{SR}^{\text{ip}}(t)H_{SR}^{\text{ip}}(t-\tau)\rho^{\text{ip}}(t)\rho_R + \text{hc} \right) \quad (\text{A.10})$$

Using the form of the system-reservoir coupling (A.1) and assuming anomalous correlations to vanish,  $\text{tr}_R \sigma^\pm(t)\sigma^\pm(t-\tau)\rho_R = 0$ , we get

$$\begin{aligned} \partial_t \rho^{\text{ip}}(t) = & \int_0^\infty d\tau f_l \left( a^{\text{ip}}(t-\tau)\rho^{\text{ip}}(t)a^{\dagger\text{ip}}(t)\Gamma_{-+}(\tau) - a^{\dagger\text{ip}}(t)a^{\text{ip}}(t-\tau)\rho^{\text{ip}}(t)\Gamma_{-+}(\tau) + \text{hc} \right) \\ & + f_g \left( a^{\dagger\text{ip}}(t-\tau)\rho^{\text{ip}}(t)a^{\text{ip}}(t)\Gamma_{+-}(-\tau) - a^{\text{ip}}(t)a^{\dagger\text{ip}}(t-\tau)\rho^{\text{ip}}(t)\Gamma_{+-}(-\tau) + \text{hc} \right) \end{aligned} \quad (\text{A.11})$$

where we defined the bath hybridization greater  $(-+)$  and lesser  $(+-)$  functions

$$f_l \Gamma_{-+}(\tau) = \sum_k |V_k|^2 \text{tr}_R \left( \sigma^{-\text{ip}}(t)\sigma^{+\text{ip}}(t-\tau)\rho_R \right) \quad (\text{A.12})$$

$$f_g \Gamma_{+-}(-\tau) = \sum_k |V_k|^2 \text{tr}_R \left( \sigma^{+\text{ip}}(t)\sigma^{-\text{ip}}(t-\tau)\rho_R \right) \quad (\text{A.13})$$

where  $f_l$  and  $f_g$  are positive coefficients. We note that the greater accounts for the process of creating a particle in the reservoir and losing one in the system, while the lesser describe a gain one particle for the system. We assume that  $\rho_R$  is stationary with respect to the bath dynamics, such that

those hybridization functions depend only on the time difference  $\tau$  and not on  $t$ . Also we note that  $\Gamma_{-+}(\tau)^* = \Gamma_{-+}(-\tau)$  and  $\Gamma_{+-}(\tau)^* = \Gamma_{+-}(-\tau)$ . The assumption (A.6) becomes  $\text{tr}_R [\sigma_-^{\text{ip}}(t), \rho_R] = \text{tr}_R [\sigma_+^{\text{ip}}(t), \rho_R] = 0$ . We can now go back to the Schröedinger picture, using  $\partial_t \rho(t) = -i [H_S, \rho(t)] + e^{-iHst} (\partial_t \rho^{\text{ip}}(t)) e^{iHst}$ . This accounts for removing all the ip indices and the  $t$  times. We also write explicitly the hermitian conjugates.

$$\begin{aligned} \partial_t \rho(t) &= -i [H_S, \rho(t)] + \\ &+ \int_0^\infty d\tau f_l \left( a(-\tau) \rho(t) a^\dagger \Gamma_{-+}(\tau) - a^\dagger a(-\tau) \rho(t) \Gamma_{-+}(\tau) + a \rho(t) a^\dagger(-\tau) \Gamma_{-+}(-\tau) - \rho(t) a^\dagger(-\tau) a \Gamma_{-+}(-\tau) \right) \\ &+ f_g \left( a^\dagger(-\tau) \rho(t) a \Gamma_{+-}(-\tau) - a a^\dagger(-\tau) \rho \Gamma_{+-}(-\tau) + a^\dagger \rho(t) a(-\tau) \Gamma_{+-}(\tau) - \rho(t) a(-\tau) a^\dagger \Gamma_{+-}(\tau) \right) \end{aligned} \quad (\text{A.14})$$

The first of the last two lines is a loss dissipator, while the second is a pump one. We can define the following modified annihilation and creation operators

$$\tilde{a}_l = \int_0^\infty d\tau \Gamma_{-+}(\tau) a(-\tau) \quad \tilde{a}_l^\dagger = \int_0^\infty d\tau \Gamma_{-+}(-\tau) a^\dagger(-\tau) \quad (\text{A.15})$$

$$\tilde{a}_g = \int_0^\infty d\tau \Gamma_{+-}(-\tau) a^\dagger(-\tau) \quad \tilde{a}_g^\dagger = \int_0^\infty d\tau \Gamma_{+-}(\tau) a(-\tau) \quad (\text{A.16})$$

where  $\tilde{a}_l^\dagger = (\tilde{a}_l)^\dagger$ ,  $\tilde{a}_g^\dagger = (\tilde{a}_g)^\dagger$ . Finally we introduce the modified dissipator (4.16),  $\tilde{\mathcal{D}}[X, Y] = X \rho Y^\dagger + Y \rho X^\dagger - X^\dagger Y \rho - \rho Y^\dagger X$ , getting the non-secular master equation

$$\partial_t \rho(t) = -i [H_S, \rho(t)] + \tilde{\mathcal{D}}[a, \tilde{a}_l] + \tilde{\mathcal{D}}[a^\dagger, \tilde{a}_p^\dagger] \quad (\text{A.17})$$

$$\tilde{\mathcal{D}}[a, \tilde{a}_l] = f_l \left( \tilde{a}_l \rho(t) a^\dagger + a \rho(t) \tilde{a}_l^\dagger - a^\dagger \tilde{a}_l \rho(t) - \rho(t) \tilde{a}_l^\dagger \right) \quad (\text{A.18})$$

$$\tilde{\mathcal{D}}[a^\dagger, \tilde{a}_p^\dagger] = f_g \left( \tilde{a}_g^\dagger \rho(t) a + a^\dagger \rho(t) \tilde{a}_g - a \tilde{a}_g^\dagger \rho(t) - \rho(t) \tilde{a}_g a^\dagger \right) \quad (\text{A.19})$$

The modified creation and annihilation operators can be computed more easily in the basis of Fock states, in terms of the Fourier transform of  $\Gamma_{-+}(t), \Gamma_{+-}(t)$ . Let's focus on the gain operator  $\tilde{a}_g = \int_0^\infty d\tau \Gamma_{+-}(\tau) a(-\tau)$ . Projecting it on the basis of Fock states, we get

$$\tilde{a}_g = \sum_n \Gamma_{+-}^R(\varepsilon(n+1) - \varepsilon(n)) \langle n | a | n+1 \rangle | n \rangle \langle n+1 | \quad (\text{A.20})$$

where  $\varepsilon(n)$  are the eigenvalues of the Hamiltonian and where we have defined the retarded Fourier transform

$$\Gamma_{+-}^R(\omega) = \int_{-\infty}^\infty dt \Gamma_{+-}(t) \theta(t) e^{i\omega t} = \int_0^\infty dt \Gamma_{+-}(t) e^{i\omega t} \quad (\text{A.21})$$

We also introduce the Fourier transform of  $\Gamma_{+-}(t)$

$$\Gamma_{+-}(\omega) = \int_{-\infty}^\infty dt \Gamma_{+-}(t) e^{i\omega t} \quad (\text{A.22})$$

There is a relation between  $\Gamma_{+-}^R(\omega)$  and  $\Gamma_{+-}(\omega)$ , exploiting that  $\Gamma_{+-}(\omega)$  is a real function, because  $\Gamma_{+-}(t)^* = \Gamma_{+-}(-t)$  and thus  $\Gamma_{+-}(t)$  and  $\Gamma_{+-}(-t)$  carry the same information. This relation reads

$$\Gamma_{+-}^R(\omega) = \frac{1}{2} \Gamma_{+-}(\omega) - i \mathcal{P} \int_{-\infty}^\infty \frac{d\omega'}{2\pi} \frac{\Gamma_{+-}(\omega')}{\omega' - \omega} \quad (\text{A.23})$$

where the real and imaginary part of  $\Gamma_{+-}^R(\omega)$  satisfy the Kramers-Krönig relations (2.7) because it is a retarded function. We also remark that  $[\Gamma_{+-}^R(\omega)]^* = \Gamma_{+-}^A(\omega)$ , which turns useful to write the creation operator  $\tilde{a}_g^\dagger$ .

## A.2 Cold and hot drives

In the main text we considered two driving schemes, which can be modeled using the dissipator derived in this appendix, which have been named the cold 4.2.2 and the hot drive 5.4. The cold drive corresponds to  $f_g \equiv f \neq 0$ ,  $f_l = 0$ . The hot drive corresponds to  $f \equiv f_g = f_l$  and  $\Gamma_{+-} = \Gamma_{-+}$ , thus  $\tilde{a}_g = \tilde{a}_l$ . We considered, for both drives

$$\Gamma_{+-}(\omega) \equiv \theta(\sigma - |\omega|) \quad (\text{A.24})$$

where  $\theta(\omega)$  is a step function centered in zero. This form for  $\Gamma$  implies its retarded component

$$\Gamma_{+-}^R(\omega) = \frac{1}{2}\theta(\sigma - |\omega|) - \frac{i}{2\pi} \log \left| \frac{\sigma - \omega}{\sigma + \omega} \right| \quad (\text{A.25})$$

The imaginary part  $\text{Im}\Gamma_{+-}^R(\omega)$ , is a Lamb-shift term. We note that its contribution is particularly important when  $\sigma \simeq |\varepsilon(n+1) - \varepsilon(n)|$  for which this term has a logarithmic divergence. We neglect this term in Ch. 4, where we keep our parameters far from these divergent points, while we keep it in Ch. 5, where we explore the whole phase diagram. Also, the choice of a window function with a hard cut-off for  $\Gamma_{+-}(\omega)$  is not rigorously justified, as this violates the Markovianity conditions under which the master equation was derived. In fact, we assumed that the relaxation time of the system  $\tau_R$  is much smaller than bath relaxation  $\tau_B$ . The characteristic time induced by the reservoir on the system is  $\tau_R \sim 1/f$ , while there's no other time-scale in the bath correlation dynamics, as one can see by the real time correlation function of the bath  $\Gamma_{+-}(t) = \sin(\sigma t)/(\pi t)$ . One should consider a “smooth” box-function, as in [101]:

$$\Gamma_{+-}(\omega) = \frac{1}{N} \left( \arctan \left( \frac{\sigma - \omega}{\Delta/2} \right) - \arctan \left( \frac{-\sigma - \omega}{\Delta/2} \right) \right) \quad (\text{A.26})$$

where the normalization  $N$  is chosen such that the window has height 1:  $N = \Gamma_{+-}(0) = 2 \arctan \left( \frac{2\sigma}{\Delta} \right)$ .  $\Delta$  serves as a cut-off for the bath correlations  $\tau_B \sim 1/\Delta$  as

$$\Gamma_{+-}(t) = \frac{1}{N} e^{-\Delta t/2} \frac{\sin(\sigma t)}{t} \quad (\text{A.27})$$

and the condition  $f_g \ll \Delta$  enforces the Markovian assumption. Also the Lamb-shift divergence gets cut off by  $\Delta$

$$\text{Im}\Gamma_{+-}^R(\omega) = \frac{1}{4N} \log \left( \frac{(\omega - \sigma)^2 + (\Delta/2)^2}{(\omega + \sigma)^2 + (\Delta/2)^2} \right) \quad (\text{A.28})$$

We preferred to use the simpler version with a “hard” cut-off. In fact, with the “smooth” window one has to numerically satisfy the conditions  $f_g, \kappa \ll \Delta \ll U$ , where  $\kappa$  is the loss rate, which considerably reduces the available parameters range. We checked that the choice of a “hard” rather than a “smooth” box-function produces only small quantitative differences in our results. In Ch. 4, in fact,

the choice of the “hard” box cannot be justified a priory. In Ch. 5, instead, the choice of a “hard” cut-off, that is  $\Delta \rightarrow 0$ , is consistent with the small dissipation limit  $\kappa \rightarrow 0$ , assuming the order of limits doesn’t matter; we numerically checked that indeed the two choices give qualitatively equivalent results.

## Appendix B

# More on DMFT

### B.1 Delocalization transition in DMFT

Let's consider the Bose-Hubbard model we discussed in Ch. 4,5, with an incoherent phase with  $\Phi = 0$  at low hopping separated by a second order phase transition from a broken-symmetry phase with  $\Phi \neq 0$ . In this appendix, we derive an equation for the critical point in DMFT which goes beyond the mean-field equation (4.22) for the critical hopping  $J_c$  (5.3)<sup>1</sup>

$$\frac{1}{J_c} + G_0^R(\Omega_*) = 0 \quad (\text{B.1})$$

using the simplified self-consistency relation for a Bethe lattice [226]

$$\Delta = \frac{J^2}{z} \mathbf{G} \quad (\text{B.2})$$

We remark that at  $J_c$  the off-diagonal components of  $\mathbf{G}$  vanish thus we can restrict to the first diagonal component, which we call  $G$ . The critical-point equation in DMFT reads

$$\frac{1}{J_c} + G^R(\Omega_*, J_c) + \frac{J_c}{z} [G^R(\Omega_*, J_c)]^2 = 0 \quad (\text{B.3})$$

We notice that the lattice retarded Green function enters in (B.3), rather than that of a decoupled site as in (B.1): this gives a much more non-trivial dependence of (B.3) on the critical hopping  $J_c$ . The last term in (B.3) describes  $1/z$  corrections, as expected by DMFT. Eventually (B.3) is a bold equation, i.e. involving lattice correlators, including  $1/z$  corrections. The mean-field equation (B.1) is recovered from (B.3) taking the  $z \rightarrow \infty$  limit. In fact, in this limit, lattice Green functions coincide with those of decoupled-sites  $G^R \rightarrow G_0^R$  whenever  $\Phi = 0$  and thus in particular at the critical point, as the effective action (6.3) reduces to standard mean field and describes decoupled sites in this limit.

The proof of (B.3) goes as follows. Let's sit in the early symmetry-broken phase, where the order parameter  $\Phi = \langle \mathbf{a} \rangle$  has just formed and it's small. This implies a small external field  $\Phi_{\text{eff}}$  (6.4)

$$\Phi_{\text{eff}}(t) = J\Phi(t) + \int_C dt' \Delta(t, t') \Phi(t') \quad (\text{B.4})$$

---

<sup>1</sup>we need to rescale the hopping  $J \rightarrow J/z$  in (5.3) to get (B.1)

in the DMFT effective action (6.3). We assume to be in stationary regime, such that two point correlators depend on time differences and move to Fourier space. As  $\Phi_{\text{eff}}$  is an average field  $\Phi_{\text{eff+}} = \Phi_{\text{eff-}}$ , thus (B.4) is also equivalent to

$$\Phi_{\text{eff}}(\omega) = J\Phi(\omega) + \Delta^R(\omega)\Phi(\omega) \quad (\text{B.5})$$

The response to  $\Phi_{\text{eff}}$  in linear-response theory is given by

$$\Phi(\omega) \equiv \langle \mathbf{a}(\omega) \rangle = \langle \mathbf{a}(\omega) \rangle_{\Phi_{\text{eff}}=0} - \mathbf{G}_{\Phi_{\text{eff}}=0}^R(\omega)\Phi_{\text{eff}}(\omega) \quad (\text{B.6})$$

where  $\mathbf{G}_{\Phi_{\text{eff}}=0}(\omega)$  is computed at  $\Phi_{\text{eff}} = 0$ . We also have that  $\langle \mathbf{a}(\omega) \rangle_{\Phi_{\text{eff}}=0} = 0$  for  $\Phi_{\text{eff}} = 0$ . Plugging (B.5) into (B.6), using the self-consistent equation (B.2) and retaining only first-order-in- $\Phi_{\text{eff}}$  terms, one gets

$$\Phi(\omega) = -J\mathbf{G}_{\Phi_{\text{eff}}=0}^R(\omega)\Phi(\omega) - \frac{J^2}{z}\mathbf{G}_{\Phi_{\text{eff}}=0}^R(\omega)\mathbf{G}_{\Phi_{\text{eff}}=0}^R(\omega)\Phi(\omega) \quad (\text{B.7})$$

This equation is satisfied for  $\Phi = 0$ , in the normal phase, and it must be satisfied in the early symmetry-broken phase, where  $\Phi \neq 0$ . At the critical point both solutions exist, and the second gives an equation for the critical point. As at the critical point the anomalous – non-diagonal – components of  $\mathbf{G}$  vanish, we consider the first diagonal component  $G$  only. We thus obtain the DMFT equation for the critical point (B.3), where it's not necessary to specify that the Green functions are computed at  $\Phi_{\text{eff}} = 0$ , as they are computed at  $J_c$  where  $\Phi_{\text{eff}} = 0$  by definition.

## B.2 Hubbard-I impurity solver in the symmetric phase

In this section, we introduce the simplest non-trivial solver for the impurity action (6.3). By solving the impurity problem, we mean being able to compute its one-particle Green functions. This solver is based on the Hubbard-I approximation [227, 268], where the lattice self-energy is approximated at zeroth order in the hopping; the Hubbard-I approximation is equivalent [227] to the random phase approximation (RPA) and thus to the strong-coupling approach we used in Ch. 4.5. We restrict to study the symmetric phase, i.e.  $\Phi = 0$ , where equations involve one Nambu component and to the stationary regime where convolutions turn into product under Fourier transform. From the Dyson equation for the impurity Green function we have

$$G^{-1} = G_{ni}^{-1} - \Delta - \Sigma \quad (\text{B.8})$$

where  $G_{ni}$  is the non-interacting Green function of the single-site problem – including also dissipative non-interacting terms – and  $\Sigma$  is the impurity self-energy. We approximate the impurity self-energy  $\Sigma$  at zeroth order in the bath  $\Delta$

$$\Sigma \approx G_{ni}^{-1} - G_{J=0}^{-1} \quad (\text{B.9})$$

where  $G_{J=0}$  is the Green function of an isolated site including all interactions, thus it is different from  $G_{ni}$ . By plugging this self-energy in the above Dyson equation (B.8) and using the Bethe lattice self-consistent condition (B.2), we get

$$G^{-1} = G_{J=0}^{-1} - \Delta = G_{J=0}^{-1} - \frac{J^2}{z}G \quad (\text{B.10})$$

This is a closed equation for  $G$ , which is easily solved in Fourier space, where it becomes a second-order algebraic equation. We can extract the retarded and Keldysh components from Eq. (B.10). The retarded Green function is simply given by

$$G^R(\omega) = \frac{z}{2J^2} G_{J=0}^R(\omega)^{-1} \left( 1 - \sqrt{1 - \frac{4J^2}{z} G_{J=0}^R(\omega)^2} \right) \quad (\text{B.11})$$

We extract the inverse Keldysh Green function  $[G^{-1}]^K = [G_{J=0}^{-1}]^K - \frac{J^2}{z} G^K$  from Eq. (B.10), that we invert with the standard relation  $G^K = -G^R [G^{-1}]^K G^A$ , giving

$$G^K = \frac{|G^R|^2 G_{J=0}^K}{|G_{J=0}^R|^2 \left( 1 - \frac{J^2}{z} |G^R|^2 \right)} \quad (\text{B.12})$$

We finally show that the equation determining the delocalization transition (B.3), reduces to the mean-field one (B.1) when evaluating it using the Hubbard-I impurity solver. In fact, from (B.10) we get  $J^2/z G = G_{J=0}^{-1} - G^{-1}$  that plugged into (B.3) gives  $1 + JG + G(G_{J=0}^{-1} - G^{-1}) = G(J + G_{J=0}^{-1}) = 0$ , where the last term is exactly the mean-field critical point equation (B.1). This is consistent with the fact that the Hubbard-I approximation coincides [227] with the strong-coupling approach we used to compute Green functions in Ch. 4,5, which yields the mean-field phase diagram.

# Appendix C

## Details of the NCA solver

### C.1 Stationary state

Assuming a stationary state exists for a non-Markovian map  $\mathcal{V}$  defined by the Dyson equation

$$\partial_t \mathcal{V}(t, t') = \mathcal{L} \mathcal{V}(t, t') + \int_{t'}^t dt_1 \Sigma(t, t_1) \mathcal{V}(t_1, t') \quad (\text{C.1})$$

then, setting  $t' = 0$ , it satisfies

$$\left( \mathcal{L} + \int_0^\infty dt_1 \Sigma(\infty, t_1) \right) \rho_{ss} = 0 \quad (\text{C.2})$$

In order to derive this equation, we focus on the propagator  $V(\infty, 0)$ , that projects any initial state on the stationary state:  $\rho_{ss} = V(\infty, 0)\rho(0)$ . This propagator obeys the Dyson equation

$$\lim_{t \rightarrow \infty} \partial_t V(t, 0) = \mathcal{L} V(\infty, 0) + \int_0^\infty dt_1 \Sigma(\infty, t_1) V(t_1, 0)$$

At this point we need to make some assumptions based on physical arguments.  $\mathcal{V}(t_1, 0)$  is expected to have a transient dynamics in a finite time interval of duration  $t_{\text{tr}}$ , starting at time  $t_1 = 0$ , and then to become stationary, i.e.  $\lim_{t \rightarrow \infty} \partial_t \mathcal{V}(t, 0) = 0$ . In addition, the system is supposed to lose memory of initial conditions, thus the convolution in the above Dyson equation must be cut off by the self-energy  $\Sigma(\infty, t_1)$  for  $\infty - t_1 > t_{\text{mem}}$ . Then, in the region where  $\Sigma(\infty, t_1)$  is non-zero,  $\mathcal{V}(\infty, t_1)$  is stationary and we can replace it with  $V(\infty, 0)$ . With these arguments we get  $(\mathcal{L} + \int_0^\infty dt_1 \Sigma(\infty, t_1)) V(\infty, 0) = 0$  and applying it to any initial state we find (C.2).

### C.2 Derivation of NCA self-energy

To obtain an analytic expression of the self-energy, we have to cast the  $k = 1$  term of the hybridization expansion obtained in the main text in a form in which the innermost integration time is lower than the outermost, that is with integrals of the form  $\int_{t'}^t dt_1 \int_{t'}^{t_1} dt_2$ . In doing so, sign of each contribution will be determined by the time-ordering  $T_C$ . The  $k = 1$  term of the hybridization expansion, omitting

the fermionic indices to simplify the expressions, reads

$$\begin{aligned}
i\mathcal{V}^{(1)}(t, 0) &= \sum_{\gamma_1, \gamma_2} \gamma_1 \gamma_2 \int_0^t dt_1 \int_0^t dt_2 T_F T_C \mathcal{V}_0(t, t_1) d_{(t_1 \gamma_1)}^\dagger \mathcal{V}_0(t_1, t_2) d_{(t_2 \gamma_2)} \mathcal{V}_0(t_2, 0) \Delta^{\gamma_1 \gamma_2}(t_1, t_2) = \\
&= \int_0^t dt_1 \int_0^t dt_2 T_F T_C \mathcal{V}_0(t, t_1) d_{(t_1+)}^\dagger \mathcal{V}_0(t_1, t_2) d_{(t_2+)} \mathcal{V}_0(t_2, 0) \Delta^{++}(t_1, t_2) + \\
&- \int_0^t dt_1 \int_0^t dt_2 T_F T_C \mathcal{V}_0(t, t_1) d_{(t_1+)}^\dagger \mathcal{V}_0(t_1, t_2) d_{(t_2-)} \mathcal{V}_0(t_2, 0) \Delta^{+-}(t_1, t_2) + \\
&- \int_0^t dt_1 \int_0^t dt_2 T_F T_C \mathcal{V}_0(t, t_1) d_{(t_1-)}^\dagger \mathcal{V}_0(t_1, t_2) d_{(t_2+)} \mathcal{V}_0(t_2, 0) \Delta^{-+}(t_1, t_2) + \\
&\int_0^t dt_1 \int_0^t dt_2 T_F T_C \mathcal{V}_0(t, t_1) d_{(t_1-)}^\dagger \mathcal{V}_0(t_1, t_2) d_{(t_2-)} \mathcal{V}_0(t_2, 0) \Delta^{--}(t_1, t_2)
\end{aligned} \tag{C.3}$$

where we have summed on contour indices  $\gamma_1$  and  $\gamma_2$ . Now we break the integrals in two pieces, for  $t_2 > t_1$  and  $t_2 < t_1$ , which allows to put the operators in a time-ordered fashion according to  $T_C$ .

$$\begin{aligned}
i\mathcal{V}^{(1)}(t, 0) &= \\
&= \int_0^t dt_1 \int_0^{t_1} dt_2 T_F \mathcal{V}_0 d_{(t_1+)}^\dagger \mathcal{V}_0 d_{(t_2+)} \mathcal{V}_0 \Delta^{++}(t_1, t_2) + \xi \int_0^t dt_1 \int_{t_1}^t dt_2 T_F \mathcal{V}_0 d_{(t_2+)} \mathcal{V}_0 d_{(t_1+)}^\dagger \mathcal{V}_0 \Delta^{++}(t_1, t_2) + \\
&- \xi \int_0^t dt_1 \int_0^{t_1} dt_2 T_F \mathcal{V}_0 d_{(t_2-)} \mathcal{V}_0 d_{(t_1+)}^\dagger \mathcal{V}_0 \Delta^{+-}(t_1, t_2) - \xi \int_0^t dt_1 \int_{t_1}^t dt_2 T_F \mathcal{V}_0 d_{(t_2-)} \mathcal{V}_0 d_{(t_1+)}^\dagger \mathcal{V}_0 \Delta^{+-}(t_1, t_2) + \\
&- \int_0^t dt_1 \int_0^{t_1} dt_2 T_F \mathcal{V}_0 d_{(t_1-)}^\dagger \mathcal{V}_0 d_{(t_2+)} \mathcal{V}_0 \Delta^{-+}(t_1, t_2) - \int_0^t dt_1 \int_{t_1}^t dt_2 T_F \mathcal{V}_0 d_{(t_1-)}^\dagger \mathcal{V}_0 d_{(t_2+)} \mathcal{V}_0 \Delta^{-+}(t_1, t_2) + \\
&+ \xi \int_0^t dt_1 \int_0^{t_1} dt_2 T_F \mathcal{V}_0 d_{(t_2-)} \mathcal{V}_0 d_{(t_1-)}^\dagger \mathcal{V}_0 \Delta^{--}(t_1, t_2) + \int_0^t dt_1 \int_{t_1}^t dt_2 T_F \mathcal{V}_0 d_{(t_1-)}^\dagger \mathcal{V}_0 d_{(t_2-)} \mathcal{V}_0 \Delta^{--}(t_1, t_2)
\end{aligned} \tag{C.4}$$

where we omitted the time arguments of the  $\mathcal{V}_0$  operators. The  $T_F$  time ordering will now sort the operators in ascending order in time from right to left:

$$\begin{aligned}
i\mathcal{V}^{(1)}(t, 0) &= \\
&= \int_0^t dt_1 \int_0^{t_1} dt_2 \mathcal{V}_0 d_{(t_1+)}^\dagger \mathcal{V}_0 d_{(t_2+)} \mathcal{V}_0 \Delta^{++}(t_1, t_2) + \xi \int_0^t dt_1 \int_{t_1}^t dt_2 \mathcal{V}_0 d_{(t_2+)} \mathcal{V}_0 d_{(t_1+)}^\dagger \mathcal{V}_0 \Delta^{++}(t_1, t_2) + \\
&- \xi \int_0^t dt_1 \int_0^{t_1} dt_2 \mathcal{V}_0 d_{(t_1+)}^\dagger \mathcal{V}_0 d_{(t_2-)} \mathcal{V}_0 \Delta^{+-}(t_1, t_2) - \xi \int_0^t dt_1 \int_{t_1}^t dt_2 \mathcal{V}_0 d_{(t_2-)} \mathcal{V}_0 d_{(t_1+)}^\dagger \mathcal{V}_0 \Delta^{+-}(t_1, t_2) + \\
&- \int_0^t dt_1 \int_0^{t_1} dt_2 \mathcal{V}_0 d_{(t_1-)}^\dagger \mathcal{V}_0 d_{(t_2+)} \mathcal{V}_0 \Delta^{-+}(t_1, t_2) - \int_0^t dt_1 \int_{t_1}^t dt_2 \mathcal{V}_0 d_{(t_2+)} \mathcal{V}_0 d_{(t_1-)}^\dagger \mathcal{V}_0 \Delta^{-+}(t_1, t_2) + \\
&+ \xi \int_0^t dt_1 \int_0^{t_1} dt_2 \mathcal{V}_0 d_{(t_1-)}^\dagger \mathcal{V}_0 d_{(t_2-)} \mathcal{V}_0 \Delta^{--}(t_1, t_2) + \int_0^t dt_1 \int_{t_1}^t dt_2 \mathcal{V}_0 d_{(t_2-)} \mathcal{V}_0 d_{(t_1-)}^\dagger \mathcal{V}_0 \Delta^{--}(t_1, t_2)
\end{aligned} \tag{C.5}$$

Using the fact that  $\int_0^t dt_1 \int_{t_1}^t dt_2 = \int_0^t dt_2 \int_0^{t_2} dt_1$  and exchanging the integration times in the second column we get

$$\begin{aligned}
& i\mathcal{V}^{(1)}(t, 0) = \\
&= \int_0^t dt_1 \int_0^{t_1} dt_2 [\mathcal{V}_0 d_{(t_1+)}^\dagger \mathcal{V}_0 d_{(t_2+)} \mathcal{V}_0 \Delta^{++}(t_1, t_2) + \xi \mathcal{V}_0 d_{(t_1+)} \mathcal{V}_0 d_{(t_2+)}^\dagger \mathcal{V}_0 \Delta^{++}(t_2, t_1) + \\
&\quad - \xi \mathcal{V}_0 d_{(t_1+)}^\dagger \mathcal{V}_0 d_{(t_2-)} \mathcal{V}_0 \Delta^{+-}(t_1, t_2) - \xi \mathcal{V}_0 d_{(t_1-)} \mathcal{V}_0 d_{(t_2+)}^\dagger \mathcal{V}_0 \Delta^{+-}(t_2, t_1) + \\
&\quad - \mathcal{V}_0 d_{(t_1-)}^\dagger \mathcal{V}_0 d_{(t_2+)} \mathcal{V}_0 \Delta^{-+}(t_1, t_2) - \mathcal{V}_0 d_{(t_1+)} \mathcal{V}_0 d_{(t_2-)}^\dagger \mathcal{V}_0 \Delta^{-+}(t_2, t_1) + \\
&\quad + \xi \mathcal{V}_0 d_{(t_1-)}^\dagger \mathcal{V}_0 d_{(t_2-)} \mathcal{V}_0 \Delta^{--}(t_1, t_2) + \mathcal{V}_0 d_{(t_1-)} \mathcal{V}_0 d_{(t_2-)}^\dagger \mathcal{V}_0 \Delta^{--}(t_2, t_1)] = \\
&= \sum_{\alpha\beta\in\{+,-\}} \alpha^{(1+\xi)/2} \beta \int_0^t dt_1 \int_0^{t_1} dt_2 \times \\
&\quad \times \mathcal{V}_0(t, t_1) \left[ d_{(t_1\beta)}^\dagger \mathcal{V}_0(t_1, t_2) d_{(t_2\alpha)} \Delta^{\beta\alpha}(t_1, t_2) + \xi d_{(t_1\beta)} \mathcal{V}_0(t_1, t_2) d_{(t_2\alpha)}^\dagger \Delta^{\alpha\beta}(t_2, t_1) \right] \mathcal{V}_0(t_2, 0)
\end{aligned} \tag{C.6}$$

which defines the NCA self-energy

$$\Sigma(t_1, t_2) = \sum_{\alpha\beta\in\{+,-\}} -\alpha^{(1+\xi)/2} \beta i \left[ d_\beta^\dagger \mathcal{V}(t_1, t_2) d_\alpha \Delta^{\beta\alpha}(t_1, t_2) + \xi d_\beta \mathcal{V}(t_1, t_2) d_\alpha^\dagger \Delta^{\alpha\beta}(t_2, t_1) \right] \tag{C.7}$$

### C.3 Trace preservation

The evolution super-operator  $\mathcal{V}$  obtained in the non-crossing approximation preserves the trace of the density operator, that is

$$\text{tr} \{ \mathcal{V}(t, t') \bullet \} = \text{tr} \{ \bullet \}$$

Writing  $\mathcal{V}(t, t') \bullet$  means applying the super-operator  $\mathcal{V}$  on a generic operator  $\bullet$ ; we recall that in the usual representation where the operator  $\bullet$  is a matrix, this is not a matrix product. To prove this, we take the trace of the NCA Dyson equation and we use the fact that  $\mathcal{V}_0$  does preserve the trace

$$\begin{aligned}
\text{tr} [\mathcal{V}(t, t') \rho_I(t')] &= \text{tr} [\mathcal{V}_0(t, t') \rho_I(t')] + \int_{t'}^t dt_1 \int_{t'}^{t_1} dt_2 \text{tr} [\mathcal{V}_0(t, t_1) \Sigma(t_1, t_2) \mathcal{V}(t_2, t') \rho_I(t')] = \\
&= \text{tr} [\rho_I(t')] + \int_{t'}^t dt_1 \int_{t'}^{t_1} dt_2 \text{tr} [\Sigma(t_1, t_2) \mathcal{V}(t_2, t') \rho_I(t')]
\end{aligned} \tag{C.8}$$

Then, using the expression for the self-energy Eq. (C.7), we can prove that the integrand vanishes, which completes the proof. In order to show that, we remark that for the cyclic property of the trace it holds that  $\text{tr}[X_+ \bullet] = \text{tr}[X_- \bullet]$ ,  $X$  being a generic super-operator. Then we can fix the  $d_\beta^\dagger, d_\beta$  super-operators to be  $d_+^\dagger, d_+$  under the trace, getting

$$\begin{aligned}
& \text{tr} [\Sigma(t_1, t_2) \mathcal{V}(t_2, t') \rho_I(t')] = \\
&= \sum_{a,b} \sum_{\alpha\beta\in\{+,-\}} -\alpha^{(1+\xi)/2} \beta i \text{tr} \left\{ \left[ \Delta_{ba}^{\beta\alpha}(t_1, t_2) d_{\beta b}^\dagger \mathcal{V}(t_1, t_2) d_{\alpha a} + \xi \Delta_{ab}^{\alpha\beta}(t_2, t_1) d_{\beta b} \mathcal{V}(t_1, t_2) d_{\alpha a}^\dagger \right] \mathcal{V}(t_1, t') \rho_I(t') \right\} = \\
&= \sum_{a,b} \sum_{\alpha\beta\in\{+,-\}} -\alpha^{(1+\xi)/2} \beta i \text{tr} \left\{ \left[ \Delta_{ba}^{\beta\alpha}(t_1, t_2) d_{+b}^\dagger \mathcal{V}(t_1, t_2) d_{\alpha a} + \xi \Delta_{ab}^{\alpha\beta}(t_2, t_1) d_{+b} \mathcal{V}(t_1, t_2) d_{\alpha a}^\dagger \right] \mathcal{V}(t_1, t') \rho_I(t') \right\}
\end{aligned} \tag{C.9}$$

By summing over  $\beta$ , one gets the two terms  $\Delta_{ba}^{+\alpha}(t_1, t_2) - \Delta_{ba}^{-\alpha}(t_1, t_2)$  and  $\Delta_{ab}^{\alpha+}(t_2, t_1) - \Delta_{ab}^{\alpha-}(t_2, t_1)$ , which vanish because of the following identities, holding for  $t_1 > t_2$ :

$$\begin{aligned}\Delta^{++}(t_1, t_2) &= \Delta^{-+}(t_1, t_2) & \Delta^{++}(t_2, t_1) &= \Delta^{+-}(t_2, t_1) \\ \Delta^{+-}(t_1, t_2) &= \Delta^{--}(t_1, t_2) & \Delta^{-+}(t_2, t_1) &= \Delta^{--}(t_2, t_1)\end{aligned}$$

These identities hold because of the definition of  $\Delta$ , given in the main text, in terms of contour time-ordered Green functions, i.e.  $\Delta^{\alpha,\beta}(t_1, t_2) \sim -i\langle T_C c(t_1, \alpha) c^\dagger(t_2, \beta) \rangle$ , and remembering that times on the  $-$  contour branch come after times on the  $+$  one. Using these arguments, we notice that the trace vanishes for the operators with the following structure, which include the self-energy, and this will be useful to derive the formula for computing Green functions from  $\mathcal{V}$ :

$$\sum_{\beta \in \{+, -\}} \beta \text{tr} \left[ \Delta^{\beta\alpha}(t_1, t_2) X_\beta \bullet \right] = 0 \quad (\text{C.10})$$

$$\sum_{\beta \in \{+, -\}} \beta \text{tr} \left[ \Delta^{\alpha\beta}(t_2, t_1) X_\beta \bullet \right] = 0 \quad (\text{C.11})$$

Here  $X_\beta$  is a generic super-operator acting only from the left (right),  $\beta = 1(-1)$ , and  $\bullet$  is a generic target operator.

### C.3.1 Spectral properties the propagator $\mathcal{V}$

We call  $\lambda_i(t, t')$ ,  $v_i^R(t, t')$ ,  $v_i^L(t, t')$  the eigenvalues and right and left eigenvectors of  $\mathcal{V}(t, t')$ , which depend on time. As it preserves the trace,  $\mathcal{V}(t, t')$  must have at least one eigenvalue equal to one, say  $\lambda_0 \equiv 1$ . If we assume this eigenvalue is non-degenerate, then all the others eigenvectors with  $i \neq 0$ , are traceless. The proof of these properties goes as follows.  $\text{tr}[\mathcal{V}(t, t')\rho] = \text{tr}[\rho]$  in the matrix notation reads  $\langle \mathbb{1} | \bar{\mathcal{V}}(t, t') | \rho \rangle = \langle \mathbb{1} | \rho \rangle$  which holds for every  $|\rho\rangle$  as the trace is preserved; then  $\langle \mathbb{1} |$  must be a left eigenvector of  $\mathcal{V}(t, t')$ ,  $\langle v_0^L | \equiv \langle \mathbb{1} |$ , with eigenvalue  $\lambda_0 = 1$ . If we assume that there is only one eigenvector with eigenvalue 1, then all the others right-eigenvectors of  $\mathcal{V}(t, t')$  must be orthogonal to  $\langle \mathbb{1} |$ , that is they must have zero trace:  $\langle \mathbb{1} | v_i^R(t, t') \rangle = \text{tr}[v_i^R(t, t')] = 0$ , for  $i \neq 0$ .

## C.4 Hermiticity preservation

A quantum dynamical map evolving the density operator should preserve its Hermiticity: will show that this property is not spoiled by the NCA approximation. The proof is inductive and goes as showing that, if  $\mathcal{V}(t, t')$  preserves Hermiticity, then  $\mathcal{V}(t+dt, t')$  does; given the initial condition  $\mathcal{V}(t', t') = \mathbb{1}$ , that obviously preserves Hermiticity, then it follows that  $\mathcal{V}(t, t')$  is Hermiticity preserving  $\forall t$ . Assuming  $\mathcal{V}(t, t')$  is analytic in  $t$ , then its increment is given by its Taylor series

$$\mathcal{V}(t + dt, t') = \mathcal{V}(t, t') + dt \partial_t \mathcal{V}(t, t') + \frac{dt^2}{2} \partial_t^2 \mathcal{V}(t, t') + \dots \quad (\text{C.12})$$

From the Dyson equation (C.1), we can show that if  $\mathcal{V}(t, t')$  preserves Hermiticity, then all its derivatives do, which in turn implies, from the Taylor expansion, that  $\mathcal{V}(t+dt, t')$  does. This ultimately comes for the causal structure of the Dyson equation.

We will restrict to show that  $\partial_t \mathcal{V}(t, t')$  is Hermiticity preserving, assuming  $\mathcal{V}(t, t')$  is. This result can be generalized to higher order derivatives, obtained by taking derivatives of the Dyson equation (C.1), with two observations: the n-th derivative of  $\mathcal{V}$  depends only on its lower order derivatives; the structure of the equation for the n-th derivative is such that, if the lower order derivatives are Hermiticity preserving, then also the n-th derivative is.

We now assume  $\mathcal{V}(t, t')$  Hermiticity preserving and show that this implies  $\partial_t \mathcal{V}(t, t')$  also is. With  $\bullet$  an Hermitian operator, Hermiticity preservation of  $\mathcal{V}$  means  $(\mathcal{V}\bullet)^\dagger = \mathcal{V}\bullet$ .  $\mathcal{L}$  preserves Hermiticity as it is a Lindblad generator. Then, taking the hermitian conjugate of the Dyson equation (C.1) we get

$$\begin{aligned} (\partial_t \mathcal{V}(t, t') \bullet)^\dagger &= \left( \mathcal{L}\mathcal{V}(t, t') \bullet + \int_{t'}^t dt_1 \Sigma(t, t_1) \mathcal{V}(t_1, t') \bullet \right)^\dagger = \\ &= \mathcal{L}\mathcal{V}(t, t') \bullet + \int_{t'}^t dt_1 (\Sigma(t, t_1) \mathcal{V}(t_1, t') \bullet)^\dagger \end{aligned} \quad (\text{C.13})$$

We need to determine the hermitian conjugate of  $\Sigma(t_1, t_2) \bullet$ .  $\Sigma(t_1, t_2)$  in the NCA approximation is given by (C.7) and it depends on the hybridization function  $\Delta$ . Defining the Keldysh indices  $\bar{\alpha} = -\alpha$ ,  $\bar{\beta} = -\beta$  and with  $*$  meaning complex conjugation, the following property holds

$$(\Delta^{\alpha\beta}(t_1, t_2))^* = -\Delta^{\bar{\beta}\bar{\alpha}}(t_2, t_1)$$

that can be proven from the definition of  $\Delta^{\alpha,\beta}(t_1, t_2) \propto -i\langle T_C c(t_1, \alpha) c^\dagger(t_2, \beta) \rangle$  and writing down explicitly its Keldysh components. It also holds that

$$(X_\alpha \bullet)^\dagger = X_{\bar{\alpha}}^\dagger \bullet^\dagger$$

as  $(X_+ \bullet)^\dagger = (X \bullet)^\dagger = \bullet^\dagger X^\dagger = X_-^\dagger \bullet^\dagger$  and  $(X_- \bullet)^\dagger = (\bullet X)^\dagger = X^\dagger \bullet^\dagger = X_+^\dagger \bullet^\dagger$ . For a nested application of super-operators as it appears in the self-energy, this property gives  $(X_{1\alpha} \mathcal{V} X_{2\beta} \bullet)^\dagger = X_{1\bar{\alpha}}^\dagger \mathcal{V} X_{2\bar{\beta}}^\dagger \bullet$ , where we have used that the our ansatz for  $\mathcal{V}$  preserves hermiticity and that  $\bullet$  is hermitian. Using these two results it follows that  $(\Sigma(t_1, t_2) \bullet)^\dagger = \Sigma(t_1, t_2) \bullet$  as

$$\begin{aligned} (\Sigma(t_1, t_2) \bullet)^\dagger &= \left( \sum_{\alpha\beta \in \{+, -\}} -\alpha^{(1+\xi)/2} \beta i \left[ d_\beta^\dagger \mathcal{V}(t_1, t_2) d_\alpha \Delta^{\beta\alpha}(t_1, t_2) + \xi d_\beta \mathcal{V}(t_1, t_2) d_\alpha^\dagger \Delta^{\alpha\beta}(t_2, t_1) \right] \bullet \right)^\dagger = \\ &= \sum_{\alpha\beta \in \{+, -\}} +\alpha^{(1+\xi)/2} \beta i \left[ d_{\bar{\beta}}^\dagger \mathcal{V}(t_1, t_2) d_{\bar{\alpha}} \left( -\Delta^{\bar{\alpha}\bar{\beta}}(t_2, t_1) \right) + \xi d_{\bar{\beta}}^\dagger \mathcal{V}(t_1, t_2) d_{\bar{\alpha}} \left( -\Delta^{\bar{\beta}\bar{\alpha}}(t_1, t_2) \right) \right] \bullet = \\ &= \sum_{\bar{\alpha}\bar{\beta} \in \{+, -\}} \xi (-1)^{(1+\xi)/2} \bar{\alpha}^{(1+\xi)/2} \bar{\beta} i \left[ \xi d_{\bar{\beta}}^\dagger \mathcal{V}(t_1, t_2) d_{\bar{\alpha}}^\dagger \Delta^{\bar{\alpha}\bar{\beta}}(t_2, t_1) + d_{\bar{\beta}}^\dagger \mathcal{V}(t_1, t_2) d_{\bar{\alpha}} \Delta^{\bar{\beta}\bar{\alpha}}(t_1, t_2) \right] \bullet = \\ &= \Sigma(t_1, t_2) \bullet \end{aligned} \quad (\text{C.14})$$

In the one but last equality,  $\xi (-1)^{(1+\xi)/2} = -1$ , for both bosons and fermions ( $\xi = \pm 1$ ). This

completes the proof as

$$\begin{aligned} (\partial_t \mathcal{V}(t, t') \bullet)^\dagger &= \mathcal{V}(t, t') \bullet + \int_{t'}^t dt_1 (\Sigma(t, t_1) \mathcal{V}(t_1, t') \bullet)^\dagger = \\ &= \mathcal{V}(t, t') \bullet + \int_{t'}^t dt_1 \Sigma(t, t_1) \mathcal{V}(t_1, t') \bullet = \partial_t \mathcal{V}(t, t') \bullet \end{aligned} \quad (\text{C.15})$$

## C.5 Green Functions

In this section we show how to compute impurity Green functions knowing  $\mathcal{V}(t, t')$ . Writing the Keldysh path integral of the impurity coupled to a bath as in Eq. (6.8) and integrating out the bath, one obtains the expression for the partition function of the impurity

$$Z = \int \mathcal{D} [\bar{d}(t) d(t)] \exp \left\{ iS_{imp} - i \int_0^\infty dt_1 \int_0^\infty dt_2 \sum_{\alpha\beta} \bar{d}_\alpha(t_1) \alpha\beta \Delta^{\alpha\beta}(t_1, t_2) d_\beta(t_2) \right\} \quad (\text{C.16})$$

where  $\Delta$  is the hybridization function in Eq. (6.15) and where the fields are expressed in the  $+ -$  basis and the indices  $\alpha, \beta \in \{+, -\}$  are Keldysh indices. One-particle Green functions are obtained as functional derivatives of the partition function

$$G_{\alpha\beta}(t, t') = -i \langle d_\alpha(t) \bar{d}_\beta(t') \rangle = \alpha\beta\xi \frac{\delta Z}{\delta \Delta^{\beta\alpha}(t', t)} \quad (\text{C.17})$$

The same partition function is obtained by  $Z = \text{tr} [\rho_I(\infty)] = \text{tr} [\mathcal{V}(\infty, 0) \rho_I(0)]$ . Using the Dyson equation (6.29) for  $\mathcal{V}(\infty, 0)$ , we get

$$G_{\alpha\beta}(t, t') = \alpha\beta\xi \text{tr} \left\{ \int_0^\infty dt_1 \int_0^{t_1} dt_2 \left[ \mathcal{V}_0(\infty, t_1) \frac{\delta \Sigma(t_1, t_2)}{\delta \Delta^{\beta\alpha}(t', t)} \mathcal{V}(t_2, 0) + \mathcal{V}_0(\infty, t_1) \Sigma(t_1, t_2) \frac{\delta \mathcal{V}(t_2, 0)}{\delta \Delta^{\beta\alpha}(t', t)} \right] \rho_0 \right\} \quad (\text{C.18})$$

In the last expression we can drop all  $\mathcal{V}_0$ s as they leave the trace unchanged. The second contribution to the trace vanishes because  $\text{tr}(\Sigma \bullet) = 0$  and we get that, for a generic self-energy

$$G_{\alpha\beta}(t, t') = \alpha\beta\xi \text{tr} \left\{ \int_0^\infty dt_1 \int_0^{t_1} dt_2 \frac{\delta \Sigma(t_1, t_2)}{\delta \Delta^{\beta\alpha}(t', t)} \mathcal{V}(t_2, 0) \rho_0 \right\} \quad (\text{C.19})$$

We now consider the NCA self-energy (6.31), which we report here dropping mode indices  $a, b$  for simplicity

$$\Sigma(t_1, t_2) = \sum_{\alpha\beta \in \{+, -\}} -\alpha^{(1+\xi)/2} \beta i \left[ \Delta^{\beta\alpha}(t_1, t_2) d_\beta^\dagger \mathcal{V}(t_1, t_2) d_\alpha + \xi \Delta^{\alpha\beta}(t_2, t_1) d_\beta \mathcal{V}(t_1, t_2) d_\alpha^\dagger \right] \quad (\text{C.20})$$

and take its functional derivative with respect to  $\Delta$ . We get two contributions of the form  $\simeq \text{tr} (\frac{\delta \Delta}{\delta \Delta} X_1 \mathcal{V} X_2 + \Delta X_1 \frac{\delta \mathcal{V}}{\delta \Delta} X_2)$  where the second one vanishes because it's a trace of the type (C.10). Remembering that  $t_1 > t_2$  in the Dyson equation, we get

$$\frac{\delta \Sigma(t_1, t_2)}{\delta \Delta_{\beta,\alpha}(t', t)} = -i \left[ \beta^{(1+\xi)/2} \alpha \xi d_\alpha \mathcal{V}(t, t') d_\beta^\dagger \theta(t - t') + \alpha^{(1+\xi)/2} \beta d_\beta^\dagger \mathcal{V}(t', t) d_\alpha \theta(t' - t) \right] \quad (\text{C.21})$$

The non-equilibrium Green functions are then given by

$$G_{\alpha\beta}(t, t') = -i \left\{ \beta^{\frac{1-\xi}{2}} \text{tr} \left[ d_\alpha \mathcal{V}(t, t') d_\beta^\dagger \mathcal{V}(t', 0) \rho_0 \right] \theta(t - t') + \xi \alpha^{\frac{1-\xi}{2}} \text{tr} \left[ d_\beta^\dagger \mathcal{V}(t', t) d_\alpha \mathcal{V}(t, 0) \rho_0 \right] \theta(t' - t) \right\} \quad (\text{C.22})$$

This equation has the same form of quantum regression formulae 2.4.1 for one-particle Green functions for Markovian systems. This result naturally generalizes the quantum regression formulae to our non-Markovian NCA impurity solver.

# Bibliography

- [1] O. Scarlatella, A. A. Clerk, and M. Schirò, “Spectral functions and negative density of states of a driven-dissipative nonlinear quantum resonator,” *New Journal of Physics* **21**, 043040 (2018).
- [2] O. Scarlatella, R. Fazio, and M. Schirò, “Emergent finite frequency criticality of driven-dissipative correlated lattice bosons,” *Physical Review B* **99**, 064511 (2019).
- [3] M. Schiro and O. Scarlatella, “Quantum impurity models coupled to Markovian and non-Markovian baths,” *The Journal of Chemical Physics* **151**, 044102 (2019).
- [4] P. A. M. Dirac, “Quantum Mechanics of Many-Electron Systems,” *Proceedings of the Royal Society A: Mathematical, Physical and Engineering Sciences* **123**, 714–733 (1929).
- [5] J. Bardeen, L. N. Cooper, and J. R. Schrieffer, “Microscopic Theory of Superconductivity,” *Physical Review* **106**, 162–164 (1957).
- [6] K. G. Wilson, “The renormalization group: Critical phenomena and the Kondo problem,” *Reviews of Modern Physics* **47**, 773–840 (1975).
- [7] H. J. Carmichael, *Statistical Methods in Quantum Optics 1* (Springer Berlin Heidelberg, Berlin, Heidelberg, 1999).
- [8] I. R. Senitzky, “Dissipation in quantum mechanics. the harmonic oscillator,” *Physical Review* **119**, 670–679 (1960).
- [9] I. R. Senitzky, “Dissipation in Quantum Mechanics. The Harmonic Oscillator. II,” *Physical Review* **124**, 642–648 (1961).
- [10] A. Caldeira and A. Leggett, “Quantum Tunnelling in a Dissipative System,” *Annals of Physics* **153**, 445 (1984).
- [11] M. J. Hartmann, F. G. S. L. Brandao, and M. B. Plenio, “Strongly Interacting Polaritons in Coupled Arrays of Cavities,” *Nature Physics* **2**, 849–855 (2006).
- [12] M. J. Hartmann, F. G. Brandão, and M. B. Plenio, “Quantum many-body phenomena in coupled cavity arrays,” *Laser and Photonics Reviews* **2**, 527–556 (2008).

- [13] M. Aichhorn, M. Hohenadler, C. Tahan, and P. B. Littlewood, “Quantum Fluctuations, Temperature, and Detuning Effects in Solid-Light Systems,” *Physical Review Letters* **100**, 216401 (2008).
- [14] G. Roumpos, M. Lohse, W. H. Nitsche, J. Keeling, M. H. Szymańska, P. B. Littlewood, A. Löffler, S. Höfling, L. Worschech, A. Forchel, and Y. Yamamoto, “Power-law decay of the spatial correlation function in exciton-polariton condensates,” *Proceedings of the National Academy of Sciences of the United States of America* **109**, 6467–6472 (2012).
- [15] A. Le Boité, G. Orso, and C. Ciuti, “Bose-Hubbard model: Relation between driven-dissipative steady states and equilibrium quantum phases,” *Physical Review A* **90**, 063821 (2014).
- [16] M. Schiró, C. Joshi, M. Bordyuh, R. Fazio, J. Keeling, and H. E. Türeci, “Exotic Attractors of the Nonequilibrium Rabi-Hubbard Model,” *Physical Review Letters* **116**, 143603 (2016).
- [17] R. M. Wilson, K. W. Mahmud, A. Hu, A. V. Gorshkov, M. Hafezi, and M. Foss-Feig, “Collective phases of strongly interacting cavity photons,” *Physical Review A* **94**, 33801 (2016).
- [18] M. Foss-Feig, J. T. Young, V. V. Albert, A. V. Gorshkov, and M. F. Maghrebi, “Solvable Family of Driven-Dissipative Many-Body Systems,” *Physical Review Letters* **119**, 190402 (2017).
- [19] P. C. L. Vázquez and R. S. Silva, “Analytic solutions to various dissipation models of the simple and driven quantum harmonic oscillator,” [arXiv:1801.05943](https://arxiv.org/abs/1801.05943).
- [20] E. T. Owen, J. Jin, D. Rossini, R. Fazio, and M. J. Hartmann, “Quantum correlations and limit cycles in the driven-dissipative Heisenberg lattice,” *New Journal of Physics* **20**, 045004 (2018).
- [21] N. Shammah, S. Ahmed, N. Lambert, S. De Liberato, and F. Nori, “Open quantum systems with local and collective incoherent processes: Efficient numerical simulations using permutational invariance,” *Physical Review A* **98**, 063815 (2018).
- [22] B. Buča, J. Tindall, and D. Jaksch, “Non-stationary coherent quantum many-body dynamics through dissipation,” *Nature Communications* **10**, 1804.06744 (2019).
- [23] F. Vicentini, F. Minganti, A. Biella, G. Orso, and C. Ciuti, “Optimal stochastic unraveling of disordered open quantum systems: Application to driven-dissipative photonic lattices,” *Physical Review A* **99**, 032115 (2019).
- [24] D. Kilda and J. Keeling, “Fluorescence spectrum and thermalization in a driven coupled cavity array,” *Physical Review Letters* **122**, 043602 (2017).

- [25] R. Bouganne, M. B. Aguilera, A. Ghermaoui, J. Beugnon, and F. Gerbier, “Anomalous momentum diffusion in a dissipative many-body system,” [arXiv:1905.04808](https://arxiv.org/abs/1905.04808) .
- [26] C. Lledó, T. K. Mavrogordatos, and M. H. Szymańska, “Driven Bose-Hubbard dimer under nonlocal dissipation: A bistable time crystal,” *Physical Review B* **100**, 054303 (2019).
- [27] F. Piazza and H. Ritsch, “Self-Ordered Limit Cycles, Chaos, and Phase Slippage with a Superfluid inside an Optical Resonator,” *Physical Review Letters* **115**, 163601 (2015).
- [28] F. Iemini, A. Russomanno, J. Keeling, M. Schirò, M. Dalmonte, and R. Fazio, “Boundary Time Crystals,” *Physical Review Letters* **121**, 035301 (2018).
- [29] A. D. Greentree, C. Tahan, J. H. Cole, and L. C. Hollenberg, “Quantum phase transitions of light,” *Nature Physics* **2**, 856–861 (2006).
- [30] M. H. Szymańska, J. Keeling, and P. B. Littlewood, “Nonequilibrium quantum condensation in an incoherently pumped dissipative system,” *Physical Review Letters* **96**, 230602 (2006).
- [31] J. Kasprzak, M. Richard, S. Kundermann, A. Baas, P. Jeambrun, J. M. J. Keeling, F. M. Marchetti, M. H. Szymańska, R. André, J. L. Staehli, V. Savona, P. B. Littlewood, B. Deveaud, and L. S. Dang, “Bose-Einstein condensation of exciton polaritons,” *Nature* **443**, 409–414 (2006).
- [32] A. Mitra, S. Takei, Y. B. Kim, and A. J. Millis, “Nonequilibrium Quantum Criticality in Open Electronic Systems,” *Physical Review Letters* **97**, 236808 (2006).
- [33] D. G. Angelakis, M. F. Santos, and S. Bose, “Photon-blockade-induced Mott transitions and XY spin models in coupled cavity arrays,” *Physical Review A - Atomic, Molecular, and Optical Physics* **76**, 31805 (2007).
- [34] S. Diehl, A. Tomadin, A. Micheli, R. Fazio, and P. Zoller, “Dynamical phase transitions and instabilities in open atomic many-body systems,” *Physical Review Letters* **105**, 15702 (2010).
- [35] K. Baumann, C. Guerlin, F. Brennecke, and T. Esslinger, “Dicke quantum phase transition with a superfluid gas in an optical cavity,” *Nature* **464**, 1301–1306 (2010).
- [36] A. Tomadin, S. Diehl, and P. Zoller, “Nonequilibrium phase diagram of a driven and dissipative many-body system,” *Physical Review A - Atomic, Molecular, and Optical Physics* **83**, 13611 (2011).
- [37] E. M. Kessler, G. Giedke, A. Imamoglu, S. F. Yelin, M. D. Lukin, and J. I. Cirac, “Dissipative phase transition in a central spin system,” *Physical Review A - Atomic, Molecular, and Optical Physics* **86**, 12116 (2012).

- [38] M. Schiró, M. Bordyuh, B. Öztop, and H. E. Türeci, “Phase Transition of Light in Cavity QED Lattices,” *Physical Review Letters* **109**, 053601 (2012).
- [39] M. Schiró, M. Bordyuh, B. Öztop, and H. E. Türeci, “Quantum phase transition of light in the Rabi-Hubbard model,” *Journal of Physics B: Atomic, Molecular and Optical Physics* **46**, 224021 (2013).
- [40] F. Brennecke, R. Mottl, K. Baumann, R. Landig, T. Donner, and T. Esslinger, “Real-time observation of fluctuations at the driven-dissipative dicke phase transition,” *Proceedings of the National Academy of Sciences of the United States of America* **110**, 11763–11767 (2013).
- [41] L. M. Sieberer, S. D. Huber, E. Altman, and S. Diehl, “Dynamical Critical Phenomena in Driven-Dissipative Systems,” *Physical Review Letters* **110**, 195301 (2013).
- [42] L. M. Sieberer, S. D. Huber, E. Altman, and S. Diehl, “Nonequilibrium functional renormalization for driven-dissipative Bose-Einstein condensation,” *Physical Review B - Condensed Matter and Materials Physics* **89**, 134310 (2014).
- [43] H. J. Carmichael, “Breakdown of photon blockade: A dissipative quantum phase transition in zero dimensions,” *Physical Review X* **5**, 31028 (2015).
- [44] J. Klinder, H. Keßler, M. Wolke, L. Mathey, and A. Hemmerich, “Dynamical phase transition in the open Dicke model,” *Proceedings of the National Academy of Sciences of the United States of America* **112**, 3290–3295 (2015).
- [45] M. F. Maghrebi and A. V. Gorshkov, “Nonequilibrium many-body steady states via Keldysh formalism,” *Physical Review B* **93**, 14307 (2016).
- [46] J. Marino and S. Diehl, “Quantum dynamical field theory for nonequilibrium phase transitions in driven open systems,” *Physical Review B* **94**, 85150 (2016).
- [47] J. M. Fink, A. Dombi, A. Vukics, A. Wallraff, and P. Domokos, “Observation of the Photon-Blockade Breakdown Phase Transition,” *Phys. Rev. X* **7**, 11012 (2017).
- [48] S. R. K. Rodriguez, W. Casteels, F. Storme, N. Carlon Zambon, I. Sagnes, L. Le Gratiet, E. Galopin, A. Lemaître, A. Amo, C. Ciuti, and J. Bloch, “Probing a Dissipative Phase Transition via Dynamical Optical Hysteresis,” *Physical Review Letters* **118**, 247402 (2017).
- [49] F. Minganti, A. Biella, N. Bartolo, and C. Ciuti, “Spectral theory of Liouvillians for dissipative phase transitions,” *Physical Review A* **98**, 042118 (2018).
- [50] F. Vicentini, F. Minganti, R. Rota, G. Orso, and C. Ciuti, “Critical slowing down in driven-dissipative Bose-Hubbard lattices,” *Physical Review A* **97**, 013853 (2018).
- [51] R. Rota, F. Minganti, A. Biella, and C. Ciuti, “Dynamical properties of dissipative XYZ Heisenberg lattices,” *New Journal of Physics* **20**, 45003 (2018).

- [52] D. Roscher, S. Diehl, and M. Buchhold, “Phenomenology of first-order dark-state phase transitions,” *Physical Review A* **98**, 062117 (2018).
- [53] R. Rota, F. Minganti, C. Ciuti, and V. Savona, “Quantum Critical Regime in a Quadratically Driven Nonlinear Photonic Lattice,” *Physical Review Letters* **122**, 110405 (2019).
- [54] T. Fink, A. Schade, S. Höfling, C. Schneider, and A. Imamoglu, “Signatures of a dissipative phase transition in photon correlation measurements,” *Nature Physics* **14**, 365–369 (2018).
- [55] J. T. Young, A. V. Gorshkov, M. Foss-Feig, and M. F. Maghrebi, “Non-equilibrium fixed points of coupled Ising models,” [arXiv:1903.02569](https://arxiv.org/abs/1903.02569).
- [56] C. A. Mead, “Scaling of MOS technology to submicrometer feature sizes,” *Feynman and Computation* **21**, 93–115 (2018).
- [57] I. Bloch, J. Dalibard, and S. Nascimbène, “Quantum simulations with ultracold quantum gases,” *Nature Physics* **8**, 267–276 (2012).
- [58] M. Greiner, O. Mandel, T. Esslinger, T. W. Hänsch, and I. Bloch, “Quantum phase transition from a superfluid to a Mott insulator in a gas of ultracold atoms,” *Nature* **415**, 39–44 (2002).
- [59] A. Wallraff, D. I. Schuster, A. Blais, L. Frunzio, R. S. Huang, J. Majer, S. Kumar, S. M. Girvin, and R. J. Schoelkopf, “Strong coupling of a single photon to a superconducting qubit using circuit quantum electrodynamics,” *Nature* **431**, 162–167 (2004).
- [60] K. Le Hur, L. Henriet, A. Petrescu, K. Plekhanov, G. Roux, and M. Schiró, “Many-body quantum electrodynamics networks: Non-equilibrium condensed matter physics with light,” *Comptes Rendus Physique* **17**, 808–835 (2016).
- [61] M. Fitzpatrick, N. M. Sundaresan, A. C. Y. Li, J. Koch, and A. A. Houck, “Observation of a Dissipative Phase Transition in a One-Dimensional Circuit QED Lattice,” *Phys. Rev. X* **7**, 11016 (2017).
- [62] R. Ma, B. Saxberg, C. Owens, N. Leung, Y. Lu, J. Simon, and D. I. Schuster, “A dissipatively stabilized Mott insulator of photons,” *Nature* **566**, 51–57 (2019).
- [63] A. A. Houck, H. E. Türeci, and J. Koch, “On-chip quantum simulation with superconducting circuits,” *Nature Physics* **8**, 292–299 (2012).
- [64] R. Blatt and C. F. Roos, “Quantum simulations with trapped ions,” *Nature Physics* **8**, 277–284 (2012).
- [65] K. B. Davis, M. O. Mewes, M. R. Andrews, N. J. Van Druten, D. S. Durfee, D. M. Kurn, and W. Ketterle, “Bose-Einstein condensation in a gas of sodium atoms,” *Physical Review Letters* **75**, 3969–3973 (1995).

- [66] M. H. Anderson, J. R. Ensher, M. R. Matthews, C. E. Wieman, and E. A. Cornell, “Observation of Bose-Einstein condensation in a dilute atomic vapor,” *Science* **269**, 198–201 (1995).
- [67] M. Greiner, O. Mandel, T. Rom, A. Altmeyer, A. Widera, T. Hänsch, and I. Bloch, “Quantum phase transition from a superfluid to a Mott insulator in an ultracold gas of atoms,” *Physica B: Condensed Matter* **329-333**, 11–12 (2003).
- [68] J. Simon, W. S. Bakr, R. Ma, M. E. Tai, P. M. Preiss, and M. Greiner, “Quantum simulation of antiferromagnetic spin chains in an optical lattice,” *Nature* **472**, 307–312 (2011).
- [69] M. Schreiber, S. S. Hodgman, P. Bordia, H. P. Lüschen, M. H. Fischer, R. Vosk, E. Altman, U. Schneider, and I. Bloch, “Observation of many-body localization of interacting fermions in a quasirandom optical lattice,” *Science* **349**, 842–845 (2015).
- [70] I. Carusotto and C. Ciuti, “Quantum fluids of light,” *Reviews of Modern Physics* **85**, 299–366 (2013).
- [71] S. Haroche, “Cavity quantum electrodynamics: A review of Rydberg atom-microwave experiments on entanglement and decoherence,” in *AIP Conference Proceedings*, Vol. 464 (American Institute of Physics, 2012) pp. 45–66.
- [72] R. Miller, T. E. Northup, K. M. Birnbaum, A. Boca, A. D. Boozer, and H. J. Kimble, “Trapped atoms in cavity QED: Coupling quantized light and matter,” *Journal of Physics B: Atomic, Molecular and Optical Physics* **38**, S551–S565 (2005).
- [73] M. J. Hartmann, “Quantum simulation with interacting photons,” *Journal of Optics* **18**, 104005 (2016).
- [74] D. L. Underwood, W. E. Shanks, J. Koch, and A. A. Houck, “Low-disorder microwave cavity lattices for quantum simulation with photons,” *Physical Review A - Atomic, Molecular, and Optical Physics* **86**, 23837 (2012).
- [75] Y. Salathé, M. Mondal, M. Oppliger, J. Heinsoo, P. Kurpiers, A. Potočnik, A. Mezzacapo, U. Las Heras, L. Lamata, E. Solano, S. Filipp, and A. Wallraff, “Digital quantum simulation of spin models with circuit quantum electrodynamics,” *Physical Review X* **5**, 21027 (2015).
- [76] Y. Chen, P. Roushan, D. Sank, C. Neill, E. Lucero, M. Mariantoni, R. Barends, B. Chiaro, J. Kelly, A. Megrant, J. Y. Mutus, P. J. J. O’Malley, A. Vainsencher, J. Wenner, T. C. White, Y. Yin, A. N. Cleland, and J. M. Martinis, “Emulating weak localization using a solid-state quantum circuit,” *Nature Communications* **5**, 1–6 (2014).
- [77] R. J. Schoelkopf and S. M. Girvin, “Wiring up quantum systems,” *Nature* **451**, 664–669 (2008).

- [78] U. Vool and M. Devoret, “Introduction to quantum electromagnetic circuits,” *International Journal of Circuit Theory and Applications* **45**, 897–934 (2017).
- [79] B. D. Josephson, “The Discovery of Tunnelling Supercurrents,” *Proceedings of the IEEE* **62**, 838–841 (1974).
- [80] J. F. Annett, *Superconductivity, Superfluids and Condensates* (Oxford University Press, 2004).
- [81] M. H. Devoret and J. M. Martinis, “Implementing Qubits with Superconducting Integrated Circuits,” in *Experimental Aspects of Quantum Computing*, Vol. 3 (Springer US, Boston, MA, 2004) pp. 163–203.
- [82] C. Noh and D. G. Angelakis, “Quantum simulations and many-body physics with light,” *Reports on Progress in Physics* **80**, 16401 (2017).
- [83] M. Leib, F. Deppe, A. Marx, R. Gross, and M. J. Hartmann, “Networks of nonlinear superconducting transmission line resonators,” *New Journal of Physics* **14**, 075024 (2012).
- [84] R. Fazio and H. Van der Zant, “Quantum phase transitions and vortex dynamics in superconducting networks,” *Physics Report* **355**, 235–334 (2001).
- [85] J. Bourassa, F. Beaudoin, J. M. Gambetta, and A. Blais, “Josephson-junction-embedded transmission-line resonators: From Kerr medium to in-line transmon,” *Physical Review A* **86**, 013814 (2012).
- [86] J. Raftery, D. Sadri, S. Schmidt, H. E. Türeci, A. A. Houck, H. E. Türeci, and A. A. Houck, “Observation of a dissipation-induced classical to quantum transition,” *Physical Review X* **4**, 031043 (2014).
- [87] S. Schmidt, D. Gerace, A. A. Houck, G. Blatter, and H. E. Türeci, “Nonequilibrium delocalization-localization transition of photons in circuit quantum electrodynamics,” *Physical Review B - Condensed Matter and Materials Physics* **82**, 100507 (2010).
- [88] D. Rossini and R. Fazio, “Mott-Insulating and Glassy Phases of Polaritons in 1D Arrays of Coupled Cavities,” *Physical Review Letters* **99**, 186401 (2007).
- [89] S. Schmidt and G. Blatter, “Strong coupling theory for the Jaynes-Cummings-Hubbard model,” *Physical Review Letters* **103**, 86403 (2009).
- [90] J. Koch and K. Le Hur, “Superfluid-Mott-insulator transition of light in the Jaynes-Cummings lattice,” *Physical Review A - Atomic, Molecular, and Optical Physics* **80**, 023811 (2009).
- [91] M. P. Fisher, P. B. Weichman, G. Grinstein, and D. S. Fisher, “Boson localization and the superfluid-insulator transition,” *Physical Review B* **40**, 546–570 (1989).

- [92] F. Verstraete, M. M. Wolf, and J. Ignacio Cirac, “Quantum computation and quantum-state engineering driven by dissipation,” *Nature Physics* **5**, 633–636 (2009).
- [93] R. Ma, C. Owens, A. Houck, D. I. Schuster, and J. Simon, “Autonomous stabilizer for incompressible photon fluids and solids,” *Physical Review A* **95**, 043811 (2017).
- [94] Y. Lu, S. Chakram, N. Leung, N. Earnest, R. K. Naik, Z. Huang, P. Groszkowski, E. Kapit, J. Koch, and D. I. Schuster, “Universal Stabilization of a Parametrically Coupled Qubit,” *Physical Review Letters* **119**, 150502 (2017).
- [95] S. Shankar, M. Hatridge, Z. Leghtas, K. M. Sliwa, A. Narla, U. Vool, S. M. Girvin, L. Frunzio, M. Mirrahimi, and M. H. Devoret, “Autonomously stabilized entanglement between two superconducting quantum bits,” *Nature* **504**, 419–422 (2013).
- [96] J. T. Barreiro, M. Müller, P. Schindler, D. Nigg, T. Monz, M. Chwalla, M. Hennrich, C. F. Roos, P. Zoller, and R. Blatt, “An open-system quantum simulator with trapped ions,” *Nature* **470**, 486–491 (2011).
- [97] J. F. Poyatos, J. I. Cirac, and P. Zoller, “Quantum reservoir engineering with laser cooled trapped ions,” *Physical Review Letters* **77**, 4728–4731 (1996).
- [98] E. Kapit, “Hardware-efficient and fully autonomous quantum error correction in superconducting circuits,” *Physical Review Letters* **116**, 150501 (2016).
- [99] E. Kapit, J. T. Chalker, and S. H. Simon, “Passive correction of quantum logical errors in a driven, dissipative system: A blueprint for an analog quantum code fabric,” *Physical Review A - Atomic, Molecular, and Optical Physics* **91**, 062324 (2015).
- [100] J. Guillaud and M. Mirrahimi, “Repetition cat-qubits: Fault-tolerant quantum computation with highly reduced overhead,” [arXiv:1904.09474](https://arxiv.org/abs/1904.09474).
- [101] J. Lebreuilly, A. Biella, F. Storme, D. Rossini, R. Fazio, C. Ciuti, and I. Carusotto, “Stabilizing strongly correlated photon fluids with non-Markovian reservoirs,” *Physical Review A* **96**, 33828 (2017).
- [102] J. Lebreuilly and I. Carusotto, “Quantum simulation of zero-temperature quantum phases and incompressible states of light via non-Markovian reservoir engineering techniques,” *Comptes Rendus Physique* **19**, 433–450 (2018).
- [103] Z. Leghtas, S. Touzard, I. M. Pop, A. Kou, B. Vlastakis, A. Petrenko, K. M. Sliwa, A. Narla, S. Shankar, M. J. Hatridge, M. Reagor, L. Frunzio, R. J. Schoelkopf, M. Mirrahimi, and M. H. Devoret, “Confining the state of light to a quantum manifold by engineered two-photon loss,” *Science* **347**, 853–857 (2015).
- [104] S. Touzard, A. Grimm, Z. Leghtas, S. O. Mundhada, P. Reinhold, C. Axline, M. Reagor, K. Chou, J. Blumoff, K. M. Sliwa, S. Shankar, L. Frunzio, R. J.

- Schoelkopf, M. Mirrahimi, and M. H. Devoret, “Coherent Oscillations inside a Quantum Manifold Stabilized by Dissipation,” *Physical Review X* **8**, 021005 (2018).
- [105] F. Minganti, N. Bartolo, J. Lolli, W. Casteels, and C. Ciuti, “Exact results for Schrödinger cats in driven-dissipative systems and their feedback control,” *Scientific Reports* **6**, 26987 (2016).
- [106] W. Casteels, R. Fazio, and C. Ciuti, “Critical dynamical properties of a first-order dissipative phase transition,” *Physical Review A* **95**, 12128 (2017).
- [107] H. Landa, M. Schiró, and G. Misguich, “Multistability of Driven-Dissipative Quantum Spins,” [arXiv:1905.10349](https://arxiv.org/abs/1905.10349).
- [108] J. Zinn-Justin, *Phase Transitions and Renormalization Group* (Oxford University Press, 2007).
- [109] B. I. Halperin, “Theory of dynamic critical phenomena,” *Physics Today* **72**, 42–43 (2019).
- [110] J. Marino and S. Diehl, “Driven Markovian Quantum Criticality,” *Physical Review Letters* **116**, 070407 (2016).
- [111] S. Sachdev, *Quantum Phase Transitions* (2007).
- [112] A. Altland and B. Simons, *Condensed Matter Field Theory*, 2nd ed. (Cambridge University Press, 2012) publication Title: Condensed Matter Field Theory.
- [113] F. Wilczek, “Quantum time crystals,” *Physical Review Letters* **109**, 160401 (2012).
- [114] P. Bruno, “Comment on ‘Quantum Time Crystals’,” *Physical Review Letters* **110**, 118901 (2013).
- [115] P. Bruno, “Impossibility of Spontaneously Rotating Time Crystals: A No-Go Theorem,” *Physical Review Letters* **111**, 070402 (2013).
- [116] H. Watanabe and M. Oshikawa, “Absence of Quantum Time Crystals,” *Physical Review Letters* **114**, 251603 (2015).
- [117] K. Sacha and J. Zakrzewski, “Time crystals: A review,” *Reports on Progress in Physics* **81**, 016401 (2018).
- [118] D. V. Else, B. Bauer, and C. Nayak, “Floquet Time Crystals,” *Physical Review Letters* **117**, 90402 (2016).
- [119] V. Khemani, A. Lazarides, R. Moessner, and S. L. L. Sondhi, “Phase Structure of Driven Quantum Systems,” *Physical Review Letters* **116**, 250401 (2016).
- [120] W. W. Ho, S. Choi, M. D. Lukin, and D. A. Abanin, “Critical Time Crystals in Dipolar Systems,” *Physical Review Letters* **119**, 010602 (2017).

- [121] S. Choi, J. Choi, R. Landig, G. Kucska, H. Zhou, J. Isoya, F. Jelezko, S. Onoda, H. Sumiya, V. Khemani, C. Von Keyserlingk, N. Y. Yao, E. Demler, and M. D. Lukin, “Observation of discrete time-crystalline order in a disordered dipolar many-body system,” *Nature* **543**, 221–225 (2017).
- [122] H. Deng, H. Haug, and Y. Yamamoto, “Exciton-polariton Bose-Einstein condensation,” *Rev. Mod. Phys.* **82**, 1489–1537 (2010).
- [123] K. Tucker, B. Zhu, R. J. Lewis-Swan, J. Marino, F. Jimenez, J. G. Restrepo, and A. M. Rey, “Shattered time: Can a dissipative time crystal survive many-body correlations?” *New Journal of Physics* **20**, 123003 (2018).
- [124] G. Stefanucci and R. Van Leeuwen, *Nonequilibrium Many-Body Theory of Quantum Systems: A Modern Introduction*, Vol. 9780521766 (Cambridge University Press, 2010).
- [125] H. Bruus and K. Flensberg, *Many-Body Quantum Theory in Condensed Matter Physics : An Introduction* (Oxford University Press, 2004).
- [126] C. W. Gardiner and M. J. Collett, “Input and output in damped quantum systems: Quantum stochastic differential equations and the master equation,” *Physical Review A* **31**, 3761–3774 (1985).
- [127] M. J. Collett and C. W. Gardiner, “Squeezing of intracavity and traveling-wave light fields produced in parametric amplification,” *Physical Review A* **30**, 1386–1391 (1984).
- [128] M. Buchhold, P. Strack, S. Sachdev, and S. Diehl, “Dicke-model quantum spin and photon glass in optical cavities: Nonequilibrium theory and experimental signatures,” *Physical Review A - Atomic, Molecular, and Optical Physics* **87**, 63622 (2013).
- [129] P. Coleman, *Introduction to Many-Body Physics* (Cambridge University Press, Cambridge, 2015).
- [130] A. A. Clerk, M. H. Devoret, S. M. Girvin, F. Marquardt, and R. J. Schoelkopf, “Introduction to quantum noise, measurement, and amplification,” *Reviews of Modern Physics* **82**, 1155–1208 (2010).
- [131] J. Schwinger, “Brownian motion of a quantum oscillator,” *Journal of Mathematical Physics* **2**, 407–432 (1961).
- [132] L. V. Keldysh, “Diagram Technique for Nonequilibrium Processes,” Sov. Phys. JETP **47**, 1515–1527 (1964).
- [133] A. Kamenev, *Field Theory of Non-Equilibrium Systems* (Cambridge University Press, Cambridge, 2011).

- [134] N. N. Nagaosa, *Quantum Field Theory in Condensed Matter Physics* (Springer Berlin Heidelberg, Berlin, Heidelberg, 1999).
- [135] L. M. Sieberer, M. Buchhold, and S. Diehl, “Keldysh field theory for driven open quantum systems,” *Reports on Progress in Physics* **79**, 96001 (2016).
- [136] H. P. Breuer and F. Petruccione, *The Theory of Open Quantum Systems*, 1st ed., Vol. 9780199213 (OUP Oxford, 2007).
- [137] P. Bocchieri and A. Loinger, “Quantum Recurrence Theorem,” *Physical Review* **107**, 337–338 (1957).
- [138] V. Gorini, A. Kossakowski, and E. C. G. Sudarshan, “Completely positive dynamical semigroups of N-level systems,” *Journal of Mathematical Physics* **17**, 821 (1976).
- [139] G. Lindblad, “On the generators of quantum dynamical semigroups,” *Communications in Mathematical Physics* **48**, 119–130 (1976).
- [140] A. A. Dzhioev and D. S. Kosov, “Super-fermion representation of quantum kinetic equations for the electron transport problem,” *Journal of Chemical Physics* **134**, 44121 (2011).
- [141] E. Arrigoni and A. Dorda, “Master Equations Versus Keldysh Green’s Functions for Correlated Quantum Systems Out of Equilibrium,” (Springer, Cham, 2018) pp. 121–188.
- [142] M. Schmutz, “Real-time green’s functions in many body problems,” *Zeitschrift für Physik B Condensed Matter and Quanta* **30**, 97–106 (1978).
- [143] T. Prosen, “Third quantization: A general method to solve master equations for quadratic open Fermi systems,” *New Journal of Physics* **10**, 043026 (2008).
- [144] T. Prosen and T. H. Seligman, “Quantization over boson operator spaces,” *Journal of Physics A: Mathematical and Theoretical* **43**, 392004 (2010).
- [145] M. Lax, “Formal theory of quantum fluctuations from a driven state,” *Physical Review* **129**, 2342–2348 (1963).
- [146] M. Lax, “Quantum noise. X. density-matrix treatment of field and population-difference fluctuations,” *Physical Review* **157**, 213–231 (1967).
- [147] D. C. Brody, “Biorthogonal quantum mechanics,” *Journal of Physics A: Mathematical and Theoretical* **47**, 035305 (2014).
- [148] V. V. Albert, “Lindbladians with multiple steady states: Theory and applications,” [arXiv:1802.00010](https://arxiv.org/abs/1802.00010).
- [149] C. Jarlskog, “Paper [1952a]: On the Definition of the Renormalization Constants in Quantum Electrodynamics,” *Portrait of Gunnar Källén* **25**, 509–527 (2013).

- [150] H. Lehmann, “Über Eigenschaften von Ausbreitungsfunktionen und Renormierungskonstanten quantisierter Felder,” *Il Nuovo Cimento* **11**, 342–357 (1954).
- [151] E. Arrigoni, M. Knap, and W. Von Der Linden, “Nonequilibrium dynamical mean-field theory: An auxiliary quantum master equation approach,” *Physical Review Letters* **110**, 86403 (2013).
- [152] A. Dorda, M. Nuss, W. Von Der Linden, and E. Arrigoni, “Auxiliary master equation approach to nonequilibrium correlated impurities,” *Physical Review B - Condensed Matter and Materials Physics* **89**, 165105 (2014).
- [153] M. I. Dykman and M. A. Krivoglaz, “Classical theory of nonlinear oscillators interacting with a medium,” in *Physica Status Solidi (B)*, Vol. 48, edited by I. M. Khalatnikov (Harwood Academic, 1971) pp. 497–512.
- [154] G. Piccitto and A. Silva, “Dynamical phase transition in the transverse field Ising chain characterized by the transverse magnetization spectral function,” *Physical Review B* **100**, 134311 (2019).
- [155] R. Orús and G. Vidal, “Infinite time-evolving block decimation algorithm beyond unitary evolution,” *Physical Review B - Condensed Matter and Materials Physics* **78**, 155117 (2008).
- [156] S. Finazzi, A. Le Boit  , F. Storme, A. Baksic, and C. Ciuti, “Corner-Space Renormalization Method for Driven-Dissipative Two-Dimensional Correlated Systems,” *Physical Review Letters* **115**, 80604 (2015).
- [157] J. Jin, A. Biella, O. Viyuela, L. Mazza, J. Keeling, R. Fazio, and D. Rossini, “Cluster mean-field approach to the steady-state phase diagram of dissipative spin systems,” *Physical Review X* **6**, 31011 (2016).
- [158] A. C. Li, F. Petruccione, and J. Koch, “Resummation for nonequilibrium perturbation theory and application to open quantum lattices,” *Physical Review X* **6**, 21037 (2016).
- [159] B. R. Mollow, “Power spectrum of light scattered by two-level systems,” *Physical Review* **188**, 1969–1975 (1969).
- [160] O. Astafiev, A. M. Zagoskin, A. A. Abdumalikov, Y. A. Pashkin, T. Yamamoto, K. Inomata, Y. Nakamura, and J. S. Tsai, “Resonance fluorescence of a single artificial atom,” *Science* **327**, 840–843 (2010).
- [161] J. C. L  pez Carre  o, E. del Valle, and F. P. Laussy, “Photon Correlations from the Mollow Triplet,” *Laser and Photonics Reviews* **11**, 1700090 (2017).

- [162] C. Lang, D. Bozyigit, C. Eichler, L. Steffen, J. M. Fink, A. A. Abdumalikov, M. Baur, S. Filipp, M. P. Da Silva, A. Blais, and A. Wallraff, “Observation of resonant photon blockade at microwave frequencies using correlation function measurements,” *Physical Review Letters* **106**, 243601 (2011).
- [163] N. Lörch, E. Amitai, A. Nunnenkamp, and C. Bruder, “Genuine Quantum Signatures in Synchronization of Anharmonic Self-Oscillators,” *Physical Review Letters* **117**, 73601 (2016).
- [164] T. E. Lee and H. R. Sadeghpour, “Quantum synchronization of quantum van der Pol oscillators with trapped Ions,” *Physical Review Letters* **111**, 234101 (2013).
- [165] S. Walter, A. Nunnenkamp, and C. Bruder, “Quantum Synchronization of a Driven Self-Sustained Oscillator,” *Physical Review Letters* **112**, 94102 (2014).
- [166] A. J. Hoffman, S. J. Srinivasan, S. Schmidt, L. Spietz, J. Aumentado, H. E. Türeci, and A. A. Houck, “Dispersive photon blockade in a superconducting circuit,” *Physical Review Letters* **107**, 53602 (2011).
- [167] W. Leoński and R. Tanaś, “Possibility of producing the one-photon state in a kicked cavity with a nonlinear Kerr medium,” *Physical Review A* **49**, R20–R23 (1994).
- [168] W. Leoński, “Fock states in a Kerr medium with parametric pumping,” *Physical Review A* **54**, 3369–3372 (1996).
- [169] A. Miranowicz, M. Paprzycka, A. Pathak, and F. Nori, “Phase-space interference of states optically truncated by quantum scissors: Generation of distinct superpositions of qudit coherent states by displacement of vacuum,” *Physical Review A - Atomic, Molecular, and Optical Physics* **89**, 33812 (2014).
- [170] M. Dykman, “Heating and cooling of local and quasilocal vibrations by a nonresonance field.pdf,” Sov. phys. Solid State **20**, 1306–1311 (1978).
- [171] M. A. Lemonde, N. Didier, and A. A. Clerk, “Nonlinear interaction effects in a strongly driven optomechanical cavity,” *Physical Review Letters* **111**, 53602 (2013).
- [172] B. A. Levitan, A. Metelmann, and A. A. Clerk, “Optomechanics with two-phonon driving,” *New Journal of Physics* **18**, 93014 (2016).
- [173] F. Marquardt, J. P. Chen, A. A. Clerk, and S. M. Girvin, “Quantum theory of cavity-assisted sideband cooling of mechanical motion,” *Physical Review Letters* **99**, 93902 (2007).
- [174] V. V. Dodonov and S. S. Mizrahi, “Exact stationary photon distributions due to competition between one-and two-photon absorption and emission,” *Journal of Physics A: Mathematical and General* **30**, 5657–5667 (1997).

- [175] M. I. Dykman and M. A. Krivoglaz, “Spectral distribution of nonlinear oscillators with nonlinear friction due to a medium,” *Physica Status Solidi (B)* **68**, 111–123 (1975).
- [176] A. C. Y. Li, F. Petruccione, and J. Koch, “Perturbative approach to Markovian open quantum systems,” *Scientific Reports* **4**, 4887 (2015).
- [177] M. Baur, S. Filipp, R. Bianchetti, J. M. Fink, M. Göppl, L. Steffen, P. J. Leek, A. Blais, and A. Wallraff, “Measurement of autler-townes and mollow transitions in a strongly driven superconducting qubit,” *Physical Review Letters* **102**, 243602 (2009).
- [178] E. Del Valle and F. P. Laussy, “Mollow triplet under incoherent pumping,” *Physical Review Letters* **105**, 233601 (2010).
- [179] N. Lörch, S. E. Nigg, A. Nunnenkamp, R. P. Tiwari, and C. Bruder, “Quantum Synchronization Blockade: Energy Quantization Hinders Synchronization of Identical Oscillators,” *Physical Review Letters* **118**, 243602 (2017).
- [180] S. E. Nigg, “Observing quantum synchronization blockade in circuit quantum electrodynamics,” *Physical Review A* **97**, 13811 (2018).
- [181] O. V. Zhirov and D. L. Shepelyansky, “Quantum synchronization,” *European Physical Journal D* **38**, 375–379 (2006).
- [182] A. Pizzi, F. Dolcini, and K. Le Hur, “Quench-induced dynamical phase transitions and  $\pi$ -synchronization in the Bose-Hubbard model,” *Physical Review B* **99**, 094301 (2019).
- [183] L. D. Landau and E. M. Lifshitz, *Statistical Physics, Part I* (1995).
- [184] M. C. Cross and P. C. Hohenberg, “Pattern formation outside of equilibrium,” *Reviews of Modern Physics* **65**, 851–1112 (1993).
- [185] M. L. Ramón, S. Boccaletti, R. Meucci, and E. Allaria, “Pattern Formation and Dynamics in an Annular Co 2 Laser,” *International Journal of Bifurcation and Chaos* **11**, 2759–2770 (2001).
- [186] W. van Saarloos, “Front propagation into unstable states,” *Physics Reports* **386**, 29–222 (2003).
- [187] J. Jin, D. Rossini, R. Fazio, M. Leib, and M. J. Hartmann, “Photon solid phases in driven arrays of nonlinearly coupled cavities,” *Physical Review Letters* **110**, 163605 (2013).
- [188] C. K. Chan, T. E. Lee, and S. Gopalakrishnan, “Limit-cycle phase in driven-dissipative spin systems,” *Physical Review A - Atomic, Molecular, and Optical Physics* **91**, 51601 (2015).

- [189] A. Biella, F. Storme, J. Lebreuilly, D. Rossini, R. Fazio, I. Carusotto, and C. Ciuti, “Phase diagram of incoherently driven strongly correlated photonic lattices,” *Physical Review A* **96**, 23839 (2017).
- [190] M. Biondi, G. Blatter, H. E. Türeci, and S. Schmidt, “Nonequilibrium gas-liquid transition in the driven-dissipative photonic lattice,” *Physical Review A* **96**, 5 (2017).
- [191] A. Le Boit , G. Orso, and C. Ciuti, “Steady-state phases and tunneling-induced instabilities in the driven dissipative bose-hubbard model,” *Physical Review Letters* **110**, 233601 (2013).
- [192] K. Sengupta and N. Dupuis, “Mott-insulator-to-superfluid transition in the Bose-Hubbard model: A strong-coupling approach,” *Physical Review A* **71**, 033629 (2005).
- [193] J. Lebreuilly, M. Wouters, and I. Carusotto, “Towards strongly correlated photons in arrays of dissipative nonlinear cavities under a frequency-dependent incoherent pumping,” *Comptes Rendus Physique* **17**, 836–860 (2016).
- [194] W. Metzner, “Linked-cluster expansion around the atomic limit of the Hubbard model,” *Physical Review B* **43**, 8549–8563 (1991).
- [195] A. Ran on and N. Dupuis, “Nonperturbative renormalization group approach to strongly correlated lattice bosons,” *Physical Review B - Condensed Matter and Materials Physics* **84**, 174513 (2011).
- [196] B. Sciolla and G. Biroli, “Quantum quenches, dynamical transitions, and off-equilibrium quantum criticality,” *Physical Review B - Condensed Matter and Materials Physics* **88**, 201110 (2013).
- [197] A. Maraga, A. Chiocchetta, A. Mitra, and A. Gambassi, “Aging and coarsening in isolated quantum systems after a quench,” *Physical Review E* **92**, 042151 (2015).
- [198] A. Chiocchetta, M. Tavora, A. Gambassi, and A. Mitra, “Short-time universal scaling in an isolated quantum system after a quench,” *Physical Review B - Condensed Matter and Materials Physics* **91**, 134311 (2015).
- [199] M. Ludwig and F. Marquardt, “Quantum many-body dynamics in optomechanical arrays,” *Physical Review Letters* **111**, 73603 (2013).
- [200] C. W. Von Keyserlingk, V. Khemani, and S. L. Sondhi, “Absolute stability and spatiotemporal long-range order in Floquet systems,” *Physical Review B* **94**, 85112 (2016).
- [201] J. Zhang, P. W. Hess, A. Kyprianidis, P. Becker, A. Lee, J. Smith, G. Pagano, I. D. Potirniche, A. C. Potter, A. Vishwanath, N. Y. Yao, and C. Monroe, “Observation of a discrete time crystal,” *Nature* **543**, 217–220 (2017).

- [202] D. Witthaut, S. Wimberger, R. Burioni, and M. Timme, “Classical synchronization indicates persistent entanglement in isolated quantum systems,” *Nature Communications* **8**, 14829 (2017).
- [203] T. Nag, R.-J. Slager, T. Higuchi, and T. Oka, “Dynamical synchronization transition in interacting electron systems,” *Physical Review B* **100**, 134301 (2019).
- [204] T. D. Kühner and S. R. White, *One-Dimensional Bose-Hubbard Model with Nearest-Neighbor Interaction*, Tech. Rep. (2000) publication Title: Physical Review B - Condensed Matter and Materials Physics.
- [205] A. Georges, G. Kotliar, W. Krauth, and M. J. Rozenberg, “Dynamical mean-field theory of strongly correlated fermion systems and the limit of infinite dimensions,” *Reviews of Modern Physics* **68**, 13–125 (1996).
- [206] J. Cui, J. I. Cirac, and M. C. Bañuls, “Variational Matrix Product Operators for the Steady State of Dissipative Quantum Systems,” *Physical Review Letters* **114**, 220601 (2015).
- [207] A. H. Werner, D. Jaschke, P. Silvi, M. Kliesch, T. Calarco, J. Eisert, and S. Montangero, “Positive Tensor Network Approach for Simulating Open Quantum Many-Body Systems,” *Physical Review Letters* **116**, 237201 (2016).
- [208] E. Mascarenhas, H. Flayac, and V. Savona, “Matrix-product-operator approach to the nonequilibrium steady state of driven-dissipative quantum arrays,” *Physical Review A* **92**, 022116 (2015).
- [209] A. Kshetrimayum, H. Weimer, and R. Orús, “A simple tensor network algorithm for two-dimensional steady states,” *Nature Communications* **8**, 1291 (2017).
- [210] A. Nagy and V. Savona, “Driven-dissipative quantum Monte Carlo method for open quantum systems,” *Physical Review A* **97**, 52129 (2018).
- [211] A. Biella, J. Jin, O. Viyuela, C. Ciuti, R. Fazio, and D. Rossini, “Linked cluster expansions for open quantum systems on a lattice,” *Physical Review B* **97**, 35103 (2018).
- [212] P. Degenfeld-Schonburg and M. J. Hartmann, “Self-consistent projection operator theory for quantum many-body systems,” *Physical Review B - Condensed Matter and Materials Physics* **89**, 245108 (2014).
- [213] A. Nagy and V. Savona, “Variational Quantum Monte Carlo Method with a Neural-Network Ansatz for Open Quantum Systems,” *Physical Review Letters* **122**, 250501 (2019).
- [214] F. Vicentini, A. Biella, N. Regnault, and C. Ciuti, “Variational Neural-Network Ansatz for Steady States in Open Quantum Systems,” *Physical Review Letters* **122**, 250503 (2019).

- [215] M. J. Hartmann and G. Carleo, “Neural-Network Approach to Dissipative Quantum Many-Body Dynamics,” *Physical Review Letters* **122**, 250502 (2019).
- [216] N. Yoshioka and R. Hamazaki, “Constructing neural stationary states for open quantum many-body systems,” *Physical Review B* **99**, 214306 (2019).
- [217] G. Carleo and M. Troyer, “Solving the quantum many-body problem with artificial neural networks,” *Science* **355**, 602–606 (2017).
- [218] W. Metzner and D. Vollhardt, “Correlated Lattice Fermions in Infinite Dimensions,” *Physical Review Letters* **62**, 324–327 (1989).
- [219] A. Georges and G. Kotliar, “Hubbard model in infinite dimensions,” *Physical Review B* **45**, 6479–6483 (1992).
- [220] G. Kotliar, S. Y. Savrasov, K. Haule, V. S. Oudovenko, O. Parcollet, and C. A. Marianetti, “Electronic structure calculations with dynamical mean-field theory,” *Reviews of Modern Physics* **78**, 865–951 (2006).
- [221] P. Anders, E. Gull, L. Pollet, M. Troyer, and P. Werner, “Dynamical mean-field theory for bosons,” *New Journal of Physics* **13**, 075013 (2011).
- [222] P. Anders, E. Gull, L. Pollet, M. Troyer, and P. Werner, “Dynamical Mean Field Solution of the Bose-Hubbard Model,” *Physical Review Letters* **105**, 096402 (2010).
- [223] J. K. Freericks, V. M. Turkowski, and V. Zlatić, “Nonequilibrium Dynamical Mean-Field Theory,” *Physical Review Letters* **97**, 266408 (2006).
- [224] P. Schmidt and H. Monien, “Nonequilibrium dynamical mean-field theory of a strongly correlated system,” [arXiv:cond-mat/0202046](https://arxiv.org/abs/cond-mat/0202046).
- [225] H. Aoki, N. Tsuji, M. Eckstein, M. Kollar, T. Oka, and P. Werner, “Nonequilibrium dynamical mean-field theory and its applications,” *Reviews of Modern Physics* **86**, 779–837 (2014).
- [226] H. U. R. Strand, M. Eckstein, and P. Werner, “Nonequilibrium dynamical mean-field theory for bosonic lattice models,” *Physical Review X* **5**, 11038 (2015).
- [227] H. U. R. Strand, M. Eckstein, and P. Werner, “Beyond the Hubbard bands in strongly correlated lattice bosons,” *Physical Review A - Atomic, Molecular, and Optical Physics* **92**, 63602 (2015).
- [228] A. O. Caldeira and A. J. Leggett, “Influence of dissipation on quantum tunneling in macroscopic systems,” *Physical Review Letters* **46**, 211–214 (1981).
- [229] A. J. Leggett, S. Chakravarty, A. T. Dorsey, M. P. A. Fisher, A. Garg, and W. Zweger, “Dynamics of the dissipative two-state system,” *Reviews of Modern Physics* **59**, 1–85 (1987).

- [230] K. Le Hur, L. Henriet, L. Herviou, K. Plekhanov, A. Petrescu, T. Goren, M. Schiro, C. Mora, and P. P. Orth, “Driven dissipative dynamics and topology of quantum impurity systems,” *Comptes Rendus Physique* **19**, 451–483 (2018).
- [231] S. Bera, S. Florens, H. U. Baranger, N. Roch, A. Nazir, and A. W. Chin, “Stabilizing spin coherence through environmental entanglement in strongly dissipative quantum systems,” *Physical Review B - Condensed Matter and Materials Physics* **89**, 121108 (2014).
- [232] S. Bera, A. Nazir, A. W. Chin, H. U. Baranger, and S. Florens, “Generalized multipolaron expansion for the spin-boson model: Environmental entanglement and the biased two-state system,” *Physical Review B - Condensed Matter and Materials Physics* **90**, 75110 (2014).
- [233] A. C. Hewson, *The Kondo Problem to Heavy Fermions* (Cambridge University Press, 2009).
- [234] D. Goldhaber-Gordon, H. Shtrikman, D. Mahalu, D. Abusch-Magder, U. Meirav, M. A. Kastner, H. Shtrikman, D. Mahalu, D. Abusch-Magder, U. Meirav, and M. A. Kastner, “Kondo effect in a single-electron transistor,” *Nature* **391**, 156–159 (1998).
- [235] M. Grobis, I. G. Rau, R. M. Potok, H. Shtrikman, and D. Goldhaber-Gordon, “Universal scaling in nonequilibrium transport through a single channel Kondo dot,” *Physical Review Letters* **100**, 246601 (2008).
- [236] Z. Iftikhar, A. Anthore, A. K. Mitchell, F. D. Parmentier, U. Gennser, A. Ouerghi, A. Cavanna, C. Mora, P. Simon, and F. Pierre, “Tunable quantum criticality and super-ballistic transport in a “charge” Kondo circuit,” *Science* **360**, 1315–1320 (2018).
- [237] G. Cohen and E. Rabani, “Memory effects in nonequilibrium quantum impurity models,” *Physical Review B - Condensed Matter and Materials Physics* **84**, 75150 (2011).
- [238] E. Gull, A. J. Millis, A. I. Lichtenstein, A. N. Rubtsov, M. Troyer, and P. Werner, “Continuous-time Monte Carlo methods for quantum impurity models,” *Reviews of Modern Physics* **83**, 349–404 (2011).
- [239] L. Mühlbacher and E. Rabani, “Real-time path integral approach to nonequilibrium many-body quantum systems,” *Physical Review Letters* **100**, 176403 (2008).
- [240] M. Schiró and M. Fabrizio, “Real-time diagrammatic Monte Carlo for nonequilibrium quantum transport,” *Phys. Rev. B* **79**, 153302 (2009).
- [241] P. Werner, T. Oka, and A. J. Millis, “Diagrammatic Monte Carlo simulation of nonequilibrium systems,” *Physical Review B - Condensed Matter and Materials Physics* **79**, 35320 (2009).

- [242] G. Cohen, E. Gull, D. R. Reichman, A. J. Millis, and E. Rabani, “Numerically exact long-time magnetization dynamics at the nonequilibrium Kondo crossover of the Anderson impurity model,” *Physical Review B - Condensed Matter and Materials Physics* **87**, 195108 (2013).
- [243] R. E. V. Profumo, C. Groth, L. Messio, O. Parcollet, and X. Waintal, “Quantum Monte Carlo for correlated out-of-equilibrium nanoelectronic devices,” *Physical Review B - Condensed Matter and Materials Physics* **91**, 245154 (2015).
- [244] G. Cohen, E. Gull, D. R. Reichman, and A. J. Millis, “Taming the Dynamical Sign Problem in Real-Time Evolution of Quantum Many-Body Problems,” *Physical Review Letters* **115**, 266802 (2015).
- [245] H.-T. T. Chen, G. Cohen, and D. R. Reichman, “Inchworm Monte Carlo for exact non-adiabatic dynamics. I. Theory and algorithms,” *Journal of Chemical Physics* **146**, 54105 (2017).
- [246] H.-T. T. Chen, G. Cohen, and D. R. Reichman, “Inchworm Monte Carlo for exact non-adiabatic dynamics. II. Benchmarks and comparison with established methods,” *Journal of Chemical Physics* **146**, 54106 (2017).
- [247] N. E. Bickers, *Review of Techniques in the Large-N Expansion for Dilute Magnetic Alloys*, Tech. Rep. (1987) publication Title: Reviews of Modern Physics.
- [248] P. Nordlander, M. Pustilnik, Y. Meir, N. S. Wingreen, and D. C. Langreth, “How Long Does It Take for the Kondo Effect to Develop?” *Physical Review Letters* **83**, 808–811 (1999).
- [249] M. Eckstein and P. Werner, “Nonequilibrium dynamical mean-field calculations based on the noncrossing approximation and its generalizations,” *Physical Review B - Condensed Matter and Materials Physics* **82**, 115115 (2010).
- [250] A. Rüegg, E. Gull, G. A. Fiete, and A. J. Millis, “Sum rule violation in self-consistent hybridization expansions,” *Physical Review B - Condensed Matter and Materials Physics* **87**, 75124 (2013).
- [251] F. Peronaci, M. Schiró, and O. Parcollet, “Resonant Thermalization of Periodically Driven Strongly Correlated Electrons,” *Physical Review Letters* **120**, 197601 (2018).
- [252] M. Nakagawa, N. Kawakami, and M. Ueda, “Non-Hermitian Kondo Effect in Ultracold Alkaline-Earth Atoms,” *Physical Review Letters* **121**, 203001 (2018).
- [253] F. Tonielli, R. Fazio, S. Diehl, and J. Marino, “Orthogonality Catastrophe in Dissipative Quantum Many-Body Systems,” *Physical Review Letters* **122**, 040604 (2019).
- [254] H. Fröml, A. Chiocchetta, C. Kollath, and S. Diehl, “Fluctuation-Induced Quantum Zeno Effect,” *Physical Review Letters* **122**, 040402 (2019).

- [255] M. R. Delbecq, V. Schmitt, F. D. Parmentier, N. Roch, J. J. Viennot, G. Fève, B. Huard, C. Mora, A. Cottet, and T. Kontos, “Coupling a quantum dot, fermionic leads, and a microwave cavity on a chip,” *Physical Review Letters* **107**, 256804 (2011).
- [256] M. Schiró and K. Le Hur, “Tunable hybrid quantum electrodynamics from nonlinear electron transport,” *Physical Review B - Condensed Matter and Materials Physics* **89**, 195127 (2014).
- [257] L. E. E. Bruhat, J. J. J. Viennot, M. C. C. Dartailh, M. M. M. Desjardins, T. Kontos, and A. Cottet, “Cavity photons as a probe for charge relaxation resistance and photon emission in a quantum dot coupled to normal and superconducting continua,” *Physical Review X* **6**, 21014 (2016).
- [258] A. Cottet, M. C. Dartailh, M. M. Desjardins, T. Cubaynes, L. C. Contamin, M. Delbecq, J. J. Viennot, L. E. Bruhat, B. Douçot, and T. Kontos, “Cavity QED with hybrid nanocircuits: From atomic-like physics to condensed matter phenomena,” *Journal of Physics Condensed Matter* **29**, 433002 (2017).
- [259] M. Schiró, “Real-time dynamics in quantum impurity models with diagrammatic Monte Carlo,” *Physical Review B - Condensed Matter and Materials Physics* **81**, 85126 (2010).
- [260] P. Danielewicz, “Quantum theory of nonequilibrium processes II. Application to nuclear collisions,” *Annals of Physics* **152**, 305–326 (1984).
- [261] P. Danielewicz, “Quantum theory of nonequilibrium processes, I,” *Annals of Physics* **152**, 239–304 (1984).
- [262] M. Wagner, “Expansions of nonequilibrium Greens functions,” *Physical Review B* **44**, 6104–6117 (1991).
- [263] P. Werner, A. Comanac, L. De Medici, M. Troyer, A. J. Millis, L. de’ Medici, M. Troyer, and A. J. Millis, “Continuous-time solver for quantum impurity models,” *Physical Review Letters* **97**, 76405 (2006).
- [264] C. Müller and T. M. Stace, “Deriving Lindblad master equations with Keldysh diagrams: Correlated gain and loss in higher order perturbation theory,” *Physical Review A* **95**, 013847 (2017).
- [265] V. Reimer and M. Wegewijs, “Density-operator evolution: Complete positivity and the Keldysh real-time expansion,” *SciPost Physics* **7**, 012 (2019).
- [266] D. Golež, M. Eckstein, and P. Werner, “Dynamics of screening in photodoped Mott insulators,” *Physical Review B - Condensed Matter and Materials Physics* **92**, 195123 (2015).

- [267] H.-T. T. Chen, G. Cohen, A. J. Millis, and D. R. Reichman, “Anderson-Holstein model in two flavors of the noncrossing approximation,” *Physical Review B* **93**, 174309 (2016).
- [268] J. Hubbard, “Electron correlations in narrow energy bands,” *Proceedings of the Royal Society of London. Series A. Mathematical and Physical Sciences* **276**, 238–257 (1963).

**Titre :** Systèmes quantiques à plusieurs corps dissipatifs et pilotés

**Mots clés :** physique quantique, matière condensée, systèmes quantiques ouverts, hors d'équilibre, problème à plusieurs corps

**Résumé :** Ma thèse de doctorat était consacrée à l'étude des systèmes quantiques à plusieurs corps dissipatifs et pilotés. Ces systèmes représentent des plateformes naturelles pour explorer des questions fondamentales sur la matière dans des conditions de non-équilibre, tout en ayant un impact potentiel sur les technologies quantiques émergentes. Dans cette thèse, nous discutons d'une décomposition spectrale de fonctions de Green de systèmes ouverts markoviens, que nous appliquons à un modèle d'oscillateur quantique de van der Pol. Nous soulignons qu'une propriété de signe des fonctions spectrales des systèmes d'équilibre ne s'imposait pas dans le cas de systèmes ouverts, ce qui produisait une surprenante "densité d'états négative", avec des conséquences physiques directes. Nous ensuite étudions la transition de phase entre une phase normale et une phase superfluide dans un système prototype de bosons dissipatifs forcés sur un réseau. Cette transition est caractérisée par une criticité à fréquence finie corres-

pondant à la rupture spontanée de l'invariance par translation dans le temps, qui n'a pas d'analogie dans des systèmes à l'équilibre. Nous discutons le diagramme de phase en champ moyen d'une phase isolante de Mott stabilisée par dissipation, potentiellement pertinente pour des expériences en cours. Nos résultats suggèrent qu'il existe un compromis entre la fidélité de la phase stationnaire à un isolant de Mott et la robustesse d'une telle phase à taux de saut fini. Enfin, nous présentons des développements concernant la théorie du champ moyen dynamique (DMFT) pour l'étude des systèmes à plusieurs corps dissipatifs et forcés. Nous introduisons DMFT dans le contexte des modèles dissipatifs et forcés et nous développons une méthode pour résoudre le problème auxiliaire d'une impureté couplée simultanément à un environnement markovien et à un environnement non-markovien. À titre de test, nous appliquons cette nouvelle méthode à un modèle simple d'impureté fermionique.

**Title :** Driven-Dissipative Quantum Many-Body Systems

**Keywords :** quantum physics, condensed matter, open quantum systems, out of equilibrium, many-body physics

**Abstract :** My PhD was devoted to the study of driven-dissipative quantum many-body systems. These systems represent natural platforms to explore fundamental questions about matter under non-equilibrium conditions, having at the same time a potential impact on emerging quantum technologies. In this thesis, we discuss a spectral decomposition of single-particle Green functions of Markovian open systems, that we applied to a model of a quantum van der Pol oscillator. We point out that a sign property of spectral functions of equilibrium systems doesn't hold in the case of open systems, resulting in a surprising "negative density of states", with direct physical consequences. We study the phase transition between a normal and a superfluid phase in a prototype system of driven-dissipative bosons on a lattice. This transition is characterized by a finite-frequency criticality correspon-

ding to the spontaneous break of time-translational invariance, which has no analog in equilibrium systems. Later, we discuss the mean-field phase diagram of a Mott insulating phase stabilized by dissipation, which is potentially relevant for ongoing experiments. Our results suggest that there is a trade off between the fidelity of the stationary phase to a Mott insulator and robustness of such a phase at finite hopping. Finally, we present some developments towards using dynamical mean field theory (DMFT) for studying driven-dissipative lattice systems. We introduce DMFT in the context of driven-dissipative models and developed a method to solve the auxiliary problem of a single impurity, coupled simultaneously to a Markovian and a non-Markovian environment. As a test, we apply this novel method to a simple model of a fermionic, single-mode impurity.

